Bi-annual (12/1/2005–5/31/2006) Performance/Technical Report for ONR YIP Award under Grant N00014-03-1-0466 Studies on Radar and Non-radar Sensor Networks

Qilian Liang
Department of Electrical Engineering
University of Texas at Arlington
Arlington, TX 76019-0016 USA
Phone: 817-272-1339, Fax: 817-272-2253
E-mail: liang@uta.edu

Abstract

During the period of 12/1/2005 – 5/30/2006, we expanded our research from generic wireless sensor networks to radar sensor networks. For radar sensor networks, we performed the following preliminary studies:

1. Waveform design and diversity in radar sensor networks with applications to automatic target recognition without or with delay-doppler uncertainty. We used constant frequency (CF) pulse waveform and linear frequency modulation (LFM) waveform in this study.
2. We proposed a Knowledge-based Ubiquitous and Persistent Sensor networks (KUPS) for threat assessment, of which "sensor" is a broad characterization concept. It means diverse data or information from ubiquitous and persistent sensor sources such as organic sensors (e.g., radar) and human intelligence sensors.
3. Spatial-temporal-frequency diversity to improve the detection performance of Radar Sensor Networks in the presence of certain types of interference (clutter, jamming, noise and interference between radar sensors) was studied.

For non-radar sensor networks, we continuously conducted the following research tasks:

1. Channel Capacity of Virtual MIMO-Based Wireless Sensor Networks with Imperfect CSI;
2. Cross-Layer Design for MIMO-Based Wireless Sensor Networks;
3. Statistical Analysis in Wireless Sensor Networks with Application to Resources Allocation;
4. MAC Protocol Design for UWB-Based Wireless Sensor Networks;
5. and Query Processing Optimization in Wireless Sensor Networks.

Fourteen papers were produced during the past six months, and are attached to this report.

1 Studies on Radar Sensor Networks

1.1 Waveform Design and Diversity in Radar Sensor Networks

In [1][2], we performed some theoretical studies on constant frequency (CF) pulse waveform design and diversity in radar sensor networks (RSN): (1) the conditions for waveform co-existence, (2) interferences among waveforms in RSN, (3) waveform diversity combining in RSN. As an application example, we applied the waveform design and diversity to automatic target recognition (ATR) in

RSN and propose maximum-likehood (ML)-ATR algorithms for nonfluctuating target as well as fluctuating target. Simulation results show that our waveform diversity-based ML-ATR algorithm performs much better than single-waveform ML-ATR algorithm for nonfluctuating targets or fluctuating targets. Conclusions are drawn based on our analysis and simulations and future research works on this research topic are discussed.

In the above ATR using CF pulse waveform design and diversity, we assumed no delay-doppler uncertainty. It is not true for ATR in target search phase because the target range and mobility are not yet perfectly known, which results in delay-doppler uncertainty. In [3][4], we studied linear frequency modulation (LFM) waveform design and diversity, and applied it to ATR with delay-doppler uncertainty using ML-ATR algorithm. Simulation results show that our RSN vastly reduces the ATR error comparing to a single radar system in ATR with delay-doppler uncertainty.

In [6], we studied waveform design and diversity using some concepts from physical layer communications such as orthogonal, non-coherent detection, and coherent detection. We also used signal representation from communication domain, i.e., taking its real part when carriers are considered. We proposed orthogonal waveforms for RSN, which eliminates interference when no doppler shift is introduced. Additionally, this approach applies the advantage of spacial diversity through equal gain combination performed by clusterhead. When doppler shift is considered and interference is unavoidable, we analyzed the performance of this design not only in coherent RSN, but in noncoherent systems as well. The latter scenario is more challenging as doppler-shift uncertainty results in more complicated implementation. Monte Carlo simulation shows that our technique provides much better detection performance than single radar for fluctuating targets, in terms of probability of false alarm and miss detection. Conclusions are drawn based on our analysis and further related research areas are discussed.

1.2 A Network Centric Warfare (NCW) Model: Knowledge-based Ubiquitous and Persistent Sensor Networks for Threat Analysis

In current and future military operational environments, such as Global War on Terrorism (GWOT) and Maritime Domain Awareness (MDA), warfighters require technologies evolved to support information needs regardless of location and consistent with the users level of command or responsibility and operational situation. To support this need, the DoD has developed the concept of Network Centric Warfare (NCW), defined as "*military operations that exploit state-of-the-art information and networking technology to integrate widely dispersed human decision makers, situational and targeting sensors, and forces and weapons into a highly adaptive, comprehensive system to achieve unprecedented mission effectiveness.*"

In the spirit of this NCW concept, in [5], we proposed a Knowledge-based Ubiquitous and Persistent Sensor networks (KUPS) for threat assessment, of which "sensor" is a broad characterization concept. It means diverse data or information from ubiquitous and persistent sensor sources such as organic sensors and human intelligence sensors. Our KUPS for threat assessment consists of two major steps: threat detection using fuzzy logic systems and threat parameter estimation using *radar sensor networks*. Our fuzzy logic systems can combine the linguistic knowledge from different intelligent sensors. We proposed a maximum-likelihood (ML) estimation algorithm for target RCS parameter estimation, and we showed that our ML estimator is *unbiased* and the variance of parameter estimation matches the *Cramer-Rao lower bound*. Simulations further validate these theoretical results.

1.3 Spatial-Temporal-Frequency Diversity in Radar Sensor Networks

In [7], spatial-temporal-frequency diversity to improve the detection performance of Radar Sensor Networks in the presence of certain types of interference (clutter, jamming, noise and interference between radar sensors) was studied. Besides the interference between radar sensors, performance of the network depends largely on other interference, especially clutter, which is extended in both angle and range, and is spread in Doppler frequency. By using the spatial-temporal diversity, we can suppress effects of these interference. In [7], we also proposed a receiver for diversity combining in RSN. As an application example, we applied the spatial-temporal-frequency diversity scheme to improve the detection performance or reduce the miss-detection probability at a low false alarm probability. Simulation results for both non-fluctuating targets and fluctuating targets show that the performance of our proposed scheme is superior to that of the single radar with the spatial-temporal diversity only.

2 Studies on Non-Radar Sensor Networks

2.1 Channel Capacity of Virtual MIMO-Based Wireless Sensor Networks with Imperfect CSI

Multiple-input multiple-output (MIMO) has recently emerged as one of the most significant technical breakthroughs in modern communications. A key feature of MIMO systems is the ability to turn multipath propagation, traditionally a pitfall of wireless transmission, into a benefit for the user. In existing works on MIMO for wireless sensor networks, virtual MIMO schemes based on the space-time block codes (STBC) have been widely used, and it's demonstrated that the full diversity and full rate are achieved which enhances power/bandwidth efficiency and reliability. However, all the existing works have generated substantial insight into the applications of MIMO to wireless sensor networks design for certain simplified models of the communication environment, such as complete channel state information (CSI), absence of interference generated by other users in the network, and persistent, homogeneous traffic from the physical layer point of view. In [8], we studied channel capacity of virtual MIMO-based wireless sensor networks with imperfect CSI. We compared the channel capacities of using equal power allocation and waterfilling strategy and considered different channel models with imperfect CSI.

2.2 Cross-Layer Design for MIMO-Based Wireless Sensor Networks

The multiple-input and multiple-output (MIMO) system can be used to increase throughtput through multiplexing or to improve PLR (Packet Loss Ratio) throught diversity. Besides physical layer factors (such as diversity gain, bandwidth, and SNR), the MAC layer and network layer protocols also affect the throughput and PLR, for example, larger number of transmitters will lead to higher link failure which may require MAC layer re-transmission and network layer re-routing. In [9], we studied cross-layer design for MIMO system considering physical layer, MAC layer and network layer design. Simulation results show that theoretical result based on pure physical layer design such as larger number of transmitters have better diversity gain and multiplexing gain does not hold when the MAC layer and network layer are also considered, which indicates that some theoretical results on MIMO may need to be revisited.

2.3 Statistical Analysis in Wireless Sensor Networks with Application to Resources Allocation

In [11], we modeled the end-to-end distance for a given number of hops in dense planar Wireless Sensor Networks. We derived that the closed-form formula for single-hop distance and postulate Beta distribution for 2-hop distance. When the number of hops increases beyond three, the multihop distance approaches Gaussian. The Gaussian approximation model is also applied to ranging, which achieves less distance error than Hop-TERRAIN and APS (Ad hoc Positioning System). Our error analysis also shows the distance error is be minimized by using our model.

In [10], we addressed a fundamental problem in Wireless Sensor Networks, how many hops does it take for a packet to be relayed for a given distance? For a deterministic topology, this question reduces to a simple geometry problem. However, a statistical study is needed for randomly deployed WSNs. We proposed a Maximum Likelihood decision based on the conditional pdf of $f(r|H_i)$. Due to the computational complexity of $f(r|H_i)$, we also proposed an attenuated Gaussian approximation for the conditional pdf. We showed that the approximation visibly simplifies the decision process and the error analysis. The latency and energy consumption estimation are also included as application examples. Simulations show that our approximation model can predict the latency and energy consumption with less than half RMSE, compared to the linear models.

2.4 MAC Protocol Design for UWB-Based Wireless Sensor Networks

In [12], we proposed a MAC protocol: throughput-maximized MAC protocol (TM-MAC), based on the characteristics of ultra wideband (UWB) technology. In UWB communication systems, the transmission parameters are tunable to match the requirements of data flow. In TM-MAC, we implement concurrent multiuser access instead of mutual exclusion method, such as TDMA and random access. For multiuser interference, we established a model to adaptively adjust the data transmission rate to ensure a satisfied signal to noise ratio (SNR) at receiver side. We also analyzed the relationship among the theoretical maximum channel capacity, the achievable maximum channel capacity and the maximum data transmission rate. According to the network topology, TM-MAC re-divides network into subsets, in which communication pairs can make communication simultaneously to enhance throughput and to exploit as fast as possible data transmission rate for reliable communication. For subset formation, we proposed a general analytical framework, which captures the unique characteristics of shared wireless channel and allows to model a large class of systemwide throughputmaximization issue via the specification of per-link utilization functions. Simulation results demonstrate that TM-MAC can implement throughput maximization to shorten latency and to enhance network processing capability.

2.5 Query Processing Optimization in Wireless Sensor Networks

Query processing has been studied extensively in traditional database systems. But few existing methods can be directly applied to wireless sensor database systems due to their characteristics, such as decentralized nature, limited computational power, imperfect information recorded, and energy scarcity of individual sensor nodes. In [13], we extended our previous work: quality-guaranteed and energy-efficient algorithm (QGEE) for wireless sensor database systems. We introduced radius of covering disk from point spread function (PSF) aspect and sample size for query quality and energy consumption control. PSF introduces ambiguity into query answers, since the sensitivity of nodes is nonuniform within monitoring region. Sample size determination refers to the process of determining exactly how many samples should be measured in order that the sampling distribution of estimators meets users' pre-specified target precision. In this paper, we formulated the criteria to

determine the optimum radius and sample size according to users' requirements on query answers. Simulation results demonstrate that the impact of sample size and monitoring coverage on query answers in terms of root mean square error (RMSE).

In [14], we proposed two methods to substitute cosine measure for vector similarity: Cosine-Length Measure (CLM) and Joint-Deference Measure (JDM). Through considering the impact of vector length on vector similarity, CLM alleviates the disadvantage of traditional VSM, in which the confidence of query answer may be degraded since truly similar nodes cannot be elected according to users' requirement. JDM upgrades the accuracy and degrades the complexity for the computation on similarity coefficient through simplifying the measure from vector domain to scalar domain. In addition, with the distributions of measurement error and environment noise known and/or unknown respectively, we formulated the criteria to determine the optimum sample size to meet users' pre-specified target precision. Through simulation, we checked the validities and sensitivities of cosine measure, CLM and JMD methods on answer quality and network lifetime. Furthermore, our simulation results, in this paper, form a set of criteria for method selection based on specific applications.

References

[1] Q. Liang, "Waveform Design and Diversity in Radar Sensor Networks: Theoretical Analysis and Application to Automatic Target Recognition," submitted to *IEEE Trans on Aerospace and Electronic Systems.*

[2] Q. Liang, "Waveform Design and Diversity in Radar Sensor Networks: Theoretical Analysis and Application to Automatic Target Recognition," accepted by *IEEE Int'l Workshop on Wireless Ad Hoc and Sensor Networks*, June 2006, New York.

[3] Q. Liang, "Radar Sensor Networks: Algorithms for Waveform Design and Diversity with Application to ATR with Delay-Doppler Uncertainty," submitted to *EURASIP Journal on Wireless Communications and Networking.*

[4] Q. Liang, "Radar Sensor Networks for Automatic Target Recognition with Delay-Doppler Uncertainty," submitted to *IEEE MILCOM*, Oct 2006, Washington, DC.

[5] Q. Liang, "KUPS: Knowledge-based Ubiquitous and Persistent Sensor networks for Threat Assessment," submitted to *IEEE MILCOM*, Oct 2006, Washington, DC.

[6] J. Liang and Q. Liang, "Orthogonal Waveform Design and Performance Analysis in Radar Sensor Networks (RSN)," submitted to *IEEE MILCOM*, Oct 2006, Washington, DC.

[7] H. Ly and Q. Liang, "Spatial-temporal-frequency diversity in radar sensor networks," submitted to *IEEE MILCOM*, Oct 2006, Washington, DC.

[8] L. Wang and Q. Liang, "Channel Capacity of Virtual MIMO-Based Wireless Sensor Networks with Impefect CSI," submitted to *IEEE MILCOM*, Oct 2006, Washington, DC.

[9] X. Xia and Q. Liang, "Cross-Layer Design for Wireless Sensor Networks based on Cooperative MIMO Techniques," submitted to *IEEE MILCOM*, Oct 2006, Washington, DC.

[10] L. Zhao and Q. Liang, "Hop-Distance Estimation in Wireless Sensor Networks with Applications to Resources Allocation," submitted to *EURASIP Journal on Wireless Communications and Networking.*

[11] L. Zhao and Q. Liang, "Modeling End-to-end Distance for Given Number of Hops in Dense Planar Wireless Sensor Networks," accepted by *IEEE Int'l Workshop on Wireless Ad Hoc and Sensor Networks*, June 2006, New York.

[12] Q. Ren and Q. Liang, "A Throughput-Maximized MAC Protocol for Ultra Wideband Communication in Wireless Sensor Networks," submitted to *IEEE Globecom*, Nov 2006, San Francisco, CA.

[13] Q. Ren and Q. Liang, "Query Processing Optimization Through Sample Size and Monitoring Coverage Controlling in Wireless Sensor Networks," accepted by *IEEE Int'l Workshop on Wireless Ad Hoc and Sensor Networks*, June 2006, New York.

[14] Q. Ren and Q. Liang, "Answer Quality and Network Lifetime Aware Query Processing Protocol in Tactical Sensor Networks," submitted to *IEEE MILCOM*, Oct 2006, Washington, DC.

Waveform Design and Diversity in Radar Sensor Networks: Theoretical Analysis and Application to Automatic Target Recognition

Qilian Liang, *Senior Member, IEEE*

Department of Electrical Engineering

University of Texas at Arlington

Arlington, TX 76019-0016 USA

E-mail: liang@uta.edu

Abstract

In this paper, we perform some theoretical studies on constant frequency (CF) pulse waveform design and diversity in radar sensor networks (RSN): (1) the conditions for waveform co-existence, (2) interferences among waveforms in RSN, (3) waveform diversity combining in RSN. As an application example, we apply the waveform design and diversity to automatic target recognition (ATR) in RSN and propose maximum-likehood (ML)-ATR algorithms for nonfluctuating target as well as fluctuating target. Simulation results show that our waveform diversity-based ML-ATR algorithm performs much better than single-waveform ML-ATR algorithm for nonfluctuating targets or fluctuating targets. Conclusions are drawn based on our analysis and simulations and future research works on this research topic are discussed.

Index Terms : radar sensor networks, waveform diversity, automatic target recognition, maximum-likelihood, interferences, ambiguity function.

1 Introduction and Motivation

The network of radar sensors should operate with multiple goals managed by an intelligent platform network that can manage the dynamics of each radar to meet the common goals of the platform, rather than each radar to operate as an independent system. Therefore, it is significant to perform signal design and processing and networking cooperatively within and between platforms of radar sensors and their communication modules.

Waveform diversity is the technology that will allow one or more sensors on board a platform to automatically change operating parameters, e.g., frequency, gain pattern, and pulse repetition frequency (PRF) to meet the varying environments. It has long been recognized that judicious use of properly designed waveforms, coupled with advanced receiver strategies, is fundamental to fully utilizing the capacity of the electromagnetic spectrum. However, it is only relatively recent advances in hardware technology that are enabling a much wider range of design freedoms to be explored. As a result, there are emerging and compelling changes in system requirements such as more efficient spectrum usage, higher sensitivities, greater information content, improved robustness to errors, reduced interference emissions, etc. The combination of these is fuelling a worldwide interest in the subject of waveform design and the use of waveform diversity techniques.

In the existing works on waveform design and selection, Fitzgerald [5] demonstrated the inappropriateness of selection of waveform based on measurement quality alone: the interaction between the measurement and the track can be indirect, but must be accounted for. Bell [3] used information theory to design radar waveform for the measurement of extended radar targets exhibiting resonance phenomena. In [2], singularity expansion method was used to design some discriminant waveforms such as K-pulse, E-pulse, and S-pulse. Sowelam and Tewfik [20] developed a signal selection strategy for radar target classification, and a sequential classification procedure was proposed to minimize the average number of necessary signal transmissions. Intelligent waveform selection

was studied in [1][9], but the effect of doppler shift was not considered. In [11], the performance of constant frequency (CF) and linear frequency modulated (LFM) waveform fusion from the standpoint of the whole system was studied, but the effects of clutter was not considered. In [19], CF and LFM waveforms were studied for sonar system, but it was assumed that the sensor is nonintelligent (i.e., waveform can't be selected adaptively). All the above studies and design methods were focused on the waveform design or selection for a single active radar or sensor. In [17], cross-correlation properties of two radars are briefly mentioned and the binary coded pulses using simulated annealing [4] are highlighted. However, the cross-correlation of two binary sequences such as binary coded pulses (e.g. Barker sequence) are much easier to study than that of two analog radar waveforms. In this paper, we will focus on the waveform diversity and design for radar sensor networks using constant frequency (CF) pulse waveform.

The rest of this paper is organized as follows. In Section 2, we study the co-existence of radar waveforms. In Section 3, we analyze the interferences among radar waveforms. In Section 4 we propose a RAKE structure for waveform diversity combining and propose maximum-likelihood (ML) algorithms for automatic target recognition (ATR). In Section 5, we provide simulation results on ML-ATR. In Section 6, we conclude this paper and provide some future works.

2 Co-existence of Radar Waveforms

In radar sensor networks (RSN), radar sensors will interfere with each other and the signal-to-interference-ratio may be very low if the waveforms are not properly designed. We will introduce orthogonality as one criterion for waveforms design in RSN to make them co-existence. Besides, the radar channel is narrow-band, so we will also consider the bandwidth constraint.

In our radar sensor networks, we choose CF pulse waveform. The CF pulse waveform can be

defined as

$$x(t) = \sqrt{\frac{E}{T}} \exp(j2\pi\beta t) \quad -T/2 \leq t \leq T/2 \tag{1}$$

In radar, ambiguity function (AF) is an analytical tool for waveform design and analysis that succinctly characterizes the behavior of a waveform paired with its matched filter. The ambiguity function is useful for examing resolution, side lobe behavior, and ambiguities in both range and Doppler for a given waveform[15]. For a single radar, the matched filter for waveform $x(t)$ is $x^*(-t)$, and the ambiguity function of CF pulse waveform is

$$\begin{aligned} A(\tau, F_D) &= \left| \int_{-T/2+\tau}^{T/2} x(t) \exp\left(j2\pi F_D s\right) x^*(t-\tau) dt \right| \\ &= \left| \frac{E \sin[\pi F_D (T - |\tau|)]}{T\pi F_D} \right| \quad -T \leq \tau \leq T \end{aligned} \tag{2}$$

Three special cases can simplify this AF:

1. When $\tau = 0$,

$$A(0, F_D) = \left| \frac{E \sin(\pi F_D T)}{T\pi(F_D)} \right|; \tag{3}$$

2. and when $F_D = 0$,

$$A(\tau, 0) = \left| \frac{E(T - |\tau|)}{T} \right|; \tag{4}$$

3. and

$$A(0, 0) = E \tag{5}$$

However, the above ambiguity is for one radar only (no co-existing radar).

For radar sensor networks, the waveforms from different radars will interfere with each other. We choose the waveform for radar i as

$$x_i(t) = \sqrt{\frac{E}{T}} \exp[j2\pi(\beta + \delta_i)t] \quad -T/2 \leq t \leq T/2 \tag{6}$$

which means there is a frequency shift δ_i for radar i. To minimize the interference from one waveform to the other, optimal values for δ_i should be determined to have the waveforms orthogonal to each other, i.e., let the cross-correlation between $x_i(t)$ and $x_n(t)$ be 0,

$$\int_{-T/2}^{T/2} x_i(t)x_n^*(t)dt = \frac{E}{T}\int_{-T/2}^{T/2} \exp[j2\pi(\beta+\delta_i)t]\exp[-j2\pi(\beta+\delta_n)t]dt \quad (7)$$

$$= E\text{sinc}[\pi(\delta_i-\delta_n)T] \quad (8)$$

If we choose

$$\delta_i = \frac{i}{T} \quad (9)$$

where i is a dummy index, then (8) can have two cases

$$\int_{-T/2}^{T/2} x_i(t)x_n^*(t)dt = \begin{cases} E & i=n \\ 0 & i\neq n \end{cases} \quad (10)$$

So choosing $\delta_i = \frac{i}{T}$ in (6) can have orthogonal waveforms, i.e., the waveforms can co-exist if the carrier spacing is $1/T$ between two radar waveforms. i.e., orthogonality amongst carriers can be achieved by separating the carriers by an interger multiple of the inverse of waveform pulse duration. With this design, all the orthogonal waveforms can work simultaneously. However, there may exist time delay and doppler shift ambiguity which will have interferences to other waveforms in RSN.

3 Interferences of Waveforms In Radar Sensor Networks

3.1 RSN with Two Radar Sensors

We are interested in analyzing the interference from one radar to another if there exist time delay and doppler shift. For a simple case where there are two radar sensors (i and n), the ambiguity

function of radar i (considering interference from radar n) is

$$A_i(t_i, t_n, F_{D_i}, F_{D_n}) = |\int_{-\infty}^{\infty} [x_i(t)\exp(j2\pi F_{D_i}t) + x_n(t-t_n)\exp(j2\pi F_{D_n}t)]x_i^*(t-t_i)dt| \quad (11)$$

$$\leq \left|\int_{-T/2+\max(t_i,t_n)}^{T/2+\min(t_i,t_n)} x_n(t-t_n)\exp(j2\pi F_{D_n}t)x_i^*(t-t_i)dt\right| + \left|\int_{-T/2+t_i}^{T/2} x_i(t)\exp(j2\pi F_{D_i}t)x_i^*(t-t_i)dt\right| \quad (12)$$

$$= \left|\int_{-T/2+\max(t_i,t_n)}^{T/2+\min(t_i,t_n)} x_n(t-t_n)\exp(j2\pi F_{D_n}t)x_i^*(t-t_i)dt\right| + \left|\frac{E\sin[\pi F_{D_i}(T-|t_i|)]}{T\pi F_{D_i}}\right| \quad (13)$$

To make analysis easier, we assume $t_i = t_n = \tau$, then (13) can be simplified as

$$A_i(\tau, F_{D_i}, F_{D_n}) \approx |E\text{sinc}[\pi(n-i+F_{D_n}T)]| + \left|\frac{E\sin[\pi F_{D_i}(T-|\tau|)]}{T\pi F_{D_i}}\right| \quad (14)$$

Some special cases of (14) are listed as follows:

1. If $F_{D_i} = F_{D_n} = 0$, and δ_i and δ_n follow (9), then (14) becomes

$$A_i(\tau, 0, 0) \approx \left|\frac{E(T-|\tau|)]}{T}\right| \quad (15)$$

2. If $\tau = 0$, then (14) becomes

$$A_i(0, F_{D_i}, F_{D_n}) \approx |E\text{sinc}[\pi(n-i+F_{D_n}T)]| + \left|\frac{E\sin(\pi F_{D_i}T)}{T\pi F_{D_i}}\right| \quad (16)$$

3. If $F_{D_i} = F_{D_n} = 0$, $\tau = 0$, and δ_i and δ_n follow (9), then (14) becomes

$$A_i(0, 0, 0) \approx E \quad (17)$$

3.2 RSN with M Radar Sensors

It can be extended to an RSN with M radars. Assuming time delay τ for each radar is the same, then the ambiguity function of radar 1 (considering interferences from all the other $M-1$ radars

with CF pulse waveforms) can be expressed as

$$A_1(\tau, F_{D_1}, \cdots, F_{D_M}) \approx \sum_{i=2}^{M} |E\text{sinc}[\pi(i-1+F_{D_i}T)]| + \left| \frac{E \sin[\pi F_{D_1}(T-|\tau|)]}{T\pi F_{D_1}} \right| \tag{18}$$

Similarly, we can have three special cases,

1. If $F_{D_1} = F_{D_2} = \cdots = F_{D_M} = 0$, and frequency shift δ_i in (6) for each radar follows (9), then (18) becomes

$$A_1(\tau, 0, 0, \cdots, 0) \approx \left| \frac{E(T-|\tau|)]}{T} \right| \tag{19}$$

comparing it against (3), it shows that our derived condition in (6) can have a radar in RSN get the same signal strength as that of a single radar (no co-existing radar) when the doppler shift is 0.

2. If $\tau = 0$, then (18) becomes

$$A_1(0, F_{D_1}, F_{D_2}, \cdots, F_{D_M}) \approx \sum_{i=2}^{M} |E\text{sinc}[\pi(i-1+F_{D_i}T)]| + \left| \frac{E \sin(\pi F_{D_1}T)}{T\pi F_{D_1}} \right| \tag{20}$$

Comparing to (4), a radar in RSN has more interferences when unknown doppler shifts exist.

3. $F_{D_1} = F_{D_2} = \cdots = F_{D_M} = 0$, $\tau = 0$, and δ_i in (6) follows (9), then (18) becomes

$$A_1(0, 0, 0, \cdots, 0) \approx E \tag{21}$$

4 Waveform Diversity and Combining with Application to Automatic Target Recognition

In RSN, The radar sensors are networked together in an ad hoc fashion. They do not rely on a preexisting fixed infrastructure, such as a wireline backbone network or a base station. They are self-organizing entities that are deployed on demand in support of various events surveillance, battlefield, disaster relief, search and rescue, etc. Scalability concern suggest a hierarchical organization of radar

sensor networks with the lowest level in the hierarchy being a cluster. As argued in [10] [7] [6] [13], in addition to helping with scalability and robustness, aggregating sensor nodes into clusters has additional benefits:

1. conserving radio resources such as bandwidth;
2. promoting spatial code reuse and frequency reuse;
3. simplifying the topology, e.g., when a mobile radar changes its location, it is sufficient for only the nodes in attended clusters to update their topology information;
4. reducing the generation and propagation of routing information; and,
5. concealing the details of global network topology from individual nodes.

In RSN, each radar can provide their waveform parameters such as δ_i to their clusterhead radar, and the clusterhead radar can combine the waveforms from its cluster members.

In RSN with M radars, the received signal for clusterhead (assume it's radar 1) is

$$r_1(u,t) = \sum_{i=1}^{M} \alpha(u) x_i(t - t_i) \exp(j2\pi F_{D_i} t) + n(u,t) \tag{22}$$

where $\alpha(u)$ stands for radar cross section (RCS) and can be modeled using non-zero constants for nonfluctuating target and four Swerling target models for fluctuating target[15]; F_{D_i} is the doppler shift of target relative to waveform i; t_i is delay of waveform i, and $n(u,t)$ is additive white Gaussian noise (AWGN). In this paper, we propose a RAKE structure for waveform diversity combining, as illustrated by Fig. 1.

According to this structure, the received $r_1(u,t)$ is processed by a bank of matched filters, then the output of branch 1 (after integration) is

$$\begin{aligned} & |Z_1(u;t_1,\cdots,t_M,F_{D_1},\cdots,F_{D_M})| \\ = & \left|\int_{-T/2}^{T/2} r_1(u,t)x_1^*(t-t_1)ds\right| \qquad (23) \\ = & \left|\int_{-T/2}^{T/2}[\sum_{i=1}^{M}\alpha_i(u)x_i(t-t_i)\exp(j2\pi F_{D_i}t)+n(u,t)]x_1^*(t-t_1)dt\right| \qquad (24) \end{aligned}$$

where $\int_{-T/2}^{T/2} n(u,t)x_1^*(t-t_1)dt$ can easily be proved to be AWGN, so

$$|n(u,t_1)| \triangleq \left|\int_{-T/2}^{T/2} n(u,t)x_1^*(t-t_1)dt\right| \qquad (25)$$

follows Rayleigh distribution. Assuming $t_1 = t_2 = \cdots = t_M = \tau$, then based on (18),

$$\begin{aligned} |Z_1(u;\tau,F_{D_1},\cdots,F_{D_M})| \approx & \sum_{i=2}^{M}|\alpha(u)E\text{sinc}[\pi(i-1+F_{D_i}T)]| \\ + & \left|\frac{\alpha(u)E\sin[\pi F_{D_1}(T-|\tau|)]}{T\pi F_{D_1}}\right| + |n(u,\tau)| \qquad (26) \end{aligned}$$

Similarly, we can get the output for any branch m ($m = 1,2,\cdots,M$),

$$\begin{aligned} |Z_m(u;\tau,F_{D_1},\cdots,F_{D_M})| \approx & \sum_{i=1,i\neq m}^{M}|\alpha(u)E\text{sinc}[\pi(i-m+F_{D_i}T)]| \\ + & \left|\frac{\alpha(u)E\sin[\pi F_{D_m}(T-|\tau|)]}{T\pi F_{D_m}}\right| + |n(u,\tau)| \qquad (27) \end{aligned}$$

So $|Z_m(u;\tau,F_{D_1},\cdots,F_{D_M})|$ consists of three parts, signal (reflected signal from radar m waveform): $\left|\frac{\alpha(u)E\sin[\pi F_{D_m}(T-|\tau|)]}{T\pi F_{D_m}}\right|$, interferences from other waveforms: $\sum_{i=1,i\neq m}^{M}|\alpha(u)E\text{sinc}[\pi(i-m+F_{D_i}T)]|$, and noise: $|n(u,\tau)|$.

We can also have three special cases for $|Z_m(u;\tau,F_{D_1},\cdots,F_{D_M})|$:

1. When $F_{D_1} = \cdots = F_{D_M} = 0$,

$$|Z_m(u;\tau,0,0,\cdots,0)| \approx \left|\frac{E\alpha(u)(T-|\tau|)]}{T}\right| + |n(u,\tau)| \qquad (28)$$

which means if there is no doppler mismatch, there will be no interference from other waveform.

2. If $\tau = 0$, then (27) becomes

$$\begin{aligned} & |Z_m(u; 0, F_{D_1}, \cdots, F_{D_M})| \\ \approx & \sum_{i=1, i\neq m}^{M} |\alpha(u) E \text{sinc}[\pi(i - m + F_{D_i} T)]| + \left| \frac{\alpha(u) E \sin[\pi F_{D_m} T]}{T \pi F_{D_m}} \right| + |n(u)| \end{aligned} \tag{29}$$

3. If $\tau = 0$, and $F_{D_1} = \cdots = F_{D_M} = 0$, then (27) becomes

$$|Z_m(u; 0, 0, 0, \cdots, 0)| \approx |E\alpha(u)| + |n(u)| \tag{30}$$

Doppler mismatch happens quite often in target search where target velocity is not yet known. However, in target recognition, generally high-resolution measurements of targets in range ($\tau = 0$) and doppler are available, so (30) will be used for automatic target recognition.

How to combine all the Z_m's ($m = 1, 2, \cdots, M$) are very similar to the diversity combining in communations to combat channel fading, and the combination schemes may be different for different applications. In this paper, we are interested in applying RSN waveform diversity to automatic target recognition (ATR), e.g., recognition that the echo on a radar display is that of an aircraft, ship, motor vehicle, bird, person, rain, chaff, clear-air turbulence, land clutter, sea clutter, bare montains, forested areas, meteors, aurora, ionized media, or other natural phenomena. Early radars were "blob" detectors in that they detected the presence of a target and gave its location in range and angle, and radar began to be more than a blob detector and could provide recognition of one type of target from another[17]. It is known that small changes in the aspect angle of complex (multiple scatter) targets can cause major changes in the radar cross section (RCS). This has been considered in the past as a means of target recognition, and is called *fluctuation of radar cross section with aspect angle*, but it has not had much success[17]. In this paper, we propose

a maximum likelihood automatic target recognition (ML-ATR) algorithm for RSN. We will study non-fluctuating target as well as fluctuating target.

4.1 ML-ATR for Non-fluctuating Targets

In some sources, the non-fluctuating target is identified as "Swerling 0" or "Swerling 5" model[18]. For non-fluctuating target, the RCS $\alpha_m(u)$ is just a constant α for a given target. In (30), $|n(u,\tau)|$ follows Rayleigh distribution since $n(u,\tau)$ is a Gaussian random variable for given τ, so $|Z_m(u;0,0,\cdots,0)|$ follows Rician distribution because signal $E|\alpha$ is a constant. Let $y_m \triangleq |Z_m(u;0,0,\cdots,0)|$, then the probability density function (pdf) of y_m is

$$f(y_m) = \frac{2y_m}{\sigma^2}\exp[-\frac{(y_m^2+\lambda^2)}{\sigma^2}]I_0(\frac{2\lambda y_m}{\sigma^2}) \tag{31}$$

where

$$\lambda = E|\alpha|, \tag{32}$$

σ^2 is the noise power (with I and Q sub-channel power $\sigma^2/2$), and $I_0(\cdot)$ is the zero-order modified Bessel function of the first kind. Let $\mathbf{y} \triangleq [y_1, y_2, \cdots, y_M]$, then the pdf of $\mathbf{y}$ is

$$f(\mathbf{y}) = \prod_{m=1}^{M} f(y_m) \tag{33}$$

Our ATR is a multiple-category hypothesis testing problem, i.e., to decide a target category (e.g. aircraft, ship, motor vehicle, bird, etc) based on $r_1(u,t)$. Assume there are totally N categories and category n target has RCS α_n, so the ML-ATR algorithm to decide a target category C can be expressed as,

$$C = \arg\max_{n=1}^{N} f(\mathbf{y}|\lambda = E|\alpha_n|) \tag{34}$$

$$= \arg\max_{n=1}^{N} \prod_{m=1}^{M} \frac{2y_m}{\sigma^2}\exp[-\frac{(y_m^2+E^2\alpha_n^2)}{\sigma^2}]I_0(\frac{2E|\alpha_n|y_m}{\sigma^2}) \tag{35}$$

4.2 ML-ATR for Fluctuating Targets

Fluctuating target modeling is more realistic in which the target RCS is drawn from either the Rayleigh or chi-square of degree four pdf. The Rayleigh model describes the behavior of a complex target consisting of many scatters, none of which is dominant. The fourth-degree chi-square models targets having many scatters of similar strength with one dominant scatter. Based on different combinations of pdf and decorrelation characteristics (scan-to-scan or pulse-to-pulse decorrelation), four Swerling models are used[15]. In this paper, we will focus on "Swerling 2" model which is Rayleigh distribution with pulse-to-pulse decorrelation. The pulse-to-pulse decorrelation implies that each individual pulse results in an independent value for RCS α.

For Swerling 2 model, the RCS $|\alpha(u)|$ follows Rayleigh distribution and its I and Q subchannels follow zero-mean Gaussian distributions with variance γ^2. Assume

$$\alpha(u) = \alpha_I(u) + j\alpha_Q(u) \tag{36}$$

and $n(u) = n_I(u) + jn_Q(u)$ follows zero-mean complex Gausian distribution with variance σ^2 for the I and Q subchannels. According to (24), (27), and (30),

$$|Z_m(u; 0, 0, 0, \cdots, 0)| \approx |E\alpha(u) + n(u)| \tag{37}$$

is a more accuate approximation. Since $\alpha(u)$ and $n(u)$ are zero-mean complex Gaussian random variables, so $E\alpha(u) + n(u)$ is a zero-mean Gaussian random variable with variance $E^2\gamma^2 + \sigma^2$ for the I and Q subchannels, which means $y_m \triangleq |Z_m(u; 0, 0, \cdots, 0)|$ follows Rayleigh distribution with parameter $\sqrt{E^2\gamma^2 + \sigma^2}$,

$$f(y_m) = \frac{y_m}{E^2\gamma^2 + \sigma^2} \exp(-\frac{y_m^2}{E^2\gamma^2 + \sigma^2}) \tag{38}$$

The mean value of y_m is $\sqrt{\frac{\pi(E^2\gamma^2+\sigma^2)}{2}}$, and variance is $\frac{(4-\pi)(E^2\gamma^2+\sigma^2)}{2}$. The variance of signal is $\frac{(4-\pi)E^2\gamma^2}{2}$ and the variance of noise is $\frac{(4-\pi)\sigma^2}{2}$.

Let $\mathbf{y} \stackrel{\triangle}{=} [y_1, y_2, \cdots, y_M]$, then the pdf of $\mathbf{y}$ is

$$f(\mathbf{y}) = \prod_{m=1}^{M} f(y_m) \tag{39}$$

Assume there are totally N categories and category n target has RCS $\alpha_n(u)$ (with variance γ_n^2), so the ML-ATR algorithm to decide a target category C can be expressed as,

$$C = \arg\max_{n=1}^{N} f(\mathbf{y}|\gamma = \gamma_n) \tag{40}$$

$$= \arg\max_{n=1}^{N} \prod_{m=1}^{M} \frac{y_m}{E^2\gamma_n^2 + \sigma^2} \exp(-\frac{y_m^2}{E^2\gamma_n^2 + \sigma^2}) \tag{41}$$

5 Simulations

Radar sensor networks will be required to detect a broad range of target classes. Too often, the characteristics of objects that are not of interest (e.g., bird) will be similar to those of threat objects (e.g., missile). Therefore, new techniques to discriminate threat against undesired detections (e.g. birds, etc.) are needed. We applied our ML-ATR to this important application, to recognize a target from many target classes. We assume that the domain of target classes is known a priori (N in Sections 4.1 and 4.2), and that the RSN is confined to work only on the known domain.

For non-fluctuating target recognition, our targets have 5 classes with different RCS values, which are summarized in Table 1[17]. We applied the ML-ATR algorithms in Section 4.1 (for nonfluctuating target case) to classify an unknown target as one of these 5 target classes. At each average SNR value, we ran Monte-Carlo simulations for 10^5 times for each target. The average SNR value is based on the average power from all targets (signal variance), so the actual SNRs for bird and missile are much lower than the average SNR value. For example, at the average SNR=16dB, the bird target SNR=-33.1646dB, and missile target SNR=0.8149dB; and at average SNR=20dB, the bird target SNR=-29.1646dB, and missile target SNR=4.8149dB. In Fig. 2(a)(b), we plotted the probability of ATR error in bird and missile recognition when they are assumed

as nonfluctuating targets. Observe both figures, single radar system can't perform well in both recognitions, and their probability of ATR error is above 10%, which can't be used for real-world ATR. However, the 5-radar RSN and 10-radar RSN can maintain very low ATR errors. In Fig. 2(c), we plotted the average probability of ATR error for all 5 targets recognition. Since the other 3 targets (different aircrafts) have much higher SNRs, so their ATR error is lower, which makes the average probability of ATR error lower.

For fluctuating target recognition, we assume the fluctuating targets follow "Swerling 2" model (Rayleigh with pulse-to-pulse decorrelation), and assume the RCS value listed in Table 1 to be the standard deviation (std) γ_n of RCS $\alpha_n(u)$ for target n. We applied the ML-ATR algorithm in Section 4.2 (for fluctuating target case) for target recognition within the 5 targets domain. Similarly we ran Monte-Carlo simulations at each SNR value. In Fig. 3(a)(b)(c), we plot the ATR performance for fluctuating targets and compared the performances of single radar system, 5-radar RSN, and 10-radar RSN. Observe that the two RSNs perform much better than the single radar system. The ATR error for missile is higher than that of bird because Rayleigh distribution of missile has lots of overlap with its neighbor targets (aircrafts). Comparing Fig. 2(a)(b)(c) to Fig. 3(a)(b)(c), it is clear that higher SNRs are needed for fluctuating target recognition comparing to nonfluctuating target recognition. According to Skolnik[17], radar performance with probability of recognition error (p_e) less than 10% is good enough. Our RSN with waveform-diversity can have probability of ATR error much less than 10% for each target ATR as well as the average ATR for all targets. However, the single radar system has probability of ATR error much higher than 10%. Observe Fig. 3(c), the average probability of ATR error of single-radar is impossible to be less than 10% even at extreme high SNR. Our RSN with waveform diversity is very promising to be used for real-world ATR.

6 Conclusions and Future Works

We have studied constant frequency pulse waveform design and diversity in radar sensor networks. We showed that the waveforms can co-exist if the carrier frequency spacing is $1/T$ between two radar waveforms. We made analysis on interferences among waveforms in RSN and proposed a RAKE structure for waveform diversity combining in RSN. As an application example, we applied the waveform design and diversity to automatic target recognition (ATR) in RSN and proposed maximum-likehood (ML)-ATR algorithms for nonfluctuating target as well as fluctuating target. Simulation results show that RSN using our waveform diversity-based ML-ATR algorithm performs much better than single radar system for nonfluctuating targets and fluctuating targets recognition.

In our future works, we will investigate the ATR when multiple targets co-exist in RSN, and the number of targets are time-varying. In this paper, we used spatial diversity combining. For multi-target ATR, we will further investigate spatial-temporal-frequency combining for waveform diversity in RSN.

Acknowledgement

This work was supported by the U.S. Office of Naval Research (ONR) Young Investigator Program Award under Grant N00014-03-1-0466.

The author would like to thank ONR Program Officer Dr. Rabinder N. Madan for his direction and insightful discussion on radar sensor networks.

References

[1] P. Baggenstoss, "Adaptive pulselength correction (APLECORR): a strategy for waveform optimization in ultrawideband active sonar," *IEEE Trans on Oceanic Engineering*, vol. 23, no. 1,

pp. 1-11, 1998.

[2] C. E. Baum, et al, "The singularity expansion method and its application to target identification", *Proc. of the IEEE*, vol 79, no. 10, Oct 1991.

[3] M. R. Bell, "Information theory and radar waveform design", *IEEE Trans on Information Theory*, vol. 39, no. 5, pp. 1578-1597, Sept 1993.

[4] H. Deng, "Synthesis of binary sequences with good correlation and cross-correlation properties by simulated annealing," *IEEE Trans on Aerospace and Electronic Systems*, vol. 32, no. 1, Jan 1996.

[5] R. Fitzgerald, "Effects of range-doppler coupling on chirp radar tracking acuracy," *IEEE Trans on Aerospace and Eletronic Systems*, vol. 10, pp. 528-532, July 1974.

[6] T.-C. Hou and T-J. Tsai, " An access-based clustering protocol for multihop wireless ad hoc networks," *IEEE J. Selected Areas in Communications*, vol. 19, no. 7, pp. 1201-1210, July 2001.

[7] A. Iwata, C. C. Chiang, G. Pei, M. Gerla, and T. W. Chen, " Scalable routing strategies for ad hoc networks," *IEEE J. Selected Areas in Communications*, vol. 17, pp. 1369-1379, 1999.

[8] R. A. Johnson and E. L. Titlebaum, "Range Doppler Uncoupling in the Doppler Tolerant Bat Signal", *Proc. of IEEE Ultrasonics Symposium*, New York, pp. 64-67, 1972.

[9] D. Kershaw and R. Evans, "Optimal waveform selection for tracking system", *IEEE Trans on Information Theory*, vol. 40, no. 5, pp. 1536-1550, 1994.

[10] C. R. Lin and M. Gerla, "Adaptive clustering in mobile wireless networks," *IEEE J. Selected Areas in Communications*, vol. 16, pp. 1265-1275, 1997.

[11] R. Niu, P. Willett, and Y. Bar-Shalom, "Tracking consideration in selection of radar waveform for range and range-rate measurements", *IEEE Transactions on Aerospace and Electronic Systems*, Vol. 38, No. 2, 2002.

[12] A. Papandreou, G. F. Boudreaux-Bartels, and S. M. Kay, "Detection and estimation of generalized chirps using time-frequency representations", *Twenty-Eighth Asilomar Conference on Signals, Systems and Computers*, vol. 1, pp. 50-54, Oct. 1994.

[13] C. E. Perkins, "Chapter 4, Cluster-Based Networks," *Ad Hoc Networking*, Edited by C. E. Perkins, pp. 75-138, Addison-Wesley, 2001.

[14] J. Roman, M. Rangaswamy, D. Davis, Q. Zhang, B. Himed, and J. Michels, "Parametric adaptive matched filter for airborne radar applications," *IEEE Trans. Aerosp. Electron. Syst.*, vol. 36, no. 2, pp. 677-692, 2000.

[15] M. A. Richards, *Fundamentals of Radar Signal Processing*, McGraw-Hill Companies, New York, 2005.

[16] T.K. Sarkar and N. Sangruji, "An adaptive nulling system for a narrow-band signal with a look-direction constraint utilizing the conjugate gradient method," *IEEE Trans. Antennas Propagat.*, vol. 37, no. 7, pp. 940-944, July 1989.

[17] M. I. Skolnik, *Introduction to Radar Systems*, 3rd ed, New York, McGraw Hill, 2001.

[18] P. Swerling, "Probability of detection for fluctuating targets", *IRE Trans on Information Theory*, vol. 6, pp. 269-308, April 1960.

[19] Y. Sun, P. Willett, and R. Lynch, "Waveform fusion in sonar signal processing", *IEEE Transactions on Aerospace and Electronic Systems*, Vol. 40, No. 2, 2004

[20] S. Sowelam and A. Tewfik, "Waveform selection in radar target classification," *IEEE Trans on Information Theory*, vol. 46, no. 3, pp. 1014-1029, 2000.

List of Tables

Table 1: RCS values at microwave frequency for 5 targets.

Index n	Target	RCS
1	Bird	0.01
2	Conventional unmanned winged missile	0.5
3	Small single-engine aircraft	1
4	Small flighter aircraft or 4 passenger jet	2
5	Large flighter aircraft	6

List of Figures

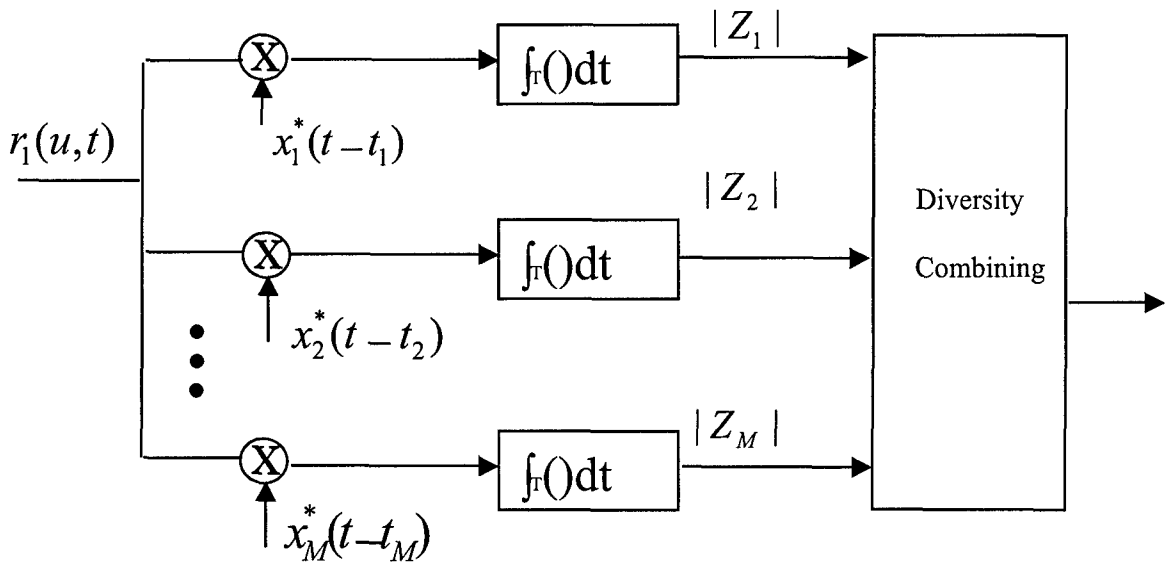

Figure 1: Waveform diversity combining by clusterhead in RSN.

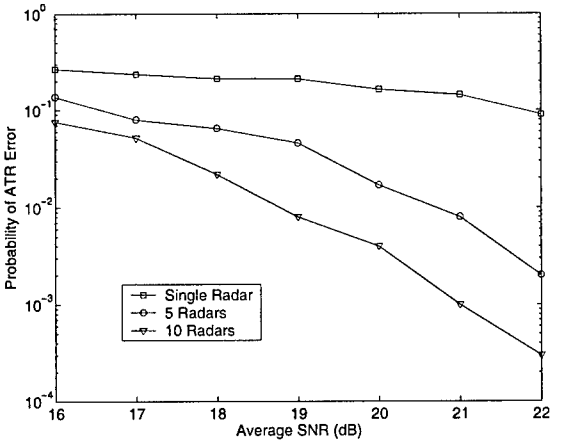

(a)

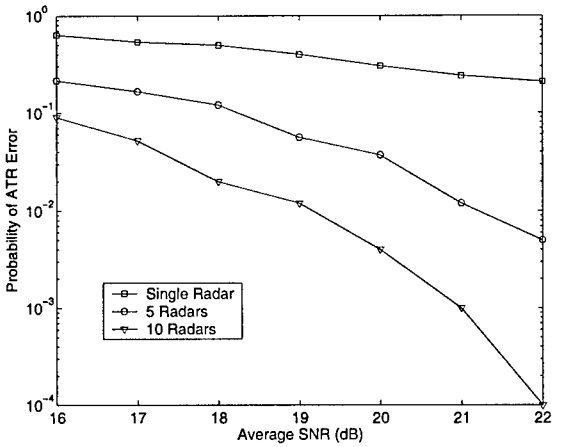

(b)

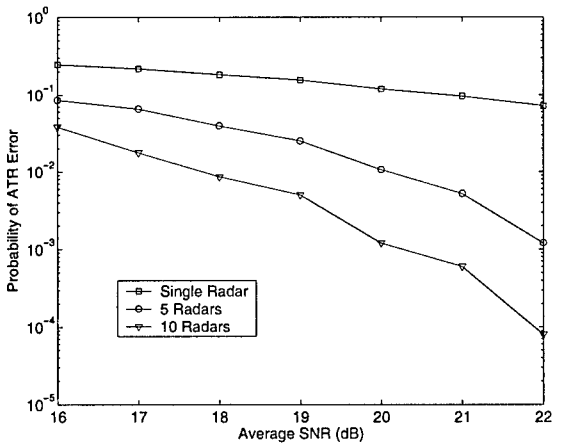

(c)

Figure 2: Probability of ATR error for *nonfluctuating* targets at different average SNR (dB) values. (a) bird, (b) missile, (c) the average probability of ATR error for 5 targets.

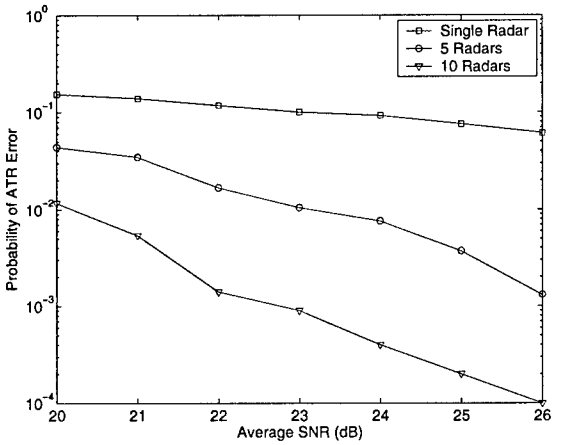

(a)

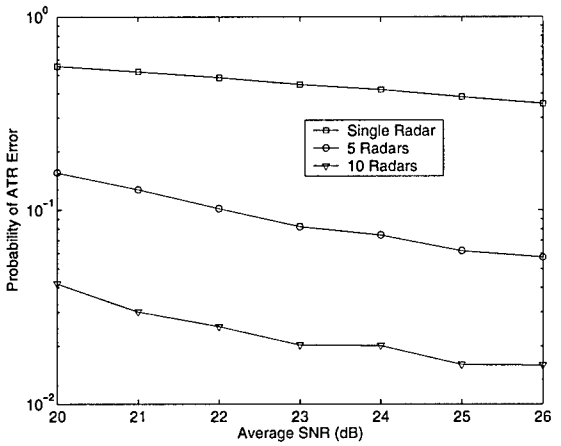

(b)

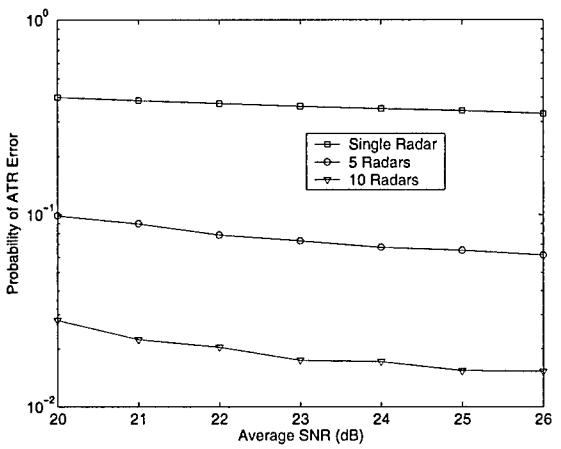

(c)

Figure 3: Probability of ATR error for *fluctuating* targets at different average SNR (dB) values. (a) bird, (b) missile, (c) the average probability of ATR error for 5 targets.

Waveform Design and Diversity in Radar Sensor Networks: Theoretical Analysis and Application to Automatic Target Recognition

Qilian Liang
Department of Electrical Engineering
416 Yates Street, Room 518
University of Texas at Arlington
Arlington, TX 76019-0016 USA
E-mail: liang@uta.edu

Abstract— **In this paper, we perform some theoretical studies on constant frequency (CF) pulse waveform design and diversity in radar sensor networks (RSN): (1) the conditions for waveform co-existence, (2) interferences among waveforms in RSN, (3) waveform diversity combining in RSN. As an application example, we apply the waveform design and diversity to automatic target recognition (ATR) in RSN and propose maximum-likehood (ML)-ATR algorithms for nonfluctuating target as well as fluctuating target. Simulation results show that our waveform diversity-based ML-ATR algorithm performs much better than single-waveform ML-ATR algorithm for nonfluctuating targets or fluctuating targets. Conclusions are drawn based on our analysis and simulations.**

I. Introduction and Motivation

The network of radar sensors should operate with multiple goals managed by an intelligent platform network that can manage the dynamics of each radar to meet the common goals of the platform, rather than each radar to operate as an independent system. Therefore, it is significant to perform signal design and processing and networking cooperatively within and between platforms of radar sensors and their communication modules. Waveform diversity is the technology that will allow one or more sensors on board a platform to automatically change operating parameters, e.g., frequency, gain pattern, and pulse repetition frequency (PRF) to meet the varying environments. It has long been recognized that judicious use of properly designed waveforms, coupled with advanced receiver strategies, is fundamental to fully utilizing the capacity of the electromagnetic spectrum. However, it is only relatively recent advances in hardware technology that are enabling a much wider range of design freedoms to be explored. As a result, there are emerging and compelling changes in system requirements such as more efficient spectrum usage, higher sensitivities, greater information content, improved robustness to errors, reduced interference emissions, etc. The combination of these is fuelling a worldwide interest in the subject of waveform design and the use of waveform diversity techniques.

In the existing works on waveform design and selection, Fitzgerald [5] demonstrated the inappropriateness of selection of waveform based on measurement quality alone: the interaction between the measurement and the track can be indirect, but must be accounted for. Bell [3] used information theory to design radar waveform for the measurement of extended radar targets exhibiting resonance phenomena. In [2], singularity expansion method was used to design some discriminant waveforms such as K-pulse, E-pulse, and S-pulse. Sowelam and Tewfik [13] developed a signal selection strategy for radar target classification, and a sequential classification procedure was proposed to minimize the average number of necessary signal transmissions. Intelligent waveform selection was studied in [1][6], but the effect of doppler shift was not considered. In [7], the performance of constant frequency (CF) and linear frequency modulated (LFM) waveform fusion from the standpoint of the whole system was studied, but the effects of clutter was not considered. In [12], CF and LFM waveforms were studied for sonar system, but it was assumed that the sensor is nonintelligent (i.e., waveform can't be selected adaptively). All the above studies and design methods were focused on the waveform design or selection for a single active radar or sensor. In [10], cross-correlation properties of two radars are briefly mentioned and the binary coded pulses using simulated annealing [4] are highlighted. However, the cross-correlation of two binary sequences such as binary coded pulses (e.g. Barker sequence) are much easier to study than that of two analog radar waveforms. In this paper, we will focus on the waveform diversity and design for radar sensor networks using constant frequency (CF) pulse waveform.

The rest of this paper is organized as follows. In Section II, we study the co-existence of radar waveforms. In Section III, we analyze the interferences among radar waveforms. In Section IV we propose a RAKE structure for waveform diversity combining and propose maximum-likelihood (ML) algorithms for automatic target recognition (ATR). In Section V, we provide simulation results on ML-ATR. In Section VI, we conclude this paper and provide some future works.

II. Co-existence of Radar Waveforms

In radar sensor networks (RSN), radar sensors will interfere with each other and the signal-to-interference-ratio may be very low if the waveforms are not properly designed. We will introduce orthogonality as one criterion for waveforms design in RSN to make them co-existence. Besides, the radar channel is narrow-band, so we will also consider the bandwidth constraint.

In our radar sensor networks, we choose CF pulse waveform. The CF pulse waveform can be defined as

$$x(t) = \sqrt{\frac{E}{T}} \exp(j2\pi\beta t) \quad -T/2 \le t \le T/2 \quad (1)$$

In radar, ambiguity function (AF) is an analytical tool for waveform design and analysis that succinctly characterizes the behavior of a waveform paired with its matched filter. The ambiguity function is useful for examing resolution, side lobe behavior, and ambiguities in both range and Doppler for a given waveform[9]. For a single radar, the matched filter for waveform $x(t)$ is $x^*(-t)$, and the ambiguity function of CF pulse waveform is

$$\begin{aligned} A(\tau, F_D) &= \left| \int_{-T/2+\tau}^{T/2} x(t) \exp(j2\pi F_D s) x^*(t-\tau) dt \right| \\ &= \left| \frac{E \sin[\pi F_D (T - |\tau|)]}{T \pi F_D} \right| \quad -T \le \tau \le T \quad (2) \end{aligned}$$

However, the above ambiguity is for one radar only (no co-existing radar).

For radar sensor networks, the waveforms from different radars will interfere with each other. We choose the waveform for radar i as

$$x_i(t) = \sqrt{\frac{E}{T}} \exp[j2\pi(\beta + \delta_i)t] \quad -T/2 \le t \le T/2 \quad (3)$$

which means there is a frequency shift δ_i for radar i. To minimize the interference from one waveform to the other, optimal values for δ_i should be determined to have the waveforms orthogonal to each other, i.e., let the cross-correlation between $x_i(t)$ and $x_n(t)$ be 0,

$$\begin{aligned} & \int_{-T/2}^{T/2} x_i(t) x_n^*(t) dt \\ = \; & \frac{E}{T} \int_{-T/2}^{T/2} \exp[j2\pi(\beta + \delta_i)t] \exp[-j2\pi(\beta + \delta_n)t] dt \\ = \; & E \mathrm{sinc}[\pi(\delta_i - \delta_n)T] \quad (4) \end{aligned}$$

If we choose

$$\delta_i = \frac{i}{T} \quad (5)$$

where i is a dummy index, then (4) can have two cases

$$\int_{-T/2}^{T/2} x_i(t) x_n^*(t) dt = \begin{cases} E & i = n \\ 0 & i \ne n \end{cases} \quad (6)$$

So choosing $\delta_i = \frac{i}{T}$ in (3) can have orthogonal waveforms, i.e., the waveforms can co-exist if the carrier spacing is $1/T$ between two radar waveforms. i.e., orthogonality amongst carriers can be achieved by separating the carriers by an interger multiple of the inverse of waveform pulse duration. With this design, all the orthogonal waveforms can work simultaneously. However, there may exist time delay and doppler shift ambiguity which will have interferences to other waveforms in RSN.

III. Interferences of Waveforms In Radar Sensor Networks

A. RSN with Two Radar Sensors

We are interested in analyzing the interference from one radar to another if there exist time delay and doppler shift. For a simple case where there are two radar sensors (i and n), the ambiguity function of radar i (considering interference from radar n) is

$$A_i(t_i, t_n, F_{D_i}, F_{D_n}) \quad (7)$$

$$= \left| \int_{-\infty}^{\infty} [x_i(t) \exp(j2\pi F_{D_i} t) + x_n(t - t_n) \exp(j2\pi F_{D_n} t)] x_i^*(t - t_i) dt \right| \quad (8)$$

$$\le \left| \int_{-T/2+\max(t_i,t_n)}^{T/2+\min(t_i,t_n)} x_n(t - t_n) \exp(j2\pi F_{D_n} t) x_i^*(t - t_i) dt \right| + \left| \int_{-T/2+t_i}^{T/2} x_i(t) \exp(j2\pi F_{D_i} t) x_i^*(t - t_i) dt \right| \quad (9)$$

$$= \left| \int_{-T/2+\max(t_i,t_n)}^{T/2+\min(t_i,t_n)} x_n(t - t_n) \exp(j2\pi F_{D_n} t) x_i^*(t - t_i) dt \right| + \left| \frac{E \sin[\pi F_{D_i} (T - |t_i|)]}{T \pi F_{D_i}} \right| \quad (10)$$

To make analysis easier, we assume $t_i = t_n = \tau$, then (10) can be simplified as

$$\begin{aligned} A_i(\tau, F_{D_i}, F_{D_n}) &\approx |E \mathrm{sinc}[\pi(n - i + F_{D_n} T)]| \\ &+ \left| \frac{E \sin[\pi F_{D_i} (T - |\tau|)]}{T \pi F_{D_i}} \right| \quad (11) \end{aligned}$$

B. RSN with M Radar Sensors

It can be extended to an RSN with M radars. Assuming time delay τ for each radar is the same, then the ambiguity function of radar 1 (considering interferences from all the other $M-1$ radars with CF pulse waveforms) can be expressed as

$$A_1(\tau, F_{D_1}, \cdots, F_{D_M}) \approx \sum_{i=2}^{M} |E\text{sinc}[\pi(i-1+F_{D_i}T)]| + \left|\frac{E\sin[\pi F_{D_1}(T-|\tau|)]}{T\pi F_{D_1}}\right| \quad (12)$$

IV. Waveform Diversity and Combining with Application to Automatic Target Recognition

In RSN, The radar sensors are networked together in an ad hoc fashion. Scalability concern suggest a hierarchical organization of radar sensor networks with the lowest level in the hierarchy being a cluster. In RSN, each radar can provide their waveform parameters such as δ_i to their clusterhead radar, and the clusterhead radar can combine the waveforms from its cluster members. In RSN with M radars, the received signal for clusterhead (assume it's radar 1) is

$$r_1(u,t) = \sum_{i=1}^{M} \alpha(u) x_i(t-t_i)\exp(j2\pi F_{D_i}t) + n(u,t) \quad (13)$$

where $\alpha(u)$ stands for radar cross section (RCS) and can be modeled using non-zero constants for nonfluctuating target and four Swerling target models for fluctuating target[9]; F_{D_i} is the doppler shift of target relative to waveform i; t_i is delay of waveform i, and $n(u,t)$ is additive white Gaussian noise (AWGN). In this paper, we propose a RAKE structure for waveform diversity combining, as illustrated by Fig. 1.

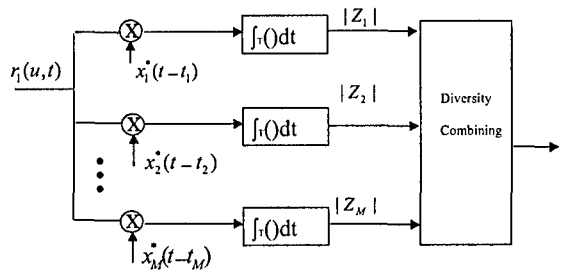

Fig. 1. Waveform diversity combining by clusterhead in RSN.

According to this structure, the received $r_1(u,t)$ is processed by a bank of matched filters, then the output of branch 1 (after integration) is

$$\begin{aligned} &|Z_1(u;t_1,\cdots,t_M,F_{D_1},\cdots,F_{D_M})| \\ =& \left|\int_{-T/2}^{T/2} r_1(u,t)x_1^*(t-t_1)ds\right| \quad (14) \\ =& \left|\int_{-T/2}^{T/2}[\sum_{i=1}^{M}\alpha_i(u)x_i(t-t_i)\exp(j2\pi F_{D_i}t) \right. \\ & \left. +n(u,t)]x_1^*(t-t_1)dt\right| \quad (15) \end{aligned}$$

where $\int_{-T/2}^{T/2} n(u,t)x_1^*(t-t_1)dt$ can easily be proved to be AWGN, so

$$|n(u,t_1)| \triangleq \left|\int_{-T/2}^{T/2} n(u,t)x_1^*(t-t_1)dt\right| \quad (16)$$

follows Rayleigh distribution. Assuming $t_1 = t_2 = \cdots = t_M = \tau$, then based on (12),

$$\begin{aligned} &|Z_1(u;\tau,F_{D_1},\cdots,F_{D_M})| \\ \approx& \sum_{i=2}^{M}|\alpha(u)E\text{sinc}[\pi(i-1+F_{D_i}T)]| \\ +& \left|\frac{\alpha(u)E\sin[\pi F_{D_1}(T-|\tau|)]}{T\pi F_{D_1}}\right| + |n(u,\tau)| \quad (17) \end{aligned}$$

Similarly, we can get the output for any branch m ($m = 1,2,\cdots,M$),

$$\begin{aligned} &|Z_m(u;\tau,F_{D_1},\cdots,F_{D_M})| \\ \approx& \sum_{i=1,i\neq m}^{M}|\alpha(u)E\text{sinc}[\pi(i-m+F_{D_i}T)]| \\ +& \left|\frac{\alpha(u)E\sin[\pi F_{D_m}(T-|\tau|)]}{T\pi F_{D_m}}\right| + |n(u,\tau)| \quad (18) \end{aligned}$$

So $|Z_m(u;\tau,F_{D_1},\cdots,F_{D_M})|$ consists of three parts, signal (reflected signal from radar m waveform): $\left|\frac{\alpha(u)E\sin[\pi F_{D_m}(T-|\tau|)]}{T\pi F_{D_m}}\right|$, interferences from other waveforms: $\sum_{i=1,i\neq m}^{M}|\alpha(u)E\text{sinc}[\pi(i-m+F_{D_i}T)]|$, and noise: $|n(u,\tau)|$.

We can have three special cases for $|Z_m(u;\tau,F_{D_1},\cdots,F_{D_M})|$:

1) When $F_{D_1} = \cdots = F_{D_M} = 0$,

$$\begin{aligned} &|Z_m(u;\tau,0,0,\cdots,0)| \\ \approx& \left|\frac{E\alpha(u)(T-|\tau|)}{T}\right| + |n(u,\tau)| \quad (19) \end{aligned}$$

which means if there is no doppler mismatch, there will be no interference from other waveform.

2) If $\tau = 0$, then (18) becomes

$$\begin{aligned} & |Z_m(u;0,F_{D_1},\cdots,F_{D_M})| \\ \approx & \sum_{i=1,i\neq m}^{M} |\alpha(u)E\text{sinc}[\pi(i-m+F_{D_i}T)]| \\ + & \left|\frac{\alpha(u)E\sin[\pi F_{D_m}T]}{T\pi F_{D_m}}\right| + |n(u)| \end{aligned} \quad (20)$$

3) If $\tau = 0$, and $F_{D_1} = \cdots = F_{D_M} = 0$, then (18) becomes

$$|Z_m(u;0,0,0,\cdots,0)| \approx |E\alpha(u)| + |n(u)| \quad (21)$$

Doppler mismatch happens quite often in target search where target velocity is not yet known. However, in target recognition, generally high-resolution measurements of targets in range ($\tau = 0$) and doppler are available, so (21) will be used for automatic target recognition.

How to combine all the Z_m's ($m = 1,2,\cdots,M$) are very similar to the diversity combining in communations to combat channel fading, and the combination schemes may be different for different applications. In this paper, we are interested in applying RSN waveform diversity to automatic target recognition (ATR), e.g., recognition that the echo on a radar display is that of an aircraft, ship, motor vehicle, bird, etc. Early radars were "blob" detectors in that they detected the presence of a target and gave its location in range and angle, and radar began to be more than a blob detector and could provide recognition of one type of target from another[10]. It is known that small changes in the aspect angle of complex (multiple scatter) targets can cause major changes in the radar cross section (RCS). This has been considered in the past as a means of target recognition, and is called *fluctuation of radar cross section with aspect angle*, but it has not had much success[10]. In this paper, we propose a maximum likelihood automatic target recognition (ML-ATR) algorithm for RSN. We will study non-fluctuating target as well as fluctuating target.

A. ML-ATR for Non-fluctuating Targets

In some sources, the non-fluctuating target is identified as "Swerling 0" or "Swerling 5" model[11]. For non-fluctuating target, the RCS $\alpha_m(u)$ is just a constant α for a given target. In (21), $|n(u,\tau)|$ follows Rayleigh distribution since $n(u,\tau)$ is a Gaussian random variable for given τ, so $|Z_m(u;0,0,\cdots,0)|$ follows Rician distribution because signal $E|\alpha$ is a constant. Let $y_m \triangleq |Z_m(u;0,0,\cdots,0)|$, then the probability density function (pdf) of y_m is

$$f(y_m) = \frac{2y_m}{\sigma^2}\exp[-\frac{(y_m^2+\lambda^2)}{\sigma^2}]I_0(\frac{2\lambda y_m}{\sigma^2}) \quad (22)$$

where

$$\lambda = E|\alpha|, \quad (23)$$

σ^2 is the noise power (with I and Q sub-channel power $\sigma^2/2$), and $I_0(\cdot)$ is the zero-order modified Bessel function of the first kind. Let $\mathbf{y} \triangleq [y_1, y_2, \cdots, y_M]$, then the pdf of $\mathbf{y}$ is

$$f(\mathbf{y}) = \prod_{m=1}^{M} f(y_m) \quad (24)$$

Our ATR is a multiple-category hypothesis testing problem, i.e., to decide a target category (e.g. aircraft, ship, motor vehicle, bird, etc) based on $r_1(u,t)$. Assume there are totally N categories and category n target has RCS α_n, so the ML-ATR algorithm to decide a target category C can be expressed as,

$$\begin{aligned} C &= \arg\max_{n=1}^{N} f(\mathbf{y}|\lambda = E|\alpha_n|) \\ &= \arg\max_{n=1}^{N} \prod_{m=1}^{M} \frac{2y_m}{\sigma^2}\exp[-\frac{(y_m^2+E^2\alpha_n^2)}{\sigma^2}]I_0(\frac{2E|\alpha_n|y_m}{\sigma^2}) \end{aligned}$$

B. ML-ATR for Fluctuating Targets

Fluctuating target modeling is more realistic in which the target RCS is drawn from either the Rayleigh or chi-square of degree four pdf. The Rayleigh model describes the behavior of a complex target consisting of many scatters, none of which is dominant. The fourth-degree chi-square models targets having many scatters of similar strength with one dominant scatter. Based on different combinations of pdf and decorrelation characteristics (scan-to-scan or pulse-to-pulse decorrelation), four Swerling models are used[9]. In this paper, we will focus on "Swerling 2" model which is Rayleigh distribution with pulse-to-pulse decorrelation. The pulse-to-pulse decorrelation implies that each individual pulse results in an independent value for RCS α.

For Swerling 2 model, the RCS $|\alpha(u)|$ follows Rayleigh distribution and its I and Q subchannels follow zero-mean Gaussian distributions with variance γ^2. Assume

$$\alpha(u) = \alpha_I(u) + j\alpha_Q(u) \quad (25)$$

and $n(u) = n_I(u) + jn_Q(u)$ follows zero-mean complex Gausian distribution with variance σ^2 for the I and Q subchannels. According to (15), (18), and (21),

$$|Z_m(u;0,0,0,\cdots,0)| \approx |E\alpha(u) + n(u)| \quad (26)$$

is a more accuate approximation. Since $\alpha(u)$ and $n(u)$ are zero-mean complex Gaussian random variables, so $E\alpha(u) + n(u)$ is a zero-mean Gaussian random variable with variance $E^2\gamma^2 + \sigma^2$ for the I and Q subchannels, which means $y_m \triangleq |Z_m(u;0,0,\cdots,0)|$ follows Rayleigh distribution with parameter $\sqrt{E^2\gamma^2+\sigma^2}$,

$$f(y_m) = \frac{y_m}{E^2\gamma^2+\sigma^2}\exp(-\frac{y_m^2}{E^2\gamma^2+\sigma^2}) \quad (27)$$

The mean value of y_m is $\sqrt{\frac{\pi(E^2\gamma^2+\sigma^2)}{2}}$, and variance is $\frac{(4-\pi)(E^2\gamma^2+\sigma^2)}{2}$. The variance of signal is $\frac{(4-\pi)E^2\gamma^2}{2}$ and the variance of noise is $\frac{(4-\pi)\sigma^2}{2}$.

Let $\mathbf{y} \triangleq [y_1, y_2, \cdots, y_M]$, then the pdf of $\mathbf{y}$ is

$$f(\mathbf{y}) = \prod_{m=1}^{M} f(y_m) \tag{28}$$

Assume there are totally N categories and category n target has RCS $\alpha_n(u)$ (with variance γ_n^2), so the ML-ATR algorithm to decide a target category C can be expressed as,

$$\begin{aligned} C &= \arg\max_{n=1}^{N} f(\mathbf{y}|\gamma=\gamma_n) \qquad (29)\\ &= \arg\max_{n=1}^{N} \prod_{m=1}^{M} \frac{y_m}{E^2\gamma_n^2+\sigma^2} \exp(-\frac{y_m^2}{E^2\gamma_n^2+\sigma^2}) \end{aligned}$$

V. Simulations

Radar sensor networks will be required to detect a broad range of target classes. Too often, the characteristics of objects that are not of interest (e.g., bird) will be similar to those of threat objects (e.g., missile). Therefore, new techniques to discriminate threat against undesired detections (e.g. birds, etc.) are needed. We applied our ML-ATR to this important application, to recognize a target from many target classes. We assume that the domain of target classes is known a priori (N in Sections IV-A and IV-B), and that the RSN is confined to work only on the known domain.

TABLE I

RCS values at microwave frequency for 5 targets.

Index n	Target	RCS (m^2)
1	Bird	0.01
2	Conventional unmanned winged missile	0.5
3	Small single-engine aircraft	1
4	Small flighter aircraft or 4 passenger jet	2
5	Large flighter aircraft	6

For non-fluctuating target recognition, our targets have 5 classes with different RCS values, which are summarized in Table I[10]. For fluctuating target recognition, we assume the fluctuating targets follow "Swerling 2" model (Rayleigh with pulse-to-pulse decorrelation), and assume the RCS value listed in Table I to be the standard deviation (std) γ_n of RCS $\alpha_n(u)$ for target n. We applied the ML-ATR algorithms in Section IV-A (for nonfluctuating target case) and Section IV-B (for fluctuating target case) to classify an unknown target as one of these 5 target classes. At each average SNR value, we ran Monte-Carlo simulations for 10^5 times for each target. The average SNR value is based on the average power from all targets (signal variance), so the actual SNRs for bird and

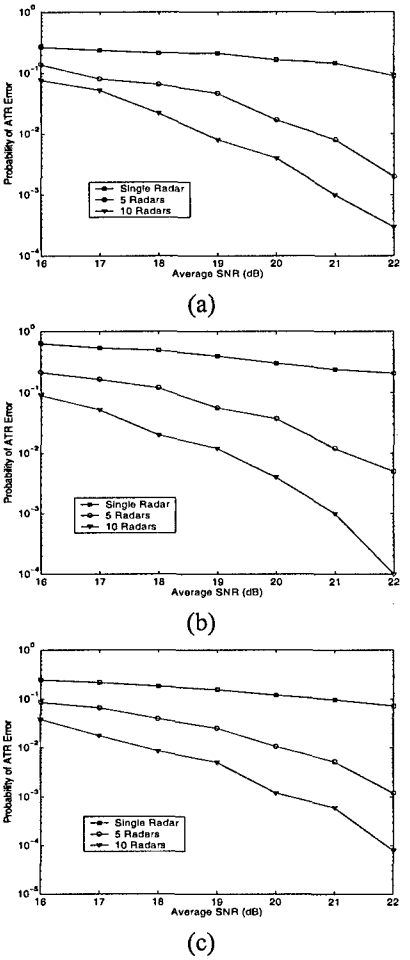

Fig. 2. Probability of ATR error for *nonfluctuating* targets at different average SNR (dB) values. (a) bird, (b) missile, (c) the average probability of ATR error for 5 targets.

missile are much lower than the average SNR value. For example, at the average SNR=16dB, the bird target SNR=-33.1646dB, and missile target SNR=0.8149dB; and at average SNR=20dB, the bird target SNR=-29.1646dB, and missile target SNR=4.8149dB. In Fig. 2(a)(b), we plotted the probability of ATR error in bird and missile recognition when they are assumed as nonfluctuating targets. Observe both figures, single radar system can't perform well in both recognitions, and their probability of ATR error is above 10%, which can't be used for real-world ATR. However, the 5-radar RSN and 10-radar RSN can maintain very low ATR errors. In Fig. 2(c), we plotted the average probability of ATR error for all 5 targets recognition. Since the other 3 targets (different aircrafts) have much higher SNRs, so their ATR error is lower, which makes the average probability of ATR error lower. Similarly, we plot the performance in fluctuating target recognition in Fig.

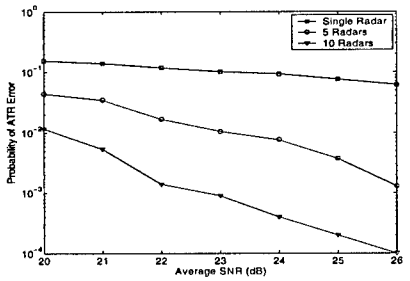

(a)

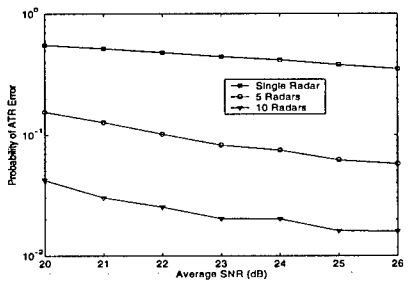

(b)

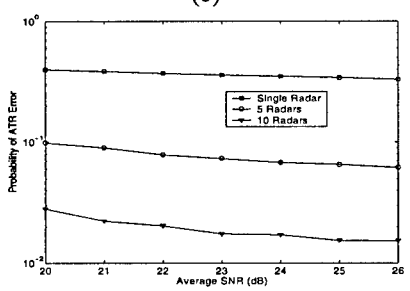

(c)

Fig. 3. Probability of ATR error for *fluctuating* targets at different average SNR (dB) values. (a) bird, (b) missile, (c) the average probability of ATR error for 5 targets.

3(a)b)(c). Comparing Fig. 2(a)(b)(c) to Fig. 3(a)(b)(c), it is clear that higher SNRs are needed for fluctuating target recognition comparing to nonfluctuating target recognition. According to Skolnik[10], radar performance with probability of recognition error (p_e) less than 10% is good enough. Our RSN with waveform-diversity can have probability of ATR error much less than 10% for each target ATR as well as the average ATR for all targets. However, the single radar system has probability of ATR error much higher than 10%. Observe Fig. 3(c), the average probability of ATR error of single-radar is impossible to be less than 10% even at extreme high SNR. Our RSN with waveform diversity is very promising to be used for real-world ATR.

VI. Conclusions

We have studied constant frequency (CF) pulse waveform design and diversity in radar sensor networks (RSN). We showed that the waveforms can co-exist if the carrier frequency spacing is $1/T$ between two radar waveforms. We made analysis on interferences among waveforms in RSN and proposed a RAKE structure for waveform diversity combining in RSN. As an application example, we applied the waveform design and diversity to automatic target recognition (ATR) in RSN and proposed maximum-likehood (ML)-ATR algorithms for nonfluctuating target as well as fluctuating target. Simulation results show that RSN using our waveform diversity-based ML-ATR algorithm performs much better than single radar system for nonfluctuating targets and fluctuating targets recognition.

Acknowledgement

This work was supported by the U.S. Office of Naval Research (ONR) Young Investigator Program Award under Grant N00014-03-1-0466.

The author would like to thank ONR Program Officer Dr. Rabinder N. Madan for his direction and insightful discussion on radar sensor networks.

References

[1] P. Baggenstoss, "Adaptive pulselength correction (APLECORR): a strategy for waveform optimization in ultrawideband active sonar," *IEEE Trans on Oceanic Engineering*, vol. 23, no. 1, pp. 1-11, 1998.

[2] C. E. Baum, et al, "The singularity expansion method and its application to target identification", *Proc. of the IEEE*, vol 79, no. 10, Oct 1991.

[3] M. R. Bell, "Information theory and radar waveform design", *IEEE Trans on Information Theory*, vol. 39, no. 5, pp. 1578-1597, Sept 1993.

[4] H. Deng, "Synthesis of binary sequences with good correlation and cross-correlation properties by simulated annealing," *IEEE Trans on Aerospace and Electronic Systems*, vol. 32, no. 1, Jan 1996.

[5] R. Fitzgerald, "Effects of range-doppler coupling on chirp radar tracking acuracy," *IEEE Trans on Aerospace and Eletronic Systems*, vol. 10, pp. 528-532, July 1974.

[6] D. Kershaw and R. Evans, "Optimal waveform selection for tracking system", *IEEE Trans on Information Theory*, vol. 40, no. 5, pp. 1536-1550, 1994.

[7] R. Niu, P. Willett, and Y. Bar-Shalom, "Tracking consideration in selection of radar waveform for range and range-rate measurements", *IEEE Transactions on Aerospace and Electronic Systems*, Vol. 38, No. 2, 2002.

[8] J. Roman, M. Rangaswamy, D. Davis, Q. Zhang, B. Himed, and J. Michels, "Parametric adaptive matched filter for airborne radar applications," *IEEE Trans. Aerosp. Electron. Syst.*, vol. 36, no. 2, pp. 677-692, 2000.

[9] M. A. Richards, *Fundamentals of Radar Signal Processing*, McGraw-Hill Companies, New York, 2005.

[10] M. I. Skolnik, *Introduction to Radar Systems*, 3rd ed, New York, McGraw Hill, 2001.

[11] P. Swerling, "Probability of detection for fluctuating targets", *IRE Trans on Information Theory*, vol. 6, pp. 269-308, April 1960.

[12] Y. Sun, P. Willett, and R. Lynch, "Waveform fusion in sonar signal processing", *IEEE Transactions on Aerospace and Electronic Systems*, Vol. 40, No. 2, 2004

[13] S. Sowelam and A. Tewfik, "Waveform selection in radar target classification," *IEEE Trans on Information Theory*, vol. 46, no. 3, pp. 1014-1029, 2000.

Radar Sensor Networks: Algorithms for Waveform Design and Diversity with Application to ATR with Delay-Doppler Uncertainty

Qilian Liang

Department of Electrical Engineering

416 Yates Street, Room 518

University of Texas at Arlington

Arlington, TX 76019-0016 USA

E-mail: liang@uta.edu

Abstract

Automatic target recognition (ATR) in target search phase is very challenging because the target range and mobility are not yet perfectly known, which results in delay-doppler uncertainty. In this paper, we firstly perform some theoretical studies on radar sensor network (RSN) design based linear frequency modulation (LFM) waveform: (1) the conditions for waveform co-existence, (2) interferences among waveforms in RSN, (3) waveform diversity in RSN. Then we apply RSN to ATR with delay-doppler uncertainty and propose maximum-likekihood (ML) ATR algorithms for fluctuating target and nonfluctuating target. Simulation results show that our RSN vastly reduces the ATR error comparing to a single radar system in ATR with delay-doppler uncertainty. The proposed waveform design and diversity algorithms can also be applied to active RFID sensor networks and underwater acoustic sensor networks.

Index Terms : radar sensor networks, waveform diversity, automatic target recognition, maximum-likelihood, interferences, delay-doppler uncertainty.

1 Introduction and Motivation

The goal for any target recognition system is to give the most accurate interpretation of what a target is at any given point in time. There are two classes of motion models of target, one for maneuvering targets and one for non-maneuvering (constant velocity and acceleration) targets. The area that is still lacking in target recognition is the ability to detect reliably when a target is beginning a maneuver where its speed and range are uncertain. The tracking system can switch the algorithms applied to the problem from a non-maneuvering set to the maneuvering set when a target is beginning a maneuver. But when the tracker does finally catch up to the target after the maneuver and then perform ATR, the latency is too high. In time critical mission situation, such latency in ATR is not tolerable. In this paper, we are interested in studying automatic target recongition with range and speed uncertainty, i.e., delay-doppler uncertainty, using radar sensor networks (RSN). The network of radar sensors should operate with multiple goals managed by an intelligent platform network that can manage the dynamics of each radar to meet the common goals of the platform, rather than each radar to operate as an independent system. Therefore, it is significant to perform signal design and processing and networking cooperatively within and between platforms of radar sensors and their communication modules. In this paper, we are interested in studying algorithms on radar sensor network (RSN) design based linear frequency modulation (LFM) waveform: (1) the conditions for waveform co-existence, (2) interferences among waveforms in RSN, (3) waveform diversity in RSN. Then we apply RSN to automatic target recognition (ATR) with delay-doppler uncertainty.

In nature, diverse waveforms are transmitted by animals for specific applications. For example, when a bat and a whale are in the search mode for food, they emit a different type of waveform than when they are trying to locate their prey. The Doppler-invariant waveforms that they transmit are environment dependent [8]. Hence, in RSN, it may be useful to transmit different waveform

from different neighbor radars and they can collaboratively perform waveforms diversity for ATR. Sowelam and Tewfik [21] developed a signal selection strategy for radar target classification, and a sequential classification procedure was proposed to minimize the average number of necessary signal transmissions. Intelligent waveform selection was studied in [1][9], but the effect of doppler shift was not considered. In [12], the performance of constant frequency (CF) and linear frequency modulated (LFM) waveform fusion from the standpoint of the whole system was studied, but the effects of clutter was not considered. In [20], CF and LFM waveforms were studied for sonar system, but it was assumed that the sensor is nonintelligent (i.e., waveform can't be selected adaptively). All the above studies and design methods were focused on the waveform design or selection for a single active radar or sensor. In [18], cross-correlation properties of two radars are briefly mentioned and the binary coded pulses using simulated annealing [4] are highlighted. However, the cross-correlation of two binary sequences such as binary coded pulses (e.g. Barker sequence) are much easier to study than that of two analog radar waveforms. In [10], CF waveform design was applied to RSN with application to ATR without any delay-doppler uncertainty. In this paper, we will focus on the waveform design fusion for radar sensor networks using LFM waveform.

The rest of this paper is organized as follows. In Section 2, we study the co-existence of LFM radar waveforms. In Section 3, we analyze the interferences among LFM radar waveforms. In Section 4 we propose a RAKE structure for waveform diversity combining and propose maximum-likelihood (ML) algorithms for automatic target recognition (ATR) with delay-doppler uncertainty. In Section 5, we provide simulation results on ML-ATR with delay-doppler uncertainty. In Section 6, we conclude this paper and provide some future works.

2 Co-existence of LFM Radar Waveforms

In radar sensor networks (RSN), radar sensors will interfere with each other and the signal-to-interference-ratio may be very low if the waveforms are not properly designed. We will introduce orthogonality as one criterion for waveforms design in RSN to make them co-existence. Besides, the radar channel is narrow-band, so we will also consider the bandwidth constraint.

In our radar sensor networks, we choose linear frequency modulation (LFM) waveform. The LFM waveform can be defined as

$$x(t) = \sqrt{\frac{E}{T}} \exp(j2\pi\beta t^2) \quad -T/2 \leq t \leq T/2 \tag{1}$$

In radar, ambiguity function (AF) is an analytical tool for waveform design and analysis that succinctly characterizes the behavior of a waveform paired with its matched filter. The ambiguity function is useful for examing resolution, side lobe behavior, and ambiguities in both range and Doppler for a given waveform[16]. For a single radar, the matched filter for waveform $x(t)$ is $x^*(-t)$, and the ambiguity function of LFM waveform is[16]

$$\begin{aligned} A(\tau, F_D) &= \left| \int_{-T/2+\tau}^{T/2} x(t) \exp(j2\pi F_D t) x^*(t-\tau) dt \right| \\ &= \left| \frac{E \sin[\pi(F_D + \beta\tau)(T - |\tau|)]}{T\pi(F_D + \beta\tau)} \right| \quad -T \leq \tau \leq T \end{aligned} \tag{2}$$

Three special cases can simplify this AF:

1. When $\tau = 0$,

$$A(0, F_D) = \left| \frac{E \sin(\pi F_D T)}{T\pi(F_D)} \right|; \tag{3}$$

2. and when $F_D = 0$,

$$A(\tau, 0) = \left| \frac{E \sin[\pi\beta\tau(T - |\tau|)]}{T\pi\beta\tau} \right| \quad -T \leq \tau \leq T \tag{4}$$

3. and

$$A(0, 0) = E \tag{5}$$

However, the above ambiguity is for one radar only (no co-existing radar).

For radar sensor networks, the waveforms from different radars will interfere with each other. We choose the waveform for radar i as

$$x_i(t) = \sqrt{\frac{E}{T}} \exp[j2\pi(\beta t^2 + \delta_i t)] \quad -T/2 \leq t \leq T/2 \tag{6}$$

which means there is a frequency shift δ_i for radar i. To minimize the interference from one waveform to the other, optimal values for δ_i should be determined to have the waveforms orthogonal to each other, i.e., let the cross-correlation between $x_i(t)$ and $x_n(t)$ be 0,

$$\begin{aligned} & \int_{-T/2}^{T/2} x_i(t) x_n^*(t) dt \\ = \; & \frac{E}{T} \int_{-T/2}^{T/2} \exp[j2\pi(\beta t^2 + \delta_i t)] \exp[-j2\pi(\beta t^2 + \delta_n t)] dt \\ = \; & E\text{sinc}[\pi(\delta_i - \delta_n)T] \end{aligned} \tag{7}$$

If we choose

$$\delta_i = \frac{i}{T} \tag{8}$$

where i is a dummy index, then (7) can have two cases

$$\int_{-T/2}^{T/2} x_i(t) x_n^*(t) dt = \begin{cases} E & i = n \\ 0 & i \neq n \end{cases} \tag{9}$$

So choosing $\delta_i = \frac{i}{T}$ in (6) can have orthogonal waveforms, i.e., the waveforms can co-exist if the carrier spacing is $1/T$ between two radar waveforms. i.e., orthogonality amongst carriers can be achieved by separating the carriers by an interger multiple of the inverse of waveform pulse duration. With this design, all the orthogonal waveforms can work simultaneously. However, there may exist time delay and doppler shift ambiguity which will have interferences to other waveforms in RSN.

3 Interferences of LFM Waveforms In Radar Sensor Networks

3.1 RSN with Two Radar Sensors

We are interested in analyzing the interference from one radar to another if there exist time delay and doppler shift. For a simple case where there are two radar sensors (i and n), the ambiguity function of radar i (considering interference from radar n) is

$$
\begin{aligned}
& A_i(t_i, t_n, F_{D_i}, F_{D_n}) && (10)\\
= & \left| \int_{-\infty}^{\infty} [x_i(t)\exp(j2\pi F_{D_i}t) + x_n(t-t_n)\exp(j2\pi F_{D_n}t)]x_i^*(t-t_i)dt \right| && (11)\\
\leq & \left| \int_{-T/2+\max(t_i,t_n)}^{T/2+\min(t_i,t_n)} x_n(t-t_n)\exp(j2\pi F_{D_n}t)x_i^*(t-t_i)dt \right| \\
+ & \left| \int_{-T/2+t_i}^{T/2} x_i(t)\exp\left(j2\pi F_{D_i}t\right)x_i^*(t-t_i)dt \right| && (12)\\
= & \left| \int_{-T/2+\max(t_i,t_n)}^{T/2+\min(t_i,t_n)} x_n(t-t_n)\exp(j2\pi F_{D_n}t)x_i^*(t-t_i)dt \right| \\
+ & \left| \frac{E\sin[\pi(F_{D_i}+\beta t_i)(T-|t_i|)]}{T\pi(F_{D_i}+\beta t_i)} \right| && (13)
\end{aligned}
$$

To make analysis easier, we assume $t_i = t_n = \tau$, then (13) can be simplified as

$$
\begin{aligned}
A_i(\tau, F_{D_i}, F_{D_n}) \approx & \; |E\text{sinc}[\pi(n-i+F_{D_n}T)]| \\
+ & \left| \frac{E\sin[\pi(F_{D_i}+\beta\tau)(T-|\tau|)]}{T\pi(F_{D_i}+\beta\tau)} \right| && (14)
\end{aligned}
$$

Some special cases of (14) are listed as follows:

1. If $F_{D_i} = F_{D_n} = 0$, then (14) becomes

$$
A_i(\tau, 0, 0) \approx \left| \frac{E\sin[\pi\beta\tau(T-|\tau|)]}{\pi\beta T\tau} \right| \qquad (15)
$$

2. If $\tau = 0$, then (14) becomes

$$
\begin{aligned}
A_i(0, F_{D_i}, F_{D_n}) \approx & \; |E\text{sinc}[\pi(n-i+F_{D_n}T)]| \\
+ & \; |E\text{sinc}(\pi F_{D_i}T)| && (16)
\end{aligned}
$$

3. If $F_{D_i} = F_{D_n} = 0$, $\tau = 0$, and δ_i and δ_n follow (8), then (14) becomes

$$A_i(0,0,0) \approx E \tag{17}$$

3.2 RSN with M Radar Sensors

It can be extended to an RSN with M radars. Assuming time delay τ for each radar is the same, then the ambiguity function of radar 1 (considering interferences from all the other $M-1$ radars with CF pulse waveforms) can be expressed as

$$\begin{aligned} A_1(\tau, F_{D_1}, \cdots, F_{D_M}) &\approx \left| \sum_{i=2}^{M} E\text{sinc}[\pi(i-1+F_{D_i}T)] \right| \\ &+ \left| \frac{E\sin[\pi(F_{D_1}+\beta\tau)(T-|\tau|)]}{T\pi(F_{D_1}+\beta\tau)} \right| \end{aligned} \tag{18}$$

Similarly, we can have three special cases,

1. If $F_{D_1} = F_{D_2} = \cdots = F_{D_M} = 0$, then (18) becomes

$$A_1(\tau, 0, 0, \cdots, 0) \approx \left| \frac{E\sin[\pi\beta\tau(T-|\tau|)]}{\pi\beta T\tau} \right| \tag{19}$$

   comparing it against (3), it shows that our derived condition in (6) can have a radar in RSN get the same signal strength as that of a single radar (no co-existing radar) when the doppler shift is 0.

2. If $\tau = 0$, then (18) becomes

$$\begin{aligned} & A_1(0, F_{D_1}, F_{D_2}, \cdots, F_{D_M}) \\ \approx & \left| \sum_{i=1}^{M} E\text{sinc}[\pi(i-1+F_{D_i}T+\beta\tau T)] \right| \end{aligned} \tag{20}$$

   Comparing to (4), a radar in RSN has more interferences when unknown doppler shifts exist.

3. $F_{D_1} = F_{D_2} = \cdots = F_{D_M} = 0$, $\tau = 0$, and δ_i in (6) follows (8), then (18) becomes

$$A_1(0,0,0,\cdots,0) \approx E \tag{21}$$

4 Application to Automatic Target Recognition (ATR) with Delay-Doppler Uncertainty

In RSN, The radar sensors are networked together in an ad hoc fashion. They do not rely on a preexisting fixed infrastructure, such as a wireline backbone network or a base station. They are self-organizing entities that are deployed on demand in support of various events surveillance, battlefield, disaster relief, search and rescue, etc. Scalability concern suggest a hierarchical organization of radar sensor networks with the lowest level in the hierarchy being a cluster. As argued in [11] [7] [6] [14], in addition to helping with scalability and robustness, aggregating sensor nodes into clusters has additional benefits:

1. conserving radio resources such as bandwidth;
2. promoting spatial code reuse and frequency reuse;
3. simplifying the topology, e.g., when a mobile radar changes its location, it is sufficient for only the nodes in attended clusters to update their topology information;
4. reducing the generation and propagation of routing information; and,
5. concealing the details of global network topology from individual nodes.

In RSN, each radar can provide their waveform parameters such as δ_i to their clusterhead radar, and the clusterhead radar can combine the waveforms from its cluster members.

In RSN with M radars, the received signal for clusterhead (assume it's radar 1) is

$$r_1(u,t) = \sum_{i=1}^{M} \alpha(u) x_i(t - t_i) \exp(j2\pi F_{D_i} t) + n(u,t) \tag{22}$$

where $\alpha(u)$ stands for radar cross section (RCS) and can be modeled using non-zero constants for nonfluctuating target and four Swerling target models for fluctuating target[16]; F_{D_i} is the doppler

shift of target relative to waveform i; t_i is delay of waveform i, and $n(u,t)$ is additive white Gaussian noise (AWGN). In this paper, we propose a RAKE structure for waveform diversity combining, as illustrated by Fig. 1.

According to this structure, the received $r_1(u,t)$ is processed by a bank of matched filters, then the output of branch 1 (after integration) is

$$\begin{aligned} & |Z_1(u;t_1,\cdots,t_M,F_{D_1},\cdots,F_{D_M})| \\ = & \left|\int_{-T/2}^{T/2} r_1(u,t)x_1^*(t-t_1)ds\right| \qquad (23) \\ = & \left|\int_{-T/2}^{T/2}[\sum_{i=1}^{M}\alpha_i(u)x_i(t-t_i)\exp(j2\pi F_{D_i}t)+n(u,t)]x_1^*(t-t_1)dt\right| \qquad (24) \end{aligned}$$

where $\int_{-T/2}^{T/2} n(u,t)x_1^*(t-t_1)dt$ can easily be proved to be AWGN, let

$$n(u,t_1) \triangleq \int_{-T/2}^{T/2} n(u,t)x_1^*(t-t_1)dt \qquad (25)$$

follows Rayleigh distribution. Assuming $t_1 = t_2 = \cdots = t_M = \tau$, then based on (18),

$$\begin{aligned} & |Z_1(u;\tau,F_{D_1},\cdots,F_{D_M})| \\ \approx & \left|\sum_{i=2}^{M}\alpha(u)E\mathrm{sinc}[\pi(i-1+F_{D_i}T)]\right. \\ + & \left.\frac{\alpha(u)E\sin[\pi(F_{D_1}+\beta\tau)(T-|\tau|)]}{T\pi(F_{D_1}+\beta\tau)}+n(u,\tau)\right| \qquad (26) \end{aligned}$$

Similarly, we can get the output for any branch m ($m = 1,2,\cdots,M$),

$$\begin{aligned} & |Z_m(u;\tau,F_{D_1},\cdots,F_{D_M})| \\ \approx & \left|\sum_{i=1,i\neq m}^{M}\alpha(u)E\mathrm{sinc}[\pi(i-m+F_{D_i}T)]\right. \\ + & \left.\frac{\alpha(u)E\sin[\pi(F_{D_m}+\beta\tau)(T-|\tau|)]}{T\pi(F_{D_m}+\beta\tau)}+n(u,\tau)\right| \qquad (27) \end{aligned}$$

So $|Z_m(u;\tau,F_{D_1},\cdots,F_{D_M})|$ consists of three parts, signal (reflected signal from radar m waveform): $\left|\frac{\alpha(u)E\sin[\pi(F_{D_m}+\beta\tau)(T-|\tau|)]}{T\pi(F_{D_m}+\beta\tau)}\right|$, interferences from other waveforms: $\sum_{i=1,i\neq m}^{M}|\alpha(u)E\mathrm{sinc}[\pi(i-m+F_{D_i}T)]|$,

and noise: $|n(u,\tau)|$. Delay-doppler uncertainty happens quite often in target search and recognition where target range and velocity are not yet perfectly known.

We can also have three special cases for $|Z_m(u;\tau,F_{D_1},\cdots,F_{D_M})|$:

1. When $F_{D_1}=\cdots=F_{D_M}=0$,

$$\begin{aligned} & |Z_m(u;\tau,0,0,\cdots,0)| \\ \approx\ & |\frac{\alpha(u)E\sin[\pi\beta\tau(T-|\tau|)]}{T\pi\beta\tau}+n(u,\tau)| \end{aligned} \tag{28}$$

2. If $\tau=0$, then (27) becomes

$$\begin{aligned} & |Z_m(u;0,F_{D_1},\cdots,F_{D_M})| \\ \approx\ & |\sum_{i=1}^{M}\alpha(u)E\mathrm{sinc}[\pi(i-m+F_{D_i}T)]+n(u)| \end{aligned} \tag{29}$$

3. If $\tau=0$, and $F_{D_1}=\cdots=F_{D_M}=0$, then (27) becomes

$$|Z_m(u;0,0,0,\cdots,0)|\approx|E\alpha(u)+n(u)| \tag{30}$$

How to combine all the Z_m's ($m=1,2,\cdots,M$) are very similar to the diversity combining in communations to combat channel fading, and the combination schemes may be different for different applications. In this paper, we are interested in applying RSN waveform diversity to automatic target recognition (ATR), e.g., recognition that the echo on a radar display is that of an aircraft, ship, motor vehicle, bird, person, rain, chaff, clear-air turbulence, land clutter, sea clutter, bare montains, forested areas, meteors, aurora, ionized media, or other natural phenomena. Early radars were "blob" detectors in that they detected the presence of a target and gave its location in range and angle, and radar began to be more than a blob detector and could provide recognition of one type of target from another[18]. It is known that small changes in the aspect angle of complex (multiple scatter) targets can cause major changes in the radar cross section (RCS). This

has been considered in the past as a means of target recognition, and is called *fluctuation of radar cross section with aspect angle*, but it has not had much success[18]. In this paper, we propose a maximum likelihood automatic target recognition (ML-ATR) algorithm for RSN. We will study both fluctuating target and non-fluctuating target.

4.1 ML-ATR for Fluctuating Targets with Delay-Doppler Uncertainty

Fluctuating target modeling is more realistic in which the target RCS is drawn from either the Rayleigh or chi-square of degree four pdf. The Rayleigh model describes the behavior of a complex target consisting of many scatters, none of which is dominant. The fourth-degree chi-square models targets having many scatters of similar strength with one dominant scatter. Based on different combinations of pdf and decorrelation characteristics (scan-to-scan or pulse-to-pulse decorrelation), four Swerling models are used[16]. In this paper, we will focus on "Swerling 2" model which is Rayleigh distribution with pulse-to-pulse decorrelation. The pulse-to-pulse decorrelation implies that each individual pulse results in an independent value for RCS α.

For Swerling 2 model, the RCS $|\alpha(u)|$ follows Rayleigh distribution and its I and Q subchannels follow zero-mean Gaussian distributions with variance γ^2. Assume

$$\alpha(u) = \alpha_I(u) + j\alpha_Q(u) \tag{31}$$

and $n(u) = n_I(u) + jn_Q(u)$ follows zero-mean complex Gausian distribution with variance σ^2 for the I and Q subchannels. Observe (27), for given τ, F_{D_i} $(i = 1, \cdots, M)$,

$$\begin{aligned} & \sum_{i=1, i\neq m}^{M} \alpha(u) E \mathrm{sinc}[\pi(i - m + F_{D_i}T)] + \frac{\alpha(u) E \sin[\pi(F_{D_m} + \beta\tau)(T - |\tau|)]}{T\pi(F_{D_m} + \beta\tau)} \\ = \; & \alpha(u) E[\sum_{i=1, i\neq m}^{M} \mathrm{sinc}[\pi(i - m + F_{D_i}T)] + \frac{\sin[\pi(F_{D_m} + \beta\tau)(T - |\tau|)]}{T\pi(F_{D_m} + \beta\tau)}] \end{aligned} \tag{32}$$

follows zero-mean complex Gaussian distributions with variance $E^2\gamma^2[\sum_{i=1, i\neq m}^{M} \mathrm{sinc}[\pi(i - m + F_{D_i}T)] + \frac{\sin[\pi(F_{D_m}+\beta\tau)(T-|\tau|)]}{T\pi(F_{D_m}+\beta\tau)}]^2$ for the I and Q subchannels. Since $n(u, \tau)$ also follows zero-mean

Gaussian distribution, so $|Z_m(u;\tau,F_{D_1},\cdots,F_{D_M})|$ of (27) follows Rayleigh distribution. In real world, the perfect values of τ and F_{D_i} are not known in the target search phase and the mean values of τ and F_{D_i} are 0, so we just assume the parameter of this Rayleigh distribution $b=\sqrt{E^2\gamma^2+\sigma^2}$ (when τ and F_{D_i} equal to 0).

Let $y_m \triangleq |Z_m(u;\tau,F_{D_1},\cdots,F_{D_M})|$, then

$$f(y_m)=\frac{y_m}{E^2\gamma^2+\sigma^2}\exp(-\frac{y_m^2}{E^2\gamma^2+\sigma^2}) \tag{33}$$

The mean value of y_m is $\sqrt{\frac{\pi(E^2\gamma^2+\sigma^2)}{2}}$, and variance is $\frac{(4-\pi)(E^2\gamma^2+\sigma^2)}{2}$. The variance of signal is $\frac{(4-\pi)E^2\gamma^2}{2}$ and the variance of noise is $\frac{(4-\pi)\sigma^2}{2}$.

Let $\mathbf{y} \triangleq [y_1,y_2,\cdots,y_M]$, then the pdf of $\mathbf{y}$ is

$$f(\mathbf{y})=\prod_{m=1}^{M} f(y_m) \tag{34}$$

Our ATR is a multiple-category hypothesis testing problem, i.e., to decide a target category (e.g. different aircraft, motor vehicle, etc) based on $r_1(u,t)$. Assume there are totally N categories and category n target has RCS $\alpha_n(u)$ (with variance γ_n^2), so the ML-ATR algorithm to decide a target category C can be expressed as,

$$\begin{aligned} C &= \arg\max_{n=1,\cdots,N} f(\mathbf{y}|\gamma=\gamma_n) \\ &= \arg\max_{n=1,\cdots,N} \prod_{m=1}^{M} \frac{y_m}{E^2\gamma_n^2+\sigma^2}\exp(-\frac{y_m^2}{E^2\gamma_n^2+\sigma^2}) \end{aligned} \tag{35}$$

4.2 ML-ATR for Non-fluctuating Targets with Delay-Doppler Uncertainty

In some sources, the non-fluctuating target is identified as "Swerling 0" or "Swerling 5" model[19]. For non-fluctuating target, the RCS $\alpha(u)$ is just a constant α for a given target. Observe (27), for

given τ, F_{D_i} $(i = 1, \cdots, M)$,

$$\sum_{i=1, i\neq m}^{M} \alpha(u) E \text{sinc}[\pi(i - m + F_{D_i} T)] + \frac{\alpha(u) E \sin[\pi(F_{D_m} + \beta\tau)(T - |\tau|)]}{T\pi(F_{D_m} + \beta\tau)} \tag{36}$$

$$= \alpha E[\sum_{i=1, i\neq m}^{M} \text{sinc}[\pi(i - m + F_{D_i} T)] + \frac{\sin[\pi(F_{D_m} + \beta\tau)(T - |\tau|)]}{T\pi(F_{D_m} + \beta\tau)}] \tag{37}$$

is just a constant. Since $n(u, \tau)$ follows zero-mean Gaussian distribution, so $|Z_m(u; \tau, F_{D_1}, \cdots, F_{D_M})|$ of (27) follows Rician distribution with direct path value

$$\lambda = \alpha E[\sum_{i=1, i\neq m}^{M} \text{sinc}[\pi(i - m + F_{D_i} T)] + \frac{\sin[\pi(F_{D_m} + \beta\tau)(T - |\tau|)]}{T\pi(F_{D_m} + \beta\tau)}] \tag{38}$$

Since τ and F_{D_i} are uncertain and zero-mean, so we just use the approximation

$$\lambda = \alpha E \tag{39}$$

which is obtained when τ and F_{D_i} equal to 0.

Let $y_m \triangleq |Z_m(u; \tau, F_{D_1}, \cdots, F_{D_M})|$, then the probability density function (pdf) of y_m is

$$f(y_m) = \frac{2y_m}{\sigma^2} \exp[-\frac{(y_m^2 + \lambda^2)}{\sigma^2}] I_0(\frac{2\lambda y_m}{\sigma^2}) \tag{40}$$

where σ^2 is the noise power (with I and Q sub-channel power $\sigma^2/2$), and $I_0(\cdot)$ is the zero-order modified Bessel function of the first kind. Let $\mathbf{y} \triangleq [y_1, y_2, \cdots, y_M]$, then the pdf of $\mathbf{y}$ is

$$f(\mathbf{y}) = \prod_{m=1}^{M} f(y_m) \tag{41}$$

The ML-ATR algorithm to decide a target category C based on $\mathbf{y}$ can be expressed as,

$$\begin{aligned} C &= \arg \max_{n=1,\cdots,N} f(\mathbf{y}|\lambda = E|\alpha_n|) \\ &= \arg \max_{n=1,\cdots,N} \prod_{m=1}^{M} \frac{2y_m}{\sigma^2} \exp[-\frac{(y_m^2 + E^2\alpha_n^2)}{\sigma^2}] I_0(\frac{2E|\alpha_n| y_m}{\sigma^2}) \end{aligned}$$

5 Simulations

Radar sensor networks will be required to detect a broad range of target classes. In this paper, we applied our ML-ATR to automatic target recognition with delay-doppler uncertainty. We assume that the domain of target classes is known a priori (N in Sections 4.1 and 4.2), and that the RSN is confined to work only on the known domain.

For fluctuating target recognition, our targets have 6 classes with different RCS values, which are summarized in Table 1[18]. We assume the fluctuating targets follow "Swerling 2" model (Rayleigh with pulse-to-pulse decorrelation), and assume the RCS value listed in Table 1 to be the standard deviation (std) γ_n of RCS $\alpha_n(u)$ for target n. We applied the ML-ATR algorithm in Section 4.1 (for fluctuating target case) for target recognition within the six targets domain. We chose $T = 0.1ms$ and $\beta = 10^6$. At each average SNR value, we ran Monte-Carlo simulations for 10^5 times for each target. In Fig. 2(a)(b)(c), we plot the average ATR error for fluctuating targets with different delay-doppler uncertainty and compared the performances of single radar system, 5-radar RSN, and 10-radar RSN. Observe these three figures:

1. The two RSNs vastly reduce the ATR error comparing to a single radar system in ATR with delay-doppler uncertainty, e.g., the 10-radar RSN can achieve ATR error 2% comparing against the single radar system with ATR error 37% at $SNR = 32dB$ with delay-doppler uncertainty $\tau \in [-0.1T, 0.1T]$ and $F_{D_i} \in [-200Hz, 200Hz]$.

2. Our LFM waveform design can tolerate reasonable delay-doppler uncertainty which are testified by Fig. 2(b)(c).

3. According to Skolnik[18], radar performance with probability of recognition error (p_e) less than 10% is good enough. Our 10-radar RSN with waveform-diversity can have probability of ATR error much less than 10% for the average ATR for all targets. However, the single

radar system has probability of ATR error much higher than 10%. Our RSN with waveform diversity is very promising to be used for real-world ATR.

4. Observe Fig. 2(a)(c), the average probability of ATR error in 2(c) is not as sensitive to the SNR as that in 2(a), i.e., ATR error curve slope becomes flat with higher delay-doppler uncertainty, which means the delay-doppler uncertainty can dominate the ATR performance when it's too high.

For non-fluctuating target recognition, our targets have 6 classes with different RCS values, which are summarized in Table 1[18]. We applied the ML-ATR algorithms in Section 4.2 (for nonfluctuating target case) to classify an unknown target as one of these 6 target classes. We chose $T = 0.1ms$ and $\beta = 10^6$. At each average SNR value, we ran Monte-Carlo simulations for 10^5 times for each target. In Fig. 3(a)(b)(c), we plotted the probability of ATR error with different delay-doppler uncertainty. Observe these figures,

1. The two RSNs tremendously reduce the ATR error comparing to a single radar system in ATR with delay-doppler uncertainty, e.g., the 10-radar RSN can achieve ATR error 9% comparing against the single radar system with ATR error 22% at $SNR = 22dB$ with delay-doppler uncertainty $\tau \in [-0.2T, 0.2T]$ and $F_{D_i} \in [-500Hz, 500Hz]$.

2. Comparing Fig. 2(a)(b)(c) against Fig. 3(a)(b)(c), the gain of 10-radar RSN for fluctuating target recognition is much larger than that for non-fluctuating target recognition, which means our RSN has better capacity to handle the fluctuating targets. In real world, fluctuating targets are more meaningful and realistic.

3. Comparing Fig. 3(a)(b)(c) against Fig. 2(a)(b)(c), the ATR needs much lower SNR for nonfluctuating target recognition because Rician distribution has direct path component.

6 Conclusions and Future Works

We have studied LFM waveform design and diversity in radar sensor networks (RSN). We showed that the LFM waveforms can co-exist if the carrier frequency spacing is $1/T$ between two radar waveforms. We made analysis on interferences among waveforms in RSN and proposed a RAKE structure for waveform diversity combining in RSN. We applied the RSN to automatic target recognition (ATR) with delay-doppler uncertainty and proposed maximum-likehood (ML)-ATR algorithms for fluctuating target and non-fluctuating target. Simulation results show that RSN using our waveform diversity-based ML-ATR algorithm performs much better than single radar system for fluctuating targets and nonfluctuating targets recognition. It is also demonstrated that our LFM waveform-based RSN can handle the delay-doppler uncertainty which quite often happens for ATR in target search phase.

The waveform design and diversity algorithms proposed in this paper can also be applied to active RFID sensor networks and underwater acoustic sensor networks because LFM waveforms can also be used by these active sensor networks to perform collaborative monitoring tasks. In this paper, the ATR is for single target recognition. We will continuously investigate the ATR when multiple targets co-existence in RSN and each target has delay-doppler uncertainty. In our waveform diversity combining, we have used spatial diversity combining in this paper. We will further investigate spatial-temporal-frequency combining for RSN waveform diversity.

Acknowledgement

This work was supported by the U.S. Office of Naval Research (ONR) Young Investigator Program Award under Grant N00014-03-1-0466.

The author would like to thank ONR Program Officer Dr. Rabinder N. Madan for his direction

and insightful discussion on radar sensor networks.

References

[1] P. Baggenstoss, "Adaptive pulselength correction (APLECORR): a strategy for waveform optimization in ultrawideband active sonar," *IEEE Trans on Oceanic Engineering*, vol. 23, no. 1, pp. 1-11, 1998.

[2] C. E. Baum, et al, "The singularity expansion method and its application to target identification", *Proc. of the IEEE*, vol 79, no. 10, Oct 1991.

[3] M. R. Bell, "Information theory and radar waveform design", *IEEE Trans on Information Theory*, vol. 39, no. 5, pp. 1578-1597, Sept 1993.

[4] H. Deng, "Synthesis of binary sequences with good correlation and cross-correlation properties by simulated annealing," *IEEE Trans on Aerospace and Electronic Systems*, vol. 32, no. 1, Jan 1996.

[5] R. Fitzgerald, "Effects of range-doppler coupling on chirp radar tracking acuracy," *IEEE Trans on Aerospace and Eletronic Systems*, vol. 10, pp. 528-532, July 1974.

[6] T.-C. Hou and T-J. Tsai, " An access-based clustering protocol for multihop wireless ad hoc networks," *IEEE J. Selected Areas in Communications*, vol. 19, no. 7, pp. 1201-1210, July 2001.

[7] A. Iwata, C. C. Chiang, G. Pei, M. Gerla, and T. W. Chen, " Scalable routing strategies for ad hoc networks," *IEEE J. Selected Areas in Communications*, vol. 17, pp. 1369-1379, 1999.

[8] R. A. Johnson and E. L. Titlebaum, "Range Doppler Uncoupling in the Doppler Tolerant Bat Signal", *Proc. of IEEE Ultrasonics Symposium*, New York, pp. 64-67, 1972.

[9] D. Kershaw and R. Evans, "Optimal waveform selection for tracking system", *IEEE Trans on Information Theory*, vol. 40, no. 5, pp. 1536-1550, 1994.

[10] Q. Liang, "Waveform Design and Diversity in Radar Sensor Networks: Theoretical Analysis and Application to Automatic Target Recognition," accepted by *Int'l Workshop on Wireless Ad Hoc and Sensor Networks*, June 2006, New York.

[11] C. R. Lin and M. Gerla, "Adaptive clustering in mobile wireless networks," *IEEE J. Selected Areas in Communications*, vol. 16, pp. 1265-1275, 1997.

[12] R. Niu, P. Willett, and Y. Bar-Shalom, "Tracking consideration in selection of radar waveform for range and range-rate measurements", *IEEE Transactions on Aerospace and Electronic Systems*, Vol. 38, No. 2, 2002.

[13] A. Papandreou, G. F. Boudreaux-Bartels, and S. M. Kay, "Detection and estimation of generalized chirps using time-frequency representations", *Twenty-Eighth Asilomar Conference on Signals, Systems and Computers*, vol. 1, pp. 50-54, Oct. 1994.

[14] C. E. Perkins, "Chapter 4, Cluster-Based Networks," *Ad Hoc Networking*, Edited by C. E. Perkins, pp. 75-138, Addison-Wesley, 2001.

[15] J. Roman, M. Rangaswamy, D. Davis, Q. Zhang, B. Himed, and J. Michels, "Parametric adaptive matched filter for airborne radar applications," *IEEE Trans. Aerosp. Electron. Syst.*, vol. 36, no. 2, pp. 677-692, 2000.

[16] M. A. Richards, *Fundamentals of Radar Signal Processing*, McGraw-Hill Companies, New York, 2005.

[17] T.K. Sarkar and N. Sangruji, "An adaptive nulling system for a narrow-band signal with a look-direction constraint utilizing the conjugate gradient method," *IEEE Trans. Antennas Propagat.*, vol. 37, no. 7, pp. 940-944, July 1989.

[18] M. I. Skolnik, *Introduction to Radar Systems*, 3rd ed, New York, McGraw Hill, 2001.

[19] P. Swerling, "Probability of detection for fluctuating targets", *IRE Trans on Information Theory*, vol. 6, pp. 269-308, April 1960.

[20] Y. Sun, P. Willett, and R. Lynch, "Waveform fusion in sonar signal processing", *IEEE Transactions on Aerospace and Electronic Systems*, Vol. 40, No. 2, 2004

[21] S. Sowelam and A. Tewfik, "Waveform selection in radar target classification," *IEEE Trans on Information Theory*, vol. 46, no. 3, pp. 1014-1029, 2000.

List of Tables

Table 1: RCS values at microwave frequency for 6 targets.

Index n	Target	RCS
1	Small single-engine aircraft	1
2	Large flighter aircraft	6
3	Medium bomber or jet airliner	20
4	Large bomber or jet airliner	40
5	Jumbo jet	100
6	Pickup truck	200

List of Figures

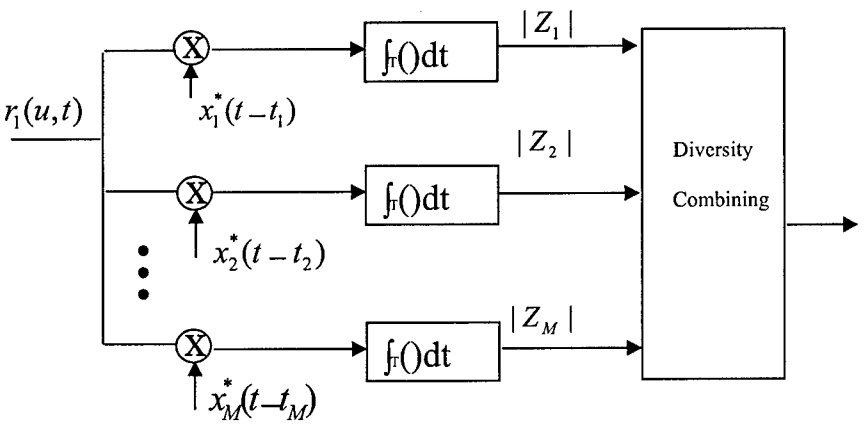

Figure 1: Waveform diversity combining by clusterhead in RSN.

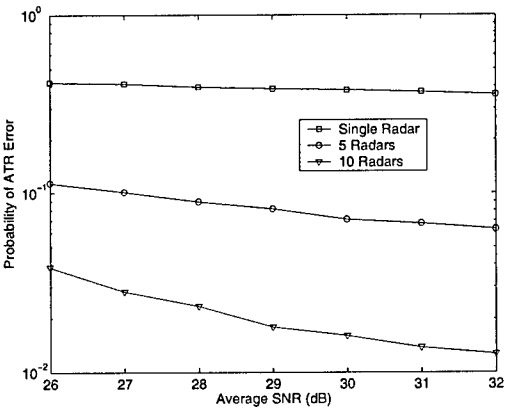

(a)

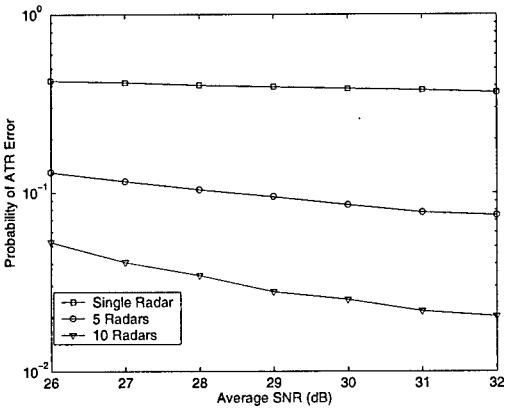

(b)

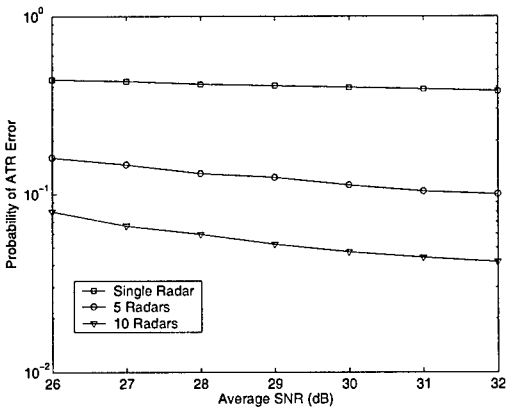

(c)

Figure 2: The average probability of ATR error for 6 *fluctuating* targets with different delay-doppler uncertainty. (a) no delay-doppler uncertainty, (b) with delay-doppler uncertainty, $\tau \in [-0.1T, 0.1T]$ and $F_{D_i} \in [-200Hz, 200Hz]$, and (c) with delay-doppler uncertainty, $\tau \in [-0.2T, 0.2T]$ and $F_{D_i} \in [-500Hz, 500Hz]$.

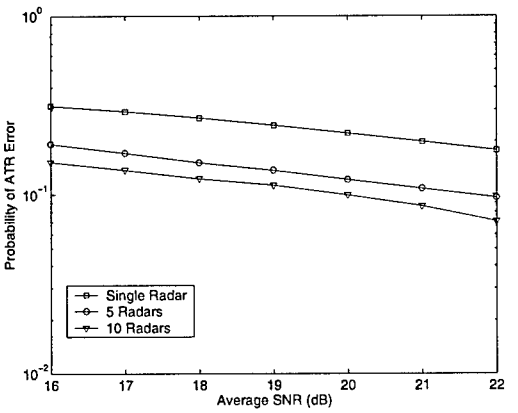

(a)

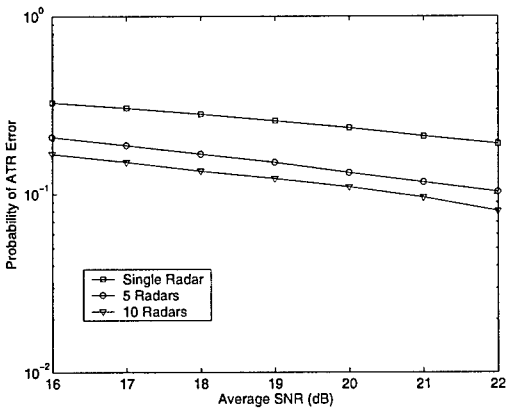

(b)

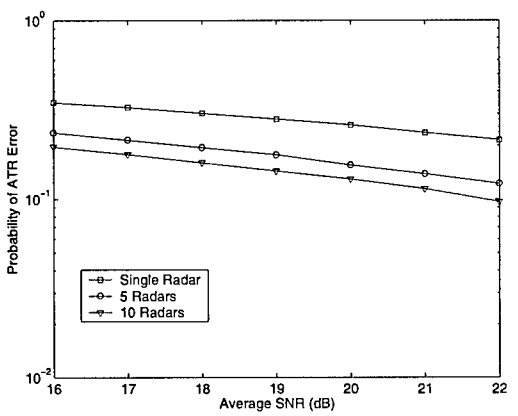

(c)

Figure 3: The average probability of ATR error for 6 *nonfluctuating* targets with different delay-doppler uncertainty. (a) no delay-doppler uncertainty, (b) with delay-doppler uncertainty, $\tau \in [-0.1T, 0.1T]$ and $F_{D_i} \in [-200Hz, 200Hz]$, and (c) with delay-doppler uncertainty, $\tau \in [-0.2T, 0.2T]$ and $F_{D_i} \in [-500Hz, 500Hz]$.

Radar Sensor Networks for Automatic Target Recognition with Delay-Doppler Uncertainty

Qilian Liang
Department of Electrical Engineering
416 Yates Street, Room 518
University of Texas at Arlington
Arlington, TX 76019-0016 USA
E-mail: liang@uta.edu

Abstract— **Automatic target recognition (ATR) in target search phase is very challenging because the target range and mobility are not yet perfectly known, which results in delay-doppler uncertainty. In this paper, we firstly perform some theoretical studies on radar sensor network (RSN) design based linear frequency modulation (LFM) waveform: (1) the conditions for waveform co-existence, (2) interferences among waveforms in RSN, (3) waveform diversity in RSN. Then we apply RSN to ATR with delay-doppler uncertainty and propose maximum-likekihood (ML) ATR algorithms for fluctuating target and nonfluctuating target. Simulation results show that our RSN vastly reduces the ATR error comparing to a single radar system in ATR with delay-doppler uncertainty.**

I. Introduction and Motivation

The goal for any target recognition system is to give the most accurate interpretation of what a target is at any given point in time. There are two classes of motion models of target, one for maneuvering targets and one for non-maneuvering (constant velocity and acceleration) targets. The area that is still lacking in target recognition is the ability to detect reliably when a target is beginning a maneuver where its speed and range are uncertain. The tracking system can switch the algorithms applied to the problem from a non-maneuvering set to the maneuvering set when a target is beginning a maneuver. But when the tracker does finally catch up to the target after the maneuver and then perform ATR, the latency is too high. In time critical mission situation, such latency in ATR is not tolerable. In this paper, we are interested in studying automatic target recongition with range and speed uncertainty, i.e., delay-doppler uncertainty, using radar sensor networks (RSN). The network of radar sensors should operate with multiple goals managed by an intelligent platform network that can manage the dynamics of each radar to meet the common goals of the platform, rather than each radar to operate as an independent system. Therefore, it is significant to perform signal design and processing and networking co-operatively within and between platforms of radar sensors and their communication modules. In this paper, we are interested in studying algorithms on radar sensor network (RSN) design based linear frequency modulation (LFM) waveform: (1) the conditions for waveform co-existence, (2) interferences among waveforms in RSN, (3) waveform diversity in RSN. Then we apply RSN to automatic target recognition (ATR) with delay-doppler uncertainty.

In nature, diverse waveforms are transmitted by animals for specific applications. For example, when a bat and a whale are in the search mode for food, they emit a different type of waveform than when they are trying to locate their prey. The Doppler-invariant waveforms that they transmit are environment dependent [8]. Hence, in RSN, it may be useful to transmit different waveform from different neighbor radars and they can collaboratively perform waveforms diversity for ATR. Sowelam and Tewfik [21] developed a signal selection strategy for radar target classification, and a sequential classification procedure was proposed to minimize the average number of necessary signal transmissions. Intelligent waveform selection was studied in [1][9], but the effect of doppler shift was not considered. In [12], the performance of constant frequency (CF) and linear frequency modulated (LFM) waveform fusion from the standpoint of the whole system was studied, but the effects of clutter was not considered. In [20], CF and LFM waveforms were studied for sonar system, but it was assumed that the sensor is nonintelligent (i.e., waveform can't be selected adaptively). All the above studies and design methods were focused on the waveform design or selection for a single active radar or sensor. In [10], CF waveform design was applied to RSN with application to ATR without any delay-doppler uncertainty. In this paper, we will focus on the waveform design fusion for radar sensor networks using LFM waveform.

The rest of this paper is organized as follows. In Section II, we study the co-existence of LFM radar waveforms. In Section III, we analyze the interferences among LFM radar

waveforms. In Section IV we propose a RAKE structure for waveform diversity combining and propose maximum-likelihood (ML) algorithms for automatic target recognition (ATR) with delay-doppler uncertainty. In Section V, we provide simulation results on ML-ATR with delay-doppler uncertainty. In Section VI, we conclude this paper and provide some future works.

II. Co-existence of LFM Radar Waveforms

In radar sensor networks (RSN), radar sensors will interfere with each other and the signal-to-interference-ratio may be very low if the waveforms are not properly designed. We will introduce orthogonality as one criterion for waveforms design in RSN to make them co-existence. Besides, the radar channel is narrow-band, so we will also consider the bandwidth constraint.

In our radar sensor networks, we choose linear frequency modulation (LFM) waveform. The LFM waveform can be defined as

$$x(t) = \sqrt{\frac{E}{T}} \exp(j2\pi\beta t^2) \quad -T/2 \le t \le T/2 \quad (1)$$

In radar, ambiguity function (AF) is an analytical tool for waveform design and analysis that succinctly characterizes the behavior of a waveform paired with its matched filter. The ambiguity function is useful for examing resolution, side lobe behavior, and ambiguities in both range and Doppler for a given waveform[16]. For a single radar, the matched filter for waveform $x(t)$ is $x^*(-t)$, and the ambiguity function of LFM waveform is[16]

$$\begin{aligned} A(\tau, F_D) &= \left| \int_{-T/2+\tau}^{T/2} x(t) \exp(j2\pi F_D t) x^*(t-\tau) dt \right| \\ &= \left| \frac{E \sin[\pi(F_D+\beta\tau)(T-|\tau|)]}{T\pi(F_D+\beta\tau)} \right| \quad -T \le \tau \le T \end{aligned} \quad (2)$$

However, the above ambiguity is for one radar only (no co-existing radar).

For radar sensor networks, the waveforms from different radars will interfere with each other. We choose the waveform for radar i as

$$x_i(t) = \sqrt{\frac{E}{T}} \exp[j2\pi(\beta t^2 + \delta_i t)] \quad -T/2 \le t \le T/2 \quad (3)$$

which means there is a frequency shift δ_i for radar i. To minimize the interference from one waveform to the other, optimal values for δ_i should be determined to have the waveforms orthogonal to each other, i.e., let the cross-correlation between $x_i(t)$ and $x_n(t)$ be 0,

$$\begin{aligned} & \int_{-T/2}^{T/2} x_i(t) x_n^*(t) dt \\ = \; & \frac{E}{T} \int_{-T/2}^{T/2} \exp[j2\pi(\beta t^2 + \delta_i t)] \exp[-j2\pi(\beta t^2 + \delta_n t)] dt \\ = \; & E\mathrm{sinc}[\pi(\delta_i - \delta_n)T] \end{aligned} \quad (4)$$

If we choose

$$\delta_i = \frac{i}{T} \quad (5)$$

where i is a dummy index, then (4) can have two cases

$$\int_{-T/2}^{T/2} x_i(t) x_n^*(t) dt = \begin{cases} E & i = n \\ 0 & i \ne n \end{cases} \quad (6)$$

So choosing $\delta_i = \frac{i}{T}$ in (3) can have orthogonal waveforms, i.e., the waveforms can co-exist if the carrier spacing is $1/T$ between two radar waveforms. i.e., orthogonality amongst carriers can be achieved by separating the carriers by an interger multiple of the inverse of waveform pulse duration. With this design, all the orthogonal waveforms can work simultaneously. However, there may exist time delay and doppler shift ambiguity which will have interferences to other waveforms in RSN.

III. Interferences of LFM Waveforms In Radar Sensor Networks

A. RSN with Two Radar Sensors

We are interested in analyzing the interference from one radar to another if there exist time delay and doppler shift. For a simple case where there are two radar sensors (i and n), the ambiguity function of radar i (considering interference from radar n) is

$$A_i(t_i, t_n, F_{D_i}, F_{D_n}) \quad (7)$$

$$= \left| \int_{-\infty}^{\infty} [x_i(t) \exp(j2\pi F_{D_i} t) + x_n(t-t_n) \exp(j2\pi F_{D_n} t)] x_i^*(t-t_i) dt \right| \quad (8)$$

$$\le \left| \int_{-T/2+\max(t_i,t_n)}^{T/2+\min(t_i,t_n)} x_n(t-t_n) \exp(j2\pi F_{D_n} t) x_i^*(t-t_i) dt \right| + \left| \int_{-T/2+t_i}^{T/2} x_i(t) \exp(j2\pi F_{D_i} t) x_i^*(t-t_i) dt \right| \quad (9)$$

$$= \left| \int_{-T/2+\max(t_i,t_n)}^{T/2+\min(t_i,t_n)} x_n(t-t_n) \exp(j2\pi F_{D_n} t) x_i^*(t-t_i) dt \right| + \left| \frac{E \sin[\pi(F_{D_i}+\beta t_i)(T-|t_i|)]}{T\pi(F_{D_i}+\beta t_i)} \right| \quad (10)$$

To make analysis easier, we assume $t_i = t_n = \tau$, then (10) can be simplified as

$$\begin{aligned} A_i(\tau, F_{D_i}, F_{D_n}) &\approx |E\mathrm{sinc}[\pi(n-i+F_{D_n}T)]| \\ &+ \left| \frac{E \sin[\pi(F_{D_i}+\beta\tau)(T-|\tau|)]}{T\pi(F_{D_i}+\beta\tau)} \right| \end{aligned} \quad (11)$$

B. RSN with M Radar Sensors

It can be extended to an RSN with M radars. Assuming time delay τ for each radar is the same, then the ambiguity function of radar 1 (considering interferences from all the

other $M-1$ radars with CF pulse waveforms) can be expressed as

$$A_1(\tau, F_{D_1}, \cdots, F_{D_M}) \approx \left|\sum_{i=2}^{M} E\text{sinc}[\pi(i-1+F_{D_i}T)]\right| + \left|\frac{E\sin[\pi(F_{D_1}+\beta\tau)(T-|\tau|)]}{T\pi(F_{D_1}+\beta\tau)}\right| \quad (12)$$

IV. Application to Automatic Target Recognition (ATR) with Delay-Doppler Uncertainty

In RSN, The radar sensors are networked together in an ad hoc fashion. They do not rely on a preexisting fixed infrastructure, such as a wireline backbone network or a base station. They are self-organizing entities that are deployed on demand in support of various events surveillance, battlefield, disaster relief, search and rescue, etc. Scalability concern suggest a hierarchical organization of radar sensor networks with the lowest level in the hierarchy being a cluster. As argued in [11] [7] [6] [14], in addition to helping with scalability and robustness, aggregating sensor nodes into clusters has additional benefits:

1) conserving radio resources such as bandwidth;
2) promoting spatial code reuse and frequency reuse;
3) simplifying the topology, e.g., when a mobile radar changes its location, it is sufficient for only the nodes in attended clusters to update their topology information;
4) reducing the generation and propagation of routing information; and,
5) concealing the details of global network topology from individual nodes.

In RSN, each radar can provide their waveform parameters such as δ_i to their clusterhead radar, and the clusterhead radar can combine the waveforms from its cluster members.

In RSN with M radars, the received signal for clusterhead (assume it's radar 1) is

$$r_1(u,t) = \sum_{i=1}^{M} \alpha(u) x_i(t-t_i)\exp(j2\pi F_{D_i}t) + n(u,t) \quad (13)$$

where $\alpha(u)$ stands for radar cross section (RCS) and can be modeled using non-zero constants for nonfluctuating target and four Swerling target models for fluctuating target[16]; F_{D_i} is the doppler shift of target relative to waveform i; t_i is delay of waveform i, and $n(u,t)$ is additive white Gaussian noise (AWGN). In this paper, we propose a RAKE structure for waveform diversity combining, as illustrated by Fig. 1.

According to this structure, the received $r_1(u,t)$ is processed by a bank of matched filters, then the output

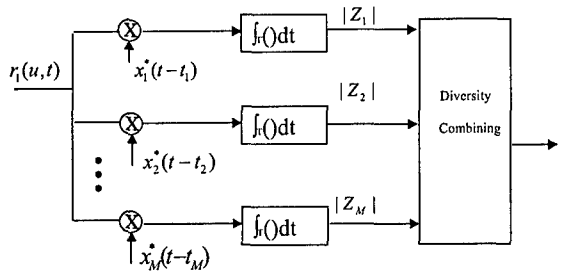

Fig. 1. Waveform diversity combining by clusterhead in RSN.

of branch 1 (after integration) is

$$\begin{aligned} &|Z_1(u;t_1,\cdots,t_M,F_{D_1},\cdots,F_{D_M})| \\ =& \left|\int_{-T/2}^{T/2} r_1(u,t)x_1^*(t-t_1)ds\right| \quad (14) \\ =& \left|\int_{-T/2}^{T/2}[\sum_{i=1}^{M}\alpha_i(u)x_i(t-t_i)\exp(j2\pi F_{D_i}t) \right. \\ & \left. +n(u,t)]x_1^*(t-t_1)dt\right| \quad (15) \end{aligned}$$

where $\int_{-T/2}^{T/2} n(u,t)x_1^*(t-t_1)dt$ can easily be proved to be AWGN, let

$$n(u,t_1) \triangleq \int_{-T/2}^{T/2} n(u,t)x_1^*(t-t_1)dt \quad (16)$$

follows Rayleigh distribution. Assuming $t_1 = t_2 = \cdots = t_M = \tau$, then based on (12),

$$\begin{aligned} &|Z_1(u;\tau,F_{D_1},\cdots,F_{D_M})| \\ \approx& \left|\sum_{i=2}^{M}\alpha(u)E\text{sinc}[\pi(i-1+F_{D_i}T)]\right. \\ &\left. + \frac{\alpha(u)E\sin[\pi(F_{D_1}+\beta\tau)(T-|\tau|)]}{T\pi(F_{D_1}+\beta\tau)} + n(u,\tau)\right| \quad (17) \end{aligned}$$

Similarly, we can get the output for any branch m ($m = 1,2,\cdots,M$),

$$\begin{aligned} &|Z_m(u;\tau,F_{D_1},\cdots,F_{D_M})| \\ \approx& \left|\sum_{i=1,i\neq m}^{M}\alpha(u)E\text{sinc}[\pi(i-m+F_{D_i}T)]\right. \\ &\left. + \frac{\alpha(u)E\sin[\pi(F_{D_m}+\beta\tau)(T-|\tau|)]}{T\pi(F_{D_m}+\beta\tau)} + n(u,\tau)\right| \quad (18) \end{aligned}$$

So $|Z_m(u;\tau,F_{D_1},\cdots,F_{D_M})|$ consists of three parts, signal (reflected signal from radar m waveform): $\left|\frac{\alpha(u)E\sin[\pi(F_{D_m}+\beta\tau)(T-|\tau|)]}{T\pi(F_{D_m}+\beta\tau)}\right|$, interferences from other waveforms: $\sum_{i=1,i\neq m}^{M}|\alpha(u)E\text{sinc}[\pi(i-m+F_{D_i}T)]|$, and noise: $|n(u,\tau)|$. Delay-doppler uncertainty happens

quite often in target search and recognition where target range and velocity are not yet perfectly known.

We can also have three special cases for $|Z_m(u;\tau,F_{D_1},\cdots,F_{D_M})|$:

1) When $F_{D_1}=\cdots=F_{D_M}=0$,

$$\begin{aligned}&|Z_m(u;\tau,0,0,\cdots,0)|\\ \approx\ &|\frac{\alpha(u)E\sin[\pi\beta\tau(T-|\tau|)]}{T\pi\beta\tau}+n(u,\tau)|\end{aligned}\quad(19)$$

2) If $\tau=0$, then (18) becomes

$$\begin{aligned}&|Z_m(u;0,F_{D_1},\cdots,F_{D_M})|\\ \approx\ &|\sum_{i=1}^{M}\alpha(u)E\text{sinc}[\pi(i-m+F_{D_i}T)]+n(u)|\end{aligned}\quad(20)$$

3) If $\tau=0$, and $F_{D_1}=\cdots=F_{D_M}=0$, then (18) becomes

$$|Z_m(u;0,0,0,\cdots,0)|\approx|E\alpha(u)+n(u)|\quad(21)$$

How to combine all the Z_m's ($m=1,2,\cdots,M$) are very similar to the diversity combining in communations to combat channel fading, and the combination schemes may be different for different applications. In this paper, we are interested in applying RSN waveform diversity to automatic target recognition (ATR), e.g., recognition that the echo on a radar display is that of an aircraft, ship, motor vehicle, bird, person, rain, chaff, clear-air turbulence, land clutter, sea clutter, bare montains, forested areas, meteors, aurora, ionized media, or other natural phenomena. Early radars were "blob" detectors in that they detected the presence of a target and gave its location in range and angle, and radar began to be more than a blob detector and could provide recognition of one type of target from another[18]. It is known that small changes in the aspect angle of complex (multiple scatter) targets can cause major changes in the radar cross section (RCS). This has been considered in the past as a means of target recognition, and is called *fluctuation of radar cross section with aspect angle*, but it has not had much success[18]. In this paper, we propose a maximum likelihood automatic target recognition (ML-ATR) algorithm for RSN. We will study both fluctuating target and non-fluctuating target.

A. ML-ATR for Fluctuating Targets with Delay-Doppler Uncertainty

Fluctuating target modeling is more realistic in which the target RCS is drawn from either the Rayleigh or chi-square of degree four pdf. The Rayleigh model describes the behavior of a complex target consisting of many scatters, none of which is dominant. The fourth-degree chi-square models targets having many scatters of similar strength with one dominant scatter. Based on different combinations of pdf and decorrelation characteristics (scan-to-scan or pulse-to-pulse decorrelation), four Swerling models are used[16]. In this paper, we will focus on "Swerling 2" model which is Rayleigh distribution with pulse-to-pulse decorrelation. The pulse-to-pulse decorrelation implies that each individual pulse results in an independent value for RCS α.

For Swerling 2 model, the RCS $|\alpha(u)|$ follows Rayleigh distribution and its I and Q subchannels follow zero-mean Gaussian distributions with variance γ^2. Assume

$$\alpha(u)=\alpha_I(u)+j\alpha_Q(u)\quad(22)$$

and $n(u)=n_I(u)+jn_Q(u)$ follows zero-mean complex Gausian distribution with variance σ^2 for the I and Q subchannels. Observe (18), for given τ, F_{D_i} ($i=1,\cdots,M$),

$$\begin{aligned}&\sum_{i=1,i\neq m}^{M}\alpha(u)E\text{sinc}[\pi(i-m+F_{D_i}T)]\\ +\ &\frac{\alpha(u)E\sin[\pi(F_{D_m}+\beta\tau)(T-|\tau|)]}{T\pi(F_{D_m}+\beta\tau)}\\ =\ &\alpha(u)E[\sum_{i=1,i\neq m}^{M}\text{sinc}[\pi(i-m+F_{D_i}T)]\\ +\ &\frac{\sin[\pi(F_{D_m}+\beta\tau)(T-|\tau|)]}{T\pi(F_{D_m}+\beta\tau)}]\end{aligned}\quad(23)$$

follows zero-mean complex Gaussian distributions with variance $E^2\gamma^2[\sum_{i=1,i\neq m}^{M}\text{sinc}[\pi(i-m+F_{D_i}T)]+\frac{\sin[\pi(F_{D_m}+\beta\tau)(T-|\tau|)]}{T\pi(F_{D_m}+\beta\tau)}]^2$ for the I and Q subchannels. Since $n(u,\tau)$ also follows zero-mean Gaussian distribution, so $|Z_m(u;\tau,F_{D_1},\cdots,F_{D_M})|$ of (18) follows Rayleigh distribution. In real world, the perfect values of τ and F_{D_i} are not known in the target search phase and the mean values of τ and F_{D_i} are 0, so we just assume the parameter of this Rayleigh distribution $b=\sqrt{E^2\gamma^2+\sigma^2}$ (when τ and F_{D_i} equal to 0).

Let $y_m\triangleq|Z_m(u;\tau,F_{D_1},\cdots,F_{D_M})|$, then

$$f(y_m)=\frac{y_m}{E^2\gamma^2+\sigma^2}\exp(-\frac{y_m^2}{E^2\gamma^2+\sigma^2})\quad(24)$$

The mean value of y_m is $\sqrt{\frac{\pi(E^2\gamma^2+\sigma^2)}{2}}$, and variance is $\frac{(4-\pi)(E^2\gamma^2+\sigma^2)}{2}$. The variance of signal is $\frac{(4-\pi)E^2\gamma^2}{2}$ and the variance of noise is $\frac{(4-\pi)\sigma^2}{2}$.

Let $\mathbf{y}\triangleq[y_1,y_2,\cdots,y_M]$, then the pdf of $\mathbf{y}$ is

$$f(\mathbf{y})=\prod_{m=1}^{M}f(y_m)\quad(25)$$

Our ATR is a multiple-category hypothesis testing problem, i.e., to decide a target category (e.g. different aircraft, motor vehicle, etc) based on $r_1(u,t)$. Assume there are totally N categories and category n target has RCS $\alpha_n(u)$

(with variance γ_n^2), so the ML-ATR algorithm to decide a target category C can be expressed as,

$$C = \arg \max_{n=1,\cdots,N} f(\mathbf{y}|\gamma = \gamma_n) \quad (26)$$

$$= \arg \max_{n=1,\cdots,N} \prod_{m=1}^{M} \frac{y_m}{E^2\gamma_n^2 + \sigma^2} \exp(-\frac{y_m^2}{E^2\gamma_n^2 + \sigma^2})$$

B. ML-ATR for Non-fluctuating Targets with Delay-Doppler Uncertainty

In some sources, the non-fluctuating target is identified as "Swerling 0" or "Swerling 5" model[19]. For non-fluctuating target, the RCS $\alpha(u)$ is just a constant α for a given target. Observe (18), for given τ, F_{D_i} $(i = 1, \cdots, M)$,

$$\sum_{i=1, i\neq m}^{M} \alpha(u) E \text{sinc}[\pi(i - m + F_{D_i}T)]$$

$$+ \frac{\alpha(u)E \sin[\pi(F_{D_m} + \beta\tau)(T - |\tau|)]}{T\pi(F_{D_m} + \beta\tau)} \quad (27)$$

$$= \alpha E[\sum_{i=1, i\neq m}^{M} \text{sinc}[\pi(i - m + F_{D_i}T)]$$

$$+ \frac{\sin[\pi(F_{D_m} + \beta\tau)(T - |\tau|)]}{T\pi(F_{D_m} + \beta\tau)}] \quad (28)$$

is just a constant. Since $n(u, \tau)$ follows zero-mean Gaussian distribution, so $|Z_m(u; \tau, F_{D_1}, \cdots, F_{D_M})|$ of (18) follows Rician distribution with direct path value

$$\lambda = \alpha E[\sum_{i=1, i\neq m}^{M} \text{sinc}[\pi(i - m + F_{D_i}T)]$$

$$+ \frac{\sin[\pi(F_{D_m} + \beta\tau)(T - |\tau|)]}{T\pi(F_{D_m} + \beta\tau)}] \quad (29)$$

Since τ and F_{D_i} are uncertain and zero-mean, so we just use the approximation

$$\lambda = \alpha E \quad (30)$$

which is obtained when τ and F_{D_i} equal to 0.

Let $y_m \triangleq |Z_m(u; \tau, F_{D_1}, \cdots, F_{D_M})|$, then the probability density function (pdf) of y_m is

$$f(y_m) = \frac{2y_m}{\sigma^2} \exp[-\frac{(y_m^2 + \lambda^2)}{\sigma^2}] I_0(\frac{2\lambda y_m}{\sigma^2}) \quad (31)$$

where σ^2 is the noise power (with I and Q sub-channel power $\sigma^2/2$), and $I_0(\cdot)$ is the zero-order modified Bessel function of the first kind. Let $\mathbf{y} \triangleq [y_1, y_2, \cdots, y_M]$, then the pdf of $\mathbf{y}$ is

$$f(\mathbf{y}) = \prod_{m=1}^{M} f(y_m) \quad (32)$$

The ML-ATR algorithm to decide a target category C based on $\mathbf{y}$ can be expressed as,

$$C = \arg \max_{n=1,\cdots,N} f(\mathbf{y}|\lambda = E|\alpha_n|)$$

$$= \arg \max_{n=1,\cdots,N} \prod_{m=1}^{M} \frac{2y_m}{\sigma^2} \exp[-\frac{(y_m^2 + E^2\alpha_n^2)}{\sigma^2}] I_0(\frac{2E|\alpha_n|y_m}{\sigma^2})$$

V. Simulations

Radar sensor networks will be required to detect a broad range of target classes. In this paper, we applied our ML-ATR to automatic target recognition with delay-doppler uncertainty. We assume that the domain of target classes is known a priori (N in Sections IV-A and IV-B), and that the RSN is confined to work only on the known domain.

TABLE I
RCS values at microwave frequency for 6 targets.

Index n	Target	RCS
1	Small single-engine aircraft	1
2	Large flighter aircraft	6
3	Medium bomber or jet airliner	20
4	Large bomber or jet airliner	40
5	Jumbo jet	100
6	Pickup truck	200

For fluctuating target recognition, our targets have 6 classes with different RCS values, which are summarized in Table I[18]. We assume the fluctuating targets follow "Swerling 2" model (Rayleigh with pulse-to-pulse decorrelation), and assume the RCS value listed in Table I to be the standard deviation (std) γ_n of RCS $\alpha_n(u)$ for target n. We applied the ML-ATR algorithm in Section IV-A (for fluctuating target case) for target recognition within the six targets domain. We chose $T = 0.1ms$ and $\beta = 10^6$. At each average SNR value, we ran Monte-Carlo simulations for 10^5 times for each target. In Fig. 2(a)(b)(c), we plot the average ATR error for fluctuating targets with different delay-doppler uncertainty and compared the performances of single radar system, 5-radar RSN, and 10-radar RSN. Observe these three figures:

1) The two RSNs vastly reduce the ATR error comparing to a single radar system in ATR with delay-doppler uncertainty, e.g., the 10-radar RSN can achieve ATR error 2% comparing against the single radar system with ATR error 37% at $SNR = 32dB$ with delay-doppler uncertainty $\tau \in [-0.1T, 0.1T]$ and $F_{D_i} \in [-200Hz, 200Hz]$.
2) Our LFM waveform design can tolerate reasonable delay-doppler uncertainty which are testified by Fig. 2(b)(c).
3) According to Skolnik[18], radar performance with probability of recognition error (p_e) less than 10%

is good enough. Our 10-radar RSN with waveform-diversity can have probability of ATR error much less than 10% for the average ATR for all targets. However, the single radar system has probability of ATR error much higher than 10%. Our RSN with waveform diversity is very promising to be used for real-world ATR.

4) Observe Fig. 2(a)(c), the average probability of ATR error in 2(c) is not as sensitive to the SNR as that in 2(a), i.e., ATR error curve slope becomes flat with higher delay-doppler uncertainty, which means the delay-doppler uncertainty can dominate the ATR performance when it's too high.

For non-fluctuating target recognition, our targets have 6 classes with different RCS values, which are summarized in Table I[18]. We applied the ML-ATR algorithms in Section IV-B (for nonfluctuating target case) to classify an unknown target as one of these 6 target classes. We chose $T = 0.1ms$ and $\beta = 10^6$. At each average SNR value, we ran Monte-Carlo simulations for 10^5 times for each target. In Fig. 3(a)(b)(c), we plotted the probability of ATR error with different delay-doppler uncertainty. Observe these figures,

1) The two RSNs tremendously reduce the ATR error comparing to a single radar system in ATR with delay-doppler uncertainty, e.g., the 10-radar RSN can achieve ATR error 9% comparing against the single radar system with ATR error 22% at $SNR = 22dB$ with delay-doppler uncertainty $\tau \in [-0.2T, 0.2T]$ and $F_{D_i} \in [-500Hz, 500Hz]$.
2) Comparing Fig. 2(a)(b)(c) against Fig. 3(a)(b)(c), the gain of 10-radar RSN for fluctuating target recognition is much larger than that for non-fluctuating target recognition, which means our RSN has better capacity to handle the fluctuating targets. In real world, fluctuating targets are more meaningful and realistic.
3) Comparing Fig. 3(a)(b)(c) against Fig. 2(a)(b)(c), the ATR needs much lower SNR for nonfluctuating target recognition because Rician distribution has direct path component.

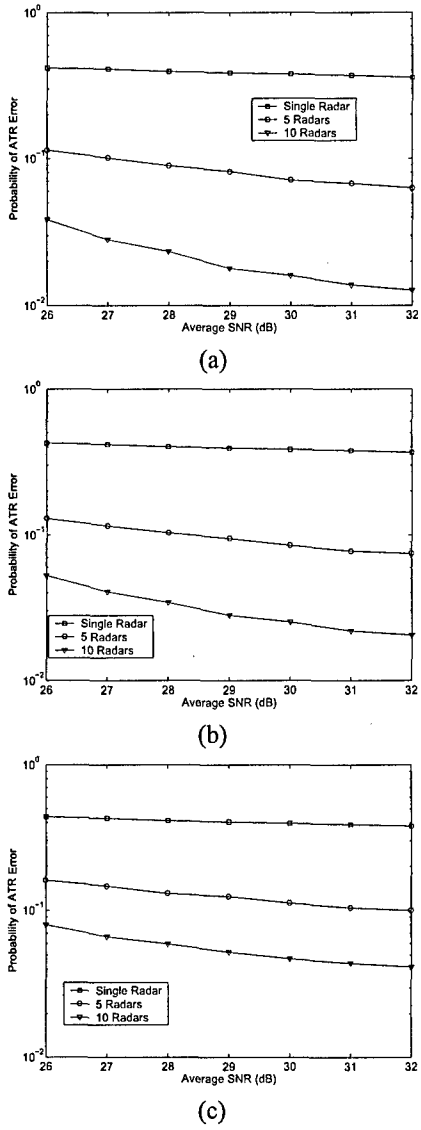

Fig. 2. The average probability of ATR error for 6 *fluctuating* targets with different delay-doppler uncertainty. (a) no delay-doppler uncertainty, (b) with delay-doppler uncertainty, $\tau \in [-0.1T, 0.1T]$ and $F_{D_i} \in [-200Hz, 200Hz]$, and (c) with delay-doppler uncertainty, $\tau \in [-0.2T, 0.2T]$ and $F_{D_i} \in [-500Hz, 500Hz]$.

VI. Conclusions and Future Works

We have studied LFM waveform design and diversity in radar sensor networks (RSN). We showed that the LFM waveforms can co-exist if the carrier frequency spacing is $1/T$ between two radar waveforms. We made analysis on interferences among waveforms in RSN and proposed a RAKE structure for waveform diversity combining in RSN. We applied the RSN to automatic target recognition (ATR) with delay-doppler uncertainty and proposed maximum-likehood (ML)-ATR algorithms for fluctuating target and non-fluctuating target. Simulation results show that RSN using our waveform diversity-based ML-ATR algorithm performs much better than single radar system for fluctuating targets and nonfluctuating targets recognition. It is also demonstrated that our LFM waveform-based RSN can handle the delay-doppler uncertainty which quite often happens for ATR in target search phase.

In this paper, the ATR is for single target recognition. We will continuously investigate the ATR when multiple targets co-existence in RSN and each target has delay-doppler uncertainty. In our waveform diversity combining,

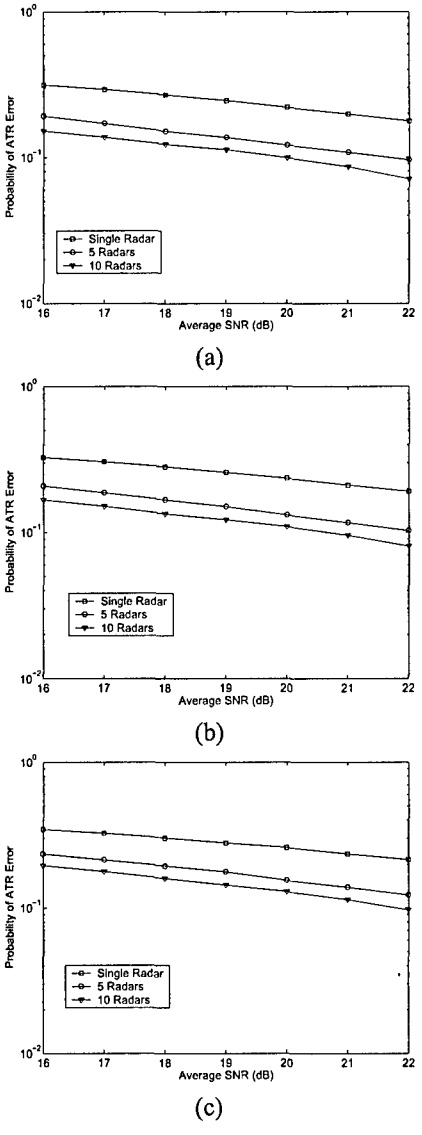

Fig. 3. The average probability of ATR error for 6 *nonfluctuating* targets with different delay-doppler uncertainty. (a) no delay-doppler uncertainty, (b) with delay-doppler uncertainty, $\tau \in [-0.1T, 0.1T]$ and $F_{D_i} \in [-200Hz, 200Hz]$, and (c) with delay-doppler uncertainty, $\tau \in [-0.2T, 0.2T]$ and $F_{D_i} \in [-500Hz, 500Hz]$.

we have used spatial diversity combining in this paper. We will further investigate spatial-temporal-frequency combining for RSN waveform diversity.

ACKNOWLEDGEMENT

This work was supported by the U.S. Office of Naval Research (ONR) Young Investigator Program Award under Grant N00014-03-1-0466.

The author would like to thank ONR Program Officer Dr. Rabinder N. Madan for his direction and insightful discussion on radar sensor networks.

REFERENCES

[1] P. Baggenstoss, "Adaptive pulselength correction (APLECORR): a strategy for waveform optimization in ultrawideband active sonar," *IEEE Trans on Oceanic Engineering*, vol. 23, no. 1, pp. 1-11, 1998.

[2] C. E. Baum, et al, "The singularity expansion method and its application to target identification", *Proc. of the IEEE*, vol 79, no. 10, Oct 1991.

[3] M. R. Bell, "Information theory and radar waveform design", *IEEE Trans on Information Theory*, vol. 39, no. 5, pp. 1578-1597, Sept 1993.

[4] H. Deng, "Synthesis of binary sequences with good correlation and cross-correlation properties by simulated annealing," *IEEE Trans on Aerospace and Electronic Systems*, vol. 32, no. 1, Jan 1996.

[5] R. Fitzgerald, "Effects of range-doppler coupling on chirp radar tracking acuracy," *IEEE Trans on Aerospace and Eletronic Systems*, vol. 10, pp. 528-532, July 1974.

[6] T.-C. Hou and T-J. Tsai, " An access-based clustering protocol for multihop wireless ad hoc networks," *IEEE J. Selected Areas in Communications*, vol. 19, no. 7, pp. 1201-1210, July 2001.

[7] A. Iwata, C. C. Chiang, G. Pei, M. Gerla, and T. W. Chen, " Scalable routing strategies for ad hoc networks," *IEEE J. Selected Areas in Communications*, vol. 17, pp. 1369-1379, 1999.

[8] R. A. Johnson and E. L. Titlebaum, "Range Doppler Uncoupling in the Doppler Tolerant Bat Signal", *Proc. of IEEE Ultrasonics Symposium*, New York, pp. 64-67, 1972.

[9] D. Kershaw and R. Evans, "Optimal waveform selection for tracking system", *IEEE Trans on Information Theory*, vol. 40, no. 5, pp. 1536-1550, 1994.

[10] Q. Liang, "Waveform Design and Diversity in Radar Sensor Networks: Theoretical Analysis and Application to Automatic Target Recognition," accepted by *Int'l Workshop on Wireless Ad Hoc and Sensor Networks*, June 2006, New York.

[11] C. R. Lin and M. Gerla, "Adaptive clustering in mobile wireless networks," *IEEE J. Selected Areas in Communications*, vol. 16, pp. 1265-1275, 1997.

[12] R. Niu, P. Willett, and Y. Bar-Shalom, "Tracking consideration in selection of radar waveform for range and range-rate measurements", *IEEE Transactions on Aerospace and Electronic Systems*, Vol. 38, No. 2, 2002.

[13] A. Papandreou, G. F. Boudreaux-Bartels, and S. M. Kay, "Detection and estimation of generalized chirps using time-frequency representations", *Twenty-Eighth Asilomar Conference on Signals, Systems and Computers*, vol. 1, pp. 50-54, Oct. 1994.

[14] C. E. Perkins, "Chapter 4, Cluster-Based Networks," *Ad Hoc Networking*, Edited by C. E. Perkins, pp. 75-138, Addison-Wesley, 2001.

[15] J. Roman, M. Rangaswamy, D. Davis, Q. Zhang, B. Himed, and J. Michels, "Parametric adaptive matched filter for airborne radar applications," *IEEE Trans. Aerosp. Electron. Syst.*, vol. 36, no. 2, pp. 677-692, 2000.

[16] M. A. Richards, *Fundamentals of Radar Signal Processing*, McGraw-Hill Companies, New York, 2005.

[17] T.K. Sarkar and N. Sangruji, "An adaptive nulling system for a narrow-band signal with a look-direction constraint utilizing the conjugate gradient method," *IEEE Trans. Antennas Propagat.*, vol. 37, no. 7, pp. 940-944, July 1989.

[18] M. I. Skolnik, *Introduction to Radar Systems*, 3rd ed, New York, McGraw Hill, 2001.

[19] P. Swerling, "Probability of detection for fluctuating targets", *IRE Trans on Information Theory*, vol. 6, pp. 269-308, April 1960.

[20] Y. Sun, P. Willett, and R. Lynch, "Waveform fusion in sonar signal processing", *IEEE Transactions on Aerospace and Electronic Systems*, Vol. 40, No. 2, 2004

[21] S. Sowelam and A. Tewfik, "Waveform selection in radar target classification," *IEEE Trans on Information Theory*, vol. 46, no. 3, pp. 1014-1029, 2000.

KUPS: Knowledge-based Ubiquitous and Persistent Sensor networks for Threat Assessment

Qilian Liang
Department of Electrical Engineering
416 Yates Street, Room 518
University of Texas at Arlington
Arlington, TX 76019-0016 USA
E-mail: liang@uta.edu

Abstract— **In this paper, we propose a Knowledge-based Ubiquitous and Persistent Sensor networks (KUPS) for threat assessment, of which "sensor" is a broad characterization concept. It means diverse data or information from ubiquitous and persistent sensor sources such as organic sensors and human intelligence sensors. Our KUPS for threat assessment consists of two major steps: threat detection using fuzzy logic systems and threat parameter estimation using radar sensor networks. Our fuzzy logic systems can combine the linguistic knowledge from different intelligent sensors. We propose a maximum-likelihood (ML) estimation algorithm for target RCS parameter estimation, and we show that our ML estimator is unbiased and the variance of parameter estimation matches the Cramer-Rao lower bound. Simulations further validate these theoretical results.**

I. Introduction and Motivation

In current and future military operational environments, such as Global War on Terrorism (GWOT) and Maritime Domain Awareness (MDA), warfighters require technologies evolved to support information needs regardless of location and consistent with the users level of command or responsibility and operational situation. To support this need, the DoD has developed the concept of Network Centric Warfare (NCW), defined as "*military operations that exploit state-of-the-art information and networking technology to integrate widely dispersed human decision makers, situational and targeting sensors, and forces and weapons into a highly adaptive, comprehensive system to achieve unprecedented mission effectiveness.*"

Some works have been reported on threat assessment. In [5], an intelligent threat assessment processor using genetic algorithms and fuzzy logic was proposed. In [16], threat assessment was studied in tactical airborne environments. In [8], neural network was applied to threat assessment for automated visual surveillance. In [4], an intelligent assistant to provide automatic situation and threat advice in the Air Defence Ground Environment was proposed. In [1], a situation and threat assessment model based on group analysis was proposed. A situation/threat assessment fusion system was proposed in [2]. Other approaches include multiple attribute decision making[3], bayesian networks[17], etc.

Current shortfalls in warfighting functionality result from limitations in technology. For example, accurate and timely information about battlespace objects and events is not available to support warfighter decision making, (includes reliable location, tracking, combat identification, and targeting information). Too often, the characteristics of objects that are not of interest will be similar to those of threat objects. The conventional approach to false alarm control is to reduce sensitivity of the radar in areas of clutter, using Sensitivity Time Control (STC) [21]. However, this approach is not effective for small and slow objects. In [9], we proposed a maximum-likelihood (ML) automatic target recognition (ATR) algorithm using constant frequency (CF) waveform design and diversity, and perfect delay-doppler are assumed in ATR. In [10], we applied linear frequency modulation (LFM) waveform design and diversity to ATR with delay-doppler uncertainty. The above two approaches assumed that different targets in the domain-of-classification have different radar cross section (RCS), e.g., bird has RCS value $0.01m^2$ and conventional unmanned winged missle has RCS value $0.5m^2$. However, different targets may have the same RCS values, e.g., a man and a small single-engine aircraft have the same RCS value $1m^2$ at microwave frequencies [21]. Besides, different threat targets, such as missile and large aircraft, may need different combat action, so we have to classify the threat target type. In this paper, we propose Knowledge-based Ubiquitous and Persistent Sensor networks (KUPS) for Threat Assessment.

The rest of this paper is organized as follows. In Section II, we introduce a new concept, Knowledge-based Ubiquitous and Persistent Sensor networks (KUPS); in Section III, we propose Situation-Aware Knowledge-Based Threat Assessment Using INT Sensors; in Section IV, we

propose a maximum-likelihood estimation algorithm for threat target RCS parameter estimation using radar sensor network and provide Monte Carlo simulation results. In Section V, we conclude this paper and discuss future research.

II. Introduction to Knowledge-based Ubiquitous and Persistent Sensor networks (KUPS): A New Concept

In this paper, we propose a Network Centric Warfare model, Knowledge-based Ubiquitous and Persistent Sensor networks (KUPS), of which "sensor" is a broad characterization concept. It means diverse data or information from ubiquitous and persistent sensor sources such as

- Organic sensors (e.g., radar, electro-optic and infrared, acoustic, and non-acoustic) deployed on air, ground, surface, or unattended platforms.
- Signals Intelligence (SIGINT) including Electronic Intelligence (ELINT) and Communication Intelligence (COMINT), for example, it can assign meaningful metadata to each collection, and metadata is the standardized characterization of data providing descriptors (such as stability, activity, membership, or structure).
- Human Intelligence (HUMINT), e.g., to identify specific people/cells/groups and relationships.
- Measurement and Signatures Intelligence (MASINT), e.g., to provide specific weapon system identifications, chemical compositions and material content.
- Imagery Intelligence (IMINT), e.g., to track vehicles through urban area.
- Open Source Intelligence (OSINT), e.g., to provide text data collection.

All these sources of information need to be integrated via "sensor networking" to accomplish a mission. In this paper, we apply KUPS to threat assessment, and the organic sensors we use are pulse doppler radars.

Our KUPS for threat assessment is a hierarchical architecture which consists of two major steps:

1) Step 1: Perform situation-aware knowledge-based threat assessment using INT sensors (e.g. SIGINT, HUMINT sensors). Fuzzy rules are used to represent the linguistic knowledge uncertainties from HUMINT sensors, and fuzzy logic systems are used to perform knowledge-based decision making on threat assessment (e.g., threat or non-threat), If it is assessed as a non-threat, then stops; if it is assessed as a threat, then go to the next step to classify what kind of target this threat is.
2) Step 2: Perform target RCS value estimation using radar sensor networks. We propose a maximal-likelihood (ML) estimation algorithm to estimate target RCS parameter value using radar sensor networks. Based on the estimated RCS parameter, the KUPS will advise what kind of target this threat is. The ML estimation algorithm can help to estimate the RCS parameter θ (parameter in Rayleigh distribution for fluctuating target). However, same RCS parameter may mean different targets, threat or non-threat. For example, for $\theta = 2$, the target can be a small flighter aircraft, a small pleasure boat, a bicycle[21], or any other similar size target. So we have to use Step 1 to make decision first, and only threat target requires further classification for further action.

We will discuss these two steps in the following sections.

III. Situation-Aware Knowledge-Based Threat Assessment Using INT Sensors

In knowledge-based threat assessment using INT sensors, fuzzy rules are used to represent the linguistic and numerical knowledge uncertainties from INT sensors, and fuzzy logic systems are used to perform knowledge-based decision making on threat assessment. We give a brief introduction on fuzzy logic systems first.

A. Overview of Fuzzy Logic Systems

Figure 1 shows the structure of a fuzzy logic system (FLS) [12]. When an input is applied to a FLS, the inference engine computes the output set corresponding to each rule. The defuzzifer then computes a crisp output from these rule output sets. Consider a p-input 1-output FLS, using singleton fuzzification, *center-of-sets* defuzzification [14] and "IF-THEN" rules of the form

$$R^l: \text{IF } x_1 \text{ is } \mathrm{F}_1^l \text{ and } x_2 \text{ is } \mathrm{F}_2^l \text{ and } \cdots \text{ and } x_p \text{ is } \mathrm{F}_p^l, \text{ THEN } y \text{ is } \mathrm{G}^l.$$

Assuming singleton fuzzification, when an input $\mathbf{x}' = \{x_1', \ldots, x_p'\}$ is applied, the degree of firing corresponding to the lth rule is computed as

$$\mu_{\mathrm{F}_1^l}(x_1') \star \mu_{\mathrm{F}_2^l}(x_2') \star \cdots \star \mu_{\mathrm{F}_p^l}(x_p') = \mathcal{T}_{i=1}^{p} \mu_{\mathrm{F}_i^l}(x_i') \quad (1)$$

where $\star$ and $\mathcal{T}$ both indicate the chosen t-norm. There are many kinds of defuzzifiers. In this paper, we focus, for illustrative purposes, on the center-of-sets defuzzifier [14]. It computes a crisp output for the FLS by first computing the centroid, c_{G^l}, of every consequent set G^l, and, then computing a weighted average of these centroids. The weight corresponding to the lth rule consequent centroid is the degree of firing associated with the lth rule, $\mathcal{T}_{i=1}^{p} \mu_{\mathrm{F}_i^l}(x_i')$, so that

$$y_{cos}(\mathbf{x}') = \frac{\sum_{l=1}^{M} c_{\mathrm{G}^l} \mathcal{T}_{i=1}^{p} \mu_{\mathrm{F}_i^l}(x_i')}{\sum_{l=1}^{M} \mathcal{T}_{i=1}^{p} \mu_{\mathrm{F}_i^l}(x_i')} \quad (2)$$

where M is the number of rules in the FLS.

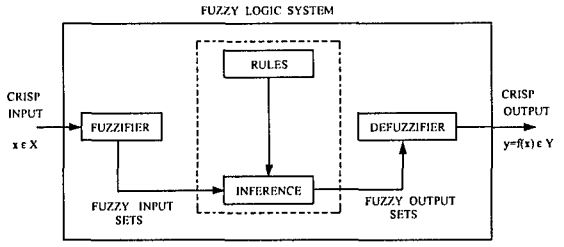

Fig. 1. The structure of a fuzzy logic system.

B. Situation-aware Knowledge-based Threat Assessment Using Fuzzy Logic Systems

In our FLS design for threat assessment, we will consider the following knowledge-based antecedents:

1) The number of switches from non-maneuvering set to the maneuvering set. When a target is beginning a maneuver from a non-maneuvering class, the tracking system can switch the algorithms applied to the problem from a non-maneuvering set to the maneuvering set. The errors in distance from where the tracker estimates the position of a target and the actual position can be very large when the incorrect motion models are applied to the problem. Additionally, when the tracker does finally catch up to the target after the maneuver, the track will "jump" across the operator's scope giving a very unrealistic and unreliable picture of what that target is actually doing. So a threat target will quite often switch from a non-maneuvering set to the maneuvering set, and vice versa, to avoid being tracked all the time. This knowledge can be used as an antecedent to make threat assessment.
2) The frequency of appearance of such type of target based on some a priori knowledge such as archival radar data. Generally threat targets are new comparing to archival radar data.
3) The importance of geolocation of this target based on the geographical information systems (GISs). Examples of important geolocations include large metroplex, landmarks, military bases, airport, etc. Threats happen quite often in such areas.

The above three antecedents are all knowledge-based and it can be collected from the INT sensors. A typical rule using the above three antecedents can be

IF the number of switches from non-maneuvering set to the maneuvering set is *High*, and the frequency of appearance of such target is *Low*, and the importance of geolocation of such type of target is *High*, THEN the possibility that this target is a threat is *Very Strong*.

The linguistic variables used to represent each antecedent were divided into three levels: *Low*, *Moderate*, and *High*. The consequent – the possibility that this target is a threat – was divided into 5 levels, *Very Strong, Strong, Medium, Weak, Very Weak*. So we need to set up $3^3 = 27$ (because every antecedent has 3 fuzzy sub-sets, and there are 3 antecedents) rules for this FLS. Table I summarizes the fuzzy rules we used in this paper. We used trapezoidal membership functions (MFs) to represent *low*, and *high*, and triangle MFs to represent *moderate*. We show these MFs in Fig. 2.

TABLE I

FUZZY RULES USED IN THE KUPS. ANTE 1 IS THE NUMBER OF SWITCHES FROM NON-MANEUVERING SET TO THE MANEUVERING SET OR VICE VERSA; ANTE 2 THE FREQUENCY OF APPEARANCE OF SUCH TYPE OF TARGET; ANTE 3 IS THE IMPORTANCE OF GEOLOCATION OF THIS TARGET; AND CONSEQUENT IS THE POSSIBILITY THAT THIS TARGET IS A THREAT.

Rule #	Ante 1	Ante 2	Ante 3	Consequent
1	low	low	low	Weak
2	low	low	moderate	Medium
3	low	low	high	Strong
4	low	moderate	low	Very Weak
5	low	moderate	moderate	Weak
6	low	moderate	high	Medium
7	low	high	low	Very Weak
8	low	high	moderate	Weak
9	low	high	high	Medium
10	moderate	low	low	Medium
11	moderate	low	moderate	Strong
12	moderate	low	high	Very Strong
13	moderate	moderate	low	Weak
14	moderate	moderate	moderate	Medium
15	moderate	moderate	high	Strong
16	moderate	high	low	Very Weak
17	moderate	high	moderate	Weak
18	moderate	high	high	Medium
19	high	low	low	Medium
20	high	low	moderate	Strong
21	high	low	high	Very Strong
22	high	moderate	low	Weak
23	high	moderate	moderate	Medium
24	high	moderate	high	Strong
25	high	high	low	Very Weak
26	high	high	moderate	Weak
27	high	high	high	Moderate

For every input (x_1, x_2, x_3), the output is computed using

$$y(x_1, x_2, x_3) = \frac{\sum_{l=1}^{27} \mu_{\mathrm{F}_l^1}(x_1)\mu_{\mathrm{F}_l^2}(x_2)\mu_{\mathrm{F}_l^3}(x_3)c_{avg}^l}{\sum_{l=1}^{27} \mu_{\mathrm{F}_l^1}(x_1)\mu_{\mathrm{F}_l^2}(x_2)\mu_{\mathrm{F}_l^3}(x_3)} \quad (3)$$

By repeating these calculations for $\forall x_i \in [0, 10]$, we obtain a hypersurface $y(x_1, x_2, x_3)$. Since it's a 4-D surface (x_1, x_2, x_3, y), it's impossible to be plot visually.

If we have $x_3 = 1$, and two other antecedents, x_1 and x_2 are variables, for every input $(x_1, x_2, 1)$, the output is

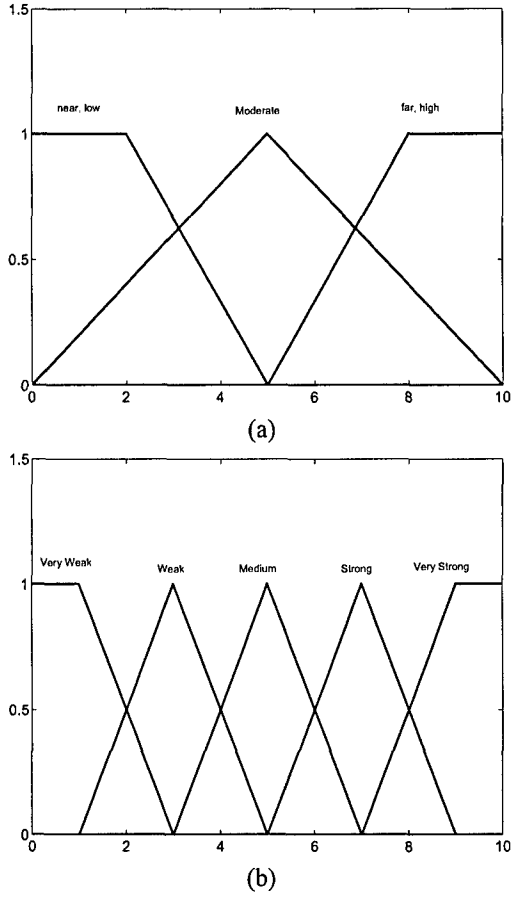

Fig. 2. The MFs used to represent the linguistic labels. (a) MFs for antecedents, and (b) MFs for consequent.

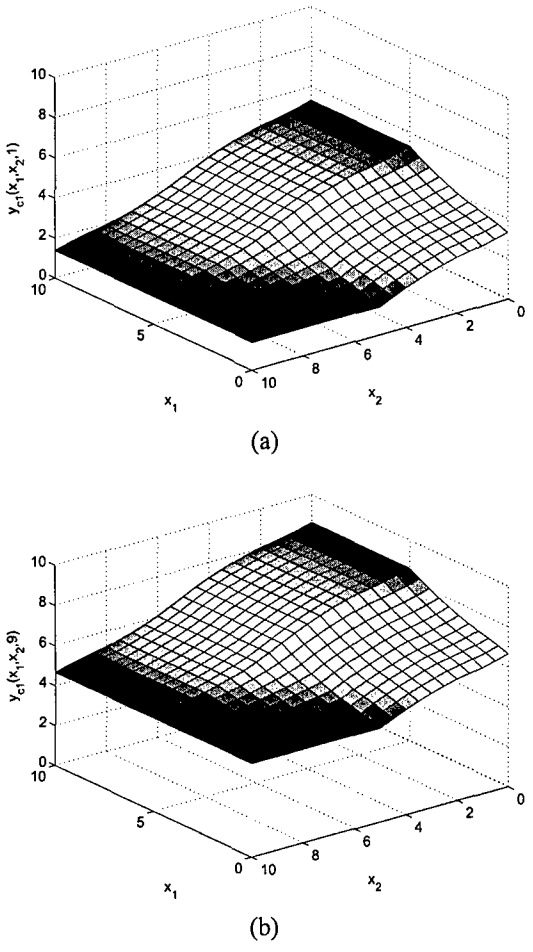

Fig. 3. The threat assessment surface for fixed importance of geolocation of this target (x_3), (a) when $x_3 = 1$, and (b) when $x_3 = 9$.

computed using

$$y(x_1, x_2, 1) = \frac{\sum_{l=1}^{27} \mu_{\mathrm{F}_l^1}(x_1)\mu_{\mathrm{F}_l^2}(x_2)\mu_{\mathrm{F}_l^3}(1)c_{cos}^l}{\sum_{l=1}^{27} \mu_{\mathrm{F}_l^1}(x_1)\mu_{\mathrm{F}_l^2}(x_2)\mu_{\mathrm{F}_l^3}(1)} \quad (4)$$

By repeating these calculations for $\forall x_1 \in [0, 10]$ and $\forall x_2 \in [0, 10]$, we obtain a hypersurface $y(x_1, x_2, 1)$, as plotted in Fig. 3(a). In contrast, if we have $x_3 = 9$, and two other antecedents, x_1 and x_2 are variables, similarly we obtain another surface $y(x_1, x_2, 9)$, as plotted in Fig. 3(b). Observe Fig. 3ab, the importance of geolocation of a target (x_3) makes a big difference in threat assessment, and the number of switches from non-maneuvering set to the maneuvering set or vice versa (x_1) and the frequency of appearance of such target (x_2) also play very important role even when the importance of geolocation (x_3) is the same.

IV. Target RCS Value Estimation Using Radar Sensor Networks

A. RCS and RCS Voltage for Fluctuating Target

Most radar analysis and measurement programs emphasize RCS measurements, which are proportional to received power. RCS is the fictional area over which the transmitter power density must be intercepted to collect a total power that would account for the received power density. Typical values of RCS for targets of interests range from $0.01m^2$ to hundreds of square meters[21]. Fluctuating target modeling is more realistic in which the target RCS is drawn from either the Rayleigh/exponential or chi-square of degree four pdf. The Rayleigh/exponential model describes the behavior of a complex target consisting of many scatters, none of which is dominant. The fourth-degree chi-square models targets having many scatters of similar strength with one dominant scatter. Based on

different combinations of pdf and decorrelation characteristics (scan-to-scan or pulse-to-pulse decorrelation), four Swerling models are used[20]. In this paper, we will focus on "Swerling 2" model which is exponential distribution with pulse-to-pulse decorrelation. The pulse-to-pulse decorrelation implies that each individual pulse results in an independent value for RCS. Sometime the RCS voltage value (square root of RCS), is of interest, particularly for use in simulations to model the composite echo from a multiple scatterer target. The RCS voltage value is the square root of RCS, so the probability density function of RCS voltage follows Rayleigh distribution[20]. In this paper, we apply radar sensor network to estimate the RCS value.

B. Introduction to Radar Sensor Networks

In [9], we performed some theoretical studies on constant frequency (CF) pulse waveform design and diversity in radar sensor networks (RSN): (1) the conditions for waveform co-existence, (2) interferences among waveforms in RSN, (3) waveform diversity combining in RSN.

For radar sensor networks, the waveforms from different radars will interfere with each other. We choose the waveform for radar i as

$$x_i(t) = \sqrt{\frac{1}{T}} \exp[j2\pi(\beta + \delta_i)t] \quad -T/2 \le t \le T/2 \quad (5)$$

which means there is a frequency shift δ_i for radar i. To minimize the interference from one waveform to the other, optimal values for δ_i should be determined to have the waveforms orthogonal to each other, i.e., let the cross-correlation between $x_i(t)$ and $x_n(t)$ be 0, we showed that choosing $\delta_i = \frac{i}{T}$ in (5) can have orthogonal waveforms, i.e., the waveforms can co-exist if the carrier spacing is $1/T$ between two radar waveforms.

In RSN, The radar sensors are networked together in an ad hoc fashion. They do not rely on a preexisting fixed infrastructure, such as a wireline backbone network or a base station. They are self-organizing entities that are deployed on demand in support of various events surveillance, battlefield, disaster relief, search and rescue, etc. Scalability concern suggest a hierarchical organization of radar sensor networks with the lowest level in the hierarchy being a cluster. As argued in [11] [7] [6] [18], in addition to helping with scalability and robustness, aggregating sensor nodes into clusters has additional benefits:

1) conserving radio resources such as bandwidth;
2) promoting spatial code reuse and frequency reuse;
3) simplifying the topology, e.g., when a mobile radar changes its location, it is sufficient for only the nodes in attended clusters to update their topology information;
4) reducing the generation and propagation of routing information; and,
5) concealing the details of global network topology from individual nodes.

In RSN, each radar can provide their waveform parameters such as δ_i to their clusterhead radar, and the clusterhead radar can combine the waveforms from its cluster members.

In RSN with M radars, the received signal for clusterhead (assume it's radar 1) is

$$r_1(u,t) = \sum_{i=1}^{M} \alpha(u) x_i(t - t_i) \exp(j2\pi F_{D_i} t) + n(u,t) \quad (6)$$

where $x_i(t)$ is the transmitted CF waveform; $\alpha(u)$ stands for voltage of radar cross section (RCS); F_{D_i} is the doppler shift of target relative to waveform i; t_i is delay of waveform i, and $n(u,t)$ is additive white Gaussian noise (AWGN). In [9], we proposed a RAKE structure for waveform diversity combining, as illustrated by Fig. 4.

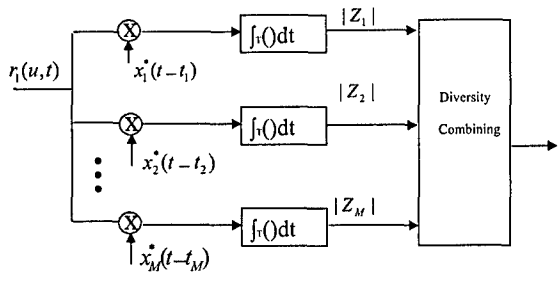

Fig. 4. Waveform diversity combining by clusterhead in RSN.

According to this structure, the received $r_1(u,t)$ is processed by a bank of matched filters, then the output of branch 1 (after integration) is[9]

$$\begin{aligned} & |Z_1(u; t_1, \cdots, t_M, F_{D_1}, \cdots, F_{D_M})| \\ = & \left| \int_{-T/2}^{T/2} r_1(u,t) x_1^*(t - t_1) ds \right| \quad (7) \\ = & \left| \int_{-T/2}^{T/2} [\sum_{i=1}^{M} \alpha_i(u) x_i(t - t_i) \exp(j2\pi F_{D_i} t) \right. \\ & \left. + n(u,t)] x_1^*(t - t_1) dt \right| \quad (8) \end{aligned}$$

where $\int_{-T/2}^{T/2} n(u,t) x_1^*(t - t_1) dt$ can easily be proved to be AWGN, so

$$|n(u,t_1)| \triangleq \left| \int_{-T/2}^{T/2} n(u,t) x_1^*(t - t_1) dt \right| \quad (9)$$

follows Rayleigh distribution. Assuming $t_1 = t_2 = \cdots = t_M = \tau$, then according to interference analysis in [9],

$$\begin{aligned} & |Z_1(u;\tau,F_{D_1},\cdots,F_{D_M})| \\ \approx & \sum_{i=2}^{M} |\alpha(u)\text{sinc}[\pi(i-1+F_{D_i}T)]| \\ + & \left|\frac{\alpha(u)\sin[\pi F_{D_1}(T-|\tau|)]}{T\pi F_{D_1}}\right| + |n(u,\tau)| \end{aligned} \quad (10)$$

Similarly, we can get the output for any branch m ($m = 1,2,\cdots,M$),

$$\begin{aligned} & |Z_m(u;\tau,F_{D_1},\cdots,F_{D_M})| \\ \approx & \sum_{i=1,i\neq m}^{M} |\alpha(u)\text{sinc}[\pi(i-m+F_{D_i}T)]| \\ + & \left|\frac{\alpha(u)\sin[\pi F_{D_m}(T-|\tau|)]}{T\pi F_{D_m}}\right| + |n(u,\tau)| \end{aligned} \quad (11)$$

So $|Z_m(u;\tau,F_{D_1},\cdots,F_{D_M})|$ consists of three parts, signal (reflected signal from radar m waveform): $\left|\frac{\alpha(u)E\sin[\pi F_{D_m}(T-|\tau|)]}{T\pi F_{D_m}}\right|$, interferences from other waveforms: $\sum_{i=1,i\neq m}^{M}|\alpha(u)E\text{sinc}[\pi(i-m+F_{D_i}T)]|$, and noise: $|n(u,\tau)|$.

We can have three special cases for $|Z_m(u;\tau,F_{D_1},\cdots,F_{D_M})|$:

1) When $F_{D_1} = \cdots = F_{D_M} = 0$,

$$\begin{aligned} & |Z_m(u;\tau,0,0,\cdots,0)| \\ \approx & \left|\frac{\alpha(u)(T-|\tau|)]}{T}\right| + |n(u,\tau)| \end{aligned} \quad (12)$$

which means if there is no doppler mismatch, there will be no interference from other waveform.

2) If $\tau = 0$, then (11) becomes

$$\begin{aligned} & |Z_m(u;0,F_{D_1},\cdots,F_{D_M})| \\ \approx & \sum_{i=1,i\neq m}^{M} |\alpha(u)\text{sinc}[\pi(i-m+F_{D_i}T)]| \\ + & \left|\frac{\alpha(u)\sin[\pi F_{D_m}T]}{T\pi F_{D_m}}\right| + |n(u)| \end{aligned} \quad (13)$$

3) If $\tau = 0$, and $F_{D_1} = \cdots = F_{D_M} = 0$, then (11) becomes

$$|Z_m(u;0,0,0,\cdots,0)| \approx |\alpha(u)| + |n(u)| \quad (14)$$

Doppler mismatch happens quite often in target search where target velocity is not yet known. However, in target recognition, generally high-resolution measurements of targets in range ($\tau = 0$) and doppler are available, so (14) will be used for RCS value estimation.

How to combine all the Z_m's ($m = 1,2,\cdots,M$) are very similar to the diversity combining in communations to combat channel fading, and the combination schemes may be different for different applications. In this paper, we are interested in applying RSN waveform diversity to estimate the RCS parameter, γ^2. In this paper, we propose a maximum likelihood algorithm for RCS parameter estimation.

C. Maximum Likelihood Algorithm for RCS Parameter Estimation

For Swerling 2 model, the RCS voltage $|\alpha(u)|$ follows Rayleigh distribution and the I and Q subchannels of $\alpha(u)$ follow zero-mean Gaussian distributions with variance γ^2 (the RCS average power value). Assume

$$\alpha(u) = \alpha_I(u) + j\alpha_Q(u) \quad (15)$$

and $n(u) = n_I(u) + jn_Q(u)$ follows zero-mean complex Gaussian distribution with variance σ^2 for the I and Q subchannels.

According to (8), (11), and (14),

$$|Z_m(u;0,0,0,\cdots,0)| \approx |\alpha(u) + n(u)| \quad (16)$$

is a more accuate approximation. Since $\alpha(u)$ and $n(u)$ are zero-mean complex Gaussian random variables, so $\alpha(u)+n(u)$ is a zero-mean Gaussian random variable with variance $\gamma^2+\sigma^2$ for the I and Q subchannels, which means $y_m \triangleq |Z_m(u;0,0,\cdots,0)|$ follows Rayleigh distribution with parameter $\sqrt{\gamma^2+\sigma^2}$,

$$f(y_m) = \frac{y_m}{\gamma^2+\sigma^2}\exp[-\frac{y_m^2}{2(\gamma^2+\sigma^2)}] \quad (17)$$

The mean value of y_m is $\sqrt{\frac{\pi(\gamma^2+\sigma^2)}{2}}$, and variance is $\frac{(4-\pi)(\gamma^2+\sigma^2)}{2}$. The variance of signal is $\frac{(4-\pi)\gamma^2}{2}$ and the variance of noise is $\frac{(4-\pi)\sigma^2}{2}$.

Let $\mathbf{y} \triangleq [y_1, y_2, \cdots, y_M]$, then the pdf of $\mathbf{y}$ is

$$f(\mathbf{y}) = \prod_{m=1}^{M} f(y_m) \quad (18)$$

so the ML algorithm to estimate the RCS average value (γ^2), let

$$\theta \triangleq \gamma^2 \quad (19)$$

then (18) can be expressed as,

$$\begin{aligned} \hat{\theta}_{ML}(\mathbf{y}) &= \arg\sup_{\theta\in R^+} f(\mathbf{y}) \\ &= \arg\sup_{\theta\in R^+} \prod_{m=1}^{M} \frac{y_m}{\theta+\sigma^2}\exp[-\frac{y_m^2}{2(\theta+\sigma^2)}] \end{aligned} \quad (20)$$

Maximizing $f(\mathbf{y})$ is equivalently to maximizing $\log f(\mathbf{y})$ (natural logarithm),

$$\log f(\mathbf{y}) = \sum_{m=1}^{M}[\log(\frac{y_m}{\theta+\sigma^2}) - \frac{y_m^2}{2(\theta+\sigma^2)}] \quad (21)$$

since it is a continuous function for $y_m > 0$ and $\theta > 0$, so a necessary condition for the ML estimation is

$$\frac{\partial}{\partial\theta}\log f(\mathbf{y})|_{\theta=\hat{\theta}_{ML}(\mathbf{y})} = \frac{\sum_{m=1}^{M} y_m^2 - 2M(\theta+\sigma^2)}{2(\theta+\sigma^2)^2} = 0 \tag{22}$$

which has the unique solution

$$\hat{\theta}_{ML}(\mathbf{y}) = \frac{\sum_{m=1}^{M} y_m^2}{2M} - \sigma^2 \tag{23}$$

Considering $\theta \geq 0$,

$$\hat{\theta}_{ML}(\mathbf{y}) = \max\left[\frac{\sum_{m=1}^{M} y_m^2}{2M} - \sigma^2, 0\right] \tag{24}$$

Since

$$\frac{\partial^2}{\partial\theta^2}\log f(\mathbf{y})|_{\theta=\hat{\theta}_{ML}(\mathbf{y})} = -\frac{4M^3}{(\sum_{m=1}^{M} y_m^2)^2} < 0 \tag{25}$$

this solution gives the unique maximum of $\log f(\mathbf{y})$. The expectation of $\hat{\theta}_{ML}(\mathbf{y})$ is

$$\begin{aligned} E_\theta[\hat{\theta}_{ML}(\mathbf{y})] &= \int_0^\infty \frac{\sum_{m=1}^{M} y_m^2}{2M} f(y_m)dy_m - \sigma^2 \\ &= \int_0^\infty \frac{\sum_{m=1}^{M} y_m^2}{2M} \frac{y_m}{\theta+\sigma^2}\exp[-\frac{y_m^2}{2(\theta+\sigma^2)}]dy_m - \\ &= \theta \end{aligned}$$

so it's an unbiased estimator.

Fisher's information for this case can be computed via

$$I_\theta = -E_\theta[\frac{\partial^2}{\partial\theta^2}\log f(\mathbf{y})] = -E_\theta\left[\frac{M(\theta+\sigma^2) - \sum_{m=1}^{M} y_m^2}{(\theta+\sigma^2)^3}\right] \tag{28}$$

The mean value of y_m is $\sqrt{\frac{\pi(\theta+\sigma^2)}{2}}$, and variance is $\frac{(4-\pi)(\theta+\sigma^2)}{2}$, so the Cramer-Rao lower bound (CRLB) is

$$Var_\theta[\hat{\theta}(\mathbf{y})] \geq \frac{1}{I_\theta} = \frac{(\theta+\sigma^2)^2}{M} \tag{29}$$

Since $\frac{\partial}{\partial\theta}\log f(\mathbf{y})$ in (22) is of the form $k(\theta)[\hat{\theta}_{ML}(y) - E_\theta[\hat{\theta}(\mathbf{y})]$ for

$$k(\theta) = \frac{1}{4M(\theta+\sigma^2)^2} \tag{30}$$

we conclude that $\hat{\theta}_{ML}(\mathbf{y})$ can achieve the CRLB theoretically [13]. From 29, it's clear that CRLB is inverse proportionally to the number of radars M in RSN, which means RSN with larger M will have much lower CRLB.

D. Simulations

For fluctuating target with RCS parameter $\theta = 2$ (Rayleigh distribution), we ran Monte Carlo simulations for 10^6 realizations at each SNR value, and we applied the ML estimation algorithm to estimate the parameter $\hat{\theta}$ for each realization. In Fig. 5, we plotted the variance of the RCS ML estimator with different number of radars in RSN. Observe that

1) the actual variance of $\hat{\theta}$ matches exactly with the CRLB for different number of radars in RSN, which validates our theoretical results: our ML estimator on RCS parameter is an unbiased estimator and the variance of parameter estimation matches CRLB.
2) the actual variance of $\hat{\theta}$ reduces as M increases, and numerically it is reverse proportional to M as we shown in Section IV.

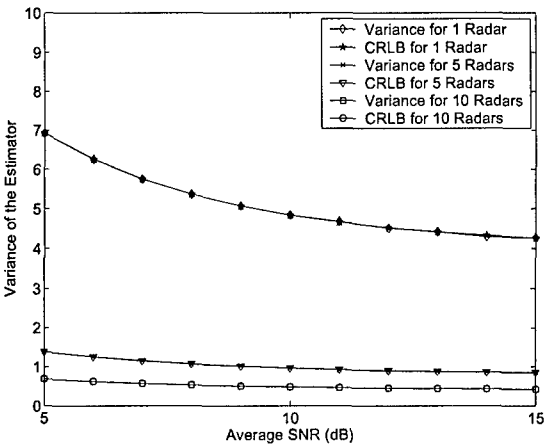

Fig. 5. Variance of the RCS ML estimator with different number of radars in RSN.

V. Conclusions and Future Works

We have proposed a Knowledge-based Ubiquitous and Persistent Sensor networks (KUPS) for threat assessment, of which "sensor" is a broad characterization concept, and it can be organic sensors, HUMINT sensors, SIGINT sensors, etc. Our KUPS for threat assessment consists of two major steps: threat detection using fuzzy logic systems and threat parameter estimation using radar sensor networks. Our fuzzy logic systems can combine the linguistic knowledge from different intelligent sensors which contains lots of uncertainties. We propose a ML estimation algorithm for target RCS parameter estimation. Theoretically we show that our ML estimator is unbiased and the variance of parameter estimation matches the Cramer-Rao lower bound. Simulations further validate these theoretical results.

The proposed techniques will increase the sensitivity and performance of existing and future NCW, enhancing ship self defense modes against stealthy, sea skimming, anti-ship cruise missiles. In future works, we will also infer intent of objects/entities, or groups of objects, in the regions of interest. We will also study methods for

constructing and learning a wide variety of models of threat behavior; methods for reasoning with uncertain and incomplete information for assessing threats from object activities.

ACKNOWLEDGEMENT

This work was supported by the U.S. Office of Naval Research (ONR) Young Investigator Program Award under Grant N00014-03-1-0466.

The author would like to thank ONR Program Officer Dr. Rabinder N. Madan for his direction and insightful discussion on radar sensor networks.

REFERENCES

[1] Y. Cai, et al, "A Situation and Threat Assessment Model Based on Group Analysis," *Proceedings of 2005 International Conference on Machine Learning and Cybernetics*, Aug. 2005, pp. 356 - 361.

[2] J. W. Choi; J. W. Joo; D. L. Cho, "Situation/Threat Assessment Fusion System (STAFS)," *Proceedings of the Fifth International Conference on Information Fusion*, July 2002, pp. 1374 - 1380.

[3] Q. Changwen, H. You, "A method of threat assessment using multiple attribute decision making," *6th International Conference on Signal Processing*, Aug. 2002, pp. 1091 - 1095.

[4] I. W. Dall, "Threat assessment without situation assessment," *Proc of Information, Decision and Control*, Feb. 1999, pp. 365 - 370.

[5] P. Gonsalves, el al, "Intelligent threat assessment processor (ITAP) using genetic algorithms and fuzzy logic," *Proceedings of the Third International Conference on Information Fusion*, 2000.

[6] T.-C. Hou and T-J. Tsai, " An access-based clustering protocol for multihop wireless ad hoc networks," *IEEE J. Selected Areas in Communications*, vol. 19, no. 7, pp. 1201-1210, July 2001.

[7] A. Iwata, C. C. Chiang, G. Pei, M. Gerla, and T. W. Chen, " Scalable routing strategies for ad hoc networks," *IEEE J. Selected Areas in Communications*, vol. 17, pp. 1369-1379, 1999.

[8] T. Jan, "Neural network based threat assessment for automated visual surveillance," *IEEE International Joint Conference on Neural Networks*, vol. 2, July 2004, pp. 1309 - 1312.

[9] Q. Liang, "Waveform Design and Diversity in Radar Sensor Networks: Theoretical Analysis and Application to Automatic Target Recognition," accepted by *Int'l Workshop on Wireless Ad Hoc and Sensor Networks*, June 2006, New York.

[10] Q. Liang, "Radar Sensor Networks: Algorithms for Waveform Design and Diversity with Application to ATR with Delay-Doppler Uncertainty," submitted to *EURASIP J. on Wireless Communications and Networking.*

[11] C. R. Lin and M. Gerla, "Adaptive clustering in mobile wireless networks," *IEEE J. Selected Areas in Communications*, vol. 16, pp. 1265-1275, 1997.

[12] J. M. Mendel, "Fuzzy Logic Systems for Engineering : A Tutorial," *Proceedings of the IEEE*, vol. 83, no. 3, pp. 345-377, March 1995.

[13] J. M. Mendel, *Lessons in Estimation Theory for Signal Processing, Communications, and Control*, Prentice-Hall, Upper Saddle River, NJ, 1995.

[14] J. M. Mendel, *Uncertain Rule-Based Fuzzy Logic Systems*, Prentice-Hall, Upper Saddle River, NJ, 2001.

[15] J. E. Manley, G. M. Mineart, A. E. Sheridan, "Underwater marine domain awareness for first responders: a low cost approach," *MTS/IEEE TECHNO-OCEAN '04* vol. 3, 2004, pp. 1695 - 1700.

[16] X. T. Nguyen, "Threat assessment in tactical airborne environments," *Proceedings of the Fifth International Conference on Information Fusion*, July 2002.

[17] N. Okello, G. Thorns, "Threat assessment using bayesian networks," *Proceedings of the Sixth International Conference of Information Fusion*, vol. 2, pp. 1102 - 1109, 2003.

[18] C. E. Perkins, "Chapter 4, Cluster-Based Networks," *Ad Hoc Networking*, Edited by C. E. Perkins, pp. 75-138, Addison-Wesley, 2001.

[19] J. Roman, M. Rangaswamy, D. Davis, Q. Zhang, B. Himed, and J. Michels, "Parametric adaptive matched filter for airborne radar applications," *IEEE Trans. Aerosp. Electron. Syst.*, vol. 36, no. 2, pp. 677-692, 2000.

[20] M. A. Richards, *Fundamentals of Radar Signal Processing*, McGraw-Hill Companies, New York, 2005.

[21] M. I. Skolnik, *Introduction to Radar Systems*, 3rd ed, New York, McGraw Hill, 2001.

[22] P. Swerling, "Probability of detection for fluctuating targets", *IRE Trans on Information Theory*, vol. 6, pp. 269-308, April 1960.

[23] G. Petterson, el al, "Multi-source integration and temporal situation assessment in air combat," *1999 Information, Decision and Control*, Feb. 1999, pp. 371 - 375.

[24] A. N. Steinberg, "An approach to threat assessment," *2005 8th International Conference on Information Fusion*, vol. 2, July 2005.

Orthogonal Waveform Design and Performance Analysis in Radar Sensor Networks (RSN)

Jing Liang and Qilian Liang
Department of Electrical Engineering
University of Texas at Arlington
416 Yates Street
Nedderman Hall, Rm 518
Arlington, TX 76019
Email: jliang@wcn.uta.edu, liang@uta.edu

Abstract— **In radar sensor networks (RSN), radar sensors are likely to interfere with each other if their waveforms are not properly designed. We propose orthogonal waveforms for RSN, which eliminate interference when no doppler shift is introduce. Additionally, this approach applies the advantage of spacial diversity through equal gain combination performed by clusterhead. When doppler shift is considered and interference is unavoidable, we analyzed the performance of this design not only in coherent RSN, but in noncoherent systems as well. The latter scenario is more challenging as doppler-shift uncertainty results in more complicated implementation. Monte Carlo simulation shows that our technique provides much better detection performance than single radar for fluctuating targets, in terms of probability of false alarm and miss detection. Conclusions are drawn based on our analysis and further related research areas are discussed.**

I. Introduction and Motivation

It is known to all that slow fluctuations of target radar cross section (RCS) result in radar target fades, which is a main factor in performance degradation [8]. Faced with the challenge from weak RCS targets, such as cruise missiles and stealth targets, modern radar sensors demand higher capability of accurate target detection and range estimation. In order to satisfy this requirement, much attention has been paid to waveform design.

Among the existing works, Bell [1] applied information theory to design radar waveforms. He demonstrated that when the transmitted radar waveform is scattered by the target, larger SIR is achieved, so in order to better detect target, distributing energy may be a perfect choice. Sowelam and Tewfik [2] studied signal selection procedure for sequential radar target classification. In their design, the criterion to chose signal is whether it maximizes the Kullback-Leiber information numbers. Their research focused on two-class signal selection and Gaussian unequal mean target models. In [3] Sun *et al.* applied several fusion schemes to study constant frequency (CF) and linear frequency modulated (LFM) waveforms, which improved detection probability and estimation accuracy. However, all the above research involves only single radar.

In nature, a network of multiple radar sensors can been introduced to combat performance degradation of single radar along with waveform optimization. These radar sensors are managed by an intelligent clusterhead that combines waveform diversity in order to satisfy the common goals of the network other than each radar operate substantively.

Apart from better performance, RSN are capable to solve blind speed problem. Radar blind speed occurs when the doppler shift is equal to the same or a multiple of the pulse repetition frequency (PRF). Under these circumstances, target return is suppressed so that a zero signal is obtained [7]. As for RSN, if PRF of each member is properly designed, for instance, co-prime to each other, the probability of blind speed occurrence will be tremendously reduced.

Although the idea of multistatic radar which employs multiple transmitters or receivers to sample the target static scattering behavior is not new, spatial diversity is still neonatal to radar research. Fishler *et al.* presented statistical MIMO radar system in [5]. Their system applied target spatial diversity, thus obtained approximately constant average received energy and superior detection performance to that achieved through coherent processing. However, effects of doppler shift and clutter were not considered. In [4], Liang performed theoretical studies on constant frequency (CF) pulse waveform design and proposed maximum-likehood (ML) automatic target recognition (ATR) approach for both nonfluctuaing and fluctuating targets. Nevertheless these studies also assumed no delay-doppler uncertainty.

This paper leans heavily on prior research on radar waveform design and spacial diversity. What distinguishes it is its detailed performance analysis for both coherent and noncoherent RSN when doppler shift is considered. The rest of this paper is organized as follows. Section II describes our propagation models. Section III and IV analyzes coherent and noncoherent detection respectively. Simulations are given in Section V and Section VI concludes the paper.

II. Waveform Model and Problem Formulation

We assume our RSN consists of N radars networked together in a self-organizing fashion. Their propagation and target model is shown in Fig.1. The ith radar transmits a

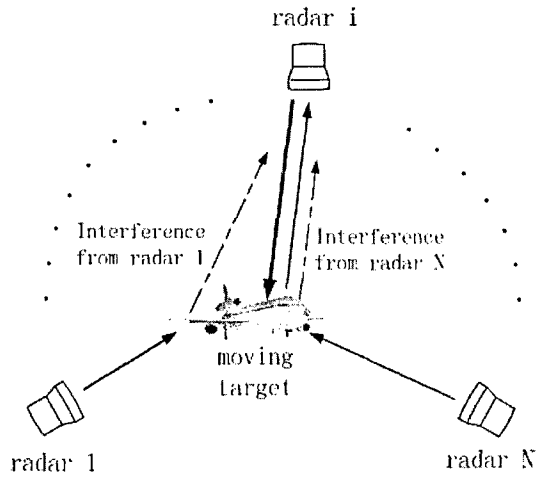

Fig. 1. Propagation and target model for RSN

waveform typically modeled as

$$\tilde{S}_i(t) = A_{si}(t) \cdot \sqrt{\frac{2}{T_p}} \cos[2\pi(f_c + \Delta_i)t] \quad (1)$$

where tilde on S_i denotes that the signal has been modulated. $A_{si}(t)$ is the constant amplitude pulse envelope [7]. $\sqrt{\frac{2}{T_p}}$ is a normalization factor to ensure that $\int_0^{T_p} \left\{\sqrt{\frac{2}{T_p}} \cdot \cos[2\pi(f_c + \Delta_i)t]\right\}^2 dt = 1$. Here T_p is the time duration for radar pulses and each oscillator of radar works at a different frequency: $f_i = f_c + \Delta_i, f_c \gg \Delta_i$, where f_c is the system carrier frequency and Δ_i must satisfies the following equation:

$$\Delta_k - \Delta_i = (k - i) \cdot \frac{1}{T_p} \quad (2)$$

Here k and i are unequal integers to provide orthogonality waveform for each radar member [9].

Consider a point moving target at an instant range R_i. t_i second after transmitting the pulse, the ith radar receives waveforms of useful back-scattered radiation from the target with inteference from other radar sensors as well as clutter and noise. The useful signal can be modeled as

$$\tilde{S_{ri}}(t) = A_i(t) \cdot \sqrt{\frac{2}{T_p}} \cos[2\pi(f_c + \Delta_i + f_{di})(t - t_i)] \quad (3)$$

where $A_i(t)$ represents amplitude of the returned useful signal. As a fluctuating target is more realistic than nonfluctuating object, it is more reasonable to apply "Swerling II" model in our situation and thus $A_i(t)$ follows Rayleigh distribution [8]. The target mobility introduces doppler shift in returned signal, which is denoted by f_{di}. Assume the target is moving at the speed v, than f_{di} is

$$f_{di} = \frac{v(f_c + \Delta_i)}{c} \cdot cos\phi \quad (4)$$

where c is the speed of light, and ϕ follows uniform distribution within $[0, 2\pi]$. As $f_c \gg \Delta_i$,

$$f_{di} \cong \frac{v f_c}{c} \cdot cos\phi \quad (5)$$

In addition, the estimated instant range to the target is $R_i = c \cdot \frac{t_i}{2}$ [6].

As all of the radar sensors are transmitting signals, the ith radar not only receives its own back-scattered waveform, but also scattered signals generated by other radars, and therefore under the condition of timing synchronization, interference waveforms received by the ith radar can be modeled as

$$\tilde{I}_i(t) = \sum_{k=1, k\neq i}^{N} B_k(t) \cdot \sqrt{\frac{2}{T_p}} \cos[2\pi(f_c + \Delta_k + f_{dk})(t - t_i)] \quad (6)$$

where $B_k(t)$ is the amplitude of interference from the kth radar, which also follows Rayleigh distribution, and f_{dk} is the doppler shift for kth radar. This is illustrated in Fig.1. As the interference from other radars is the dominant interference that results in target fade, we may ignore clutter under these circumstances. Apart from interference, the ith radar also receives additive white Gaussian noise (AWGN) $n_i(t)$ with mean value zero and variance $N_0/2$. Therefore, the combined received waveform for the ith radar is

$$\tilde{R}_i(t) = \tilde{S_{ri}}(t) + \tilde{I}_i(t) + n_i(t) \quad (7)$$

After introducing our propagation and target model, further analysis on coherent and noncoherent RSN are carried out respectively.

III. Coherent Detection

In coherent RSN, radar members are smart enough to extract the knowledge of the exact doppler shift introduced by moving targets, so based on the a-priori information, the demodulator of each radar can be constructed as shown in Fig.2. According

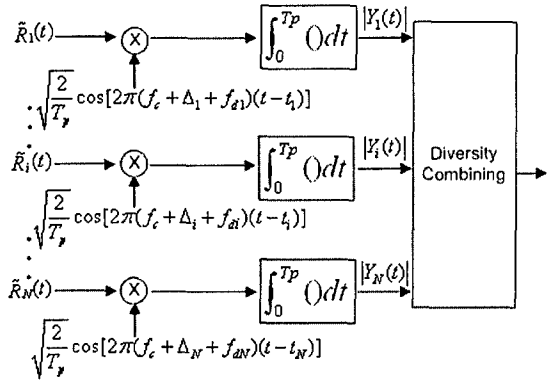

Fig. 2. Coherent RSN demodulation and waveform combining

to this structure, the combined received waveform $\tilde{R}_i(t)$ is

processed by its corresponding matched filter. The output of the ith branch $Y_i(t)$is

$$Y_i(t) = \int_{t_i}^{t_i+T_p} \tilde{R}_i(t) \cdot \sqrt{\frac{2}{T_p}} \cos[2\pi(f_c + \Delta_i + f_{di})(t - t_i)]dt \tag{8}$$

It can also be represented as

$$Y_i(t) = S_i(t) + I_i(t) + n_i(t) \tag{9}$$

where $S_i(t)$, $I_i(t)$, $n_i(t)$ denotes the output of useful signal, interference and noise respectively.

$$S_i(t) = \int_{t_i}^{t_i+T_p} \tilde{S_{ri}}(t) \cdot \sqrt{\frac{2}{T_p}} \cos[2\pi(f_c + \Delta_i + f_{di})(t - t_i)]dt \tag{10}$$

It can be easily derived that

$$S_i(t) = A_i(t) \tag{11}$$

Similarly, $I_i(t)$ is given by

$$I_i(t) = \int_{t_i}^{t_i+T_p} \tilde{I}_i(t) \cdot \sqrt{\frac{2}{T_p}} \cos[2\pi(f_c + \Delta_i + f_{di})(t - t_i)]dt \tag{12}$$

Simplifies the above equation, we can obtain that

$$I_i(t) = \sum_{k=1,k\neq i}^{N} \frac{B_k(t) sin[2\pi(f_{dk} - f_{di})T_p]}{2\pi\left[(k-i) + (f_{dk} - f_{di})T_p\right]} \tag{13}$$

As for noise, it can be easily proved that $n_i(t)$ is still an AWGN with mean value zero and variance $N_0/2$. Therefore the output of the ith radar is

$$|Y_i(t)| = |A_i(t) + \sum_{k=1,k\neq i}^{N} \frac{B_k(t) sin[2\pi(f_{dk} - f_{di})T_p]}{2\pi\left[(k-i) + (f_{dk} - f_{di})T_p\right]} + n_i(t)| \tag{14}$$

Assume each radar works at the same level of detection accuracy, the RSN clusterhead can apply equal gain combining algorithm before making a final decision.

Since Swerling II models is applied, $A_i(t)$ follows Rayleigh distribution, which can be modeled as

$$A_i(t) = A_i^I(t) + jA_i^Q(t) \tag{15}$$

In the same way, noise is given by

$$n_i(t) = n_i^I(t) + jn_i^Q(t) \tag{16}$$

both I and Q subchannels of $A_i(t)$ and $n_i(t)$ follow zero-mean Gaussian distribution with corresponding variance γ_i^2 and σ_i^2 [4]. Assume each $\left|\frac{B_k(t) sin[2\pi(f_{dk}-f_{di})T_p]}{2\pi[(k-i)+(f_{dk}-f_{di})T_p]}\right|$ in above equation follows Rayleigh distribution with variance β_k^2 for its I and Q subchannels, then $|Y_i(t)|$ follows Rayleigh distribution with parameter

$$\alpha_i = \sqrt{\gamma_i^2 + \beta_i^2 + \sigma_i^2} \tag{17}$$

where

$$\beta_i^2 \triangleq \sum_{k=1,k\neq i}^{N} \beta_k^2 \tag{18}$$

so when there is a moving target, the pdf for $|Y_i(t)|$ is

$$f_s(y_i) = \frac{y_i}{\alpha_i^2} exp(-\frac{y_i^2}{2\alpha_i^2}) \tag{19}$$

The mean value of y_i is $\alpha_i\sqrt{\frac{\pi}{2}}$, and variance is $(2 - \frac{\pi}{2})\alpha_i^2$. The variance of useful signal is $(2 - \frac{\pi}{2})\gamma^{2_i}$ and the vaiance of noise is $(2 - \frac{\pi}{2})\sigma_i^2$. Therefore, SNR is $\frac{\gamma_i^2}{\sigma_i^2}$ and it is worth mentioning that SIR for coherent RSN is $\frac{\gamma_i^2}{\beta_i^2}$.

After equal gain diversity combination, the synthesized pdf becomes

$$f_s(\mathbf{y}) = \prod_{i=1}^{N} \frac{y_i}{\alpha_i^2} exp(-\frac{y_i^2}{2\alpha_i^2}) \tag{20}$$

In case of no target, i.e. there exits only noise , and hence the pdf of $|Y_i(t)|$ is given by

$$f_n(y_i) = \frac{y_i}{\sigma_i^2} exp(-\frac{y_i^2}{2\sigma_i^2}) \tag{21}$$

and accordingly the synthesized pdf becomes

$$f_n(\mathbf{y}) = \prod_{i=1}^{N} \frac{y_i}{\sigma_i^2} exp(-\frac{y_i^2}{2\sigma_i^2}) \tag{22}$$

Based on the knowledge of pdf, we apply Bayesian's rule to obtain our decision criterion ,which is

$$\frac{f_s(\mathbf{y})}{f_n(\mathbf{y})} \underset{no\ target}{\overset{target\ exists}{\gtrless}} \frac{P_n}{P_s} \tag{23}$$

where P_n denotes the probability of no target but noise and P_s represents the probability of target occurrence.

IV. Noncoherent Detection

As far as noncoherent RSN is concerned, the difference from the above system is that radars have no knowledge of the accurate doppler shift introduced by moving targets, so each matched filter applies the same frequency as transmitted carrier. Although this situation is more complicated to handle, as for modern military it is more practical. Our construction of RSN demodulators is shown in Fig.3.

In terms of this structure, the received signals of the ith radar is first multiplied by separate cosine and sine waveforms generated by the local oscillator. The receiver then sums of the sine and cosine correlations, extracts its envelope, and then transmits the result to RSN cluterhead, which will make final decision based on the combined information colletcted by each radar member. It is obvious that because of not knowing the doppler shift, this system involves nonlinear operations unlike the coherent RSN in the above section.

As for the ith radar, the output of inphase branch is

$$Y_i^I(t) = \int_{t_i}^{t_i+T_p} \tilde{R}_i(t) \cdot \sqrt{\frac{2}{T_p}} \cos[2\pi(f_c + \Delta_i)(t - t_i)]dt \tag{24}$$

Similar to equation(9), it can be also represented as

$$Y_i^I(t) = S_i^I(t) + I_i^I(t) + n_i^I(t) \tag{25}$$

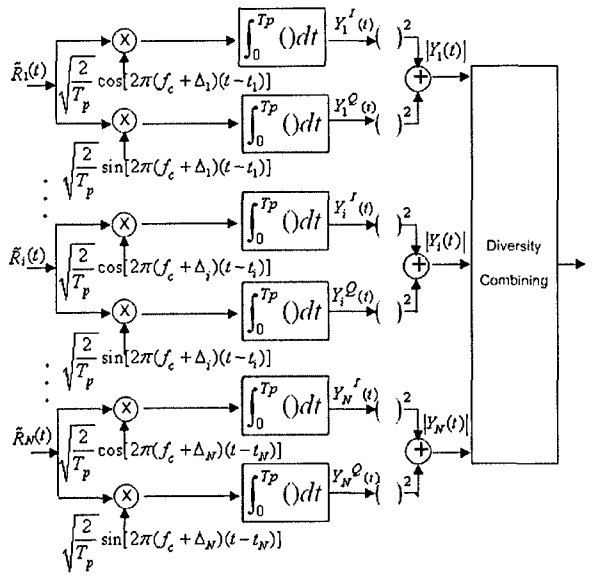

Fig. 3. Noncoherent RSN demodulation and waveform combining

where

$$S_i^I(t) = A_i(t) \cdot sinc(2\pi f_{di} T_p) \tag{26}$$

$$I_i^I(t) = \sum_{k=1,k\neq i}^{N} B_k(t) sinc\left[2\pi(\Delta_k - \Delta_i + f_{dk})T_p\right] \tag{27}$$

And $n_i^I(t)$ is the noise in inphase branch. In the same way, the output of quadrature branch is

$$Y_i^Q(t) = \int_{t_i}^{t_i+T_p} \tilde{R}_i(t) \cdot \sqrt{\frac{2}{T_p}} \sin[2\pi(f_c+\Delta_i)(t-t_i)]dt \tag{28}$$

which can also be given as

$$Y_i^Q(t) = S_i^Q(t) + I_i^Q(t) + n_i^Q(t) \tag{29}$$

where

$$S_i^Q(t) = \frac{A_i(t)\left[cos(2\pi f_{di}T_p) - 1\right]}{2\pi f_{di} T_p} \tag{30}$$

$$I_i^Q(t) = \sum_{k=1,k\neq i}^{N} \frac{B_k(t)\left\{cos[2\pi(\Delta_k - \Delta_i + f_{dk})T_p] - 1\right\}}{2\pi(\Delta_k - \Delta_i + f_{dk})T_p} \tag{31}$$

and $n_i^Q(t)$ is the noise in quadrature branch.

To simplify the computation, we can define

$$\theta_i \triangleq \pi f_{di} T_p \tag{32}$$

so equation(26)(27)(30)(31) are also respectively given by

$$S_i^I(t) = \frac{A_i(t) sin\theta_i cos\theta_i}{\theta_i} \tag{33}$$

$$I_i^I(t) = \sum_{k=1,k\neq i}^{N} \frac{B_k(t) sin\theta_k cos\theta_k}{\pi(k-i)+\theta_k} \tag{34}$$

$$S_i^Q(t) = -\frac{A_i(t) sin^2\theta_i}{\theta_i} \tag{35}$$

$$I_i^Q(t) = \sum_{k=1,k\neq i}^{N} -\frac{B_k(t) sin^2\theta_k}{\pi(k-i)+\theta_k} \tag{36}$$

Based on the above equations and the construction in Fig.3, it can derived that

$$|Y_i(t)| = \frac{\sqrt{\frac{A_i^2(t)sin^2\theta_i}{\theta_i^2} + \sum_{k=1,k\neq i}^{N} \frac{2A_i(t)B_k(t)sin\theta_i sin\theta_k cos(\theta_i-\theta_k)}{[\pi(k-i)+\theta_k]\theta_i} + \sum_{k=1,k\neq i}^{N} \frac{B_k^2 sin^2\theta_k}{[\pi(k-i)+\theta_k]^2} + \sum_{m\neq j\neq i}^{N} \frac{2B_m B_j sin\theta_m sin\theta_j cos(\theta_m-\theta j)}{[\pi(m-i)+\theta_m][\pi(j-i)+\theta_j]} + n_i^2(t)}}{} \tag{37}$$

We can have two special cases as follows:

1) If there is no doppler shift, i.e. $f_{di} = 0$ and $\theta_i = 0$, then $\frac{sin^2\theta_i}{\theta_i^2}$=1 and thus equation(37) becomes

$$|Y_i(t)| = \sqrt{A_i^2(t) + n_i^2(t)} \tag{38}$$

2) If there is only one radar, then equation(37) becomes

$$|Y_i(t)| = \sqrt{A_i^2(t)\frac{sin^2\theta_i}{\theta_i^2} + n_i^2(t)} \tag{39}$$

Similar to coherent system, in equation(37) we may assume that $\left|\frac{A_i(t)sin\theta_i}{\theta_i}\right|$, $\sqrt{\sum_{k=1,k\neq i}^{N} \frac{2A_i(t)B_k(t)sin\theta_i sin\theta_k cos(\theta_i-\theta_k)}{[\pi(k-i)+\theta_k]\theta_i} + \sum_{k=1,k\neq i}^{N} \frac{B_k^2 sin^2\theta_k}{[\pi(k-i)+\theta_k]^2} + \sum_{m\neq j\neq i}^{N} \frac{2B_m B_j sin\theta_m sin\theta_j cos(\theta_m-\theta j)}{[\pi(m-i)+\theta_m][\pi(j-i)+\theta_j]}}$ and $|n_i(t)|$ follow Rayleigh distribution with variance γ_i^2, η_i^2 and σ_i^2 for their corresponding I and Q subchannels, and therefore $|Y_i(t)|$ follows Rayleigh distribution with parameter

$$\alpha_i = \sqrt{\gamma_i^2 + \eta_i^2 + \sigma_i^2} \tag{40}$$

Similarly, we may apply the equation(19)(20) (21)(22)(23) in coherent RSN to analyze the dection performance and in noncoherent RSN, SIR is $\frac{\gamma_i^2}{\eta_i^2}$.

V. Simulations

In order to study the performance versus the number of radars in RSN under the condition of doppler shift, we apply our waveform models and equal gain combination technique in our simulation with following parameters:

1) $\frac{vf_c}{c} = 5000Hz$, i.e. $(f_{di})max = 5000Hz$
2) $T_p = 1ms$
3) $P_n = P_s$
4) the mean value and variance of $B_k(t)$ are equal to those of $A_i(t)$
5) 10^6 Monte-Carlo simulations

The average SNR value refers to the average SNR of all the members in RSN. Specifically SNR of each member is the power of received useful back-scattered signal to that of noise.

The performance of the envelope detector in single radar, 3-radar and 6-radar coherent RSN are compared in Fig.4 and

Fig.5, in terms of the probability of false alarm and probability of miss detection respectively. Fig.4 shows that, to achieve the same $P_{FA} = 0.1$, single radar requires about 7dB greater than the SNR of 6-radar RSN. In latter system, even SNR is 1dB, P_{FA} is around 0.1, which is good enough [6].

Observe Fig.5, we can see that P_M of single radar is much larger than 0.1 even SNR reaches 10dB. When $P_M = 0.1$, SNR of 3-radar and 6-radar are around 8.3dB and 4dB respectively. These two figures demonstrate that our coherent RSN could provide superior detection performance to that of single radar.

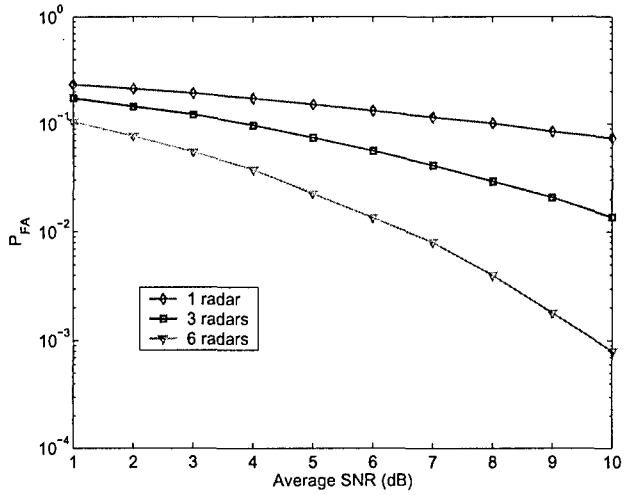

Fig. 4. Probability of false alarm for coherent RSN

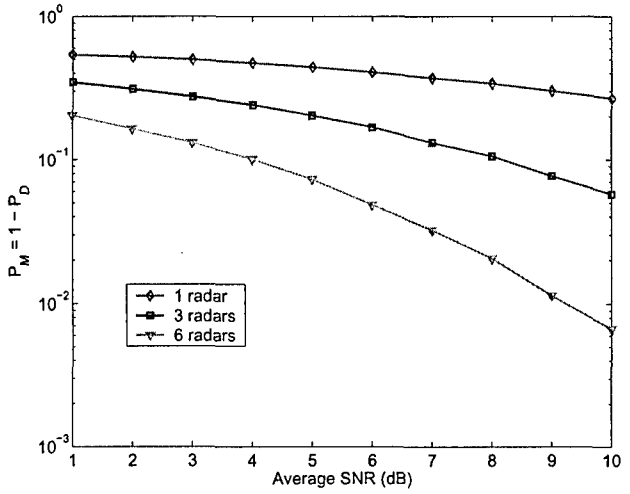

Fig. 5. Probability of miss detection for coherent RSN

In noncoherent RSN, the probability of false alarm and probability of miss detection are shown in Fig.6 and Fig.7. These two figures clearly illustrate that performance of noncoherent single radar is extremely worse than that of coherent system and it can not work properly while SNR is below

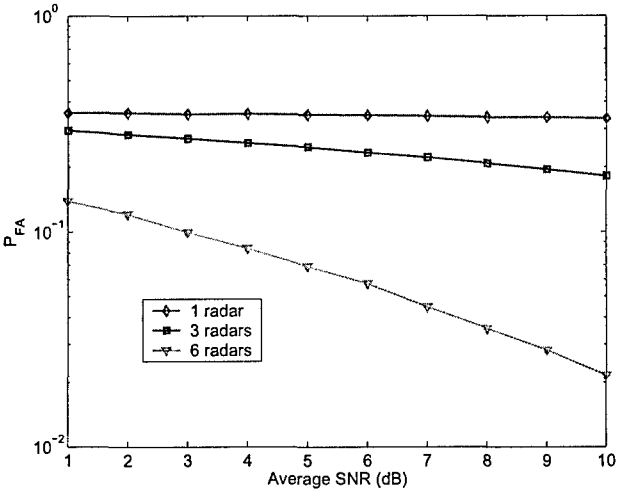

Fig. 6. Probability of false alarm for noncoherent RSN

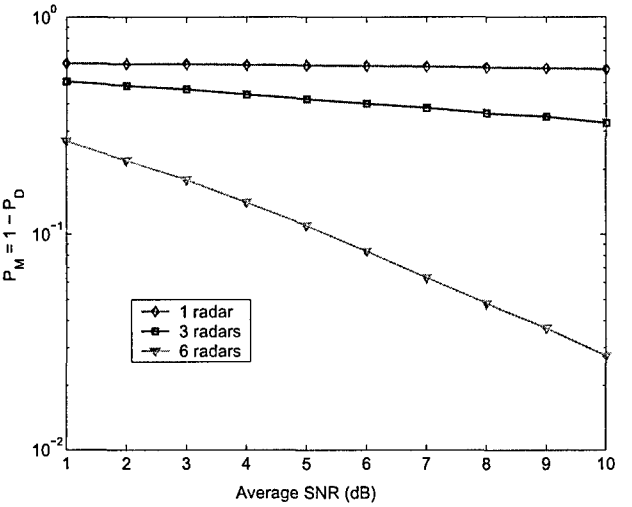

Fig. 7. Probability of miss detection for noncoherent RSN

or even equal to 10dB. Clearly, even 3-radar RSN could not provide enough performance improvement. Applying 6-radar RSN, performance has been improved a lot compared to single radar. Here $P_{FA} = 0.1$ is achieved when SNR is greater than 3dB and to satisfy $P_M \leq 0.1$, SNR must be increased to around 5.3 dB.

Meanwhile, it is clear to see no matter how many radars have been exploited in our RSN, the performances of noncoherent RSN are worse the coherent system, i.e., noncoherent RSN demand higher energy in order to achieve the same performance.

From the above figures, it is obvious that although doppler shift generates interference between each radar sensor, promising detection performance has been obtained applying our orthogonal waveform and combination technique. Particularly, this design provides greater performance in case of noncoher-

ent 10-radar RSN.

VI. Conclusion and Future Works

We have studied orthogonal waveforms and spacial diversity under the condition of doppler shift in radar sensor networks (RSN). Both cases of coherent detection and noncoherent detection have been analyzed. In case of no doppler shift, our orthogonal waveforms eliminate interference between each member. However, when there is doppler shift, there exists interference that can not be avoid. Simulation results show that applying equal gain combination technique through clusterhead to our signal models, better detection performance than single radar is achieved for fluctuating targets. This design not only satisfies higher demanding criterion for detection accuracy in modern military and security affairs, but also offers advantage to combat the blind speed problem.

One can extend the above procedure in several directions:

1) In this paper we only considered constant frequency (CF) pulse waveform design. Naturally, we would like to extend our results to other forms, such as linear frequency modulation (LFM) and binary phase-coded pulse, and analyze their performances.
2) For simplicity, we assumed perfect timing here, so the performance of RSN can be studied when timing ambiguity is considered.
3) In our model, we only assume there is one moving target and thus multiple targets co-existence and corresponding performance can be further investigated.

Acknowledgement

This work was supported by the Office of Naval Research (ONR) Young Investigator Award under Grant N00014-03-1-0466.

References

[1] M. R. Bell, "Information Theory and Radar Waveform Design" , *IEEE Transactions on Information Theory*, vol. 39, no. 5, pp.1578-1597, Sept. 1993.

[2] S. M. Sowelam, A. H. Tewfik, "Waveform Selection in Radar Target Classification" , *IEEE Transactions on Information Theory*, vol. 46, no. 3, pp.1014-1029, May 2000.

[3] Y. Sun, P. Willett, R. Lynch, "Waveform fusion in Sonar Signal Processing" , *IEEE Transactions on Aerospace and Electronic Systems*, vol. 40, no. 2, pp.462-477, April 2004.

[4] Q. Liang, "Waveform Design and Diversity in Radar Sensor Networks: Theoretical Analysis and Application to Automatic Target Recognition", accepted by *IEEE Int'l Workshop on Wireless Ad Hoc and Sensor Networks*, New York, June 2006.

[5] E. Fishler, A. Haimovich, R. S. Blum, L. J. Cimini, D. Chizhik, A. Valenzuela, "Spatial Diversity in Radars - Models and Detection Performance" , *IEEE Transactions on Sigal Processing*, vol. 54, No. 3, pp. 823-838, March 2006.

[6] M. I. Skolnik, *Introduction to Radar Systems* , 3rd ed, New York, McGraw Hill, 2001.

[7] M. A. Richards, *Fundamentals of Radar Signal Processing* , McGraw-Hill Companies, New York, 2005.

[8] N. Levanon, *Radar Principles*, New York, Wiley, 1988.

[9] M. K. Simon, S. M. Hinedi, W. C. Lindsey *Digital Communication Techniques*, PTR Prentice Hall, New Jersey, 1995.

SPATIAL-TEMPORAL-FREQUENCY DIVERSITY IN RADAR SENSOR NETWORKS

Hung D. Ly and Qilian Liang
Department of Electrical Engineering
The University of Texas at Arlington
Arlington, TX 76019-0016, USA
E-mail: ly@wcn.uta.edu, liang@uta.edu

Abstract— **In this paper, the spatial-temporal-frequency diversity to improve the detection performance of Radar Sensor Networks (RSN) in the presence of certain types of interference (clutter, jamming, noise and interference between radar sensors) is studied. In order to reduce the interference between radar sensors and maximize the signal-to-interference-plus-noise ratio (SINR), we propose a method using the orthogonality criterion to design waveforms for radar sensors in the network. Besides the interference between radar sensors, performance of the network depends largely on other interference, especially clutter, which is extended in both angle and range, and is spread in Doppler frequency. By using the spatial-temporal diversity, we can suppress effects of these interference. In this paper, we also propose a receiver for diversity combining in RSN. As an application example, we apply the spatial-temporal-frequency diversity scheme to improve the detection performance or reduce the miss-detection probability at a low false alarm probability. Simulation results for both non-fluctuating targets and fluctuating targets show that the performance of our proposed scheme is superior to that of the single radar with the spatial-temporal diversity only.**

I. INTRODUCTION

Radar sensor network (RSN) consists of collaboratively operating radar sensors which are deployed ubiquitously (possibly randomly placed) on airborne, surface and sub-surface unmanned vehicles. Each sensor in the network has capabilities for radar sensing, signal processing and wireless communication. Autonomous radar sensors operating in the microwave spectrum are used to detect, classify and track visible, obscured or hidden targets such as tactical weapons, aircraft, ships, spacecraft, vehicles, people, and the natural environment in the presence of both noise and interference (clutter, jamming and interference between sensors). Information about a target is wirelessly forwarded to the central processor, where target identification and network-wide tracking are conducted using sensor data from every sensor in the network, along with their position and timing information.

In the radar sensor network, radar sensors are networked together in an ad-hoc fashion, i.e., they do not depend on any preexisting infrastructure. They are self-organizing entities that are deployed on demand in support of various events such as surveillance, battlefield, disaster relief, search and rescue, etc. RSN has advantages compared to a single radar system in improving the system sensitivity, reducing obscuration effects and vulnerability as well as increasing the detection performance. However, when deploying the RSN, we have to solve some challenging problems such as networking between radar sensors, canceling effects of interference, power efficient communication, and reducing complexity of signal processing schemes, etc. Only few work doing research on these aspects has been developed. Recently, S. Kadambe [1] proposed a minimax entropy-based technique to reduce the processing complexity in the RSN. In [2], relative merits of the RSN and the balance between increased performance, complexity, and cost were discussed. In this paper, we will propose a method to design the waveform in order to cancel the interference between radar sensors and maximize the signal-to-interference-plus-noise ratio (SINR). In research literature on the waveform design, Fitzgerald [3] demonstrated the inappropriateness of waveform selection based on measurement quality alone: the interaction between the measurement and the track can be indirect, but must be taken into account. Bell [4] used the information theory to design waveform for the measurement of extended radar targets exhibiting resonance phenomena. Baum [5] used the singularity expansion method to design some discriminant waveforms. However, these design methods were used for the single radar only. In [18], radar sensor networks for automatic target recognition was studied, but clutter and jammer were not considered.

Performance of the RSN depends largely on the interference which is extended in both angle and range, and is spread in Doppler frequency because of motion of the platform and target. Space-Time Adaptive Processing (STAP) or spatial-temporal diversity has become an excellent technique to suppress effects of interference. STAP refers to the simultaneous processing of the spatial samples from an array antenna and the temporal samples provided by the echoes from multiple pulses of a coherent processing interval (CPI). A considerable amount of work has been done to develop STAP for processing data from airborne or space-borne radars to reliably detect moving targets of interest in the presence of strong clutter returns and jamming [6] - [9]. By combining waveform design and spatial-temporal diversity, we can perform spatial-temporal-frequency diversity in RSN. Studies in this paper will show that using our proposed diversity scheme will improve the detection performance with a low false alarm probability.

The remainder of this paper is organized as follows. In section II, we propose a method to design waveforms. Spatial-temporal diversity and interference analysis are discussed in

the section III. In section IV, we propose a diversity combining scheme and analyze detection performance for non-fluctuating targets as well as fluctuating targets using our proposed diversity scheme. Simulation results and performance analysis are discussed in section V, and in section VI, we conclude the paper.

II. Waveform design

In radar sensor networks, radar sensors will interfere with one another and SINR will be very low if waveforms are not properly chosen. In order to have waveforms designed properly and coexisted in the network, we propose orthogonality as one criterion to design waveforms.

In our radar sensor networks, we choose constant frequency (CF) pulse waveform. The CF waveform can be defined as

$$x(t) = \sqrt{\frac{E}{T}} exp(j2\pi ft) \qquad 0 \le t \le T \tag{1}$$

where E is the energy of the waveform and T is the waveform pulse duration.

We know that the waveforms from different radar sensors will interfere with one another. We choose the waveform for radar i as

$$x_i(t) = \sqrt{\frac{E}{T}} exp(j2\pi(f + \Delta_i)t) \qquad 0 \le t \le T \tag{2}$$

which means that there is a frequency shift Δ_i for the radar sensor i. In order to minimize the interference between radar sensors, we will find a set of frequency shifts $\{\Delta_i\}_{i=0}^{M-1}$ (M is the number of radar sensors) for which the waveforms are orthogonal. Let $R(k,l)$ denote the cross-correlation between the waveforms $x_k(t)$ and $x_l(t)$.

$$\begin{aligned} R(k,l) &= \int_0^T x_k(t) x_l^*(t) dt \\ &= E sinc[(\Delta_k - \Delta_l)T] exp[j\pi(\Delta_k - \Delta_l)T] \end{aligned} \tag{3}$$

If $\pi(\Delta_k - \Delta_l)T = i\pi$, the waveforms $x_k(t)$ and $x_l(t)$ are orthogonal, i.e.,

$$R(k,l) = \begin{cases} 0 & k \ne l \\ E & k = l \end{cases}$$

So, we can choose a set of frequency shifts $\{\Delta_i\}_{i=0}^{M-1}$ as below [18]:

$$\Delta_i = \Delta_k - \Delta_l = \frac{i}{T} \qquad i = 0, 1, ..., M-1 \tag{4}$$

Based on (4), we can confirm that the waveforms can co-exist if the frequency shift is i/T between two waveforms, i.e., orthogonality among waveforms can be achieved by separating frequencies of waveforms by multiplying an integer with the inverse of the waveform pulse duration. So, we will choose the waveforms by this method to get radar sensors coexisted in the network. Moreover, by using this waveform design method, we can perform a frequency diversity in the RSN.

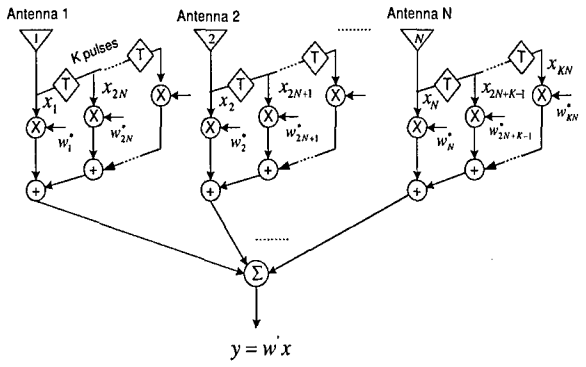

Fig. 1. Space-time beamformer consisting of an N-element ULA and a coherent processing interval (CPI) comprising K pulses with a fixed PRI [9]

III. Spatial - Temporal diversity and interference analysis

A. Spatial - Temporal diversity

At each radar sensor, we use a receiver with an array antenna as shown in Fig. 1. This array consists of an N-element ULA with inter-element spacing d_i (spatial degrees of freedom) and K pulse repetition interval (PRI) time taps (temporal degrees of freedom). Now, we consider a signal $s_i(t) = Ae^{j\Omega_i t}$ impinging on the array. If the wave's angle of arrival relative to the array is θ, the signal observed at the n^{th} array element is

$$m_n(t) = Ae^{j[\Omega_i(t - nd_i sin\theta/c) + \phi_0]} \qquad n = 0, 1, .., N-1 \tag{5}$$

where the phase offset ϕ_0 accounts for the absolute phase at the first element. We consider N samples formed from N array elements at a time t_0 and map these N element samples into a vector form to have a snapshot of the array at a fixed time.

$$\begin{aligned} m &= A_1[1 \quad e^{-j2\pi d_i sin\theta/\lambda_i} \quad ... \quad e^{-j2\pi(N-1)d_i sin\theta/\lambda_i}]' \\ &= A_1 a_s(\overline{\theta}_i) \end{aligned} \tag{6}$$

where $A_1 = Ae^{j(\Omega_i t + \phi_0)}$, $\overline{\theta}_i = d_i sin\theta/\lambda_i$ is the normalized angle, $(.)'$ denotes the transpose operation, and $a_s(\overline{\theta}_i)$ is the spatial steering vector.

$$a_s(\overline{\theta}_i) = [1 \quad e^{-j2\pi\overline{\theta}_i} \quad ... \quad e^{-j2\pi(N-1)\overline{\theta}_i}]' \tag{7}$$

Since the target is in motion, the normalized Doppler shift at the target induced on the radar sensor i at an angle θ is

$$\overline{f}_{di} = \frac{2v_i T}{\lambda_i} sin\theta = \beta\overline{\theta}_i \tag{8}$$

where v_i is the velocity of the radar sensor i and $\beta = \frac{2v_i T}{d_i} = \frac{4v_i T}{\lambda_i}\Big|_{d_i = \frac{\lambda_i}{2}}$. Each vector of array outputs from successive pulses due to the target will have a temporal linear phase progression, i.e., at the k^{th} PRI, snapshot of the target takes the form [9], [10]

$$e(\overline{\theta}_i, \overline{f}_{di}) = e^{j2\pi(k-1)\overline{f}_{di}} a_s(\overline{\theta}_i) \qquad k = 1, 2, .., K \tag{9}$$

If K pulses are to be processed in a coherent pulse interval (CPI), the KN dimensional space-time steering vector (snapshot) corresponding to a possible target at look angle θ and

Doppler frequency $\overline{f}_{di}$ is given by

$$e(\overline{\theta}_i, \overline{f}_{di}) = b_t(\overline{f}_{di}) \otimes a_s(\overline{\theta}_i) \quad (10)$$

where $\otimes$ denotes the Knonecker product and $b_t(\overline{f}_{di})$ is the K-dimensional Doppler steering vector

$$b_t(\overline{f}_{di}) = [1 \quad e^{j2\pi\overline{f}_{di}} \quad \ldots \quad e^{j2\pi(K-1)\overline{f}_{di}}]' \quad (11)$$

By introducing the complex weighting vector w_i, the output response of the space-time beamformer can be maximized for any desired angle of arrival. More specifically, let x_i and y_i denote the received data at the radar sensor i and beamformer output, respectively.

$$y_i = w_i' x_i \quad (12)$$

In any case, the optimum weight vector, $w_i \in C^{NK}$, that maximizes SINR, satisfies the Weiner-Hopf equation

$$w_i = R_{di}^{-1} e(\overline{\theta}_i, \overline{f}_{di}) \quad (13)$$

where $R_{di} \in C^{NK \times NK}$ is the interference-plus-noise covariance matrix.

However, in practice, the covariance matrix R_{di} is unknown and must be estimated. To solve this problem, researchers have produced extensively algorithms [12] - [15] to choose an optimal set of complex space-time weights w_i in order to maximize SINR.

B. Interference analysis in Radar Sensor Networks

1) Clutter: Clutters generate unwanted radar returns that may interfere with the desired signal. Parasitic returns that enter the radar through the antenna's main-lobe are called main-lobe clutter; otherwise they are called side-lobe clutter. Clutter can be classified into two main categories: surface clutter (including trees, vegetation, ground terrain, man-made structures, and sea surface) and volume clutter (including chaff, rain, birds, and insects). Surface clutter changes from one area to another, while volume clutter may be predictable. In many scenarios, the dominant interference is not noise, but clutter. Consequently, the signal-to-clutter ratio (SCR) is often of more important than the signal-to-noise ratio (SNR).

The integrated clutter can be generally approximated as the sum of N_c elemental clutter patches. For clutter patch i, the space-time data vector [9] is

$$P_i = \gamma_i b_t(\overline{f}_{d_{ci}}) \otimes a_s(\overline{\theta}_{ci}) = \gamma_i u_i \quad (14)$$

where γ_i is a complex scalar random variable that accounts for the amplitude and phase of the i^{th} clutter patch, $u_i = b_t(\overline{f}_{d_{ci}}) \otimes a_s(\overline{\theta}_{ci})$. $b_t(\overline{f}_{d_{ci}})$ and $a_s(\overline{\theta}_{ci})$ are temporal vector and spatial vector of clutter signal from clutter patch i, respectively. $\overline{f}_{d_{ci}}$ and $\overline{\theta}_{ci}$ are the normalized Doppler shift and angle of arrival of the i^{th} clutter patch, respectively. The total clutter vector equals to

$$X_c = \sum_{i=1}^{N_c} P_i = \sum_{i=1}^{N_c} \gamma_i b_t(\overline{f}_{d_{ci}}) \otimes a_s(\overline{\theta}_{ci}) = \sum_{i=1}^{N_c} \gamma_i u_i \quad (15)$$

The covariance matrix of the clutter [9] is given by

$$R_c = E\{X_c X_c'\} = \sum_{i=1}^{N_c} \sum_{j=1}^{N_c} E\{\gamma_i \gamma_j'\} u_i u_j' = \sum_{i=1}^{N_c} G_i u_i u_i' \quad (16)$$

2) Jamming: Jamming signals are generated by hostile interfering signal sources that seek to degrade the performance of radar sensors by mechanisms such as degrading SINR by increasing the noise level, or generating false detections to overwhelm the radar with false targets. One of the most common forms of jamming is a simple noise jammer that radiates a relatively high-power waveform at the victim radar sensor from a specific platform. A commonly employed model for N_j jamming signals [6]

$$J = \sum_{m=1}^{N_j} z_m \otimes a_j(\overline{\theta}_m) \quad (17)$$

where z_m contains voltage samples of the m^{th} jammer waveform taken at PRI. The different jammer waveforms are uncorrelated with each other.

3) Interference between radar sensors: When we deploy the radar sensor network, interference between radar sensors need to be studied. In [18], interference between radar sensors was analyzed in detail. Since radar sensors operate at different frequencies, they will interfere one another. To suppress this interference, we should choose waveforms correctly. In this paper, we choose the orthogonality criterion to design the waveforms.

4) Noise: The echo signal received from a target or clutter inevitably competes with noise. Noise can be received through antenna from external sources or generated in the radar receiver itself. Of these various sources, thermal noise due to ohmic losses at the radar receiver is normally dominant. We can use the Gaussian process to model the thermal noise.

IV. Diversity combining and target detection

A radar sensor network is composed of many radar sensors deployed in a large geographical area. The radar sensors (nodes) are networked together in an ad-hoc fashion, i.e., they do not depend on any preexisting infrastructure. In fact, they are self-organizing entities that are deployed on demand to perform various tasks such as surveillance, disaster relief, search and rescue, etc. Scalability concerns suggest a hierarchical organization of the radar sensor networks with the lowest level in the hierarchy being a cluster. The clusters are independently controlled and dynamically reconfigured as nodes move. Thus, this network architecture has some main advantages as follows [16]

1) Using the radio resources efficiently. For example, bandwidth can be shared or reserved in a controlled fashion in each cluster.
2) Providing spatial and frequency reuse due to node clustering.
3) Robustness with topological changes caused by node motion, node failure, and node insertion/removal.
4) Concealing the details of global network topology from individual nodes.

In this paper, we perform the waveform design for radar sensors in the network. Each sensor in the network will be assigned a waveform with specific parameters. Radar sensors

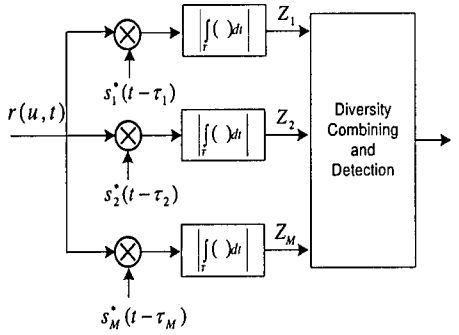

Fig. 2. Receiver at the clusterhead for diversity combining

can provide their parameters about waveforms to the cluster-head. Cluster-head will collect and combine waveforms from cluster members.

The received data at each radar sensor i consists of the desired signal and interference, i.e.,

$$\begin{aligned} x_i(u,t) &= \alpha_i(u)e(\overline{\theta}_i,\overline{f}_{di})s_i(t-\tau_i)+C_i+J_i+I_i+n_i \\ &= \alpha_i(u)e(\overline{\theta}_i,\overline{f}_{di})s_i(t-\tau_i)+d_i \end{aligned} \quad (18)$$

where $d_i = C_i + J_i + I_i + n_i$ presents the overall interference, i.e., the sum of the clutter vector C_i, the jammer vector J_i, the interference between radar sensors I_i, and the background white noise n_i. $\alpha_i(u)$ is a random variable that models the radar cross section (RCS), $e(\overline{\theta}_i,\overline{f}_{di})$ is a spatial-temporal steering vector that models the target return for a specific angle-Doppler, and $s_i(t-\tau_i)$ is the return of waveform with delay τ_i.

The data at the output of the i^{th} sensor is the multiplication of the received data $x_i(u,t)$ and the spatial-temporal weight vector w_i, i.e.,

$$\begin{aligned} y_i(u,t) &= w_i^{'}x_i(u,t) \\ &= w_i^{'}[\alpha_i(u)e(\overline{\theta}_i,\overline{f}_{di})s_i(t-\tau_i)+d_i] \\ &= \alpha_i(u)s_i(t-\tau_i)L_i(\overline{\theta}_i,\overline{f}_{di})+D_i \end{aligned} \quad (19)$$

where $D_i \triangleq w_i^{'}d_i$ and $L_i(\overline{\theta}_i,\overline{f}_{di}) \triangleq w_i^{'}e(\overline{\theta}_i,\overline{f}_{di})$.

Assuming the radar sensor network with M radar sensors, the received signal $r(u,t)$ at the cluster-head is

$$\begin{aligned} r(u,t) &= \sum_{i=1}^{M} y_i(u,t) \\ &= \sum_{i=1}^{M}\{\alpha_i(u)s_i(t-\tau_i)L_i(\overline{\theta}_i,\overline{f}_{di})+D_i\} \end{aligned} \quad (20)$$

Note that $\alpha_i(u)$ can be modeled using non-zero constants for non-fluctuating targets and four Swerling target models for fluctuating targets [17]. Target fluctuation lowers the probability of detection, or equivalently reduces SINR.

At the cluster-head, we propose a receiver [18] as shown in the Fig. 2 to combine waveforms. According to this receiver, the received signal $r(u,t)$ is processed by a bank of matched filters. After integration, the output of the branch 1 is given by

$$\begin{aligned} Z_1(u) &= \left|\int_0^T r(u,t)s_1^*(t-\tau_1)dt\right| \quad (21) \\ &= \left|\sum_{i=1}^{M}\alpha_i(u)L_i(\overline{\theta}_i,\overline{f}_{di})\int_0^T s_i(t-\tau_i)s_1^*(t-\tau_1)dt\right. \\ &\quad \left.+\sum_{i=1}^{M}\int_0^T s_1^*(t-\tau_1)D_i dt\right| \\ &= |Z_{11}(u)+Z_{12}(u)| \quad (22) \end{aligned}$$

where $Z_{11}(u)$ and $Z_{12}(u)$ are defined as below

$$\begin{aligned} Z_{11}(u) &\triangleq \sum_{i=1}^{M}\alpha_i(u)L_i(\overline{\theta}_i,\overline{f}_{di})\int_0^T s_i(t-\tau_i)s_1^*(t-\tau_1)dt \\ &= \sum_{i=2}^{M}\alpha_i(u)L_i(\overline{\theta}_i,\overline{f}_{di})\int_0^T s_i(t-\tau_i)s_1^*(t-\tau_1)dt \\ &\quad + E\alpha_1(u)L_1(\overline{\theta}_1,\overline{f}_{d1}) \quad (23) \\ Z_{12}(u) &\triangleq \sum_{i=1}^{M}\int_0^T s_1^*(t-\tau_1)D_i dt \quad (24) \end{aligned}$$

Based on (4), $Z_{11}(u)$ can be rewritten as

$$Z_{11}(u) = E\alpha_1(u)L_1(\overline{\theta}_1,\overline{f}_{d1}) \quad (25)$$

Assuming that waveforms are designed properly. So, the interference between radar sensors is negligible. Since the detection performance of RSN is greatly affected by the clutter, we consider the clutter the primary interference source. The overall interference can be given by

$$d_i = C_i(\overline{f}_{d_{ci}},\overline{\theta}_{ci})+n_i = \sum_{j=1}^{N_c}\gamma_{ij}u_{ij}+n_i \quad (26)$$

where $u_{ij} = b_t(\overline{f}_{d_{cij}}) \otimes a_s(\overline{\theta}_{cij})$. Thus, $Z_{12}(u)$ becomes

$$Z_{12}(u) = \sum_{i=1}^{M}\int_0^T w_i^{'}d_i s_1^*(t-\tau_1)dt \quad (27)$$

Since γ_{ij} is a complex random variable, we assume γ_{ij} is a complex Gaussian random variable. So, it is not difficult to prove that Z_{12} is a complex Gaussian noise $n(u)$. The output of the branch 1 becomes

$$Z_1(u) \approx |E\alpha_1(u)L_1(\overline{\theta}_1,\overline{f}_{d1})+n(u)| \quad (28)$$

Similarly, the output of the i^{th} branch (i = 1, 2, ..., M) is

$$Z_i(u) \approx |E\alpha_i(u)L_i(\overline{\theta}_i,\overline{f}_{di})+n(u)| \quad (29)$$

Based on (29), we can recognize that the output of the i^{th} branch is composed of the signal from the radar sensor i and noise. Note that when we compute $Z_i(u)$, we still have to estimate the interference-plus-noise covariance matrix.

Now, our objective is to combine all the outputs of all branches. We will use diversity combining method to combine these outputs. In this paper, we are interested in using the spatial-temporal-frequency diversity in RSN to solve the target detection problem. The purpose of detection problem is to figure out the presence and motion of the desired targets such as missiles, tanks, fighter aircrafts, other tactical weapons from

the enemy, illegal intruders at the border of the country, over-speeded vehicles or strange ships at sea, etc. In this paper, we will apply the spatial-temporal-frequency diversity to improve the detection performance and use a maximum likelihood criterion to analyze the detection performance of RSN for both non-fluctuating targets and fluctuating targets. The detection problem in RSN can be formulated as follows:

$$\begin{aligned} H_0 &: \text{Target is not present} \\ H_1 &: \text{Target is present} \end{aligned} \tag{30}$$

A. Non-fluctuating targets

Non-fluctuating targets can be modeled as the Swerling 0 or equivalently Swerling V [11], [17]. The radar cross section (RCS) $\alpha_i(u)$ of non-fluctuating targets is constant and unknown. We assume that $\alpha_1(u) = \alpha_2(u) = ... = \alpha_M(u) = \alpha(u)$. Under hypothesis H_0, $Z_i(u)$ follows the Rayleigh distribution. The probability density function (pdf) of Z_i is

$$f(z_i|H_0) = \frac{2z_i}{\sigma^2} exp[-\frac{z_i^2}{\sigma^2}] \tag{31}$$

Under hypothesis H_1, $Z_i(u)$ follows the Rician distribution. The pdf of Z_i with the parameter m_i is

$$f(z_i|H_1) = \frac{2z_i}{\sigma^2} exp[-\frac{z_i^2 + m_i^2}{\sigma^2}] I_0(\frac{2m_i z_i}{\sigma^2}) \tag{32}$$

where $m_i = E\alpha(u) L_i(\overline{\theta}_i, \overline{f}_{di})$, $\sigma^2/2$ is the noise power for each branch I, Q, and $I_0(.)$ is the zero-order modified Bessel function of the first kind. We assume that $Z_1, Z_2, ..., Z_m$ are independent random variables. Let $Z \triangleq [Z_1, Z_2, ..., Z_M]$, the joint pdf of the variable Z for each hypothesis:

$$f(z|H_0) = \prod_{i=1}^{M} \frac{2z_i}{\sigma^2} exp[-\frac{z_i^2}{\sigma^2}] \tag{33}$$

$$f(z|H_1) = \prod_{i=1}^{M} \frac{2z_i}{\sigma^2} exp[-\frac{z_i^2 + m_i^2}{\sigma^2}] I_0(\frac{2m_i z_i}{\sigma^2}) \tag{34}$$

Our objective is to decide whether or not a target is present based on the received signal at the cluster-head. Using the maximum likelihood criterion, we can derive the detection threshold T, false alarm probability P_{FA} and miss-detection probability P_{MD}.

$$\begin{aligned} P_{FA} &= \int_T^{\infty} \frac{z^{M-1}}{(M-1)!} e^{-z} dz \\ &= 1 - I(\frac{T}{\sqrt{M}}, M-1) \end{aligned} \tag{35}$$

$$P_{MD} = 1 - \int_T^{\infty} (\frac{z}{Mx})^{(M-1)/2} e^{-z-Mx} I_{M-1}(2\sqrt{Mxz}) dz \tag{36}$$

where x is the average signal-to-clutter-plus-noise ratio (SCNR), $I_{M-1}(.)$ is the $(M-1)$ order modified Bessel function of the first kind, and $I(a,b)$ is the incomplete gamma function.

B. Fluctuating targets

In practice, RCS is normally fluctuating. Based on different combinations of pdf and decorrelation (pulse to pulse or scan to scan), Swerling [17] proposed four Swerling models. He also showed that the statistics associated with Swerling I and II models are applied to targets consisting of many small RCS scatters of comparable RCS values, while the statistics associated with Swerling III and IV models are applied to targets consisting of one large scatter and many small equal RCS scatters [11].

In this paper, we focus on the Swerling II model. The magnitude $|\alpha(u)|$ of Swerling II targets fluctuates independently from pulse to pulse according to a chi-square probability density function with two degree of freedom, i.e., a Rayleigh probability density function.

$$\alpha(u) = \alpha_I(u) + j\alpha_Q(u) \tag{37}$$

where $\alpha_I(u)$ and $\alpha_Q(u)$ follow Gaussian distribution with the variance $\rho^2/2$ for each branch I, Q. Under hypothesis H_0, $Z_i(u)$ follows the Rayleigh distribution. The pdf of $Z_i(u)$ is

$$f(z_i|H_0) = \frac{2z_i}{\sigma^2} exp[-\frac{z_i^2}{\sigma^2}] \tag{38}$$

Under hypothesis H_1, $Z_i(u)$ follows the Rayleigh distribution. The pdf of $Z_i(u)$ is given by

$$f(z_i|H_1) = \frac{2z_i}{\sigma_i^2} exp(-\frac{z_i^2}{\sigma_i^2}) \tag{39}$$

where $\sigma_i = \sqrt{(EL_i(\overline{\theta}_i, \overline{f}_{di}))^2 \rho^2 + \sigma^2}$. We assume that $Z_1, Z_2, ..., Z_m$ are independent random variables. Let $Z \triangleq [Z_1, Z_2, ..., Z_M]$, the joint pdf of the variable Z for each hypothesis:

$$f(z|H_0) = \prod_{i=1}^{M} \frac{2z_i}{\sigma^2} exp[-\frac{z_i^2}{\sigma^2}] \tag{40}$$

$$f(z|H_1) = \prod_{i=1}^{M} \frac{2z_i}{\sigma_i^2} exp[-\frac{z_i^2}{\sigma_i^2}] \tag{41}$$

Our objective is to decide whether or not a target is present based on the received signal at the cluster-head. Using the maximum likelihood criterion, we can derive the detection threshold T, false alarm probability P_{FA} and miss-detection probability P_{MD}.

$$\begin{aligned} P_{FA} &= \int_T^{\infty} \frac{z^{M-1}}{(M-1)!} e^{-z} dz \\ &= 1 - I(\frac{T}{\sqrt{M}}, M-1) \end{aligned} \tag{42}$$

$$P_{MD} = 1 - \int_T^{\infty} \frac{z^{M-1}}{(1+x)^M (M-1)!} e^{-z/(1+x)} dz \tag{43}$$

where x is the average SCNR, and $I(a,b)$ is the incomplete gamma function.

V. Simulation results and performance analysis

A. Simulated data model

In this paper, we use the modified Joint Domain Localized (JDL) algorithm proposed by Adve *et.al* [12] to determine the space-time weights at sensors. The data generation scheme uses the physical model presented by Ward [8].

As mentioned in the section III, the clutter is modeled as a sum of the contributions of many discrete far field sources. In this paper, amplitude of each discrete source is a complex Gaussian random variable whose average power is set by a chosen clutter-to-noise ratio (CNR). The normalized Doppler shift associated with each clutter source depends on the velocity of the platform.

Thermal noise is modeled as a Gaussian white noise process. The average power is set to unity allowing the clutter and target powers to be referenced to the white noise power. Simulations do not consider the effects of Jammers. Parameters used in simulations are listed in the Table I [12].

TABLE I - Parameters used in simulations

Parameters	Values
Array elements	8
Pulses	8
Element spacing	$\lambda_i/2$
Pulse Repetition Frequency (PRF)	1024 Hz
The number of clutter sources	181
Target normalized Doppler shift	1/3
Thermal noise power	Unity
Clutter to noise ratio (CNR)	50 dB
The number of Doppler bins in LPR	3
The number of Angle bins in LPR *(LPR: Local Processing Region)*	3

The interference-plus-noise covariance matrix R_d is given

$$R_d = R_N + p_c(k)R_c \tag{44}$$

where R_N is the covariance of noise, R_c is the clutter covariance computed in (16), and $p_c(k)$ is a random variable used to model the clutter power of the k^{th} range cell. $p_c(k)$ often follows $Weibull$ or gamma distribution [19] [20]. In homogeneous environments, the average clutter power does not depend on k. We assume the average CNR equals 50 dB.

B. Detection performance analysis of the radar sensor network

In RSN, each radar sensor transmits a known waveform. This waveform is reflected back from the target toward the receiving sensor. RSN's tasks are to detect the existence of the target and to estimate its unknown parameters, e.g., range speed and direction. In this paper, we use the spatial-temporal-frequency diversity in RSN to improve the detection performance. Fig. 3(a) presents the probability of miss-detection P_{MD} as a function of SCNR and $P_{FA} = 10^{-6}$ while Fig. 3(b) presents the miss-detection probability P_{MD} as the function of false alarm probability P_{FA}, $SCNR = 8dB$ and $SCNR = 10dB$ for non-fluctuating targets. Similarly, Fig. 4(a) presents the probability of miss-detection P_{MD} as a function of SCNR and $P_{FA} = 10^{-6}$ while Fig. 4(b) presents the miss-detection probability P_{MD} as the function of false alarm probability P_{FA}, $SCNR = 10dB$ and $SCNR = 12dB$ for fluctuating targets.

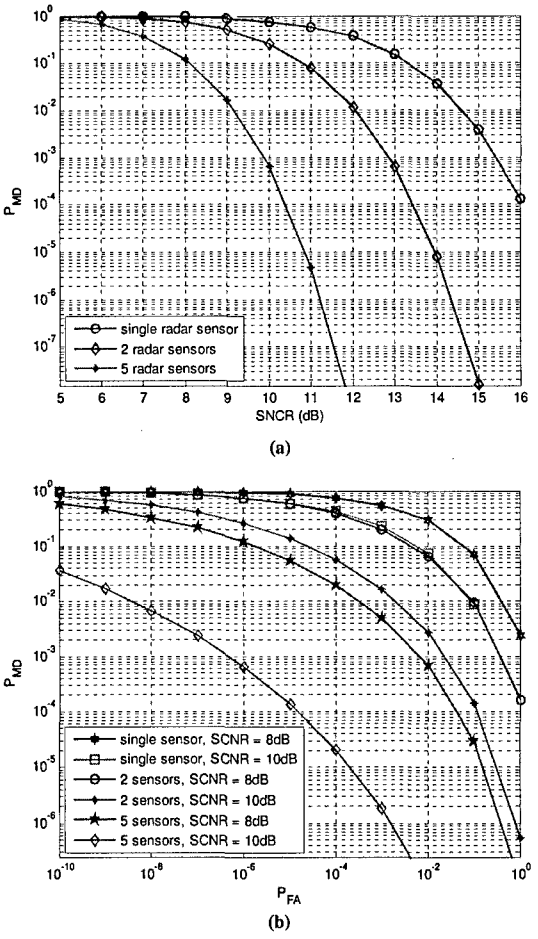

Fig. 3. Non-fluctuating target models: (a) Probability of miss-detection P_{MD} as a function of $SCNR$, $P_{FA} = 10^{-6}$, (b) Miss-detection probability P_{MD} as the function of false alarm probability P_{FA}, $SCNR = 8dB$ and $SCNR = 10dB$

Based on these results, we recognize that the probability of miss-detection P_{MD} at the same SCNR decreases when the number of radar sensors in the network increases, e.g., at SCNR=10 dB, P_{MD} of the 5-radar RSN is much lower than that of the 2-radar RSN. It is desirable for P_{MD} to be as low as possible. In the real world, P_{MD} less than 10% is reasonable. We can observe that it is very difficult to achieve this P_{MD} with a single radar at low P_{FA} and if possible, the SCNR must be very high. However, the 5-radar RSN can maintain very low P_{MD} at a low P_{FA}.

We also notice that it requires more SCNR with fluctuating targets than with non-fluctuating targets to achieve the same P_{MD}. For example, when we use 5 radar sensors and P_{MD} is about 10%, SCNR is 9.3 dB for fluctuating targets but less than 9 dB for non-fluctuating targets. At the same values of P_{MD} and SCNR, P_{FA} for non-fluctuating targets is lower than for

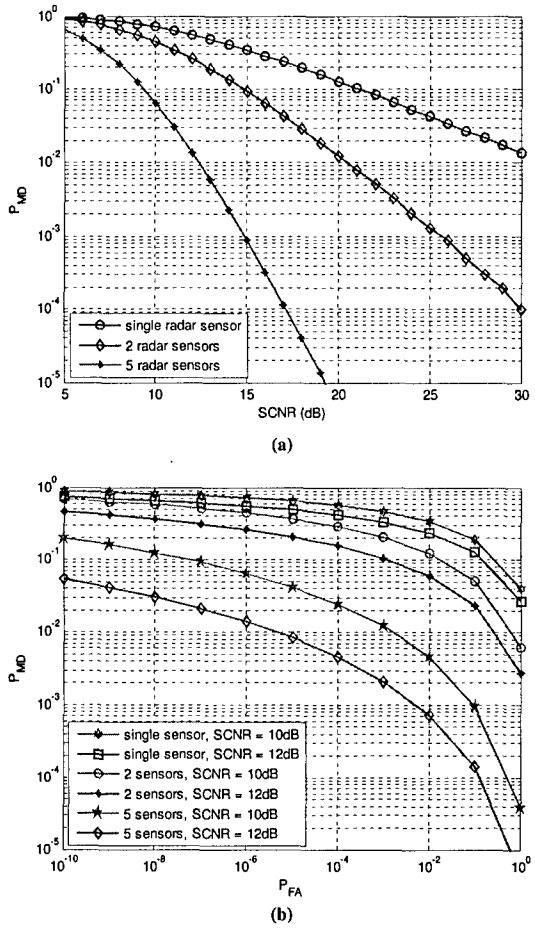

Fig. 4. Fluctuating target models: (a) Probability of miss-detection P_{MD} as a function of $SCNR$, $P_{FA} = 10^{-6}$, (b) Miss-detection probability P_{MD} as the function of false alarm probability P_{FA}, $SCNR = 10dB$ and $SCNR = 12dB$

fluctuating targets. So, depending on specific scenarios, we can choose P_{FA} and SCNR logically in order to get the desired detection performance.

VI. Conclusion

In this paper, we investigated and applied the spatial-temporal-frequency diversity to improve the detection performance of RSN. We also proposed a receiver for diversity combining in RSN. The probability of miss-detection as a function of the false alarm probability and the signal-to-clutter-plus-noise (SCNR) is analyzed for both non-fluctuating targets and fluctuating targets. Simulation results showed that the detection performance of our diversity scheme-based radar sensor network is much better than that of single radar system using the spatial-temporal diversity only.

However, in this paper, we do not consider other factors that affect the performance of RSN such as crab angle, mutual coupling and beam mismatch between target and steering vector. Although we also study interference in nonhomogeneous environments, we only limit our simulations to the homogeneous environments. In subsequent papers, we will investigate methods to solve the above restrictions and develop our scheme to solve advanced problems in radar sensor networks: target search and target recognition.

Acknowledgement

This work was supported by the Office of Naval Research (ONR) Young Investigator Award under Grant N00014-03-1-0466

References

[1] S. Kadambe, "Feature discovery and sensor discrimination in a network of distributed radar sensors for target tracking" *HRL Laboratories, LLC, 2001.*

[2] C.J. Baker, A.L.Hume, "Netted Radar Sensing," *IEEE A&E Systems Magazine, Feb. 2002.*

[3] R. Fitzgerald, "Effects of range-doppler coupling on chirp radar tracking acuracy," *IEEE Trans on Aerospace and Eletronic Systems,* vol. 10, pp. 528-532, July 1974.

[4] M. R. Bell, "Information theory and radar waveform design," *IEEE Trans on Information Theory,* vol. 39, no. 5, pp. 1578-1597, Sept. 1993.

[5] C. E. Baum, et al, "The singularity expansion method and its application to target identification," *Proc. of the IEEE,* vol 79, no. 10, Oct 1991.

[6] William L. Melvin, "A STAP Overview," *IEEE A&E Systems Magazine,*, Vol 19, no. 1 , Jan. 2004, pp. 19-35.

[7] R. Klemm, "Introduction to Space-Time Adaptive Processing," *Electronics & Communication Engineering Journal, Feb. 1999.*

[8] Ward, J., "Space-Time Adaptive Processing for Airborne Radar," *Lincoln Laboratory Technical Report 1015, Dec. 1994.*

[9] J.R Guerci, *Space-Time Adaptive Processing for Radar, Artech House, 2003.*

[10] Mark A. Richards, *Fundamentals of Radar Signal Processing, McGraw-Hill Companies, New York 2005.*

[11] Bassem R. Mahafza, *Radar Systems Analysis and Design, Chapman & Hall, 2005.*

[12] Raviraj S. Adve and et.al, "Practical Joint Domain Localized Adaptive Processing in Homogeneous and Non-homogeneous Environments: Part I - Homogeneous Environments," *IEE Part F: Proceedings on Radar, Sonar and Navigation, Oct. 1999.*

[13] H.Wang and L. Cai, "A localized adaptive MTD processor," *IEEE Transaction on Aerospace and Electronic Systems,, Vol 27, no.3, pp 532-539, 1991.*

[14] J. Goldstein, L. Scharf, and I. Reed, "A multistage representation of the Wiener filter based on orthogonal projections," *IEEE Trans. Inform. Theory,, vol. 44, no. 7, pp. 29432959, 1998.*

[15] T.K. Sarkar and N. Sangruji, "An adaptive nulling system for a narrow-band signal with a look-direction constraint utilizing the conjugate gradient method," *IEEE Trans. Antennas Propagat., vol. 37, no. 7, pp. 940944, July 1989.*

[16] Chunhung Richard Lin and Mario Gerla, "Adaptive Clustering for Mobile Wireless Networks," *IEEE journal on selected areas in communications,, vol. 15, no. 7, Sep. 1997.*

[17] Swerling, P., "Probability of Detection for Fluctuating Targets," *IRE Transactions on Information Theory,, vol IT-6, pp. 269-308, April 1960.*

[18] Q. Liang, "Waveform design and diversity in radar sensor networks: Theoretical analysis and application to Automatic Target Recognition", *accepted by Intl Workshop on Wireless Ad Hoc and Sensor Networks, June 2006, New York.*

[19] R. Nitzberg, "An effect of range-heterogeneous clutter on adaptive doppler filters," *IEEE Transaction on Aerospace and Electronic Systems, Vol 26, no.3, pp 475-480, May 1990.*

[20] William L. Melvin, "Space-time adaptive radar performance in heterogeneous clutter," *IEEE Transaction on Aerospace and Electronic Systems, Vol 36, no.2, pp 621-633, April 2000.*

Channel Capacity of Virtual MIMO-Based Wireless Sensor Networks with Impefect CSI

Lingming Wang and Qilian Liang
Department of Electrical Engineering
University of Texas at Arlington
Arlington, TX 76019-0016. USA
E-mail:wang@wcn.uta.edu. liang@uta.edu

Abstract— **Virtual multiple-input multiple-output (MIMO) communication architecture is popularly used in Wireless Sensor Networks (WSN) recently to counteract the severe communication. Channel state information (CSI) is a crucial factor to MIMO communication system. Waterfilling strategy based on the CSI at transmitter (CSIT) is an optimal power allocation scheme, especially at low signal-to-noise ratio (SNR) scenario. However, CSIT is usually imperfect in practice. In this paper, we will analyze the how the estimation error would impact the channel capacity for the MIMO system at low SNR region.**

Index Terms— **Wireless sensor networks, channel capacity, channel state information, estimation error.**

I. Introduction

The infusion and maturation of the Micro Mechanical System(MEMS), computations, and wireless communication technologies has advanced the development of Wireless Sensor Networks (WSN). In WSN, a large amount of low cost sensor nodes are densely deployed to monitor the environment of interest. Due to the various applications [7] [16], WSN has generated flurry of research activity.

The sensor nodes are miniature devices equipped with a sensor, a transceiver and the necessary electronic circuites and able to collect and forward information[10]. These nodes are designed to be deployed randomly or strategically in area and left operating until their battery is totally used up. Obviously, WSN is power, bandwidth, and complexity limited.

Virtual multiple-input multiple-output (MIMO) communication architecture have recently been applied in energy-constraint, distributed WSN so as to economize energy consumption [5] [14] [15]. In these implementations, the underlying MIMO concepts include the simple Alamouti scheme [1] and the virtual Bell Labs Layered Space-time (V-BLAST) architecture [23].

In addition to the potential advantage of energy efficiency in MIMO , the theoretical capacity gain of MIMO channels is also enormous. It has been proved that MIMO capacity nominally increases linearly with the number of antenna elements. However, MIMO channel capacity depends heavily on how accurately we know the channel. Specifically, when the instantaneous channel gains, called channel state information (CSI), are known perfectly at both the transmitter and the receiver of the MIMO system, the transmitter can adapt its transmission strategy relative to the instantaneous channel state, so the maximum MIMO channel capacity can be achieved.

Channel capacity for MIMO channel has been intensively studied in different scenarios since the pioneer work by Winters [18] and Telatar [17]. Most of them modeled the channel as fully scattering, *i.e.*, Rayleigh fading channel. The Rayleigh fading model is a reasonable assumption for many fading environments encountered in practical communication systems. However in some other cases, (*e.g.*, in WLAN application, and for sure, WSN fits in this scope), there is a strong deterministic Line-Of-Sight (LOS) component between the transmitter and receiver, which gives rise to Rician fading model. The Rician distribution is characterized by the Rice factor, k, which reflects the relative strength of the direct LOS path component. When $k = 0$, this model reduces to Rayleigh fading and $k \to \infty$ the model reduces to AWGN channel. The capacity of a Rician channel with receiver CSI but without any knowledge even the Rice factor at the transmitter has been studied in [8] [6]. [13] assumes that there is perfect CSI at receiver (CSIR), meanwhile the transmitter has partial CSI, *i.e.*, the knowledge of the value of the Rice factor.

In this paper, we assume that the transmitter has full/partial CSI, however, there is error of the CSI. We will investigate how the error impact the channel capacity.

The remainder of this paper is organized as follows. In section II we briefly present the relay virtual MIMO architecture for WSN and the underlying one-hop MIMO system model. Whereafter, we investigate the channel capacity with imperfect CSI in sectionIII. The numerical results will be presented in sectionIV. And we make the conclusion and propose the future work in sectionV.

II. Virtual MIMO architecture and System Model

A. Virtual MIMO architecture

In this section, we will first briefly review the virtual MIMO architecture applied in WSN.

The nodes in a WSN is usually of small dimensions. Thus it may not be realistic to assume these inexpensive sensor nodes are equipped with multiple antennas. [5] first proposed to realize MIMO communication architecture in a WSN consisting of single-antenna sensor nodes via sensor cooperation. The MIMO architecture applied here is shown in Fig. 1

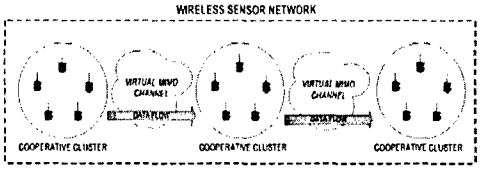

Fig. 1. Virtual MIMO architecture in WSN

There is a transmitter cluster, which is composed of a group of N_T cooperative sensor nodes, communicating with a receiver cluster, which is compose of a set of N_R cooperative sensor nodes. In order to fulfil the communication, the transmitter cluster should do:

- broadcasting the data within the cluster, so that all the active sensor nodes inside the cluster can encode and send out the data during the MIMO transmission;
- transmitting the data via the $N_T * N_R$ MIMO channel.

These two functionalities should be carried out in two orthogonal channel. Here, we assume time division (TD) scheme is applied. These two TD channels are referred as *Intracluster* channel and *Intercluster* channel. For *Intracluster* channel, it is falling into the broadcast capacity region. In the *Intercluster*, the N_T sensor nodes jointly transmit data to the receiver cluster by using a $N_T * N_R$ virtual MIMO channel. So, we will mainly focus on the *Intercluster* MIMO channel.

B. System model

In this paper, we only consider single user scenario. N_T transmitter sensor nodes and N_R receiver sensor nodes equal to N_T transmitting antenna and N_R receiving antenna respectively. Throughout, we assume that $N_R \geq N_T$. The discrete-time received signal in such a system can be modeled in matrix form as

$$\mathbf{y}(i) = \mathbf{H(i)x(i)} + \eta(i) \tag{1}$$

where at symbol time i, $\mathbf{x}(i)$ is the $N_T \times 1$ vector of transmitted signal on the N_T transmitting sensor nodes, $\mathbf{y}(i)$ is the $N_R \times 1$ vector of received signal on the N_R receiving sensor nodes, and $\eta(i)$ is the $N_R \times 1$ additive receiver noise vector. We assume the components of the noise $\eta(i)$ to be independent, zero-mean, circularly symmetric complex Gaussian with independent real and imaginary parts having equal variances. The noise is also assumed to be independent with respect to the time index, and $R_\eta = E[\eta(i)\eta(i)^H] = \sigma_\eta^2 I_{N_R}$, where $I_{N_R} \in \mathbb{C}^{N_R \times N_R}$ denotes the identity matrix, and A^H denotes the hermitian conjugate of the matrix A.

The CSI is the channel matrix $\mathbf{H}(i) \in \mathbb{C}^{N_R \times N_T}$. The (m,n)-th element of the matrix $\mathbf{H}(i)$ represents the fading coefficient value at time i between the m-th receiving sensor node to the n-th transmitting sensor node. The $\mathbf{H}(i)$ corresponding to each channel use is assumed to be independent from that of other uses, *i.e.*, $\mathbf{H}(i)$ and $\mathbf{H}(j)$ are independent when $i \neq j$. In this sense, the time index i can be dropped so as to simplify notation.

In Rician fading the elements of $\mathbf{H}$ are nonzero mean, complex Gaussian variables. Hence, we can model the channel matrix $\mathbf{H}$ as a sum of two components, a fixed (LOS) component and a variable (or scattered) component,

$$\mathbf{H} = \overline{\mathbf{H}} + \widetilde{\mathbf{H}} \tag{2}$$

and

$$\begin{aligned} \overline{\mathbf{H}} &= E\{\mathbf{H}\} \\ &= \frac{\mu}{\sqrt{2}}(1+i)\Psi_{N_R,N_T} \end{aligned} \tag{3}$$

where Ψ_{N_R,N_T} is defined as the $N_R \times N_T$ matrix of all ones. $E\{\cdot\}$ is an expectation operation. $\widetilde{\mathbf{H}}$ is a complex distributed matrix with zero-mean, denoted as $\widetilde{\mathbf{H}} \sim \mathcal{N}_c(\mathbf{0}, \mathbf{I}_{N_T} \bigotimes \mathbf{\Sigma})$, with the probability density function (pdf) [4] [12]

$$f_{\widetilde{H}}(\widetilde{\mathbf{H}}) = \frac{1}{(\pi)^{N_T N_R} |\Sigma|^{N_T}} e^{-tr[\Sigma^{-1}\widetilde{H}\widetilde{H}^H]}, \tag{4}$$

where *tr* denotes the trace of a matrix, Σ is the Hermitian covariance matrix of the columns (assumed to be the same for all the columns) of $\widetilde{\mathbf{H}}$,

$$\Sigma = 2\,\sigma^2\,\mathbf{I}_{N_R}. \tag{5}$$

The strength of the LOS component can be indicated by the *Rician K* factor,

$$K = 10\,log_{10}(\frac{|\mu|^2}{2\sigma^2})\,dB. \tag{6}$$

In the case of Rayleigh fading, which is an extreme scenario of Rician fading, $K = 0$, which also implies that $\mu = 0$. The parameters should be normalized as

$$|\mu|^2 + 2\,\sigma^2 = 1, \tag{7}$$

so that the signal-to-noise ratio (SNR) will not be scaled by the channel. We also assume that the channel is block

fading [3], *i.e.*, $\mathbf{H}$ remains constant over $T \geq N_T$ symbol periods and changes in an independent fashion from block to block.

III. One Hop Channel Capacity of MIMO Rician Fading Channel

The CSI is the channel matrix $\mathbf{H}$. Based on different knowledge of the CSI, we can get different system performance, including channel capacity.

A. Error Model

In a realistic scenario, however, the CSI is generally imperfect. The receiving sensor node can estimate the CSI, *i.e.*, the matrix $\mathbf{H}$, using training sequences, *e.g.*, pilot symbols. For CSIT, basically there are two ways [2],

- The transmitting sensor nodes can estimate the channel using the signals received in the reverse link, and use it as an estimate in the forward link, because of the channel reciprocity principle. During the procedure of estimation, estimation error will be introduced without doubt. Suppose the estimation is unbiased, the estimated CSI, $\hat{\mathbf{H}}$ can be formulated as

$$\hat{\mathbf{H}} = \mathbf{H} + \xi \tag{8}$$

  where ξ is the estimation error. The entries of ξ are assumed to be i.i.d. and zero-mean circularly symmetric complex Gaussian. ξ is independent from the real channel realization.
- The transmitter can obtain the CSI through a feedback channel from the receiver to the transmitter. Besides the Gaussian estimation error at the receiver, due to the finite capacity of the feedback channel, the channel response has to be quantized, which will introduce the another quantization noise to the CSIT. The receiving sensor nodes can uniformly quantize the real and imaginary parts of all the entries of the CSI matrix $\mathbf{H}$. Suppose the quantization step size is Δ_q, assume that there will be no error in the transmission, the quantization signal-to-noise ratio SNR_q is given in [19] as,

$$SNR_q = \frac{6\sigma_h^2}{\Delta_q^2} \tag{9}$$

  where σ_h^2 is the variance of each component of $\mathbf{H}$. Notice that when the Δ_q is sufficiently small, the quantization SNR_q will be very large.

We will focus on the Gaussian estimation error in the following analysis. And we make the following assumption.

- The transmitting sensor nodes have a total power constraint P, however, they can adapt their power allocation according to the channel fading so as the maximize capacity. The power constraint condition can be mathematically presented as,

$$E(P) = E(tr(Q)) \leq \bar{P}. \tag{10}$$

- Either there exist a perfect and instantaneous feedback channel from the receiver to the transmitter, or the delay from the obtaining reverse-channel information to applying the information to the forward-link is negligible. So the only error we consider is the estimation error in (8).

B. Channel Capacity with Perfect CSIR and CSIT

If CSI is known both at the transmitting and receiving sensor nodes, the transmitting sensor nodes can adapt its transmission strategy according to this CSI. The channel capacity of such a MIMO system with perfect CSIR and CSIT is nothing but the average of the capacities achieved with each channel realization. The formula is given in [9]

$$C = \mathbb{E}_{\mathbf{H}}[\max_{Q:tr(Q)=P} \log|\mathbf{I}_{\mathbf{N_R}} + \mathbf{HQH^H}|] \tag{11}$$

where $\mathbf{Q}$ is the input covariance matrix as

$$\mathbf{Q} = E(\mathbf{x}\mathbf{x}^{\mathbf{H}}). \tag{12}$$

C. Optimal power allocation strategy: waterfilling

With CSI at both the receiver and the transmitter, optimal power allocation strategy based on the $\mathbf{H}$ should be applied to maximize the channel capacity in (11) [22]. The joint singular value decomposition (SVD) and *waterfilling* power allocation technique provides the optimum solution [20].

The SVD of the channel matrix $\mathbf{H}$ is presented as

$$\mathbf{H} = \mathbf{U}\,\mathbf{\Lambda}\,\mathbf{V}^H \tag{13}$$

where $\mathbf{U} \in \mathbb{C}^{N_R \times N_R}$ is an unitary matrix of orthonormalized eigenvector of $\mathbf{H}\mathbf{H}^T$, $\mathbf{V} \in \mathbb{C}^{N_T \times N_T}$ is an unitary matrix of orthonormalized eigenvector of $\mathbf{H}^T\mathbf{H}$, and $\mathbf{\Lambda} \in \mathbb{C}^{N_R \times N_T}$ is a rectangular matrix whose diagonal elements are non-negative real numbers and whose off-diagonal elements are zero. The diagonal elements $\lambda_1, \lambda_2, \ldots, \lambda_{N_{min}}$ denotes the i^{th} singular value of $\mathbf{H}$, and $\lambda_1 \geq \lambda_2 \geq \cdots \geq \lambda_{N_{min}} > 0$, where $N_{min} = min(N_T, N_R)$.

The MIMO channel can then be represented as a parallel channel [22] based on the ordered singular value λ_i as

$$\tilde{y}_i = \lambda_i \tilde{x}_i + \tilde{\eta}_i, \qquad i = 1, \cdots, N_{min} \tag{14}$$

and

$$\begin{aligned} \tilde{\mathbf{x}} &= \mathbf{V}^H\mathbf{x}, \\ \tilde{\mathbf{y}} &= \mathbf{U}^H\mathbf{y}, \\ \tilde{\eta} &= \mathbf{U}^H\eta. \end{aligned}$$

Substituting (13) into (11), we can get

$$C = \max_{p_i:\sum_i p_i \le P} \sum_{i=1}^{N_{min}} \log(1 + \frac{\lambda_i^2 p_i}{\sigma_\eta^2}), \quad (15)$$

The transmitting powers are allocated to each sub-channel based on their strength according to the waterfilling strategy,

$$\frac{p_i}{P} = (0, \mu - \frac{\sigma_\eta^2}{\lambda_i^2 P})^+ \quad (16)$$

where $(A)^+ = \max(0, A)$, and μ is the waterfilling level which should be chosen so that the total power constraint is satisfied:

$$\sum_{i=1}^{N_{min}} (\mu - \frac{\sigma_\eta^2}{\lambda_i^2 P}) = 1. \quad (17)$$

Therefore, the maximum channel capacity can be obtained as:

$$C_{max} = \sum_{i,p_i>0} \log(1 + \frac{p_i \lambda_i^2}{\sigma_\eta^2}) \quad (18)$$

D. Channel Capacity with imperfect CSIT

When there is error in the estimation as discussed in section III-A, what the transmitter knows is the estimated channel matrix $\hat{\mathbf{H}}$ in (8). Hereby, the decomposition of the MIMO channel and the application of waterfilling strategy in section III-C are both based on $\hat{\mathbf{H}}$, which contains zero-mean Gaussian Noise. Apparently, the singular value $\hat{\lambda}_i$ obtained from $\hat{\mathbf{H}}$ will be different from λ_i. Consequently, the maximum channel capacity in (18) is no long tenable because the power allocation is not optimized. we will show how the estimation error impact the channel capacity in section IV.

IV. Numerical Results and Discussions

Numerical results are presented to show how Gaussian estimation errors degrade the channel capacity in i.i.d. Rician fading MIMO channel based on Monte-Carlo simulations.

Two MIMO systems, where $N_T = N_R = 3$ and $N_T = N_R = 6$, respectively were simulated. The MIMO channels were treated as 9 and 36 i.i.d. single-input-single-output (SISO) Rician channels applying the Jakes's model [21] [11].

In Figure 2, we compare the average channel capacity using equal power allocation, waterfilling strategy with perfect CSIT, and waterfilling strategy with channel estimation error as $\sigma_\xi^2 = 0.1, 0.25, 0.5, 1$ respectively in a $N_T = 3, N_R = 3$ MIMO system with the Rician fading parameter as $K = 10$ for all the independent $3 \times 3 = 9$ sub-channels, and f_d is randomly chosen from $0 \sim 30Hz$ for sub-channels.

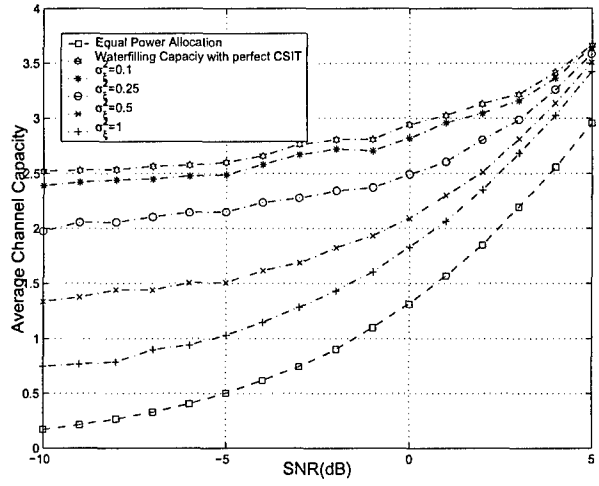

Fig. 2. Average Channel Capacity for $N_T = N_R = 3$ in Rician fading MIMO system with $K = 10$.

We can see clearly that the waterfilling scheme performs much better than the equal power allocation scheme, which does not need CSIT, even with estimation error, especially at the low SNR. At high SNR, the difference between waterfilling and equal power allocation scheme becomes slimmer.

We then set the Rice factor $K = 0$ for all the sub-channels, which means it is Rayleigh fading. The results are shown in Figure 3.

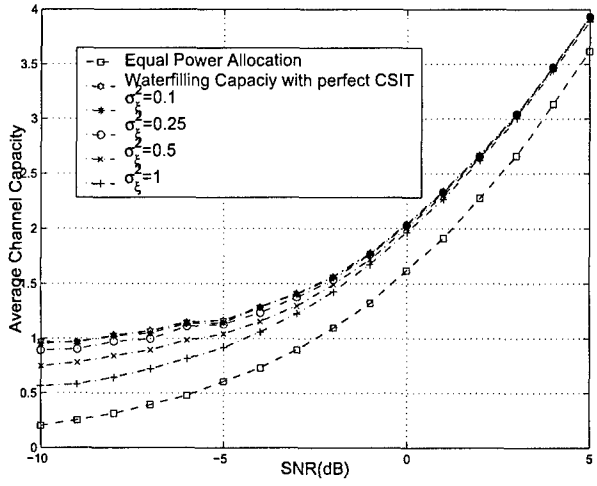

Fig. 3. Average Channel Capacity for $N_T = N_R = 3$ in Rayleigh fading MIMO system.

For Rayleigh fading MIMO channel, channel capacity is more sensitive to the SNR, but less sensitive to the estimation error.

Figure 4 5 show the results of the simulation of $N_T =$

$N_R = 6$ system.

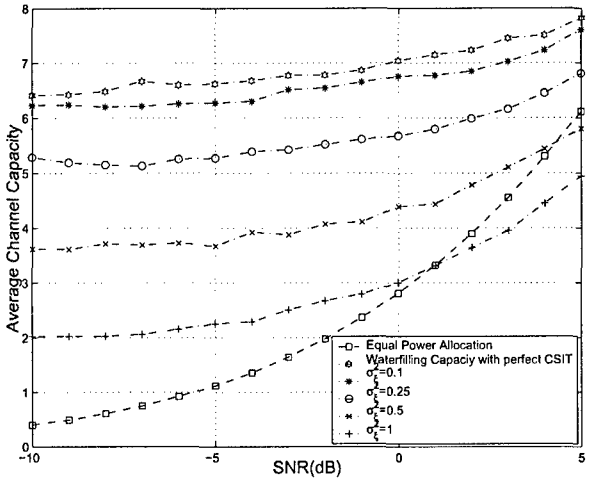

Fig. 4. Average Channel Capacity for $N_T = N_R = 6$ in Rician fading MIMO system with $K = 10$.

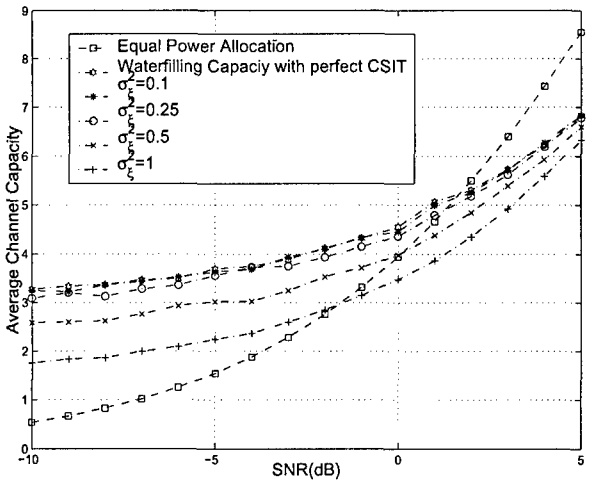

Fig. 5. Average Channel Capacity for $N_T = N_R = 6$ in Rayleigh fading MIMO system.

We notice that the average channel capacities of equal power allocation strategy are larger than the ones of waterfilling strategy at high SNR. When we perform the waterfilling scheme, some of the decomposed parrallel channels may not be assigned any power, so that some of the diversity gain is lost.

We compare the average channel capacities of $N_T = N_R = 3$ and $N_T = N_R = 6$ MIMO systems at Figure 6. The Rician fading parameters K and f_d for each independent sub-channel are chosen from $0 \sim 10$ and $0 \sim 30Hz$ respectively.

Without any doubt, the average channel capacity of the $N_T = N_R = 6$ MIMO system is much larger than the one of the $N_T = N_R = 3$ MIMO system.

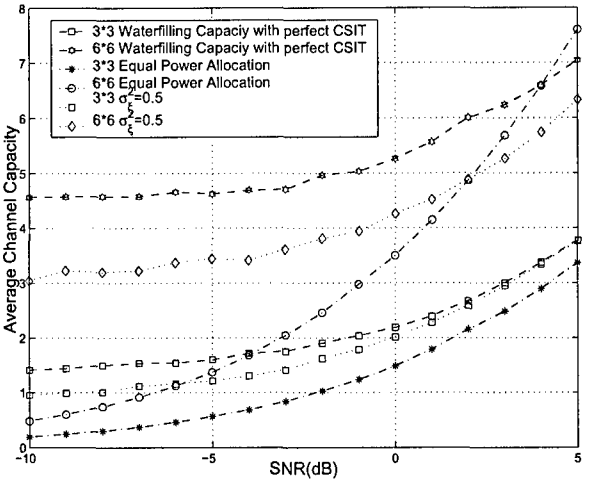

Fig. 6. Average Channel Capacities for $N_T = N_R = 3$ and $N_T = N_R = 6$ MIMO systems.

Figure 7 shows the average channel capacities get from $N_R = 3, N_T = 6$ and $N_R = 6, N_T = 3$ MIMO systems.

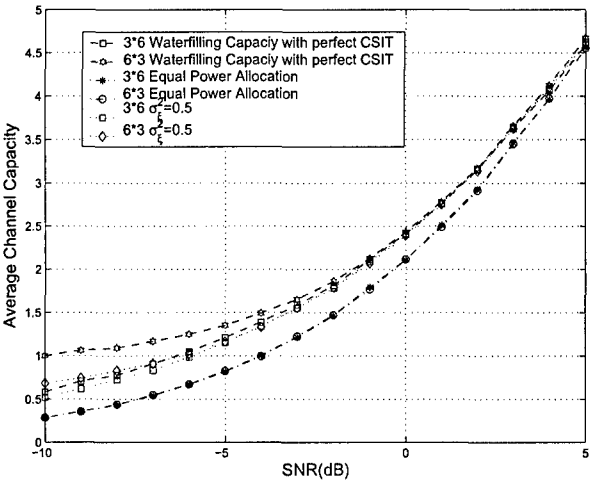

Fig. 7. Average Channel Capacities for $N_R = 3, N_T = 6$ and $N_R = 6, N_T = 3$ MIMO systems.

For equal power allocation algorithm, the channel capacities for the two systems are exactly the same. However, for waterfilling strategy, more gains can be obtained from the receiving part.

V. Conclusions and Future Works

A. Conclusions

Virtual MIMO structure is very attractive to WSN due to its potential huge diversity gain. WSN is power constraint,

however, with CSIT, waterfilling algorithm can be applied to optimize the power allocation in each sub-channel of the MIMO system based on the estimated channel matrix $\mathbf{H}$, so as to maximize the channel capacity of the system even in deep fading scenario. However, in reality, both the estimation error and the quantization noise will be introduced when estimate the channel.

In this paper, we first discuss the virtual MIMO structure in WSN, then set up the MIMO system model focused on one-hop intercluster transmission. Afterwards, the error model of the channel estimation is investigated, and how the estimation error will impact the optimal waterfilling strategy is analyzed. Numerical results were presented based on the Monte-Carlo simulations.

B. Future work

- In WSN, transmission are generally multi-hopped, as shown in section II-A. In this paper, we only focused on the one-hop channel capacity, however, the overall capacity including relaying hops should be derived.
- We only consider the estimation error in this paper. Delay of the estimation, i.e., $\mathbf{H}(t-T) \neq \mathbf{H}(t)$, and only $\mathbf{H}(t-T)$ is available, can also impact the system performance.
- Wireless sensor nodes are usually small-sized with limited computing capability. Waterfilling algorithm is based on the singular values of MIMO channel matrix, which needs considerable computing. Besides the overhead to the transmitting sensor nodes is also not negligible. Simple but efficient power allocation algorithms should be developed.

ACKNOWLEDGEMENT

This work was supported by the Office of Naval Research (ONR) Young Investigator Award under Grant N00014-03-1-0466.

REFERENCES

[1] S. M. Alamouti, "A simple transmit diversity techinique for wireless communications," *IEEE J. Sel. Areas. Commun.*, vol. 16, no. 8, pp. 1451-1458, Oct. 1998.

[2] M. Bengtsson, and B. Ottersten "Optimal and suboptimal transmit beamforming," in *Handbook of Antennas in Wireless Communications.*, L. C. Godara, Ed. Boca Raton, Fl: CRC, 2001.

[3] E. Biglieri, J. Proakis, and S. Shamai, "Fading channels: Information-theoretic and communication aspects," *IEEE Trans. Inf. Theory*, vol. 44, no. 6, pp. 2619-2692, Oct. 1998.

[4] A. G. Constantine, "Some non-central distribution problems in multivariate analysis," *Ann. Math. Stat.*, vol. 34, pp. 1270-1285, Dec. 1963.

[5] S. Cui, A. J. Goldsmith, and A. Bahai, "Energy-efficiency of MIMO and cooperative MIMO techniques in sensor networks," *IEEE J. Sel. Areas. Commun.*, vol. 22, no. 6, pp. 1089-1098, Aug. 2004.

[6] P. F. Driessen, and G. J. Foschini, "On the capacity formula for multiple-input multiple-output wireless channels: A geometric interpretation ," *IEEE Trans. Commun.*, vol. 2, pp. 173-176, Feb. 1999.

[7] D. Estrin, and R. Govindan, " Next century chanlleges:scalable coordination in sensor networks ," *Mobicom 1999, Seattle, WA.*, pp. 263-270, August 1999.

[8] F. R. Farokhi, G. J. Foschini, A. Lozano, and R. A. Valenzuela, "Link-optimal space-time processing with multiple transmit and receiver antennas", *IEEE Commun. Lett.*, vol. 5, pp. 85-87, Mar. 2001.

[9] A. Goldsmith, S. A. Jafar, N. Jindal, and S. Vishwanath "Capacity limits of MIMO channels," *IEEE J. Sel. Areas. Commun.*, vol. 21, no. 5, pp. 684-702, June 2003.

[10] Jason L. Hill, and David E. Culler, " Mica: A Wireless Platform for Deeply Embedded Networks ," *Micro, IEEE,*, Volume: 22, Issue: 6, pp. 12-24, Nov.-Dec. 2002.

[11] W. C. Jakes Jr., *Mircowave Mobile Communications* New York: Wiley, 1974

[12] A. T. James, "Distributions of matric variates and latent roots derived from normal samples," *Ann. Math. Stat.*, vol. 35, pp. 475-501, June 1964.

[13] S. K. Jayaweera, and H. V. Poor, "MIMO Capacity results for Rician fading channels," *Proc. IEEE Global Telecommunications Conference*, vol. 4, pp. 1806-1810, Dec. 2003.

[14] S. K. Jayaweera, "Energy analysis of MIMO techniques in wireless sensor networks," *38th Annual Conf. on Inform. Sci. and Syst. (CISS 04)* Princeton, NJ, Mar. 2004

[15] S. K. Jayaweera, "An energy-efficient virtual MIMO communications architecture based on V-BLAST processing for distributed wireless sensor networks," *Proc. IEEE Secon.*, Santa Clara, CA, USA, Oct. 2004

[16] G. J. Pottie, and W. J. Kaiser, " Wireless integrated network sensors ," *Communications of the ACM*, vol. 43, no. 5, pp. 551-558, May 2000.

[17] I. E. Telatar, "Capacity of multi-antenna Gaussian channels", *Eur. Trans. Telecomm. ETT*, vol. 10, no. 6, pp. 585-596, Nov. 1999.

[18] J. Winters, "On the capacity of radio communication systems with diversity in a Rayleigh fading environment," *IEEE J. Sel. Areas. Commun.*. vol. 5, pp. 871-878, June 1987.

[19] A. Pascula-Iserte, D. P. Palomar, A. I. Perez-Neira, and M. A. Lagunas "A Robust maximin approach for MIMO communications with imperfect channel state information based on convex optimization," *IEEE. Trans. Singal Proc.*, vol. 54, no. 1, pp. 346-359, Jan. 2006.

[20] G. G. Raleigh, and J. M. Cioffi, "Spatio-temporal coding for wireless communication," *IEEE. Trans. Commun.*, vol. 46, pp. 357-366, Mar. 1998.

[21] T. S. Rappaport, *Wireless Communications* Englewood Cliffs, NJ: Prentice Hall, 1996

[22] D. Tse, and P. Viswanath, *Fundamentals of Wireless Communications* Cambridge, U.K.: Cambridge Univ. Press, 2005

[23] P. W. Wolniansky, G. J. Foschini, G. D. Golden, and R. A. Valenzuela, "V-BLAST: An architecture for realizing very high data rates over the rich-scattering wireless channel," *Proc. ISSSE*, Pisa, Italy, Sep. 1998, invited.

Cross-Layer Design for Wireless Sensor Networks based on Cooperative MIMO Techniques

Xinsheng Xia and Qilian Liang
Department of Electrical Engineering
The University of Texas at Arlington
416 Yates Street, Rm 518
Arlington, TX 76010-0016
Email: xia@wcn.uta.edu, liang@uta.edu

Abstract— **The multiple-input and multiple-output(MIMO) system can be used to increase throughtput throught multiplexing or to improve PLD(Packet Loss Ration) throught diversity. However, the throughtput and PLR will also be determined by MAC layer and network layer protocols. In this paper, we coordinate physical layer, data-link layer and network layer for cross-layer design. Performance analysis and simulations show that throughput and packet performance will have different performance compared with only consider the MIMO scheme in physical layer as the increase of the number of transmitters.**

I. Introduction

The demand for energy efficiency and Quality of Service (QoS) in wireless sensor networks is growing in a rapid speed. A strict layered design is not flexible enough to cope with the dynamics of the wireless sensor networks [1]. To enhance the energy efficiency and QoS, we consider the combination of physical layer, data-link layer and network layer together, a cross-layer approach. Cross-layer design could introduce the layer interdependencies to optimize overall network performance.

The general methodology of cross-layer design is to maintain the layered architecture, capture the important information that influence other layers, exchange the information between layers and implement adaptive protocols and algorithms at each layer to optimize the performance.

However, cross-layer design can produce unintended interactions among protocols, such as an adaptation loops. It is hard to characterize the interaction at different layers and joint optimization across layers may lead to complex algorithm.

MIMO systems can support higher data rate under the same transmit power budget and bit-error-rate performance requirement as single-input-single-output (SISO) systems. However, direct application of multi-antenna techniques to sensor networks is impractical duo to the limited physical size of a sensor node that is typically can only support a single antenna. Fortunately, if we allow individual single-antenna nodes to cooperate on information transmission and/or reception, a cooperative MIMO system can be constructed such that energy efficient MIMO scheme can be deployed [2].

Using cooperative MIMO, we show that the end-to-end performance can be dramatically improved. Moreover, the novel approach of distributed Alamouti [3] coding provides diversity gain with no local information exchange, as is typically required in node cooperation.

However, the routing and MAC layer protocols have different effects on network performance compared with cooperative MIMO technique. Performance analysis and simulation results have been illustrate this situation

The remainder of this paper is structured as following. In section II, we introduce the preliminaries. In section III, we make the performance analysis for all the layers. In section IV, we make the performance analysis for cross-layer model. Simulation results and discussions are presented in section V. In section VI, we conclude the paper.

II. Preliminaries

A. IEEE 802.11a OFDM PHY

The physical layer is the interface between the wireless medium and the MAC [4]. The principle of OFDM is to divide a high-speed binary signal to be transmitted over a number of low data-rate subcarriers. A key feature of the IEEE 802.11a PHY is to provide 8 PHY modes with different modulation schemes and coding rates, making the idea of link adaptation feasible and important. BPSK, QPSK, 16-QAM and 64-QAM are the supported modulation schemes. The OFDM provides a

data transmission rates from 6 to 54MBPS. The higher code rate of 2/3 and 3/4 are obtained by puncturing the original rate 1/2 code.

B. IEEE 802.11 MAC

The 802.11 MAC uses Carrier-Sense Multiple Access with Collision Avoidance (CSMA/CA) to achieve automatic medium sharing between compatible stations. In CSMA/CA, a station senses the wireless medium to determine if it is idle before it starts transmission. If the medium appears to be idle, the transmission may proceed, else the station will wait until the end of the in-progress transmission. A station will ensure that the medium has been idle for the specified inter-frame interval before attempting to transmit.

Besides carrier sense and RTS/CTS mechanism, an acknowledgment (ACK) frame will be sent by the receiver upon successful reception of a data frame. Only after receiving an ACK frame correctly, the transmitter assumes successful delivery of the corresponding data frame. The sequence for a data transmission is: RTS-CTS-DATA-ACK.

A mobile node will retransmit the data packet when finding failing transmission. Retransmission of a signal packet can achieve a certain probability of delivery. There is a relationship between the probability of delivery p and retransmission times n [5]:

$$n = 1.45 \ln \frac{1}{1-p} \tag{1}$$

The IEEE 802.11 standard requires that the transmitter's MAC discard a data frame after certain number of unsuccessful transmission attempts. According to the requirement of probability of delivery, we choose the minimum number of retransmission. The advantage is we can save energy through avoiding unnecessary retransmission, and ensure probability of delivery.

C. Network Layer

The Ad hoc On Demand Distance Vector (AODV) routing algorithm is a routing protocol designed for ad hoc mobile networks [6]. AODV is capable of both unicast and multicast routing. It is an on demand algorithm, meaning that it builds routes between nodes only as desired by source nodes. It maintains these routes as long as they are needed by the sources. Additionally, AODV forms trees which connect multicast group members. The trees are composed of the group members and the nodes needed to connect the members. AODV uses sequence numbers to ensure the freshness of routes. It is loop-free, self-starting, and scales to large numbers of mobile nodes.

AODV builds routes using a route request/route reply query cycle. As long as the route remains active, it will continue to be maintained. A route is considered active as long as there are data packets periodically travelling from the source to the destination along that path. Once the source stops sending data packets, the links will time out and eventually be deleted from the intermediate node routing tables. If a link break occurs while the route is active, the node upstream of the break propagates a route error message to the source node to inform it of the now unreachable destinations.

Multicast routes are set up in a similar manner. AODV maintains routes for as long as the route is active. This includes maintaining a multicast tree for the life of the multicast group. Because the network nodes are mobile, it is likely that many link breakages along a route will occur during the lifetime of that route.

D. Billiard Mobility

Pick a uniform random direction, advance in that direction. A new random direction is selected every T seconds, where T is exponentially distributed. Boundaries are reflecting, i.e. a node bounces off as off of a mirror.

E. Node Mobility and Channel Fading

Mobility of a mobile node generates a doppler shift, which is a key parameter of fading channel. The doppler shift is

$$f_d = \frac{v}{c} f_c \tag{2}$$

where v is the ground speed of a mobile node, c is the speed of light ($3 \times 10^8 m/s$), and f_c is the carrier. In our simulation, we used the carrier is $6GHz$. For reference, if a node moves with speed $10m/s$, the doppler shift is $200Hz$.

We model channel fading in wireless sensor networks as Rayleigh fading. Rayleigh fading occurs when there is a strong specular (direct path or line of sight component) signal in addition to the scatter (multipath) components. For example, in communication between two infrared nodes, there exist a direct path. The channel gain,

$$g(t) = g_I(t) + j g_Q(t) \tag{3}$$

can be treated as a wide-sense stationary complex Gaussian random process, and $g_I(t)$ and $g_Q(t)$ are Gaussian random processes with zero means; and they have same

variance σ^2, then the magnitude of the received complex envelop has a Rayleigh distribution,

$$p_\alpha(x) = \frac{x}{\sigma^2}\exp\{-\frac{x^2}{2\sigma^2}\} \quad x \geq 0 \tag{4}$$

This kind of channel is known as Rayleigh fading channel. A Rayleigh channel is characterized by parameter, the Doppler spread (or single-sided fading bandwidth) f_d. The Rayleigh fade generator is based on Jakes' model [7] in which an ensemble of sinusoidal waveforms are added together to simulate the coherent sum of scattered rays with Doppler spread f_d arriving from different directions to the receiver.

For the values of M for MPSK(Mary phase shift keying), one can use the approximate BER expression obtained by Lu et al [8]. For the AWGN(Additive white Gaussian niose), which is accurate for a wide range of SNRs, again making the substitution $\gamma log_2 M$ for E_b/N_0 followed by averaging over the PDF of γ. Using the alternative form of the Gaussian Q-function, it is straightforward to show that the result of the evaluation is given by:

$$P_b(E) \cong \frac{2}{max(\log_2 M,2)}\sum_{i=1}^{max(\frac{M}{4},1)}\frac{1}{\pi}\times \int_0^{\frac{\pi}{2}} M_\gamma(-\frac{1}{\sin^2\theta}\frac{E_b\log_2 M}{N_0}\sin^2\frac{(2i-1)\pi}{M})d\theta \tag{5}$$

where $M_\gamma(s)$ is the MGF(Moment generating function)of the instantneous fading power γ. For a Rayleigh fading channel, we obtain the following analogous to:

$$P_b(E) \cong \frac{1}{max(\log_2 M,2)}\sum_{i=1}^{max(\frac{M}{4},1)} (1-\sqrt{\frac{\frac{E_b log_2 M}{N_0}sin^2\frac{(2i-1)\pi}{M}}{1+\frac{E_b log_2 M}{N_0}sin^2\frac{(2i-1)\pi}{M}}}) \tag{6}$$

For BPSK, we get the result:

$$P_b(E) \cong \frac{1}{2}(1-\sqrt{\frac{\frac{E_b}{N_0}}{1+\frac{E_b}{N_0}}}) \tag{7}$$

III. Performance Analysis

A. MIMO

It is wildly understood that in a system with multiple transmit and receive antennas, the spectral efficiency is much higher than that of the conventional single-antenna channels, i.e., a MIMO system can provide two types of gains: diversity gain and multiplexing gain.

1) MIMO Diversity Gain: The multiple antennas at the transmitter and receiver can be used to obtain diversity gain: This scheme is also referred to as MIMO beamforming [9] [10]. Beamforming provides diversity gain via coherent combining of the multiple signal paths. Channel knowledge at the receiver is assumed, since this is required for coherent combining. A beamforming strategy corresponds to the precoding and shaping matrices being just column vectors: V=v and U = u.The transmit symbol x is sent over the ith antenna with weight v_i. On the receive side, the signal received on the ith antenna is weighted by u_i^*. The resulting received signal is given by:

$$y = u^H Hvx + u^H n \tag{8}$$

The performance gain then depends on whether or not the channel is known at the transmitter. When the channel matrix H is known, the received SNR is optimized by choosing u and v as the principal left and right vectors of the channel matrix H. That is, the reveived SNR can be shown to equal $\gamma = \sigma_{max}^2\rho$, where σ_{max} is the largest singular value of H.

When the channel is not known to the transmitter, for M_t=2 the Alamouti scheme described in [3] can be used to extract an array gain of M_r and the maximum diversity gain of $2M_r$.

Two-Branch Transmit Diversity with one receiver the scheme uses two transmit antennas and one receive antenna and may be defined by the following three functioin: the ending and transmission sequence of information symbols at the transmitter; the combining scheme at the receiver; the decision rule for maximum likelihood detection.

The encoding and transmission sequence: at a given symbole period, two signals are simultaneously tansmitted from the two antennas. The signal transmitted from antenna zero is denoted by c_1 and from antenna one by c_2. During the next symbol period signal (-c_2^*) is transmiited from antenna zero, and signal c_1^* is transmitted from antenna one where * is the complex conjugate operation.

$$r_1 = h_1c_1 + h_2c_2 + n_1 \tag{9}$$

$$r_2 = -h_1c_2^* + h_2c_1^* + n_2 \tag{10}$$

where r_1 and r_2 are the received signals at time t and t+T and n_1 and n_2 are complex random variables representing receiver noise and interference.

We will build the following two combined signals that are sent to the maximum likelihood detector:

$$\tilde{c_1} = (\alpha_1^2 + \alpha_2^2)c_1 + h_1^* n_1 + h_1 n_2^* \quad (11)$$

$$\tilde{c_2} = (\alpha_1^2 + \alpha_2^2)c_2 + h_1 n_2^* + h_1^* n_1 \quad (12)$$

The combined signals are then sent to the maximum likelihood detector, uses the decision rule to decide the signals c_1 or c_2.

It is further shown that the scheme may easily be generalize to M transmit antennas and one receive antenna to provide diversity gain M.

2) MIMO Multiplexing Gain: One mechanism for utilizing to improve wireless system performance is to obtain gain by decomposing the MIMO channel into parallel channels and multiplexing different data streams onto these channels. By multiplexing independent data onto these independent channels, we get an increase in data rate in comparison to a system with just one antenna at the transmitter and receiver. This increased data rate is called multiplexing gain.

3) MIMO Diversity-Multiplexing Gain Tradeoffs: The MIMO diversity-multiplexing gain tradeoffs is essentially the tradeoff between the error probability and the data rate of a system.

A. Optimal Tradeoff Curve

A schemec(SNR)is said to achieve spatial multiplexing gain r and diversity gain d if the data rate [11]:

$$\lim_{SNR\to\infty} \frac{R(SNR)}{\log SNR} = r \quad (13)$$

and the average error probability

$$\lim_{SNR\to\infty} \frac{\log P_e(SNR)}{\log SNR} = -d \quad (14)$$

For each r, the optimal diversity gain $d_{opt}(r)$ is maximum diversity gain that can be achieved by any scheme.

$$d_{opt}(r) = (M_t - r)(M_r - r) \quad (15)$$

$$0 \le r \le min(M_t, M_r) \quad (16)$$

Equation(15)(16) are plotted in Figure 1.

This figure implies if we use all transmit and receive antennas for diversity then we get full diversity gain $M_t M_r$ and we can use some of these antennas to increase data rate at the expense of diversity gain.

B.Outage Formulation

Channel outage is usually discussed for nonergodic fading channels, i.e., the channel matrix H is choosen

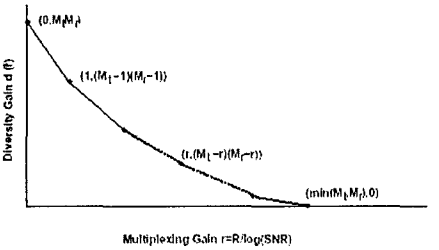

Fig. 1. Diversity-multiplexing trade-offs

randomly but is held fixed for all time. This nonergodic channel can be written as:

$$y_t = \sqrt{\frac{SNR}{m}} H x_t + w_t \quad (17)$$

where $x_t \in C^m$, $y_t \in C^n$ are the transmitted and received signal at time t, and $w_t \in C^n$ is the additive Gaussian noise. An outage is defined as the event that the mutual information of this channel does not support a target data rate:

$$H : I(x_t; y_t | H = H) < R \quad (18)$$

The mutual information is function of the input distribution P(x_t) and the channel realization. Without loss of optimality, the input distribution can be taken to be Gaussian with a covariance matrix Q, in which case

$$I(x_t; y_t | H = H) = logdet(I + \frac{SNR}{M_t} HQH^+) \quad (19)$$

Optimzing over all input distributions, and on the scale of interest, the bounds are tight, we have

$$P_{out}(R) \doteq P[logdet(I + SNRHH^+) < R] \quad (20)$$

For the multiple-antenna channel, let the data rate be R= rlog SNR, with $r \le mim(M_t, M_r)$. The outage probability satisfies

$$P_{out}(r \log SNR) \doteq SNR^{-d_{out}(r)} \quad (21)$$

where

$$d_{out}(r) = \inf_{\alpha \in A} \sum_{i=1}^{min(M_t, M_r)} 2i - 1 + |M_t - M_r|\alpha_i \quad (22)$$

and

$$\alpha_i = -\log \mu_i / \log SNR \quad (23)$$

B. IEEE 802.11 MAC Protocol

p_c is the probability of a collision seen by a packet being transmitted on the medium [12] [13] [14]. Assuming that there are n stations in the wireless LAN we are considering, we observe that p_c is also the probability that there is at least one packet transmission in the medium among other (n-1) stations in the interference range of the station under consideration. This yields:

$$p_c = 1 - [1 - (1 - p_0)\tau]^{n-1} \tag{24}$$

where p_0 is the probability that there is no packet ready to transmit at the MAC layer in wireless station under consideration, and τ is the packet transmission probability that the station transmits in a randomly chosen slot time given that the station has packets to transmit at the MAC layer. In non-saturated scenario, p_c mainly depends on the total number of packets attempting to transmit by all neighbouring stations. However, in saturated scenario, i.e. the stations always have packets to transmit, the total number of packets attempting to transmit equals to the total number of neighboring stations, hence p_c is mainly dependent on the total number of neighboring stations.

A queue model can be characterized by the service time distribution and the arrival process in addition to the service dicipline. In this paper, we assume that the packet arrivals at each mobile station follow the Poisson process or a deterministic distribution with average arrival rate λ. The packet transmission process at each station can be modeled as a general single server. The buffer size at each station is K. Thus the queueing model for each station can be modeled as an M/G/1/K when Poisson arrivals of packets are assumed.

Let p_n represent the steady-state probability of n packets in the queueing system, and let π_n represent the probability of n packets in the queueing system upon a departure at the steady state, λ' is the average arrival rate, $\overline{T_s}$ is the duration of time taken for a state transition from the start state (beginning to be served) to the end state (being transmitted successfully or discarded after maximum α times retranmission failures), ρ is the traffic internsity $\rho = \lambda'\overline{T_s}$. For the finite system size K with Poisson input [15], we have

$$p_0 = \frac{p_0}{\pi_0 + \rho} \tag{25}$$

$$p_n = \frac{p_n}{\pi_0 + \rho} \tag{26}$$

$$p_K = 1 - \frac{1}{\pi_0 + \rho} \tag{27}$$

The average queue length, blocking probability, and average waiting time including MAC sevice time are given by,

$$L = \sum_{i=0}^{K} i \times p_i \tag{28}$$

$$p_B = 1 - \frac{1}{\pi_0 + \rho} \tag{29}$$

$$W = \frac{L}{\lambda(1 - p_b)} \tag{30}$$

If we know the blocking probability p_B, then the throughput S can be computed easily by:

$$S = (1 - p_B)(1 - p_c^{\alpha+1}) \tag{31}$$

where α is the maximum retransmission times, $p_c^{\alpha+1}$ is the packet discard probability due to tranmission failure.

Suppose α is constant, as n increase, p_c increase, the he packet discarding probability at MAC layer increase.

Throughput linearly increases with the offered load at the non-saturated status and maintains a constant value with different total number of transmitting stations at the saturated status. As the n increases, the constant value decrease.

C. AODV Routing Protocol

Using the Opnet and NS-2, we could conduct an extensive set of performance experiments for the AODV routing protocol [16] [17] [18].

1) With the increase of number of hops, throughput degrades due to the higher delay.
2) With the increase of loads (i.e. application traffic), throughput can again be degraded due to the loss at the link layer. Link layer losses could be due to problems of hidden/exposed node or collisions in the wireless media.
3) the connectivity between nodes decreases, throughput also decrease.
4) the mobility increase, throughput decrease.

IV. Cross-layer Analysis

When we combine the Physical layer, MAC layer and network layer, we need to analyze two performance parameters: throughput and packet loss ratio(PLR).

1) Throughput: From the performance analysis of the physical layer, MIMO scheme could achieve multiplexing gain to increase the throughput as the number of T_x increases.

For the CSMA/CA MAC protocol, in non-saturated scenario, throughput linearly increases with the offered load, i.e., the throughtput will increase. as the number of T_x increase. As the T_x increases, it will be the saturated scenario. The throughput will decrease as the number of T_x increases.

For AODV routing protocol, if we increase the number of T_x, we need more routing paths, the connectivity between nodes dreases, throughtput decrease.

2) Packet Loss Ratio: MIMO scheme could achieve diversity gain to increase the performance as the number of T_x increases. So the BER will decrease. If each bit inside the L length packet has the same BER and bit-errors are uncorrelated, the PER can be related to the BER through [19]:

$$PER = 1 - (1 - BER)^L \tag{32}$$

We could conclude that for MIMO scheme, the PER will decrease as the number of T_x increase.

For CSMA/CA MAC protocol, as T_x increases, the total number of packets attempte to transmit will increase, the collision probability will increase, suppose block probability is given, the maximum retransmission times is constant, the packet discard probability will increase shown in equation (31).

In AODV routing protocol, the node density keeps unchanged as the increase of the number of the transmitters. It is hard to establish enough routing paths. The buffer size in each sensor node is constant, the arriving packets rate is constant, more packets will be discarded when the buffer is full.

V. Simulations

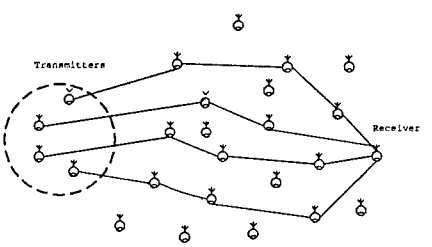

Fig. 2. System Architecture for cross-layer design

Figure 2 illustrates the system architecture for cross-layer design. Only the source sensor nodes send out the packets. The source sensor nodes need to set up paths to the destination sensor node. There are three phases during the packets transmissions.

1) MIMO scheme for physical layer.
2) set up the link in MAC layer.
3) routing path discovery in network layer.

We use Matlab to obtain the BER-SNR curves for MIMO schemes. We run 1000 Monte-Carlo simulations to get the physical layer curves.

We implemented the cross-layer model using the OPNET modeler. The simulation region is 1000×1000 meters. The wireless communcation range is 300 meters. There were 49 mobile nodes in the simulation model, and the nodes were roaming independently with variable ground speed between 0 to 10 meters per second. The mobility model was called billiard mobility model. the maximum retransmission times is 7 and arriving packet distribution is Poisson. The modulation scheme is BPSK.

3) Throughput: Figure 3 is the throughput performance for the cross-layer model. It shows when the throught is maximum when the number the transmitter is 11. As the number of T_x increases, throughput will increase for the MIMO scheme. For the MAC layer, when T_x is small, it is the non-saturated scenario. As the T_x increase, throughput will increase. When T_x is large enough, it is the saturated scenario. As the T_x increases, throughput will decrease. For AODV protocol, the collision probability will increase as the the T_x increases. The simulation result is consented with the analysis result.

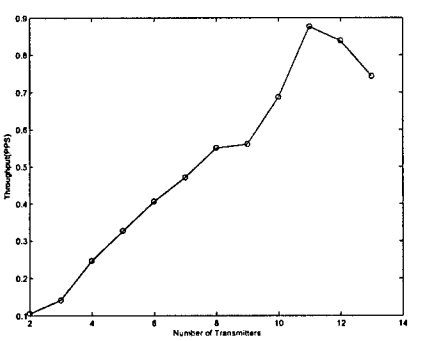

Fig. 3. Throughput Vs Number of Transmitters

4) Packet Loss Ratio: Figure 4 is the packet loss rate performance for the cross-layer model. The change of curve in fig.4 is instability, but the best performance for PLR was achieved when the number of transmitter is 10. As the T_x increases, BER decreases, so PER decreases,

more packets will be discarded, PLR decreases. For MAC layer protocol, when T_x increases, the probability of collision will increase. The packet loss ratio will keep stable for retransmission could solve the collision problem. If the number of T_x is big enough, retransmission number will exceed the maximum retransmission number α, large number of prackets will be discarded, the PLR will increase sharply. For AODV protocol, as the increase of the T_x, it is hard ro set up enough routing pathes. Large number of packets will jam in the finite-size buffer, more packets will be discarded. The simulation result matched well with the performance analysis.

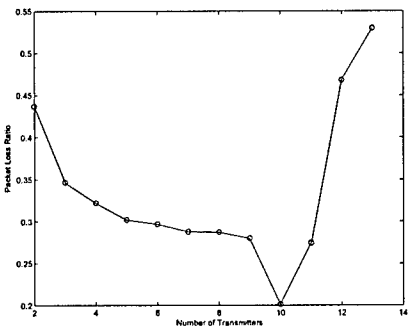

Fig. 4. PLR Vs Number of Transmitters

VI. Conclusion

MIMO scheme is a effective method to improve the performance of the wireless sensor networks. We apply the cross-layer design to combine physical layer, data-link layer and network layer together. For the data-link and network layer protocolas have different effect on the WSN performance. Throughput and packet performance will be have different performance compared with only consider the MIMO scheme in physical layer as the increase of the number of transmitters.

Acknowledgment

This work was supported by the U.S. Office of Naval Research (ONR) Young Investigator Award under Grant N00014-03-1-0466.

References

[1] Goldsmith A.J.; Wicker, S.B.; " Design Challenges for Energy-Constrained Ad Hoc Wireless Networks," *IEEE Wireless Comm.,*, vol. 9, No. 4 ,2002 , pp. 8-27.

[2] Cui, S.; Goldsmith A.J.; " Cross-Layer Optimization of Sensor Networks based on Cooperative MIMO Techniques with Rate Adaptation," *Proceedings: IEEE workshop on Signal Processing Advances in Wireless Communications (SPAWC)*, New York, NY, pp. 960-964, Jun 2005.

[3] Almouti, S.; "A simple Transmit Diversity Technique for Wireless Communications", *IEEE Journal on Select Area In Communication,* Vol. 16, No. 8, October 1998 .

[4] D. Qiao, S. Choi, and K. G. Shin, " Goodput Analysis and Link Adaption for IEEE 802.11a Wireless LANs", *IEEE Transactions On Mobile Computing*, Oct. 2002.

[5] Bao, L.H.; Garcia-Luna-Aceves, J.J.; " Hybrid Channel Access Scheduling in Ad Hoc Networks", *IEEE Computer Society,* Washington, DC, USA.

[6] Chakeres, I. etc; "The Ad hoc On Demand Distance Vector (AODV) routing algorithm", University of California at Santa Barbara , Santa Barbara , CA, USA.

[7] G.L. Stuber; "Principles of Mobile Communcation" *Kluwer Academic Press*, 2001.

[8] k. Simon, et al, *"Digital Communication over Fading Channels,"* Wiley Interscience, 2005.

[9] Tarokh, V.; Jafarkhani H.; Calderbank A. R.; "Space-Time Block Coding for Wireless Communications: Performance Result", *IEEE Journal on Selected Areas in Communications,* Vol.17, No.3, March 1999.

[10] Goldsmith, A.; "Wireless Communication", *Cambridge University, 2005.*

[11] Zheng, L. and Tse, D.N.C.; " Diversity and Multiplexing: A Fundamental Tadeoff in Multiple-Antenna Channels," *IEEE Transaction On Information Theory*, Vol. 49 , No. 5 , May 2003.

[12] Bianchi, G.; "Performance Analysis of IEEE 802.11 Distributed Coordination Function", *IEEE Journal on Selected in Communications. Vol. 18, No. 3, March 2000.*

[13] Zeng, G.; Chlamtac I.; "A Finite Queueing Model For IEEE 802.11 MAC Protocol", *IEEE 59th Vehicular Technology Conference,* VTC 2004-Spring, Vol 4, 17-19 May pp. 2037 - 2041.

[14] Zhai, H.; Fang Y.; "Performance of Wireless LANs Based on IEEE 802.11 MAC Protocols", *14th IEEE International Symposium on Personal, Indoor and Mobile Radio Communications (PIMRC'03),* Beijing, China, September, 2003.

[15] Gross,D and Harris, C. M.; "Fundamental of Queueing Theory", 3rd ed., John Wiley & Sons, Inc, 1998.

[16] Ari, I.; Jethani, N.; Rangnekar, A.; Natarajan, S.; " Performance Analysis and Comparision of Ad-Hoc Routing Protocols," *UMBC*, CMSC 691T,Mobile Computing, Project Report.

[17] Gerasimov, I.; Simon, R.; " Performance Analysis for Ad Hoc QoS Routing Protocols," *International Mobility and Wireless Access Workshop (MobiWac'02)*, 2002.

[18] Kuladinithi, K.; Gorg, R.; " Performance Analysis of Ad hoc On-demand Distance Vector routing (AODV) using OPNET Simulator," *University of Bremen*, Communication Networks, Project Report.

[19] Liu, Q., Zhou, S. and Giannakis, G.; " Cross-Layer Combining of Adaptive Modulation and Coding with Truncated ARQ over Wireless Links ," *IEEE Transactions on Wireless Communications*, Volume: 3 , Issue: 5 , Sept. 2004 pp. 1746 - 1755.

Hop-Distance Estimation in Wireless Sensor Networks with Applications to Resources Allocation

Liang Zhao and Qilian Liang
Department of Electrical Engineering
University of Texas at Arlington
Arlington, TX 76010, USA
Email: zhao@wcn.uta.edu, liang@uta.edu

Abstract

In this paper, we address a fundamental problem in Wireless Sensor Networks, how many hops does it take for a packet to be relayed for a given distance? For a deterministic topology, this question reduces to a simple geometry problem. However, a statistical study is needed for randomly deployed WSNs. We propose a Maximum Likelihood decision based on the conditional pdf of $f(r|H_i)$. Due to the computational complexity of $f(r|H_i)$, we also propose an attenuated Gaussian approximation for the conditional pdf. We show that the approximation visibly simplifies the decision process and the error analysis. The latency and energy consumption estimation are also included as application examples. Simulations show that our approximation model can predict the latency and energy consumption with less than half RMSE, compared to the linear models.

I. Introduction

The recent advances in MEMS, embedded systems and wireless communications enable the realization and deployment of wireless sensor networks (WSN), which consist of a large number of densely deployed and self-organized sensor nodes [1]–[3]. The potential applications of WSN, such as environment monitor, often emphasize the importance of location information. Fortunately, with the advance of localization technologies, such location information can be accurately estimated [4]–[7]. Accordingly geographic routing [8]–[10] was proposed to route packets not to a specific node, but to a given location. An interesting

question arises as "how many hops does it take to reach a given location?" The prediction of the number of hops is important not only in itself but also in helping estimating the latency and energy consumption, which are both important to the viability of WSN.

The question could become very simple if the sensor nodes are manually placed. However, if sensor nodes are deployed in a random fashion, the answer is beyond the reach of simple geometry. The stochastic nature of the random deployment calls for a statistical study.

The relation between the Euclidean distance and network distance (in terms of the number of hops) catches a lot of research interest recently. In [11], Huang, Lu and Roman defined the Γ-compactness of a geometric graph $G(V, E)$ to be the minimum ratio of the Euclidean distance to the network distance,

$$\gamma = \min_{i,j \in V} \frac{d(i,j)}{h(i,j)} \tag{1}$$

where $d(i,j)$ and $h(i,j)$ are the Euclidean distance and network distance between node i and j, respectively. The constant value γ is a good lower bound, but might not be enough to describe the non-linear relation between Euclidean distance and network distance. Fortunately, a lot of probabilistic study has been applied to this question. In [12], Hou and Li studied the 2-D Poisson distribution to find an optimal transmission range. They found that the hop-distance distribution is determined not only by node density and transmission range but also by the routing strategy. They showed results for three routing strategies, Most Forward with Fixed Radius, Nearest with Forward Progress, and Most Forward with Variable Radius. Cheng and Robertazzi in [13] studied the one-dimension Poisson point and found the pdf of r given the number of hops. They also pointed out the 2-D Poisson point distribution is analogous to the 1-D case, replacing the length of the segment by the area of the range. Vural and Ekici re-examined the study under the sensor networks circumstances in [14], and gave the mean and variance of multi-hop distance for 1-D Poisson point distribution. They also proposed to approximate the multi-hop distance using Gaussian. Zorzi and Rao derive the mean number of hops of the minimal hop-count route through simulations and analytic bounds in [10]. Chandler [15] derives an expression for t-hop outage probability for 2-D Poisson node distribution. However, Mukherjee and Avidor [16] argue that one of Chandler's assumptions is flawed and thus his expression is in fact a lower bound on the desired probability. They also rigorously derive the pdf of the minimal number of hops for a given distance in a fading environment. Although the exact analytic results are available in the literature, their monstrous computational complexity limits their applications. Therefore,

we try to approximate the hop-distance relation and simplify the decision process and error analysis in this paper. Considering the application of resource allocation, only large-scale path loss is considered and thus the fading is ignored.

The rest of this paper is organized as follows. We provide some preliminaries on skewness and kurtosis in Section II. The number of hops predication problem is addressed and solved in Section III. Since this problem has no closed-form solution, we propose an attenuated Gaussian approximation and show how to simplify the error analysis in Section III-A. Application examples are shown in Section IV. Section V concludes this paper.

II. Preliminaries :Skewness and Kurtosis

In this section, we provide some preliminaries on statistical methods [17]. Skewness is a measure of symmetry, or more precisely, the lack of symmetry. A distribution, or sample set, is symmetric if it looks the same to the left and right of the center point.

Definition 1: [17] For a given sample set X,

$$m_3 = \Sigma(X - \bar{X})^3/n, \tag{2}$$

$$m_2 = \Sigma(X - \bar{X})^2/n, \tag{3}$$

where $\bar{X}$ is the sample mean of X, and n is the size of X. Then a *sample estimate of skewness coefficient* is given by

$$g_1 = \frac{m_3}{m_2^{\frac{3}{2}}}. \tag{4}$$

Skewness is zero for a symmetric distribution. Positive skewness indicates right skewness and negative indicates left.

Kurtosis is a measure of whether the data are peaked or flat relative to a normal distribution.

Definition 2: [17] A sample estimate of kurtosis for a sample set X is given by

$$g_2 = m_4/m_2^2 - 3, \tag{5}$$

where $m_4 = \Sigma(X - \bar{X})^4/n$ is the fourth-order moment of $\bar{X}$ about its mean.

Skewness and kurtosis is useful in determining whether a sample set is normal. Note that the skewness and kurtosis of a normal distribution are both zero; significant skewness and kurtosis clearly indicate that data are not normal.

III. Estimation of Network Distance Based on Euclidean Distance

Suppose the sensor nodes are placed on a plane at random at an average density of λ nodes per square meters. Let $N(A)$ be the number of nodes in area A, it can be shown that $N(A)$ is a two-dimensional Poisson point process with density λ. The problem of interest is to find the number of hops, denoted H_i needed to reach a specific destination r from a given source node. We can make a Maximum Likelihood (ML) decision,

$$\hat{H} = \arg\max f(r|H_i), i = 1, 2, 3, \cdots, \tag{6}$$

where H_i can also be described as "the minimum number of hops is i from the source to the specific node with Euclidean distance r". In the following discussion, we are trying to approximate $f(r|H_i)$ for 2-D Poisson distribution. Note that $r < R \rightarrow H_1$, we are more interested in multiple-hop distance relation, especially for i is relatively large.

A. Attenuated Gaussian Approximation

TABLE I

Statistics of $f(r|H_i)$

Number of Hops	Mean	Std	Skewness	Kurtosis
1	19.991	7.0651	-0.57471	-0.58389
2	45.132	7.8365	-0.16958	-1.0763
3	72.01	8.2129	-0.10761	-1.0332
4	99.45	8.391	-0.07938	-0.97857
5	127.14	8.5323	-0.06445	-0.93104
6	154.96	8.6147	-0.05341	-0.9004
7	182.68	8.573	-0.07738	-0.91687

Since $f(r|H_i)$ is awkward to evaluate even using numerical methods, we use histograms collected from Monte Carlo simulations as substitute to the joint pdf. All the simulation data are collected from such a scenario that N sensor nodes were uniformly distributed in a circular region of radius of R_{Bound} meters. For convenience, polar coordinates were used. The source node was placed at $(0, 0)$. The transmission range was set as R meters. For each setting of (N, R_{Bound}, R), we ran 300 simulations, in each of which all nodes are re-deployed at random. We ran simulations for extensive settings of node density λ and transmission range R. Due to space constraints, only the histograms for $(N = 1000, R_{Bound} = 200, R = 30)$

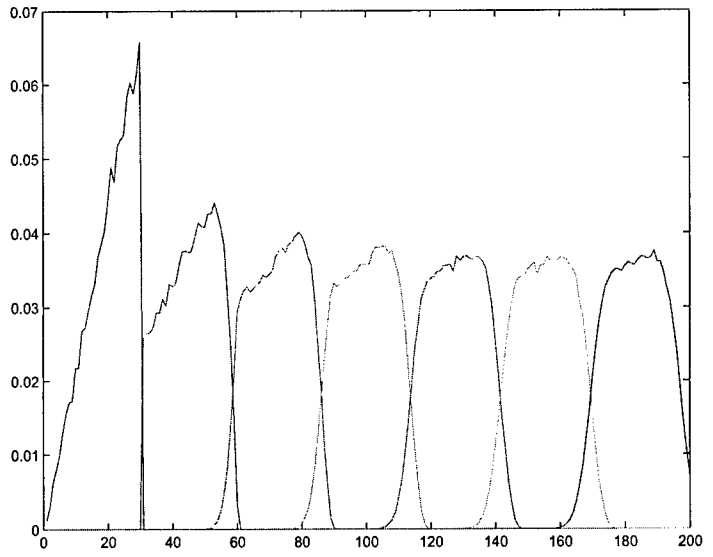

Fig. 1. Histograms of hop-distance joint distribution. ($N = 1000, R_{Bound} = 200, R = 30$)

are plotted in Fig. 1, which approximately shows that $f(r|H_i)$ approach the normal when H_i increases. Table I lists the first-, second-, third- and fourth-order statistics of $f(H, r)$. The skewness and kurtosis clearly satisfy the Gaussianity condition within tolerance of error. Furthermore, The postulated distribution and histogram are drawn together in Fig. 2 (d)(e)(f), which clearly shows a close match for each case.

Thus, the objective function can be approximated by

$$\begin{aligned} f(r|H_i) &= \alpha^n \mathcal{N}(m_n, \sigma_n) \\ &= \frac{\alpha^n}{2\pi\sigma} e^{-\frac{(r-m_n)^2}{2\sigma_n^2}}, \end{aligned} \tag{7}$$

where α is the equivalent attenuation base, m_n and σ_n are the mean and standard deviation(std), respectively. The specific values of these parameters can be estimated from simulations. Our extensive simulations show that, even for only relatively large H_i, $f(r|H_i)$ has following properties,

1) $\sigma_n \approx \sigma_{n-1}$, which means the neighboring joint pdf's have similar spread.
2) $m_n - m_{n-1} \approx m_{n+1} - m_n$, which means the joint pdf's are evenly spaced.
3) $3 < \frac{m_n - m_{n-1}}{\sigma_n} < 5$, which means the overlap between the neighboring joint pdf's is small but not negligible. (As a rule of thumbs, $Q(3)$ is considered relatively small and $Q(5)$ is regarded negligible.)

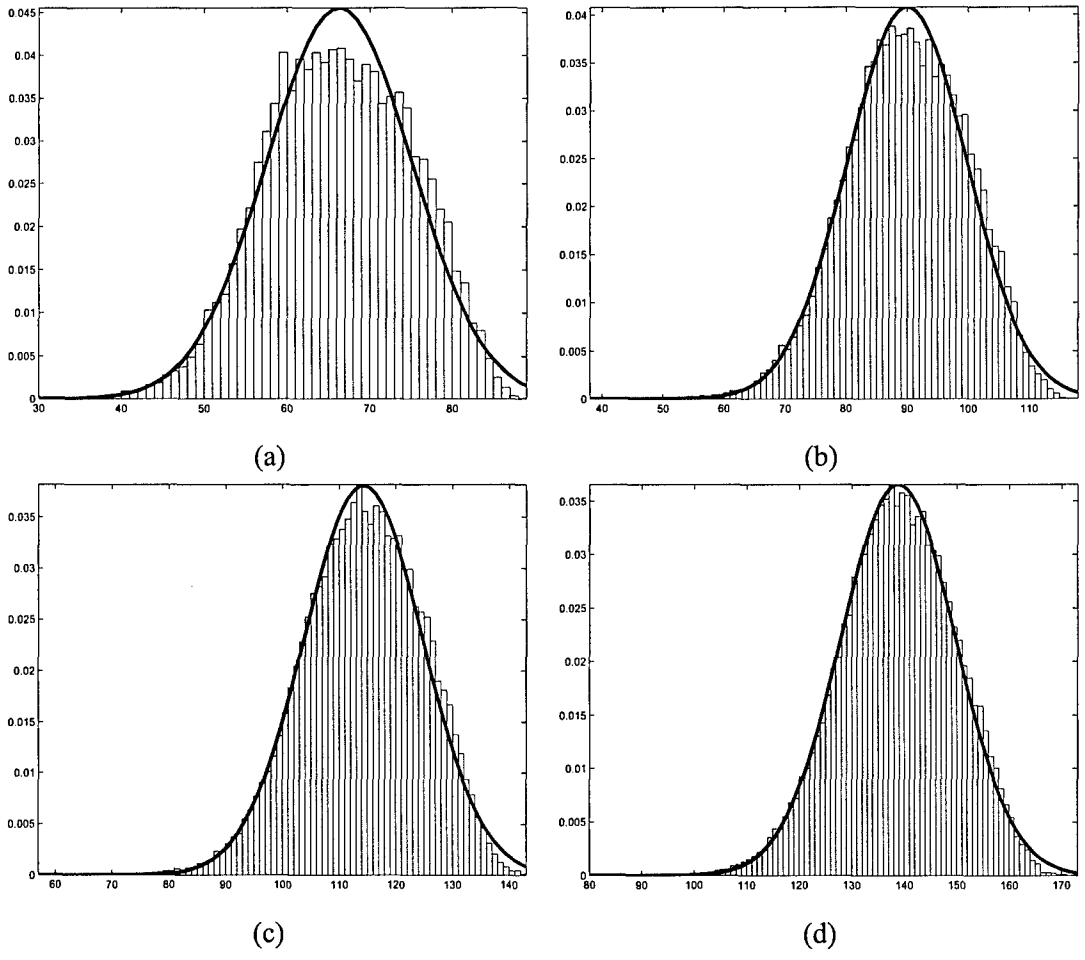

Fig. 2. The histogram vs. postulated distribution for end-to-end distances for given number of hops. (a) Three-hop. (b) Four-hop. (c) Five-hop. (d) Six-hop.

4) $\frac{m_n - m_{n-2}}{\sigma_n} \gg 5$, which means the overlap between the non-neighboring joint pdf's is negligible.

5) $\alpha < 1$. For large density λ, $\alpha \to 1$. Along with Property 1, this tell us that the neighboring joint pdf's have nearly identical shape.

As shown in the following discussion, these properties largely simplify the decision rule and the error analysis. Another interesting observation, besides these properties, is that the following equations do not stand true.

$$m_n = nm_1 \tag{8}$$

$$m_n = nR \tag{9}$$

$$m_n = (n-1)R + R/2 \tag{10}$$

Although these equations sound plausible, they all give visible errors. The aforementioned estimator $[r/R]+1$ for H_i, though widely used, is not good in the new light shed by this study.

B. Decision Boundaries

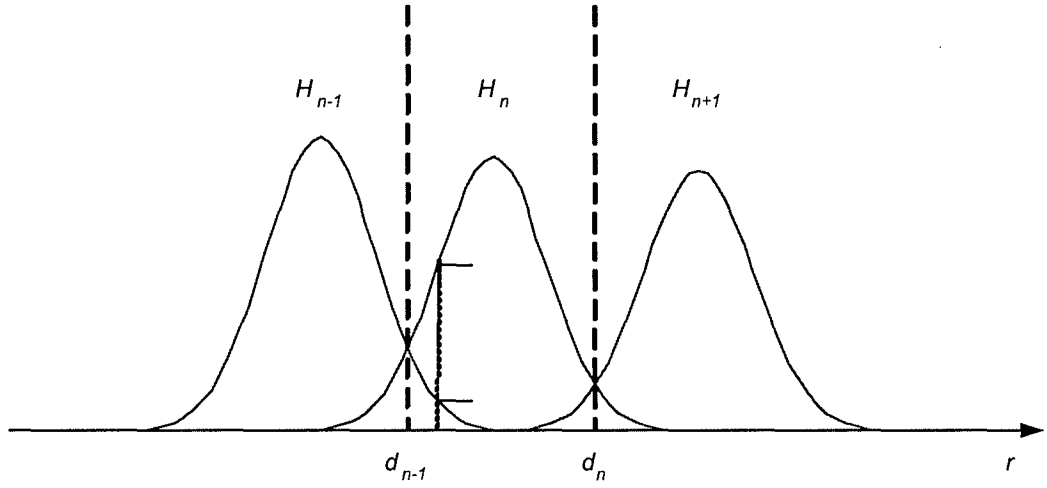

Fig. 3. Gaussian Approximation.

Following (6), and observe the $f(r|H_i)$ in Fig. 3, the decision is needed only between neighboring H_i, that is,

$$f(r|H_n) \underset{n+1}{\overset{n}{\gtrless}} f(r|H_n+1). \tag{11}$$

This is because, for a specific value of r, there are only two values of H_i with dominating $f(r|H_i)$, compared to which $f(r|H_i)$ for other values of H_i is negligible. Substitute (7) into (11), we obtain the decision boundary d_n between the regions H_n and H_n+1.

$$\begin{aligned} d_n &= \frac{B+\sqrt{B^2+AC)}}{A} \\ A &= \sigma_{n+1}^2 - \sigma_n^2 \\ B &= m_n\sigma_{n+1}^2 - m_{n+1}\sigma_n^2 \\ C &= m_n^2\sigma_{n+1}^2 - m_{n+1}^2\sigma_n^2 + 2\sigma_n^2\sigma_{n+1}^2 \ln\alpha \end{aligned} \tag{12}$$

Using Property 1,

$$d_n = \frac{m_{n+1}^2 - m_n^2 - 2\sigma_n^2 \ln \alpha}{2(m_{n+1} - m_n)} \tag{13}$$

For large density λ, Property 5 is applicable, (12) simplifies to

$$d_n = \frac{\sigma_n^2 m_{n+1} + \sigma_{n+1}^2 m_n}{\sigma_n^2 + \sigma_{n+1}^2} \tag{14}$$

Applying Property 1 to (14),

$$d_n = \frac{m_n + m_{n+1}}{2} \tag{15}$$

No matter which approximate solution we choose for d_n, the decision rule is given by

$$r \underset{n}{\overset{n+1}{\gtrless}} d_n. \tag{16}$$

In other words,

$$\text{we decide } \hat{n} \text{ if } d_{\hat{n}-1} < r \leq d_{\hat{n}}. \tag{17}$$

C. Error Performance Analysis

For our decision rule, a decision error occurs only when H_n but we decide $\hat{n} \neq n$. Thus, the probability of error for a specific r is

$$p(\epsilon|r) = \sum_{n \neq \hat{n}} f(H_n|r), \tag{18}$$

where $f(H|r)$ is related to $f(r|H_i)$ by the Bayesian rule. The total probability of error is obtained by integrating (18) over all possible r.

$$p(\epsilon) = \int p(\epsilon|r) f_r(r) dr \tag{19}$$

According to Property 4, only $f(r|H = n-1)$ and $f(r|H = n+1)$ could have outstanding value over the decision region $[d_{n-1}, d_n]$.

$$\begin{aligned} p(\epsilon) &\approx \sum_{n=2}^{\infty} \int_{d_{n-1}}^{d_n} f(r|H = n-1)p(H_n - 1) + f(r|H_n + 1)p(H_n + 1)dr \\ &= \sum_{n=2}^{\infty} \alpha^{n-1} p(H_n - 1)[Q(\frac{d_{n-1} - m_{n-1}}{\sigma_{n-1}}) - Q(\frac{d_n - m_{n-1}}{\sigma_{n-1}})] \\ &\quad + \alpha^{n+1} p(H_n + 1)[Q(\frac{m_{n+1} - d_n}{\sigma_{n+1}}) - Q(\frac{m_{n+1} - d_{n-1}}{\sigma_{n+1}})] \end{aligned} \tag{20}$$

Note that

$$\begin{aligned} & \frac{d_n - m_{n-1}}{\sigma_{n-1}} - \frac{d_{n-1} - m_{n-1}}{\sigma_{n-1}} \\ = \; & \frac{d_n - d_{n-1}}{\sigma_{n-1}} \gg 1, \end{aligned} \tag{21}$$

therefore, $Q(\frac{d_n - m_{n-1}}{\sigma_{n-1}})$ is negligible compared to $Q(\frac{d_{n-1} - m_{n-1}}{\sigma_{n-1}})$. Similarly, $Q(\frac{m_{n+1} - d_n}{\sigma_{n+1}})$ is negligible. (20) is approximated by

$$\begin{aligned} p(\epsilon) \; \approx \; & \alpha^3 p(H_3) Q(\frac{m_3 - d_2}{\sigma_3}) + \sum_{n=3}^{\infty} [\alpha^{n-1} p(H_n - 1) Q(\frac{d_{n-1} - m_{n-1}}{\sigma_{n-1}}) \\ & + \alpha^{n+1} p(H_n + 1) Q(\frac{m_{n+1} - d_n}{\sigma_{n+1}})] \\ = \; & \alpha^2 p(H_2) Q(\frac{d_2 - m_2}{\sigma_2}) + \sum_{n=3}^{\infty} \alpha^n p(H_n) [Q(\frac{m_n - d_{n-1}}{\sigma_n}) \\ & + Q(\frac{d_n - m_n}{\sigma_n})] \end{aligned} \tag{22}$$

Substituting an appropriate solution of d_n into (22) would give us the probability of error within required accuracy. For example, if we choose (15),

$$\begin{aligned} p(\epsilon) \; \approx \; & \alpha^2 p(H_2) Q(\frac{m_3 - m_2}{2\sigma_2}) + \sum_{n=3}^{\infty} \alpha^n p(H_n) [Q(\frac{m_n - m_{n-1}}{2\sigma_n}) \\ & + Q(\frac{m_{n+1} - m_n}{2\sigma_n})] \end{aligned} \tag{23}$$

IV. Application Examples

We provide two application examples, latency and energy estimation, in this section. To emphasize the role of the number of hops in the estimation, we use general time and energy models. On how to derive the parameters such as $T_{rx}, T_{tx}$for a specific routing scheme, readers are referred to [18], [19].

A. Latency Estimation

We use a simple time model, in which the latency increases linearly with the number of hops [20]. Suppose it takes T_{rx}, T_{tx} for a sensor node to process 1 bit of incoming and

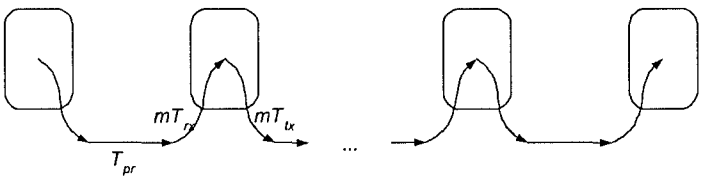

Fig. 4. Time model.

outgoing message, respectively. And T_{pr} is the required time to transmit 1 bit of message through a band-limited channel. Therefore, the latency introduced for each hop is

$$T_{hop} = T_{tx} + T_{pr} + T_{rx} \tag{24}$$

Shown in Fig. 4, given the end-to-end distance r, we can find the required number of hops $\hat{n}$ according to (16), thus, a good estimator of the total latency of a l-bit message is

$$l\hat{n}T_{hop} \tag{25}$$

B. Energy Consumption Estimation

The following model is adopted from [21] where perfect power control is assumed. To transmit l bits over distance r, the sender's radio expends

$$E_{tx}(l,r) = \begin{cases} lE_{elec} + l\epsilon_{fs}r^2 & r < r_0 \\ lE_{elec} + l\epsilon_{mp}r^4 & r \geq r_0 \end{cases} \tag{26}$$

and the receiver's radio expends

$$E_{rx}(l,r) = lE_{elec}. \tag{27}$$

E_{elec} is the unit energy consumed by the electronics to process one bit of message, ϵ_{fs} and ϵ_{mp} are the amplifier factor for free-space and multi-path models, respectively, and d_0 is the reference distance to determine which model to use. The values of these communication energy parameters are set as in Table II.

Let s_n denote the single-hop distance from the $(n-1)$th-hop to the nth-hop. Obviously, $s_n \leq R$. In our experimental setting, $R = 30m < d_0$ so that the free space model is always used. This agrees well with most applications, in which multi-hop short-range transmission

TABLE II

ENERGY CONSUMPTION PARAMETERS

Name	Value
r_0	86.2m
E_{elec}	$50nJ/bit$
E_{DA}	$5nJ/bit$
ϵ_{fs}	$10pJ/bit/m^2$
ϵ_{mp}	$0.0013pJ/bit/m^4$

is preferred to avoid the exponential increase in energy consumption for long-range transmission. Naturally, the end-to-end energy consumption for sending l bits over distance r is given by

$$E_{total}(l,r) = \sum_{1}^{\hat{n}} \{E_{tx}(l,r_1) + E_{rx}(l)\} \tag{28}$$

where $\hat{n}$ is the estimated number of hops for given r and r_1 is the single-hop distance because the message is relayed hop by hop.

On the average,

$$\begin{aligned} \bar{E}_{total}(l,r) &= \hat{n}l(E_{elec} + \epsilon_{fs}E[r_1^2] + E_{elec}) \\ &= \hat{n}l(2E_{elec} + \epsilon_{fs}(m_1^2 + \sigma_1^2) \end{aligned} \tag{29}$$

C. Simulation

We used the same scenario described in Section III-A and varied the node density λ and transmission range R. In each simulation, the number of hops is estimated for each node using (14) and (16), and then the latency and energy consumption are estimated using (25) and (29), respectively. As comparison to our proposed statistic-based estimator, we chose a widely used linear estimator.

$$\begin{aligned} &\text{Linear Estimator 1} \quad \hat{n} = [r/R] + 1, \\ &\text{Linear Estimator 2} \quad \hat{n} = [r/R] + 2, \end{aligned} \tag{30}$$

where r is the given distance, R the transmission range and $[r/R]$ is the maximum number less than r/R. We plot the average of latency and energy consumption in Fig.5(a) (b) and the RMSE in Fig.6(a) (b), respectively. The latency is plotted in units of T_{hop} while the

energy consumption in units of Joules. The ripple shape of RMSE is due to the fact decision errors occurs more often in the overlapping zones of neighboring $f(r|H_i)$. Fig.5 show that the linear estimator 1 performs well at the shorter range but suffers visibly at larger range, while the linear estimator does the opposite. The linear estimators, no matter what value their parameters take, may significantly underestimate or overestimate the latency and energy consumption as already pointed out in Section III-A, while our statistic-based model keeps close to the actual latency and energy consumption at all ranges except for the border. This is also verified by Fig.6, which also shows that our model can reduce RMSE to at least half for both latency and energy consumption. These results show that linear models cannot identify network behavior accurately, as also confirmed by our extensive simulations for different settings of node density and transmission range, which is not shown here due to space constraints.

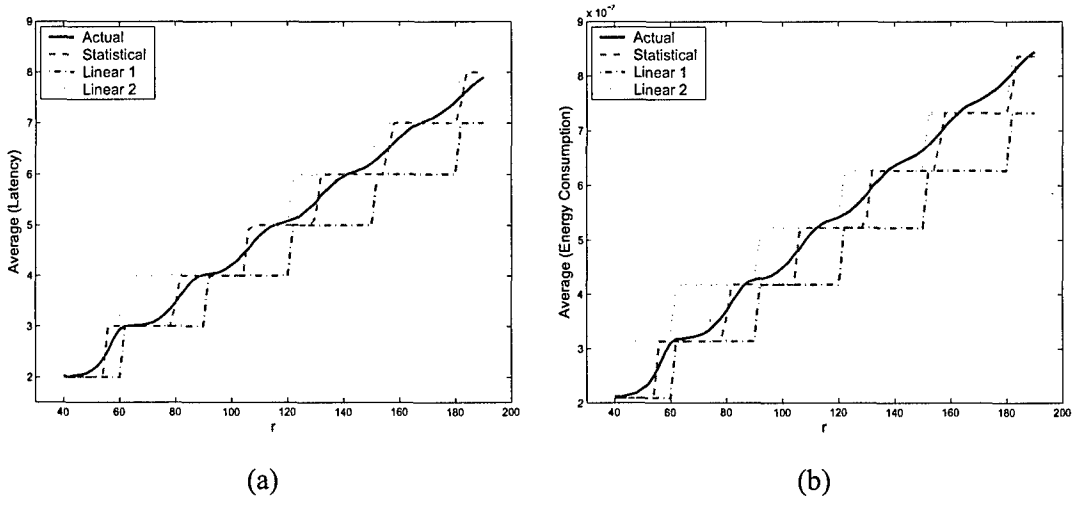

(a) (b)

Fig. 5. Estimation Average. (a) Latency. (b) Energy consumption.

V. Conclusion

To address the fundamental problem "how many hops does it take for a packet to be relayed for a given distance?", we make both probabilistic and statistic studies. We proposed a Bayesian decision based on the conditional pdf of $f(r|H_i)$. Since $f(r|H_i)$ is computationally complex, we also proposed an attenuated Gaussian approximation for the conditional pdf, which visibly simplifies the decision process and the error analysis. We also show that several linear models, though intuitively sound and widely used, may give significant bias error.

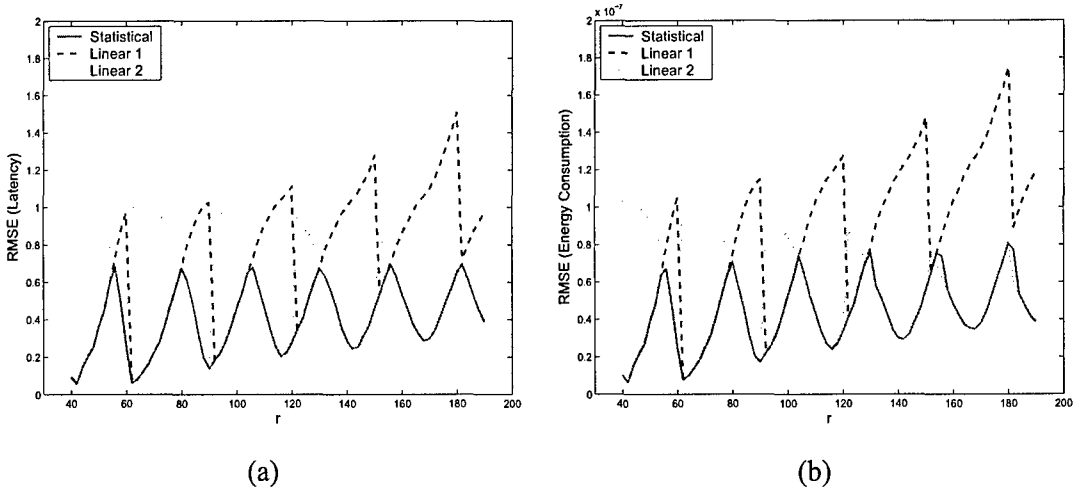

Fig. 6. Estimation RMSE. (a) Latency. (b) Energy consumption.

We apply our approximation to the latency and energy consumption estimation in dense WSN. Simulations show that our approximation model can predict the latency and energy consumption with less than half RMSE, compared to the aforementioned linear models.

ACKNOWLEDGMENT

This work was supported by the U.S. Office of Naval Research (ONR) Young Investigator Award under Grant N00014-03-1-0466.

REFERENCES

[1] I. F. Akyildiz, W. Su, Y. Sankarasubramaniam, and E. Cayirci, "A survey on sensor networks," *IEEE Commun. Mag.*, vol. 20, pp. 102–114, Aug. 2002.

[2] R. Min, M. Bhardwaj, S.-H. Cho, N. Ickes, E. Shih, A. Sinha, A. Wang, and A. Chandrakasan, "Energy-centric enabling technologies for wireless sensor networks," *IEEE Wireless Communications*, vol. 9, no. 4, pp. 28 – 39, Aug. 2002.

[3] V. Raghunathan, C. Schurgers, S. Park, and M. Srivastava, "Energy-aware wireless microsensor networks," *IEEE Signal Processing Magazine*, vol. 19, no. 2, pp. 40 – 50, March 2002.

[4] H. Lim and J. Hou, "Localization for anisotropic sensor networks," in *IEEE Infocom'05*, March 2005.

[5] S. Caruso, A and; Chessa, S. De, and A. Urpi, "Gps free coordinate assignment and routing in wireless sensor networks," in *IEEE Infocom*, March 2005.

[6] L. Fang, W. Du, and P. Ning, "A beacon-less location discovery scheme for wireless sensor networks," in *IEEE Infocom*, March 2005.

[7] N. Priyantha, H. Balakrishnan, E. Demaine, and S. Teller, "Mobile-assisted localization in wireless sensor networks," in *IEEE Infocom*, March 2005.

[8] R. Jain, A. Puri, and R. Sengupta, "Geographical routing using partial information for wireless ad hoc networks," *IEEE Personal Communications*, vol. 8, pp. 48 – 57, Feb 2001.

[9] Y. Xu, J. Heidemann, and D. Estrin, "Geography-informed energy conservation for ad hoc routing," in *MobiCom '01: Proceedings of the 7th annual international conference on Mobile computing and networking*. New York, NY, USA: ACM Press, 2001, pp. 70–84.

[10] M. Zorzi and R. Rao, "Geographic random forwarding (geraf) for ad hoc and sensor networks: multihop performance," *Mobile Computing, IEEE Transactions on*, vol. 2, no. 4, pp. 337–348, 2003.

[11] Q. Huang, C. Lu, and G.-C. Roman, "Spatiotemporal multicast in sensor networks," in *SenSys '03: Proceedings of the 1st international conference on Embedded networked sensor systems*. New York, NY, USA: ACM Press, 2003, pp. 205–217.

[12] T.-C. Hou and V. Li, "Transmission range control in multihop packet radio networks," *IEEE Transactions on Communications*, vol. 34, no. 1, pp. 38–44, 1986.

[13] Y.-C. Cheng and T. Robertazzi, "Critical connectivity phenomena in multihop radio models," *IEEE Transactions on Communications*, vol. 37, no. 7, pp. 770–777, 1989.

[14] S. Vural and E. Ekici, "Analysis of hop-distance relationship in spatially random sensor networks," in *MobiHoc '05: Proceedings of the 6th ACM international symposium on Mobile ad hoc networking and computing*. New York, NY, USA: ACM Press, 2005, pp. 320–331.

[15] S. Chandler, "Calculation of number of relay hops required in randomly located radio network," *Electronics Letters*, vol. 25, no. 24, pp. 1669–1671, 1989.

[16] S. Mukherjee and D. Avidor, "On the probability distribution of the minimal number of hops between any pair of nodes in a bounded wireless ad-hoc network subject to fading," in *Proceedings of the 2nd International Workshop on Wireless Ad-Hoc Networks*, Kings College, London, UK, May 2005.

[17] G. Snedecor and W. Cochran, *Statistical Methods*. Iowa State University Press / AMES, 1989.

[18] M. Zorzi and R. Rao, "Geographic random forwarding (geraf) for ad hoc and sensor networks: energy and latency performance," *IEEE Transactions on Mobile Computing*, vol. 2, no. 4, pp. 349–365, 2003.

[19] H. M. Ammari and S. K. Das, "Trade-off between energy savings and source-to-sink delay in data dissemination for wireless sensor networks," in *MSWiM '05: Proceedings of the 8th ACM international symposium on Modeling, analysis and simulation of wireless and mobile systems*. New York, NY, USA: ACM Press, 2005, pp. 126–133.

[20] W. Ye, J. Heidemann, and D. Estrin, "Medium access control with coordinated adaptive sleeping for wireless sensor networks," *IEEE/ACM Trans. Networking*, vol. 12, no. 3, pp. 493–506, 2004.

[21] W. B. Heinzelman, A. P. Chandrakasan, and H. Balakrishnan, "An application-specific protocol architecture for wireless microsensor networks," *IEEE Trans. Wireless Commun.*, vol. 1, no. 4, pp. 660 – 670, Oct. 2002.

Modeling End-to-end Distance for Given Number of Hops in Dense Planar Wireless Sensor Networks

Liang Zhao and Qilian Liang
Department of Electrical Engineering
University of Texas at Arlington
Arlington, TX 76010, USA
Email: zhao@wcn.uta.edu, liang@uta.edu

Abstract— **We model the end-to-end distance for a given number of hops in dense planar Wireless Sensor Networks in this paper. We derive that the closed-form formula for single-hop distance and postulate Beta distribution for 2-hop distance. When the number of hops increases beyond three, the multi-hop distance approaches Gaussian. The Gaussian approximation model is also applied to ranging, which achieves less distance error than Hop-TERRAIN and APS (Ad hoc Positioning System). Our error analysis also shows the distance error is be minimized by using our model.**

I. Introduction and Motivation

In Wireless Sensor Networks (WSN), knowledge of node location is often required in many applications. The examples include events report, target tracking, geographical routing, and coverage evaluation. Generally, the distances from a node with unknown location to several anchor nodes are estimated, and then a multilateration is applied to estimate the node location. Distance is often estimated based on received signal strength, time of arrival (TOA), time difference of arrival (TDOA) or angle of arrival [1]. The angle-of-arrival based ranging requires directive antennas or arrays, which is not suitable for most microsensors. Similarly, measuring time of flight requires timing device with satisfactory resolution like in GPS. Although TDOA needs much less resolution, it often requires extra acoustic or ultrasound emission, which comes with higher price, larger size and more energy consumption, all seeming impractical for microsensors. Thus, most technically available ranging is based on received signal strength; in fact, RSSI (Received Signal Strength Indication) is widely used in wireless communications to provide distance estimation.

The underlying observation is that the average large-scale path loss can be expressed as a function of distance by using a path loss exponent, n [2].

$$\bar{PL}(d) = \bar{PL}(d_0)(\frac{d}{d_0})^n \tag{1}$$

where n is the path loss exponent, which indicates the rate at which the path loss increases with distance, d_0 is the close-in reference distance, which is determined from measurement close to the transmitter, and d is the distance from the source to the receiving point. Measurements have also shown that at any value of d, the path loss $PL(d)$ at a particular location is random and distributed log-normally (normal in dB) about the mean distance-dependent value.

$$PL(d)[dB] = \bar{PL}(d)[dB] + X_\sigma, \tag{2}$$

where X_σ is a zero-mean Gaussian distributed random variable (in dB) with standard deviation σ (also in dB). The log-normal shadowing is the main source of distance error for received-signal-strength-based ranging methods. The values of n and σ are often estimated empirically, for example, n could vary from 2 to 10 for different environments, and typical value of σ in urban area is around 10 dBs.

Due to the log-normal shadowing, the RSS-based ranging could be very rough. For example, the median localization error of commodity 802.11 technology is $10ft$ [3]; such accuracy may be achieved by alternative techniques, for example, exploiting the dense deployment to estimate distance between nodes. For those applications where the sensor nodes are over-densely deployed, the distance between the nodes are short and the variance of such distance is also small. Therefore, it is quite promising to estimate the end-to-end distance based on the number of hops [4]–[6].

For example, both APS [4] and Hop-TERRAIN [6] find the number of hops from a node to each of the anchors and then multiply this hop count by a shared metric (average single-hop distance) to estimate the range between the node and each anchor. The known positions of anchor nodes and these computed ranges are then used to perform a triangulation to obtain estimated node positions. A further refinement phase is proposed in [6], which uses least squares on local computation. However, as we show later, the distance does not increase linearly with the number of hops. Therefore, a better knowledge about the hop-distance relationship can cast new light on distance estimation.

In [7], Hou and Li studied the 2-D Poisson distribution to find an optimal transmission range. They found that the hop-distance distribution is determined not only by node density and transmission range but also by the routing strategy. They showed results for three routing strategies, Most Forward with Fixed Radius, Nearest with Forward Progress, and Most Forward with Variable Radius. Cheng and Robertazzi in [8] studied the one-dimension Poisson point and found the pdf of r_i and the dependency of r_i on previous r_j, $j < i$. They also pointed out the 2-D Poisson point distribution is analogous to the 1-D case, replacing the length of the segment

by the area of the range. Vural and Ekici reexamined the study of 1-D Poisson distribution under the sensor networks circumstances in [9], and proposed to approximate the multi-hop distance using Gaussian. In this paper, we study the hop-distance relation in the planar WSN.

The rest of this paper is organized as follows. We provide some preliminaries on statistical methods in Section II.The probabilistic study is presented in Section III and statistical analysis in Section IV. Section V concludes this paper.

II. Preliminaries

In this section, we provide some preliminaries on statistical methods [10].

A. Skewness and Kurtosis

Skewness is a measure of symmetry, or more precisely, the lack of symmetry. A distribution, or sample set, is symmetric if it looks the same to the left and right of the center point.

Definition 1: [10] For a given sample set X,

$$m_3 = \Sigma(X - \bar{X})^3/n, \quad (3)$$

$$m_2 = \Sigma(X - \bar{X})^2/n, \quad (4)$$

where $\bar{X}$ is the sample mean of X, and n is the size of X. Then a *sample estimate of skewness coefficient* is given by

$$g_1 = \frac{m_3}{m_2^{\frac{3}{2}}}. \quad (5)$$

Skewness is zero for a symmetric distribution. Positive skewness indicates right skewness and negative indicates left.

Kurtosis is a measure of whether the data are peaked or flat relative to a normal distribution.

Definition 2: [10] A sample estimate of kurtosis for a sample set X is given by

$$g_2 = m_4/m_2^2 - 3, \quad (6)$$

where $m_4 = \Sigma(X - \bar{X})^4/n$ is the fourth-order moment of $\bar{X}$ about its mean.

Skewness and kurtosis is useful in determining whether a sample set is normal. Note that both the skewness and kurtosis of a normal distribution are zero; significant skewness and kurtosis clearly indicate that data are not normal.

B. Chi-Square Test

Chi-square test is widely used to determine the goodness of fit of a distribution to a set of experimental data. It works as follows:

- 1. Partition the sample space into the union of K disjoint intervals.
- 2. Compute the probability b_k that an outcome falls in the kth interval under the postulated distribution. The $m_k = nb_k$ is the expected number of outcomes that fall in the kth interval in n repetitions of the experiment.
- 3. The chi-square statistic is defined as the weighted difference between the observed number of outcomes, N_k, that fall in the kth interval, and the expected number m_k.

$$D^2 = \Sigma_{k=1}^{K} \frac{(N_k - m_k)^2}{m_k} \quad (7)$$

- 4. The hypothesis is rejected if $D^2 \geq t_\alpha$, where t_α is a threshold determined by a given significance level. Otherwise, the fit is considered good.

III. Modeling End-to-end Distance for Given Number of Hops

A. Problem Formulation

We assume a general beacon scenario, in which anchors sends out beacon packets informing other nodes about their locations. These beacon packets are also relayed so that nodes outside the anchors' transmission range could also received the beacons. Suppose the sensor nodes are placed on a plane at random at an average density of λ nodes per square meters. Nonetheless, clarifications about several terms are necessary, because they have been used in a wide variety of senses.

Firstly, our study on end-to-end distance for given number of hops is based on local coordinate system, which could be translated into a global coordinate system if enough nodes in the local coordinate system have known global coordinates. In previous research, anchors refer to beacons, whose locations are known and broadcast to other nodes. However, in our study, an anchor is simply a specific node used in establishing the local coordinate system. An anchor could have global coordinates or not, which is of no interest to our study. Therefore, our study is applicable to both anchor-based and anchor-free approaches.

Secondly, we assume the beacon packets are distributed in an ad hoc fashion. Although better routing, such as geographic routing, are proposed for WSN, they are not suitable for relaying beacon packets, because during this phase, most nodes have no knowledge about locations of their own and neighbors'. Under such circumstances, we have to assume the beacon packets are simply flooded throughout the sensor network, except that nodes can only relay the beacon packets incoming with least number of hops and discard those via more hops.

Let $N(A)$ be the number of nodes in area A, it can be shown that $N(A)$ is a two-dimensional Poisson point process with density λ. One property of the Poisson process is that *if the number of nodes occurring in the area A is N, then the individual outcomes are distributed independently and uniformly in the area A.* That is, if N nodes are placed at random in the area A, then the probability of a specific node in the subarea B is B/A, given $B \in A$.

Assume the area A is large enough so that none of the anchor nodes is near the border and the transmission range is R. The problem of interest is to find the distance from a specific node to the anchor given this node is

TABLE I
DEFINITION OF VARIABLES

Variable	Definition
$\vec{r} = (r, \theta)$	the polar coordinates of a node
t_i	the distance from the $(i-1)$-hop node to the i-hop node
H_i	the event "the specific node is within i hops, but beyond $(i-1)$ hops from the source."

within i hops from the anchor. The definitions of variables are listed in Table I. Note that the event H_i can also be described as "the minimum number of hops from the anchor to the specific node is i".

B. Single-Hop Case

Consider the first hop case, the conditional cdf can be expressed by

$$P[r_1 < r|H_1] = P[r_1 < r|r_1 < R] = \frac{r^2}{R^2} \quad (8)$$

Taking derivative,

$$f_{(r_1|H_1)}(r) = \frac{2r}{R^2} \quad (9)$$

And the conditional mean and variance are $2R/3$ and $R^2/18$, respectively, which are solely determined by the transmission range R and irrelevant to the node distribution density λ. This is due to the uniform node distribution; no matter how large the density could be, it would not give any bias to the conditional mean and variance.

C. Two-Hop Case

Conditional on the value of r_1, the cdf for t_2 is

$$P(t_2 < t|r_1|H_2) = \frac{B}{\pi R^2}, \quad (10)$$

where B is the area of the region inside the circle of center $\vec{r}_1$ but outside the circle of center $\vec{r}_0$. B is equal to

$$\pi(t_2)^2 - (t_1)^2(\phi_1 - \frac{1}{2}\sin 2\phi_1) - (t_2)^2(\phi_2 - \frac{1}{2}\sin 2\phi_2), \quad (11)$$

where

$$\phi_1 = \cos^{-1}(1 - \frac{(t_2)^2}{2(t_1)^2}), \quad (12)$$

$$\phi_2 = \cos^{-1}(\frac{t_2}{2t_1}). \quad (13)$$

The conditional pdf of t_2 is obtained by taking the derivative of (10).

$$f_{t_2|r_1|H_2}(r) = \frac{d}{dt}\frac{B}{\pi R^2}, \quad (14)$$

By taking expected value of (14),

$$f_{t_2|H_2}(t) = \int_0^R f_{r_1}(s)\frac{d}{dt}\frac{B}{\pi R^2}ds, \quad (15)$$

r_2 is determined by

$$r_2 = \sqrt{(t_1)^2 + (t_2)^2 - 2t_1t_2\cos\phi}, \quad (16)$$

where ϕ is the angle between t_1 and t_2 and uniformly distributed in $[-\phi_2, \phi_2]$. Although it is possible to derive the pdf of r_2 from (16), it is awkward to evaluate explicitly. Furthermore, note that r_n depends on r_{n-1}, a nested integral as in (17) is generally required for such evaluations. Thus, for the end-to-end distance for two and more hops, we will postulate their distribution from the collected simulation data in the next section.

$$p(r_n|H) = \int_R^{(n-1)R(n-2)R} \int_R \cdots \int_0^R p(r_n|r_1, r_2, \cdots, r_n - 1, H) f(r_{n-1}|r_1, r_2, \cdots, r_{s-2}, H) \cdots f(r_1|H)dr_1 \cdots dr_{n-2}dr_{n-1} \quad (17)$$

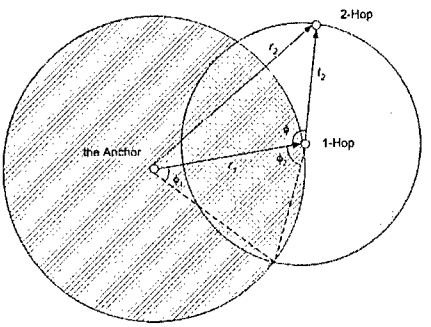

Fig. 1. Two-hop distance.

IV. STATISTICAL ANALYSIS

All the simulation data are collected from such a scenario that N sensor nodes were uniformly distributed in a circular region of radius of 300 meters. For convenience, polar coordinates were used. The anchor node was placed at $(0, 0)$. We ran simulations for extensive settings of node density λ and transmission range R. And for each setting of (N, R), we ran 300 simulations, in each of which all nodes are re-deployed from the beginning.

A. Single-Hop Distance

We plot the histogram of single-hop distance collected from simulations and compare with the theoretical result (9) in Fig. 2 (a), which clearly shows that (9) fits the experimental data very well. Furthermore, a chi-square test was carried out to determine the goodness of fit of (9) to the experimental data. The threshold for $30-1 = 29$ degrees of freedom at a 1% significance level is 49.59. Compared to this, $D^2 = 28.8728$ is well within the threshold. Thus, we establish that the data is in good agreement with (9).

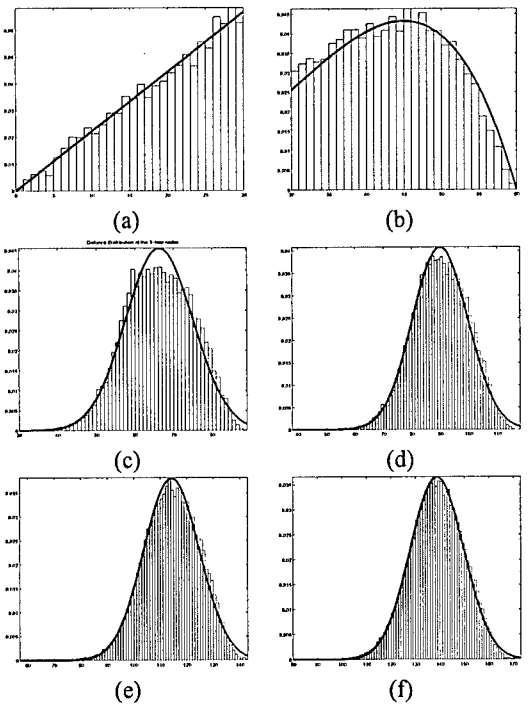

Fig. 2. The histogram vs. postulated distribution for end-to-end distances for given number of hops. (a) One-hop. (b) Two-hop. (c) Three-hop. (d) Four-hop. (e) Five-hop. (f) Six-hop.

B. Two-Hop End-to-end Distance

Since there is no closed-form formula for the conditional pdf of end-to-end distance for two and more hops, we have to find a fit for it. We postulate the following pdf for the conditional pdf of two-hop end-to-end distance according to the experimental data plotted in Fig. 2 (b), whose characteristic curve clearly shows a Beta distribution shape. The general pdf of Beta distribution is

$$f_X(x) = C(x-a)^{p-1}(b-x)^{q-1}, \qquad (18)$$

where p and q are the shape parameters, a and b are the lower and upper bounds, and C is a numerical factor to make the complete probability one. The bounds a and b can be easily determined as $a = 0$ and $b = 2R$. Since the maximum of (18) occurs at $b(p-1)/(p-1+q-1)$, which is at $3R/2$ in Fig. 2 (b), therefore, $p = 4$ and $q = 2$ would be a good guess. The remaining parameter C is determined by

$$C = \int_R^{2R} \frac{(2R-s)s^3}{B(4,2)(2R)^5}. \qquad (19)$$

The postulated Beta distribution and histogram are drawn together in Fig. 2 (b), which clearly shows a close match.

C. Three-And-More-Hop End-to-end Distance

When the number of hops increases beyond three, the end-to-end distance distribution approaches Gaussian

TABLE II
MEANS AND STDS FOR THREE-AND-MORE-HOP END-TO-END DISTANCES

Number of Hops	Mean	Std	Skewness	Kurtosis
3	72.01	8.2129	-0.10761	-1.0332
4	99.45	8.391	-0.079383	-0.97857
5	127.14	8.5323	-0.064453	-0.93104
6	154.96	8.6147	-0.053416	-0.9004

(See Fig. 2 (d)(e)(f)). For a more formal analysis about its Gaussianity, we list their skewness and kurtosis in Table II. Note that both skewness and kurtosis are well within tolerance, we postulate Gaussian distribution for three-and-more-hop end-to-end distance. The mean and std can be estimated from the experimental data (see Table II). We plot the postulated Gaussian distribution and histogram together in Fig. 2 (d)(e)(f), which clearly show a close match for each case.

D. Optimum Estimation and Error Analysis

Once the condition pdf is known, the distance estimation is straightforward. The optimum unbiased estimator is $E[r_n|H_n]$, and accordingly, the RMSE can be minimized to $\sqrt{VAR[r_n|H_n]}$. In APS/Hop-TERRAIN, the distance is assumed to increase linearly with the number of hops, and thus, a linear estimator, $n * m1$, is used to estimate nth-hop distance. Accordingly, the MSE of the linear estimator is given by

$$\begin{aligned} MSE(H_n) &= E[(r_n - nm_1)^2] \\ &= VAR[r_n|H_n] + (m_n - nm_1)^2 \end{aligned} \qquad (20)$$

The minimum RMSE and the biased RMSE given by APS/Hop-TERRAIN estimator are plotted together in Fig.3, which increases drastically even when n is only moderately large. As discussed in the Introduction, there

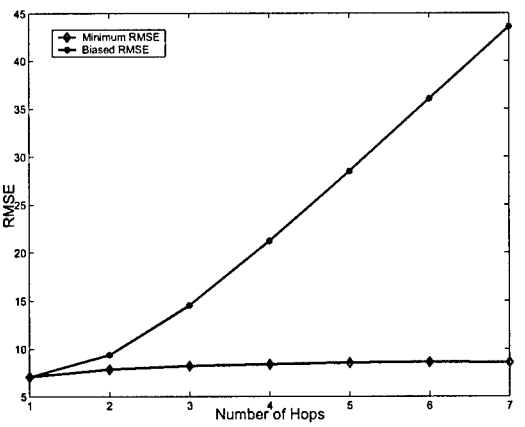

Fig. 3. The RMSE bias vs. the number of hops. R=30m

exists a lower bound of distance error for the RSS-based ranging technology. According to [3], the median localization error of commodity 802.11 technology is

$10ft \approx 3.05m$. The RMSE we obtain in our simulations is around 8 meters, which is in the same order of magnitude as the distance error bound in [3]. Furthermore, in environment with irregular terrain, obstacles or other clutters, the shadowing effect may cause higher distance error. Since hop-based distance technology is immune to shadowing effect, it may outperform RSS-base ranging in these kinds of environment.

V. Conclusions

In this paper, we study the modeling of the end-to-end distance for given number of hops in WSN. The experiments showed that the distance does not increase linearly with the number of hops. Therefore, the distance should be analyzed for each number of hops. We derived the distribution for single-hop distance and also showed that the complexity of derivation for multiple-hop distance is beyond practical interest. Thus, we postulate Beta distribution for two-hop end-to-end distance and Gaussian distribution for three-and-more-hop end-to-end distance. Computer simulations showed our postulated distributions agree well with the histograms. We also show that the distance error can be minimized by exploiting the distribution knowledge.

Acknowledgment

This work was supported by the U.S. Office of Naval Research (ONR) Young Investigator Award under Grant N00014-03-1-0466.

References

[1] J. Hightower and G. Borriello, "Location systems for ubiquitous computing," *IEEE Computer*, vol. 34, no. 8, pp. 57–66, August 2001.

[2] T. S. Rappaport, *Wireless Communications:Principles and Practice*. Upper Saddle River, NJ: Prentice-Hall, 2002.

[3] E. Elnahrawy, X. Li, and R. Martin, "The limits of localization using signal strength: a comparative study," in *Sensor and Ad Hoc Communications and Networks, 2004. IEEE SECON 2004. 2004 First Annual IEEE Communications Society Conference on*, 2004, pp. 406–414.

[4] D. Niculescu and B. Nath, "Ad hoc positioning system (aps)," in *Global Telecommunications Conference, 2001. GLOBECOM '01. IEEE*, vol. 5, 2001, pp. 2926–2931 vol.5.

[5] ——, "Dv based positioning in ad hoc networks," *Telecommunication Systems*, vol. 22(1-4), pp. 267–280, 2003.

[6] C. Savarese, J. Rabay, and K. Langendoen, "Robust positioning algorithms for distributed ad-hoc wireless sensor networks," in *USENIX Technical Annual Conference*, Monterey, CA, June 2002.

[7] T.-C. Hou and V. Li, "Transmission range control in multihop packet radio networks," *IEEE Transactions on Communications*, vol. 34, no. 1, pp. 38–44, 1986.

[8] Y.-C. Cheng and T. Robertazzi, "Critical connectivity phenomena in multihop radio models," *IEEE Transactions on Communications*, vol. 37, no. 7, pp. 770–777, 1989.

[9] S. Vural and E. Ekici, "Analysis of hop-distance relationship in spatially random sensor networks," in *MobiHoc '05: Proceedings of the 6th ACM international symposium on Mobile ad hoc networking and computing*. New York, NY, USA: ACM Press, 2005, pp. 320–331.

[10] G. Snedecor and W. Cochran, *Statistical Methods*. Iowa State University Press / AMES, 1989.

A Throughput-Maximized MAC Protocol for Ultra Wideband Communication in Wireless Sensor Networks

Qingchun Ren and Qilian Liang
Department of Electrical Engineering
University of Texas at Arlington
Arlington, TX 76019-0016 USA
E-mail: ren@wcn.uta.edu, liang@uta.edu

Abstract— **In this paper, we propose a MAC protocol: throughput-maximized MAC protocol (TM-MAC), based on the characteristics of ultra wideband (UWB) technology. In UWB communication systems, the transmission parameters are tunable to match the requirements of data flow. In TM-MAC, we implement concurrent multiuser access instead of mutual exclusion method, such as TDMA and random access. For multiuser interference, we establish a model to adaptively adjust the data transmission rate to ensure a satisfied signal to noise ratio (SNR) at receiver side. We also analyze the relationship among the theoretical maximum channel capacity, the achievable maximum channel capacity and the maximum data transmission rate. According to the network topology, TM-MAC re-divides network into subsets, in which communication pairs can make communication simultaneously to enhance throughput and to exploit as fast as possible data transmission rate for reliable communication. For subset formation, we propose a general analytical framework, which captures the unique characteristics of shared wireless channel and allows to model a large class of systemwide throughput maximization issue via the specification of per-link utilization functions. Simulation results demonstrate that TM-MAC can implement throughput maximization to shorten latency and to enhance network processing capability.**

I. Introduction

A wireless sensor network (WSN) can be thought as an *ad hoc* network consisting of sensor nodes linked by a wireless medium to perform distributed sensing tasks. Distributed WSNs have increasing potential applications because they hold the potential to revolutionize many segments of our economy and life, from environmental monitoring and conservation to manufacturing and business asset management. Ultra wideband (UWB)[1] is an attractive technology for WSNs due to its extremely high data transmission rate, low radiated power, accurate range resolution, precision distance and/or positioning measurement capabilities, relatively immune to multipath cancellation effects, as well as simple UWB transceiver devices.

As a general principle, the role of medium access control (MAC) module is to allow multiple users to share a common resource. Most of existed wireless MAC protocols assume that simultaneous transmissions result in transmission errors and thus employ mutual exclusion mechanisms to avoid them. Moreover, from layered architecture aspect, the functions executed by MAC should be defined without taking into account the underlying physical layer, which is seen by MAC as a black box offering the service of transferring bits in the form of signals appropriate for channel. From this view, there are some MAC protocols appeared for UWB communication systems. In European funded project U.C.A.N (Ultra wideband Concepts for Ad-hoc Networks), a TDMA-based MAC protocol is proposed. This MAC protocol is an adaptation for UWB from IEEE 802.15.3[2] draft standard for narrow-band wireless personal area network (WPAN). In [3], they proposed a single transceiver approach for UWB and a companion MAC layer based on busy tone multiple access (BTMA). BTMA reduces the time and the energy spent on collision as compared to handshaking protocols.

However, the design of a truely efficient MAC protocol for UWB systems should investigate some possible MAC enhancements that will take into account the inherent advantages of UWB technology. In [4], they proposed scheme providing distributed medium access through pulse sense, which is similar to carrier sense in narrowband systems. Moreover, UWB is flexible in the reconfiguration process of data transmission rate. Thus, opposite to mutual exclusion MAC protocols, another approach for MAC protocol design is issued. This kind of MAC protocol for UWB systems allows simultaneous transmission and adapts to multiuser interference. F. Cuomo et al. [5] outlined key issues to design a multi access scheme based on UWB. They selected a distributed mechanism to handle radio resource sharing, and presented a general framework of radio resource sharing to UWB wireless ad hoc networks.

In this paper, starting from the inherent characteristics of UWB technology and cross-layer design approach, we propose a MAC protocol: throughput-maximized MAC protocol (TM-MAC). We combine MAC layer and physical layer together to optimize network throughput. At MAC layer, network is re-divided into subsets based on TM-MAC. In each subset, communication pairs can make communication simultaneously to enhance throughput and to exploit as fast as possible data transmission rate for reliable communication. In subset formation, we propose a general analytical framework that captures the unique characteristics of shared wireless channel and allows to model a large class of systemwide throughput maximization issue via the specification of per-link utilization

functions. At physical layer, we analyze the connection among the theoretical maximum channel capacity, the achievable maximum channel capacity and data transmission rate. For multiuser interference, we establish a model to adaptively adjust the maximum data transmission rate to ensure a satisfied signal to noise ratio (SNR) at the receiver side.

The remainder of this paper is organized as follows. In Section II, we summarize motivations for our work. We analyze the impact of simultaneous transmission on system's transmission capability in Section III. Section IV describes our TM-MAC algorithm. Simulation results are given in Section VI. Section VI concludes this paper.

II. Our Motivation

A. Energy Constraint

One of the biggest challenges for designers of WSNs is to develop systems that will run unattended for years. This calls for not only robust hardware and software, but also lasting energy resources. However, current generation of sensor nodes is battery powered, whose available energy is limited, and replacing or recharging batteries, in many cases, may be impractical or uneconomical. Thus, protocols and applications designed for WSNs should be highly efficient and optimized in terms of energy. For WSNs, communication, not only transmitting, but also receiving, or merely scanning the channel for communication, can use up to half energy[6]. Therefore, recently, some researchers have begun studying the problem of reducing power consumption on wireless interface.

Considering that UWB is a low radiated power communication scheme. The research in [7] points out that a bit rate of $100Kbps$ over 5 meters with no more than 1 mW power consumption. UWB is the idlest choice in terms of energy efficiency for energy-constraint WSNs. However, seldom WSNs take advantage of properties of UWB technology because of the lack of an efficient MAC technology.

Related with energy constraint problem for WSNs, we have done some work in [8] and [9]. Our proposed energy-efficient MAC protocols: A-MAC and ASCEMAC, not only reserve energy to extend network lifetime but also own the capability to solve accumulative clock drift problem without network synchronization. While, both of them only suit narrow-band communication systems well. In this research, we extend our previous work into UWB communication systems.

B. Physical Layer Property

In UWB communication systems, even though bandwidth is finite, the bandwidth is at least $500MHz$ or the transmitted signal has a $10dB$ bandwidth larger than 20 percent of its center frequency based on FCC standard[1]. Compared to narrowband systems, information-theoretic results in [10] and [11] show that a Shannoncapacity of a multipath fading AWGN wideband channel is a linear function of SNR as shown in (1).

$$C = \xi \times SNR \tag{1}$$

Moreover, for UWB systems, data transmission rate R can be formulated using (2). Here N_s is the number of pulses transmitted at the pulse repetition time, N_h is the number of frames (pulses) per information bit and T_c is the bin duration.

$$R = \frac{1}{N_s N_h T_c} \tag{2}$$

Note that, UWB is flexible in the reconfiguration process of data transmission rate due to the availability of a number of transmission parameters, such as N_s N_h and T_c, which can be tuned to better match the requirements of a data flow. Therefore, for UWB systems, a consequence of rate adaptation is that an arbitrary level of interference is possible. That is, for a given level of interference at the receiver side, a sender can tune its rate by adjusting the code, in order to achieve a desired bit error rate (BER).

III. Theoretic Analysis on Throughput

A. Network Model

The network model assumed in this paper is that of "piconet" or clustered architecture. We assume that we can set up this hierarchical topology for a randomly deployed network through certain existing methods, such as energy-efficient self-organization (ESO) [12] algorithm. In each piconet, there is a cluster head and a multitude of normal nodes. Communication range determines the radius of piconet. Two nodes, which are only one hop apart, are neighbors and can communicate with each other directly. Our proposed algorithm is responsible for controlling wireless medium (or the common channel) access.

B. Physical Layer Model

In this paper, we utilize binary PPM-TH-UWB to generate the transmitted signal $x(t)$. That is, we utilize pulse position modulation (PPM) to implement modulation and time hopping (TH) to shape the spectrum of the generated signal.

$$x(t) = \sum_{j=-\infty}^{\infty} p(t - jT_f - c_j T_c - a_j \varepsilon) \tag{3}$$

where $p(t)$ denotes a unit-energy pulse. T_f is the frame duration. c_j is the dedicated pseudorandom code. a_j is the binary bit of transmitted symbols. ε is transmission time delay for each pulse.

We consider the multi-path-affected UWB radio channel for signal propagation. In this paper, we use IEEE 802.15.3a channel model[13]. The signal $r(t)$ at the receiver side can be expressed as following:

$$r(t) = \sum_{j=1}^{L(t)} \alpha_j(t) x(t - \tau_j) + \omega(t) + n(t) \tag{4}$$

where $\alpha_j(t)$ and $\tau_j(t)$ are the channel gain and the delay measured at time t for the jth path. $L(t)$ is the number of path observed at time t. $\omega(t)$ is the multiuser interference. $n(t)$ is AWGN noise.

Considering a network with N communication pairs composed of UWB terminals, each pair consists of one transmitter,

one receiver and uses one pseudorandom code. If N links are active, then the signal to interference and noise ratio ($SINR$) at the ith link's receiver at time t is formed as following[5]:

$$SINR_i = \frac{P_i g_{ii}}{R_i\{\eta_i + T_f\sigma^2 \sum_{k=1,k\neq i}^{N} P_k g_{ki}\}} \quad (5)$$

where R_i is the data transmission rate of the ith link; P_i is the average power emitted by the ith link's transmitter; g_{ij} is the path gain from the ith link's transmitter to the jth link's receiver; η_i is the background noise energy plus interference from other non-UWB systems; σ^2 is an adimensional parameter depending on the shape of monocycle.

In this case, the total multi-path gain g, which measures the total amount of energy collected over L pulses, is determined as following: $g = \sum_{l=1}^{L} \mid \alpha_l \mid^2$. Note that g is related with the attenuation suffered by the transmitted pulses during propagation. In multi-path environments, g decreases with distance according to the path-loss model as following[14]:

$$g = \frac{g_0}{d^\beta} \quad (6)$$

where g_0 is the reference value for power gain evaluated at $d_0 = 1m$ and β is the exponent of power or energy attenuation law.

C. The Impact of Simultaneous Transmission on Network Throughput

Within a network, piconets can be treated as independent with each other, since the distance among piconets is far enough to permit us ignore the interference among them (piconet formation scheme can ensure this assumption to be held). Therefore, the analysis on network throughput can be simplified into the independent analysis on the throughput for individual piconets. Then combining all results together linearly, we can obtain the impact of simultaneous transmission on network throughput. Thus, in the following part, the discussion mainly focuses on the impact of simultaneous transmission on throughput within a piconet.

In this paper, the theoretic maximum channel capacity C_{t-max} is defined as the largest channel capacity implied by channel situation, and the achievable maximum channel capacity C_{a-max} is defined as the largest channel capacity which is acquired through a data transmission rate which can ensure reliable communication. From (1) and (5), note that $C \propto \frac{1}{R}$ and we can derivate the specific data transmission rate for C_{a-max}, noted as R_{a-max}, to achieve our goal - trying to not only enhance data transmission rate to shorten the transmission latency but also ensure reliable communication and enhance network throughput. The value of R_{a-max} is calculated as following:

$$R_{a-max} = \sqrt{\frac{\xi P g}{\eta + T_f\sigma^2 \sum_{k=1,k\neq i}^{N} P_k g_k}} \quad (7)$$

In a piconet where there are N pairs of communication terminals making communication simultaneously at rate $R_{a-max,i}(i = 1, \cdots, N)$. In this case, the achieved channel capacity for each pair can also be determined by (7). Thus, the acquired throughput (TH_{put}) of this piconet at time t is calculated as following:

$$TH_{put} = \sum_{i=1}^{N} \sqrt{\frac{\xi P_i g_{ii}}{\eta_i + T_f\sigma^2 \sum_{k=1,k\neq i}^{N-1} P_k g_{ki}}} \quad (8)$$

For this existed piconet, if we add m more communication pairs. What is the influence on the throughput? Through analyzing the change of throughput when adding different number of communication pairs or picking up same number of communication pairs but located at different positions, we obtain criteria for forming simultaneous transmission subset to improve throughput.

Without making any influence on analysis, we let $U_i \triangleq T_f\sigma^2 \sum_{k=1,k\neq i}^{N-1} P_k g_{ki}$ and the newly added communication pairs are pair $N+1$ to pair $N+m$. The impact of adding more simultaneous transmissions on throughput is evaluated by the change of it, noted as $\triangle TH_{put}$ and calculated using (9).

$$\begin{aligned} \triangle TH_{put} &= TH'_{put} - TH_{put} \\ &= \sum_{i=1}^{N} \sqrt{\frac{\xi P_i g_{ii}}{\eta_i + U_i + T_f\sigma^2 \sum_{k=N+1}^{N+m} P_k g_{ki}}} \\ &+ \sum_{i=N+1}^{N+m} \sqrt{\frac{\xi P_i g_{ii}}{\eta_i + T_f\sigma^2 \sum_{k=1,k\neq i}^{N+m} P_k g_{ki}}} \\ &- \sum_{i=1}^{N} \sqrt{\frac{\xi P_i g_{ii}}{\eta_i + U_i}} \end{aligned} \quad (9)$$

We also obtain the relationship between the new data transmission rate $R'_{a-max,i}$ and the original data transmission rate $R_{a-max,i}$ for existed communication pair i ($i = 1, \cdots, N$) as following: $\frac{1}{R'^2_{a-max,i}} = \frac{1}{R^2_{a-max,i}} + \frac{T_f\sigma^2 \sum_{k=N+1}^{N+m} P_k g_{ki}}{\xi P_i g_{ii}}$. Note that, adding some communication pairs into an existed network will decrease R_{a-max}, since $\frac{T_f\sigma^2 \sum_{k=N+1}^{N+m} P_k g_{ki}}{\xi P_i g_{ii}}$ is positive. While, how much R_{a-max} will be degraded is determined by the sum interference coming from all simultaneous users.

From (9), we found that, when adding communication pairs, the change of throughput of a piconet is related with the negative influence degrading R_{a-max} for existed communication pairs and the positive influence for permitting more communication pairs work concurrently. Thus, from network perspective, letting more communication pairs work concurrently does not definitely mean enhancing/degrading throughput. There is a watershed for it. That is, when the negative influence is smaller than or equals to the positive influence of adding some communication pairs into an existed network, system performance in term of throughput will be improved, or at least not be degraded. That is $\triangle TH_{put} \geq 0$.

First, we consider the $N = 1$ and $m = 1$ scenario as the our analysis basis. We assume that the distance between transmitter and receiver is same for each communication pair (i.e., $d_{ii} = d$), and each communication pair can use same

power to make transmission. Moreover, the noise floor for communication is fixed. Thus (9) is simplied into (10).

$$\begin{aligned}\triangle TH_{put} &= \sqrt{\frac{\xi P g_0}{\eta d_{22}^{\beta} + T_f \sigma^2 P g_0 (\frac{d_{22}}{d_{12}})^{\beta}}} \\ &+ \sqrt{\frac{\xi P g_0}{\eta d_{11}^{\beta} + T_f \sigma^2 P g_0 (\frac{d_{11}}{d_{21}})^{\beta}}} \\ &- \sqrt{\frac{\xi P g_0}{\eta d_{11}^{\beta}}} \end{aligned} \quad (10)$$

In this case, $\triangle TH_{put}$ is a function of d_{12} and d_{21}. Here, d_{12} denotes the distance between the original existed communication pair's transmitter and the added communication pair's receiver, and d_{21} stands of the distance between the added communication pair's transmitter and the original existed communication pair's receiver.

Note that, to ensure the throughput to be enhanced when adding one or more communication pairs, the shortest distance for d_{12} and d_{21} should, at least, equal to a threshold d_{min}, which is related with the choice of other parameters, such as transmission power P, environment noise strength η, environment exponential β, symbol time T_f, monocycle shape σ^2, power gain g_0 and communication range of node d_{rag}, but the distance between the transmitter and the receiver of the originally existed communication pair. That is:

$$d_{min} = \{ (\frac{1}{(\sqrt{\frac{1}{\eta}} - \sqrt{\frac{1}{\eta + T_f \sigma^2 P \frac{g_0}{d_{rag}^{\beta}}}})^2} - \eta)(g_0 T_f \sigma^2 P)^{-1} \}^{\frac{1}{\beta}} \quad (11)$$

IV. Throughput-Maximized MAC Protocol (TM-MAC) Description

We ever proposed an energy-efficient MAC protocol: ASCEMAC[8] for WSNs. ASCEMAC forces nodes power on and off their batteries alternately to implement communication, as well as to reduce energy consumption on collision and idle listening to extend network lifetime. However, for UWB communication systems, TDMA-based and contention-based mutual exclusion medium access control schemes are not the best choice any more. We propose our algorithm: throughput-maximized MAC protocol specially for UWB communication systems.

Inheriting the advantages of ASCEMAC, TM-MAC also divides the system time into four phases: *T*RFR-*P*hase, *S*chedule-*B*roadcast-*P*hase, *O*n-*P*hase and *O*ff-*P*hase. *O*ff-*P*hase is preserved for all nodes to power off their radios and *O*n-*P*hase is preserved for to power on their radios to carry on communication. TRFR message, *T*RFR-*P*hase duration design, matching schedule establishment, maintenance, schedule interval design and time-slot allocation mechanisms for TM-MAC are similar to ASCEMAC's. But, in TM-MAC, during *O*n-*P*hase the further divided super-time-slots are individually occupied by subsets, a group of communication pairs. TM-MAC, based on the network topology, is responsible for further dividing a network into a set of subsets in which communication pairs can make communication simultaneously to maximize throughput, so that to improve better energy efficiency and spectrum utilization.

A. Modelling Network

The network is represented as a directed graph $G = (V, E)$. V is the set of nodes in a piconet. $e = (u, v)$ is an edge in E iff nodes u and v are transmitter and receiver of a communication pair. Fig. 1(a) shows an example, in which nodes A, C, E, G, I, K are transmitters, B, D, F, H, J, L are receivers. In our algorithm the interference caused by newly added communication pairs is untolerable when the created throughput is smaller than the original one. Otherwise, it is tolerable. The untolerable interference coming from other communication pairs are denoted by dotted lines. According to the network topology, we utilize the conclusion acquired in (11) to determine the untolerable interference from other communication pairs.

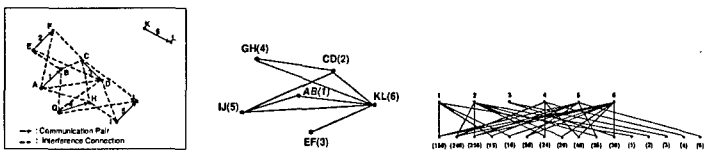

(a) (b) (c)

Fig. 1. (a) Network graph G, (b) Interference tolerable graph G' and (c)Potential Group formation graph G''

B. Forming Interference-Tolerated Relationship

We consider all communication pairs in a piconet. We generate the interference tolerable graph $G' = (V', E')$. $V' \subset E$, i.e., each node in G' is a communication pair in G. $e' = (u', v')$ is an edge in E' iff the achieved throughput is higher than the throughput generated by those two terminals separately. Fig. 1(b) presents the inference tolerable graph for the graph in Fig. 1(a).

C. Forming Potential Subset

We generate the potential subset forming graph G''. $G'' = (V_1, V_2, E'')$ is a bit-partite graph such that $V_1 = V'$, and each node in V_2 presents all cliques and sub-cliques in G'. $e'' = (u'', v'')$ is an edge in E'' iff $u'' \in V_1, v'' \in V_2$, and u'' belongs to one of cliques in G' represented by v''. Fig. 1(c) represents the potential group formation graph for the inference tolerable graph shown in Fig. 1(b).

Each clique in G' represents a potential subset of communication pairs which can make simultaneous communication to enhance throughput. We represent each node in V_1 as an one-off source which is granted and must to be used once in a super-timeslot. Then, the subset formation in a piconet represents the optimal classification for all nodes within a piconet, and a node in V_2 is permitted to occupy the channel mutually excluded if and only if it can make contribute to achieve higher throughput and one-off source is still available.

Let I_{ij} be an indicator function such that $I_{ij} = 1$ if the node $j \in V_2$ is allocated with channel by node $i \in V_1$, and $I_{ij} = 0$ otherwise. Let TH'_{put} be the sub-throughput generated by node j. Then the channel allocation problem can be represented as a set of the following linear constraints.

$$\forall i, \quad \sum_j I_{ij} = 1$$
$$\forall j \quad r_j = TH'_{put,j} \times \sum_i I_{ij} \tag{12}$$

Where r_j is the sub-throughput generated by node j in V_2, Note that this set of constraints captures the location-dependent interference on piconet throughput characteristics of UWB communication systems.

D. Maximizing Piconet Throughput

Consider a utility function $U(r)$ for a throughput r is defined as:

$$U(r) = \frac{L_{tr}}{r} \tag{13}$$

where L_{tr} stands of number of information bits waiting for transmission. The unit for r is $bits/sec$.

Since our goal for subset optimization is to improve piconet throughput as much as possible, maximizing piconet throughput problem can be modelled by the following system of equations:

$$Minimize \quad \sum_j U(r_j)$$

subject to

$$\forall i, \quad \sum_j I_{ij} = 1$$
$$\forall j, \forall i, \quad r_j = TH'_{put,j} \times \sum_i I_{ij} \tag{14}$$

V. Performance Evaluation

We do a set of simulations to evaluate the performance of our algorithm: TM-MAC. A network with amount of communication pairs is set up. Those communication pairs are deployed randomly in an area of $50 \times 50m^2$ and have no mobility. This network can be treated as one piconet in a large-scale system. Parameters for simulations are given in Table I.

We deploy 5 to 40 communication pairs separately in the same region. Then, we form simultaneous transmission subsets using our TM-MAC. We observe the number of generated subsets. We run Monte Carlo simulations and make average operation on results to remove the randomicity of simulation results. The results are shown in Table II. We also observe the chance for each communication pair being classified into different subset (See Table III).

Note that, from Table II and Table III, three to four percent of communication pairs being classified into 1-pair, 2-pair or 3-pair subset. Even with node density increase, there is more chance to form 4-pair subset, i.e., there is 10% higher probability for 40 communication pairs scenario than for 5 communication pairs scenario.

TABLE I

VALUE FOR PARAMETERS USED BY SIMULATIONS.

Parameter	Typical Value	Parameter	Typical Value
T_f	100 ns	σ^2	1.9966×10^{-3}
η	$2.568 \times 10^{-21}\ V^2s$	P	$1\ \mu W$
d	1 m	ξ	$\log_2^e$
g_0	7.9433×10^{-6}	d_{rag}	20 m

Within a piconet, we make simulation to check the actual throughput achieved by different subsets. Under various node density, we plot throughput versus various types of subset (See Fig. 2(a)). Note that, subset within which there are more communication pairs making communication simultaneously acquires higher throughput. In 40 communication pairs scenario, the throughput achieved by 4-pair subset is $119.309kbps$, which is around two times of the throughput achieved by 1-pair subset. Moreover, with the node density increase, the largest throughput which can be achieved is decreased since the interference coming from other users is increased.

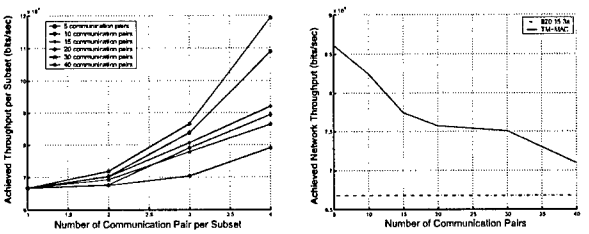

(a) (b)

Fig. 2. (a) Throughput Achieved per Subset and (b) Average Throughput Achieved

We compare our TM-MAC against 802.15.3a, which uses a mutual exclusion scheme to implement medium access control - TDMA scheme. We check the throughput achieved, transmission time needed for certain traffic load and longest latency for data packet for our TM-MAC and 802.15.3a (See Fig. 2(b), Fig. 3(a) and Fig. 3(b)). Note that, our TM-MAC can achieve higher throughput than 802.15.3a around 5.97% to 25.358%. Given same amount of traffic to networks which run TM-MAC and 802.15.3a separately, the transmission time needed for TM-MAC is shorter than the one for 80.215.3a. The reduced ratio for various nodes density from 40 communication pairs to 5 communication pairs locates within the range from 10.358% to 32.18%. Since 802.15.3a uses mutual excluded scheme for medium access control, the communication for various communication pairs is carried out serially. While, for TM-MAC, some communication pairs can make communication simultaneously. The longest latency for TM-MAC is shorter than 802.15.3a. The decreased ratio is from 18.554% to 65.869%.

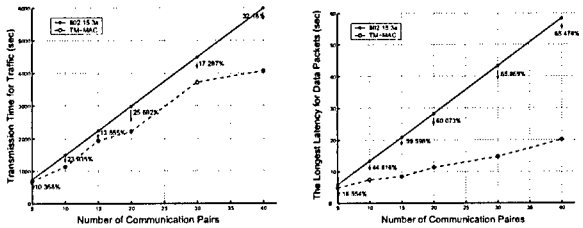

(a) (b)

Fig. 3. (a) Transmission Duration Needed and (b) Longest Latency for Data Packet

VI. Conclusion

In this paper, we propose a MAC protocol: throughput-maximized MAC protocol (TM-MAC), based on the characteristics of ultra wideband (UWB) technology. In UWB communication systems, the transmission parameters are tunable to match the requirements of data flow. In TM-MAC, we implement concurrent multiuser access instead of mutual exclusion method, such as TDMA and random access. For multiuser interference, we establish a model to adaptively adjust the data transmission rate to ensure satisfied signal to noise ratio (SNR) at receiver side. We also analyze the relationship among the theoretical maximum channel capacity, the achievable maximum channel capacity and the maximum data transmission rate. According to the network topology, TM-MAC re-divides network into subsets, in which communication pairs can make communication simultaneously to enhance throughput and to exploit as fast as possible data transmission rate for reliable communication. For subset formation, we propose a general analytical framework, which captures the unique characteristics of shared wireless channel and allows to model a large class of systemwide throughput maximization issue via the specification of per-link utilization functions.

Simulation results demonstrate that TM-MAC can implement throughput maximization to shorten latency and to enhance network processing capability.

Acknowledgement

This work was supported by the U.S. Office of Naval Research (ONR) Young Investigator Program Award under Grant N00014-03-1-0466.

References

[1] "First report and order in the matter of revision of part 15 of the commissions rules regarding ultra-wideband transmission systems, federal communications commission (fcc 02-48)," in *Std., ET Docket 98-153*, Apr. 2002.

[2] I. 802.15.3-2003, "Ieee standard for information technology - telecommunications and information exchange between systems - local and metropolitan area networks specific requirements part 15.3: wireless medium access control (mac) and physical layer (phy) specifications for high rate wireless personal area networks (wpans)," Sept. 2003.

[3] N. J. August and D. S. Ha, "An efficient uwb radio architecture for busy signal mac protocols," in *Proc. IEEE Conference on Ultra Wideband Systems and Technologies*, May 2004, pp. 325–334.

[4] N. J. August, H. Lee, and D. S. Ha, "Pulse sense: a method to detect a busy medium in pulse-based ultra wideband (uwb) networks," in *Proc. IEEE Conference on Ultra Wideband Systems and Technologies*, May 2004, pp. 366–370.

[5] F. Cuomo, C. Martello, A. Baiocchi, and F. Capriotti, "Radio resource sharing for ad hoc networking with uwb," *IEEE J. Select. Areas Commun.*, vol. 20, no. 9, pp. 1722–1732, Dec. 2002.

[6] M. Stemm and R. H. Katz, "Measuring and reducing energy consumption of network modules in hand-held devices," *IEICE Commun.*, vol. E80-B, no. 8, pp. 1125–1131, Aug. 1997.

[7] S. Biaz and Y. D. Barowski, "Gangs: an energy efficient mac protocol for sensor networks," in *Proc. 42nd annual Southeast regional conference (ACMSE'04)*, Apr. 2004, pp. 82–87.

[8] Q. Ren and Q. Liang, "An energy-efficient mac protocol for wireless sensor networks," in *Proc. IEEE Global Telecommunications Conference 2005 (GLOBECOM'2005)*, Dec. 2005, pp. 157–161.

[9] ——, "A contention-based energy-efficient mac protocol for wireless sensor networks," in *Proc. IEEE Wireless Communications and Networking Conference 2006 (WCNC2006)*, Apr. 2006.

[10] I. E. Teletar and D. N. C. Tse, "Capacity and mutual information of wideband multipath fading channels," *IEEE Trans. Inform. Theory*, vol. 46, no. 4, pp. 1384–1400, July 2000.

[11] S. Verdu, "Spectral efficiency in the wideband regime," *IEEE Trans. Commun.*, vol. 48, no. 6, pp. 1319–1343, June 2002.

[12] L. Zhao, X. Hong, and Q. Liang, "Energy-efficient self-organization for wireless sensor networks: a fully distributed approach," in *Proc. IEEE Global Telecommunications Conference 2004 (Globecom 2004)*, Nov. 2004, pp. 2726–2732.

[13] I. 802.15.SG3a, "Channel modeling sub-committee report final."

[14] M. D. Benedetto and G. Giancola, *Understanding Ultra Wide Band Radio Fundamentals*. NJ: Prentice Hall, 2004.

TABLE II

NUMBER OF DIFFERENT KIND OF SUBSET GENERATED WITH VARIOUS NODE DENSITY. 1-PAIR SUBSET, 2-PAIR SUBSET, 3-PAIR SUBSET AND 4-PAIR SUBSET SEPARATELY DENOTE THE SUBSET IN WHICH THERE IS ONE COMMUNICATION PAIR, TWO COMMUNICATION PAIRS, THREE COMMUNICATION PAIRS OR FOUR COMMUNICATION PAIRS.

	5 pairs	10 pairs	15 pairs	20 pairs	30 pairs	40 pairs
1-pair subset	1.648	2.964	4.198	5.782	8.398	10.635
2-pairs subset	0.824	1.368	2.175	3.058	5.081	7.293
3-pairs subset	0.464	0.62	0.856	1.134	1.908	2.677
4-pairs subset	0.078	0.61	0.771	1.105	1.429	1.687

TABLE III

PERCENTAGE OF COMMUNICATION PAIR BEING CLASSIFIED INTO WITHIN DIFFERENT KIND OF SUBSET FOR VARIOUS NODE DENSITY

%	5 pairs	10 pairs	15 pairs	20 pairs	30 pairs	40 pairs
1-pair subset	32.96	29.64	27.987	28.91	27.993	26.587
2-pair subset	32.96	27.36	29	30.58	33.873	36.465
3-pair subset	27.84	18.6	17.12	17.01	19.08	20.078
4-pair subset	6.24	24.4	25.893	23.5	19.053	16.87

Query Processing Optimization Through Sample Size and Monitoring Coverage Controlling in Wireless Sensor Networks

Qingchun Ren and Qilian Liang
Department of Electrical Engineering
University of Texas at Arlington
Arlington, TX 76019-0016 USA
E-mail: ren@wcn.uta.edu, liang@uta.edu

Abstract— **Query processing has been studied extensively in traditional database systems. But few of existed methods can be directly applied to wireless sensor database systems due to their characteristics, such as decentralized nature, limited computational power, imperfect information recorded, and energy scarcity of individual sensor nodes. In this paper, we extend our previous work: quality-guaranteed and energy-efficient algorithm (QGEE) for wireless sensor database systems. We introduce radius of covering disk from point spread function (PSF) aspect and sample size for query quality and energy consumption control. PSF introduces ambiguity into query answers, since the sensitivity of nodes is nonuniform within monitoring region. Sample size determination refers to the process of determining exactly how many samples should be measured in order that the sampling distribution of estimators meets users' pre-specified target precision. In this paper, we formulate the criteria to determine the optimum radius and sample size according to users' requirements on query answers. Simulation results demonstrate that the impact of sample size and monitoring coverage on query answers in terms of root mean square error (RMSE).**

I. Introduction

Recent developments in integrated circuit technology have allowed the construction of low-cost sensor nodes, which are generally equipped with sensing capabilities, wireless communication and limited power supply, CPU and memory. These devices are expected to be embedded into environment to create very dense networks[1]. High level tasks, such as monitoring specific events, are accomplished by cooperation of multiple nodes to collect and process information. Wireless sensor networks (WSNs), which operate in unattended mode, represent an emerging type of network. WSNs are intended for a broad range of environmental sensing applications from weather data collection to vehicle tracking and habitat monitoring[2][3].

The goal of monitoring through sensor nodes is to infer information about objects from measurements made from remote locations. Since inference processes are always less than perfect, there is an element of uncertainty regarding answers. When viewed from this perspective, the problem of uncertainty, which stands for the quality of query answer, is central to monitoring applications. Thus, to build useful information systems, it is necessary to learn how to represent and reason with imperfect information. As a result, Motro[4] is interested in how imperfect information may be represented in a database system. Turtle and Corft[5] in their discussion of uncertainty in information retrieval systems also argue that the issue of imperfect information cannot be ignored.

Uncertain information is typically handled by attaching a number, which represents a subjective measure of an uncertain element according to some observer, to that element. The way in which the number is manipulated depends upon the theory that underlies the number. There are possibilistic databases[6] and probabilistic databases[7][8][9]. Moreover, probabilistic approach has started to be used by WSNs to process query with limited information[10].

Most of algorithms for determining query processing strategies in WSNs are static in nature. In [11], Bodorik proposed aborted join last (AJL) method to substitute static mechanism with adaptive one, which owns low overhead delay to decide when to correct a strategy. In AJL, the decision for correction is computationally simple and, moreover, a corrective strategy is already exist when it is decided to correct. Acquisitional query processing (ACQP)[12], compared with typical methods, focuses on betaking the significant new query processing opportunity that arises in WSNs: smart sensor nodes have the capability to control over where, when, and how often data is physically acquired (i.e., sampled) and is delivered to query processing operators.

Considering energy constraint issues, some energy efficient solutions are proposed. Query processing based on random walk technique[13] is an alternative scheme to implement failure recovery in dynamic environment. The robustness of this approach under dynamic situation follows the simplicity of processing, which only requires the connectivity of moving neighbors. In-network query processing is critical for reducing network traffic when accessing and manipulating data. It requires to place not only a tree of query processing operators such as filters and aggregations but also correlations onto nodes in order to minimize the amount of data transmitted over the network. In [14], an adaptive and decentralized algorithm is proposed. This algorithm progressively refines the placement of query processing operators by walking through neighbor nodes. Thus, an initial arbitrary placement of query processing operators can be progressively refined toward an

optimal placement.

Existing query processing systems for WSNs, including Directed Diffusion[15], TinyDB[12] and Cougar[16], provide high-level interface that allows users to collect and process such continuous streams. Note that they are especially attractive as ways to efficiently implement monitoring applications without forcing users to write complex, low-level code for managing multihop network topologies or for acquiring samples from sensor nodes. TinyDB, Directed Diffusion and Cougar are relatively mature research prototypes that give some ideas on how future query processing system will function for WSNs.

Our previous work: quality-guaranteed and energy-efficient algorithm (QGEE) for wireless sensor database systems[17], considers the energy constraint problem and quality requirement from active nodes election, information collection and query answer expression. QGEE utilizes in-network query processing method to task wireless sensor database systems through declarative queries and uses confidence interval strategy to determine the closeness of a query answer to the true value. Through further study, we extend QGEE in this paper. We introduce radius of covering disk from point spread function (PSF) aspect and sample size for query quality and energy consumption control. PSF introduces ambiguity into query answers, since the sensitivity of nodes is nonuniform within monitoring region. Sample size determination refers to the process of determining exactly how many samples should be measured in order that the sampling distribution of estimators meets users' pre-specified target precision. In this paper, we formulate the criteria to determine the optimum radius and sample size according to users' requirements on query answers.

The remainder of this paper is organized as follows. Section II summarizes our previous work on QGEE algorithm. Our extending work is discussed in Section III. Simulation results are given in Section IV. Section V concludes this paper.

II. Quality-Guaranteed and Energy-Efficient (QGEE) Query Procession Protocol

QGEE employs an in-network query processing method to task networks through declarative queries, which is critical for reducing network traffic when accessing and manipulating sensor data. In QGEE algorithm, only a subset of nodes within a network will be chosen to acquire readings or samples corresponding to the fields or attributes referenced in queries. The goal of our approach is to reduce interference coming from measurements with extreme errors and to minimize energy consumption by providing service that is considerably necessary and sufficient for the needs of application. Moreover, according to the analysis and classification on sources of imperfect information, we employ probabilistic method to formulate the distribution of them in terms of probability distribution function (PDF). Finally probabilistic query answers are acquired on uncertain data. The probability in a query answer allows users to place appropriate confidence in it as opposed to having an incorrect answer or no answer at all.

From four aspects, QGEE implement quality control:

- *Query Vector Space Model (VSM) Design and Active Nodes Selection:* VSM is employed by us to combine all considering factors, such as node location, measurement quality and remaining battery capacity, to select the most related nodes to participate query processing. When a query submitted, the related top-end node fixes on optimal locations for this query and translates the query into a query VSM vector. Query VSM vector and information on optimal locations will be flooded over the whole network. A query correlation is designed to express the correlation between each node and a query. Query correlation is a function of query quality requirement, nodes' energy, measurement quantify and location. The criterion for active nodes choosing is the decision-which nodes are active to respond queries-is based on their query correlations. That is, nodes with highest query correlation among their one-hop neighbors are chosen to participate in related query processing. In QGEE, active nodes are chosen locally leveraging cooperations among nodes.
- *Optimal Location Determination:* We model the problem-determining optimal locations for a query, as a k-partial set cover problem. It is a NP problems which requires time that is exponential to the problem size. We exploit an approximation algorithm: SETCOVER[18], which can acquire the solution during polynomial time, to determine the value of k and the locations of these k disks on a plane. In QGEE, we choose centers of those k disks as our optimal locations.
- *Query Answer Expression:* Since a statistic measurement on samples can rarely, if ever, be expected to be exactly equal to a parameter, it is important that an estimation is accompanied by a statement which describes the precision of this estimation. We utilize confidence intervals[19] to state both how close the value of a statistic being likely to be value of a parameter and the chance of being close.
- *Information Collection:* After active nodes are chosen, a data centric routing algorithm, EM-GMR[20] is employed, which is a multipath, power-aware and mobility-aware routing scheme. It is used to establish route-tree from active nodes to front-end nodes for query answer return. EM-GMR uses reactive networking approach, in which it finds a route only when a message is to be delivered from source to destination. EM-GMR considers distance, remaining battery capacity, and mobility of each sensor node during route path setting up. This scheme could tremendously reduce frame loss rate and link failure rate since mobility is considered, so that incompleteness information caused by poor link quality can be reduced at certain degree.

In energy consumption control, first, in the query SVM design, node location is included besides measurement quality and remaining battery capacity, since it is directly related to

the necessary number of active nodes to cover the whole monitoring region. Through solving optimal location problem, we can employ as few as possible nodes to cover as large as possible monitoring region in order to carry out energy reservation task. Second, we tremendously reduce the frame loss rate and link failure rate through choosing more suitable nodes to set up route-tree for queries. With this improvement, we can reduce energy consumption for route-tree maintenance and information retransmission.

III. Extending Work for Energy and Quality Aware Query Processing

As a motivation for our work, we describe a scenario:

- A great multitude of temperature sensor nodes are randomly deployed in a region we are interested. Individual sensor nodes (or in short, nodes) is connected to other nodes in its vicinity through wireless communication interface, and it uses a multihop routing protocol to communicate with nodes that are spatially distant. All nodes are interconnected to at least one powered PC (front-end node) directly or through intermedial nodes. Front-end nodes are in charge of processing data, on the opposite direction, disseminating queries to related nodes. Within this WSN, each node owns equal computing and sensing capabilities, but measurement quality for sensor parts may be not identical.

A. Radius Control for k-Partial Set Cover Problem

Point spread function (PSF) of nodes introduces ambiguity into query answers. Our temperature monitoring application is interested in the temperature over a region instead of one point in space. But considering operation feasibility, cost and speed, sampling method is widely used instead of completely measuring. In this aspect, another imperfect information source is raised - PSF. PSF is caused by nonuniform sensitivity within nodes' local space. In general, nodes exhibit sensitivity variation similar to what is shown in Fig. 1. Note that, nodes are more sensitive to the center of their regions than toward the edge.

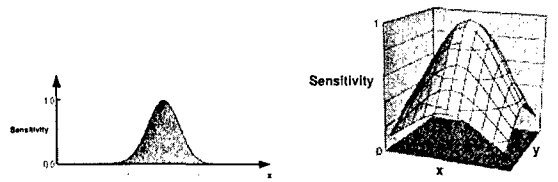

(a) (b)

Fig. 1. (a) 1-Dimension Gaussian model of a PSF and (b) 2-Dimension Gaussian model of a PSF

Among various locations within a disk, measurements of active nodes own the lowest sensitivity/confidence when they stand for the situation at this disk's edge. This nature inspires us to acquire the criterion to calculate suitable value for r. That is, if the sensitivity/confidence equals to or higher than p at the edge of disk, then we can ensure that the measurements of active nodes can represent the situation within this disk at least with p confidence.

Considering the impact of PSF on the uncertainty of query answer, we adaptively adjust the radius r of disks according to users' quality requirements instead of fixing it. We assume that PSF ($g(d)$) of nodes in a WSN is defined by (1) and confidence of query answer is required to be at least p.

$$g(d) = \frac{1}{\sigma\sqrt{2\pi}} e^{-\frac{d^2}{2\sigma^2}} \tag{1}$$

where d is the distance between a point and the center on a disk. σ^2 is the variance of d. $g(d)$ has the similar form as shown in Fig. 1(a).

We derive (2) from (1) to determine r.

$$r = \sigma\sqrt{ln(2\pi\sigma^2(1-p)^2)} \tag{2}$$

Note that r is a function of standard deviation of PSF σ and query quality requirement p. If we fixed σ, r will decrease with increasing of p. That means, with higher query quality, smaller disks are used to search the optimum locations and more active nodes are needed for a query processing.

B. Sample Size Control for Data Sensing

We have chosen a set of nodes to respond a query. However, "How many measurements should be included in one sample?" is the question we will answer in this Section. Sample (any subset of a population) size determination refers to the process of determining exactly how many samples should be measured/observed in order that the sampling distribution of estimators meets users' pre-specified target precision[21].

Since nodes' readings are subject to many small and random errors which are caused by limitations of device's hardware and environmental noise, uncertainty is inherent regarding to true values. Hence nodes reading (x) can be expressed as:

$$x = v + e_m + \eta \tag{3}$$

where v is the true value, e_m is the measurement error introduced by limitations of device's hardware, and η is the environmental noise which is considered as added white Gaussian noise in this paper and $\eta \sim N(0, \frac{N_0}{2})$. Based on central limit theorem[22], the probability distribution of measurement errors complies with a normal distribution. That is, $e_m \sim N(0, \sigma_e^2)$. Generally, in product's technical datasheet, manufactories supply the information on measurement error. For example, the bias for CXM539 is $\pm$1Gauss with 0.95 confidence[23]. That means for sensor nodes CXM593, $\sigma_e^2 = 0.1302$. For general cases, if we know the maximum bias δ and its confidence p, we can obtain the general expression of σ_e^2. That is

$$\sigma_e^2 = \frac{\delta^2}{[Q^{-1}(\frac{1-p}{2})]^2} \tag{4}$$

where $Q(x)$ stands for Q-Function, defined as $Q(x) \triangleq \int_x^\infty \frac{1}{2\pi} e^{-\frac{y^2}{2}} dy$

Moreover, e_m and η are independent. Therefore, node reading also complies with a normal distribution with μ_x-mean and σ_x-standard deviation given in (5).

$$\mu_x = v \quad and \quad \sigma_x = \sqrt{\sigma_e^2 + \frac{N_0}{2}} \tag{5}$$

Therefore the PDF $f_X(x)$ of node reading x is

$$f_X(x) = \frac{1}{\sqrt{2\pi(\sigma_e^2 + \frac{N_0}{2})^2}} e^{-\frac{(x-v)^2}{2(\sigma_e^2 + \frac{N_0}{2})^2}} \tag{6}$$

Using sample mean to estimate the mean of a random variable is an unbiased estimation. That means the estimator aims at the true value or is correct average[24]. In (5), the mean μ_x of samples x equals to the true value v. Moreover, we choose the sample mean as our estimator for true value v, i.e. $\hat{v}_n = \frac{1}{n}\sum_{j=1}^{n} x_j$. Thus, we do an unbiased estimation on true value v. Here n is the sample size. In this case, the PDF of $\hat{v}_n$ is $f_{\hat{V}_n}(\hat{v}_n)$ with $\mu_{\hat{v}_n} = \mu_x$ and $\sigma_{\hat{v}_n}^2 = \frac{1}{n}\sigma_x^2$, as shown in (7).

$$f_{\hat{V}_n}(\hat{v}_n) = \frac{\sqrt{n}}{\sqrt{2\pi(\sigma_e^2 + \frac{N_0}{2})}} e^{-\frac{n(\hat{v}_n - v)^2}{2(\sigma_e^2 + \frac{N_0}{2})}} \tag{7}$$

We let Δx as the margin between the estimator ($\hat{v}_n$) and the true value (v) to reflect the target precision of queries, and we specify our capability, ensuring the estimation error to be within this margin, is not to smaller than p. The criterion for sample size determination is simply stated as:

$$P_r\{|\hat{v}_n - v| \leq \Delta x\} \geq p \tag{8}$$

Since we have known the PDF of $\hat{v}_n$, the probability that the estimation error is not larger than Δx is

$$P_r\{|\hat{v}_n - v| \leq \Delta x\} = 1 - 2Q(\frac{\Delta x}{\sqrt{\frac{\sigma_e^2 + \frac{N_0}{2}}{n}}}) \tag{9}$$

Solving (8) and (9) for sample size n, we obtain

$$n \geq \frac{(\sigma_e^2 + \frac{N_0}{2})[Q^{-1}(\frac{1-p}{2})]^2}{\Delta x^2} \tag{10}$$

Since too large sample size implies a waste of resources, and too small sample size will diminish the utilization of results. In this paper, we exploit the smallest value that satisfies (10) to specify the value of sample size during information sensing, so that we can acquire enough samples to meet users' pre-specified target precision, and reduce energy consumption for data sensing.

IV. Simulations and Performance Evaluation

In our simulations, 100 nodes are randomly deployed in an area of $10 \times 10m^2$, and sensing range for individual nodes is 1m. We run Monte Carlo simulations to remove the randomicity of simulation results. We evaluate the performance of our extending work. In all experiments, we assume that the true value is known to us. We define the root mean square error (RMSE) to express the error of query results,

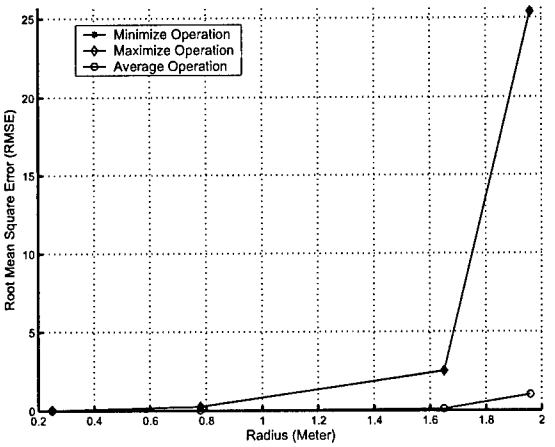

Fig. 2. Error Corresponding to Query Result Caused by Radius of Covering Disk

i.e., $RMSE = \sqrt{\sum_{i=1}^{k}(\hat{v}_i - v)^2}$. Here, k is the number of Monte Carlo simulation.

For MAXIMUM, MINIMUM and AVERAGE data aggregation operations, we check the error caused by the size of k-partial set cover disk and the sample size. In Fig. 2 and Fig. 3, we plot radius and sample size versus error corresponding to query results separately. We can see that with radius of k-partial set cover disk increasing, the error of query results, expressed by root mean square error (RMSE), is enlarged around tens times. Large sample size can make the acquired query results be more close to true values, i.e., the RMSE for 30 sample size scenario is only 30% to the one for 2 sample size scenario. Moreover, the impact of radius of disk and sample size for AVERAGE data aggregation is much smaller than for MAXIMUM and MINIMUM data aggregations. The reason is, for normal random variable, the mean operation for all samples can counteract some errors during estimation. Furthermore, we note that the impact from PSF on query answers is much bigger than the impact from sample size.

Based on (2) and (10), we acquire the optimum values for radius of k-partial set cover disk and sample size, as shown in Table I. Observe that in order to monitoring same region interested, the number of active node needed when p equals to 0.95 is 2 times when p equals to 0.5. In addition, more samples are needed to satisfy the predefined precision on query answers, such as the sample size for p=0.95 is 10 times to p=0.5. Note that, there is a tradeoff between the energy consumption and the quality of answer.

V. Conclusions

Query processing has been studied extensively in traditional database systems. But few of existed methods can be directly applied to wireless sensor database systems due to their characteristics, such as decentralized nature, limited computational power, imperfect information recorded, and energy scarcity of individual sensor nodes. In this paper, we extend

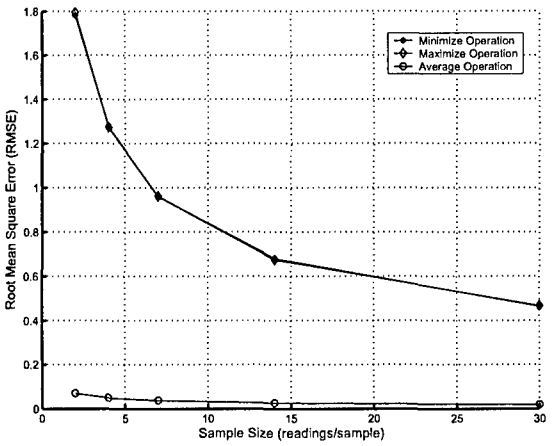

Fig. 3. Error Corresponding to Query Results Caused by Sample Size

TABLE I

OPTIMUM VALUES FOR RADIUS AND SAMPLE SIZE TO GUARANTEE QUERY QUALITY.

	p=0.95	p=0.85	p=0.75	p=0.5
Radius (meter)	1.0079	1.0732	1.217	2.1933
Sample Size (readings/sample)	10.564	5.6987	3.6391	1.2511

our previous work: quality-guaranteed and energy-efficient algorithm (QGEE) for wireless sensor database systems. We introduce radius of covering disk from point spread function (PSF) aspect and sample size for query quality and energy consumption control. PSF introduces ambiguity into query answers, since the sensitivity of nodes is nonuniform within monitoring region. Sample size determination refers to the process of determining exactly how many samples should be measured in order that the sampling distribution of estimators meets users' pre-specified target precision. In this paper, we formulate the criteria to determine the optimum radius and sample size according to users' requirements on query answers.

ACKNOWLEDGEMENT

This work was supported by the U.S. Office of Naval Research (ONR) Young Investigator Program Award under Grant N00014-03-1-0466.

REFERENCES

[1] G. J. Pottie and W. J. Kaiser, "Wireless integrated network sensors," *Commun. of the ACM.*, vol. 43, no. 5, pp. 551–558, May 2000.

[2] J. Warrior, "Smart sensor networks of the future," in *Sensor Magazine*, Mar. 1997.

[3] A. Cerpa, M. H. J. Elson, and J. Zhao, "Habitat monitoring: application driver for wireless communications technology," in *Proc. 2110 ACM SIGCOMM Workshop on Data Communications in Latin America and the Caribbean*, Apr. 2001.

[4] A. Motro, "Sources of uncertainty in information systems," in *Proc. 2nd Workshop on Uncertainty Management and Information Systems: From Needs to Solutions*, Sept. 1992, pp. 1–18.

[5] H. R. Turtle and W. B. Corft, "Uncertainty in information retrieval systems," in *Proc. 2nd Workshop on Uncertainty Management and Information Systems: From Needs to Solutions*, Sept. 1992, pp. 93–111.

[6] H. Prade and C. Testemal, "Generalizing database relational algebra for the treatment of incomplete or uncertain information and vague queries," *Information Sciences*, vol. 34, no. 2, pp. 115–143, 1984.

[7] R. Cavallo and M. Pittarelli, "The theory of probabilistic databases," in *Proc. 13th Very Large Database Conference*, Sept. 1987, pp. 71–81.

[8] M. Pittarelli, "An algebra for probabilistic databases," *IEEE Trans. Knowledge Data Eng.*, vol. 6, no. 2, pp. 293–303, 1994.

[9] ——, "Probabilistic databases for decision analysis," *International J. Intell. Sys.*, vol. 5, no. 4, pp. 209–236, 1990.

[10] R. Biswas, S. Thrun, and L. J. Guibas, "A probabilistic approach to inference with limited information in sensor networks," in *Proc. 3rd International Symposium on Information Processing in Sensor Networks (IPSN'04)*, Apr. 2004, pp. 269–276.

[11] P. Bodorik, J. S. Riordon, and J. S. Pyra, "Deciding to correct distributed query processing," *IEEE Trans. Knowledge Data Eng.*, vol. 5, no. 3, pp. 253–265, 1992.

[12] S. R. Madden, M. J. Franklin, J. M. Hellerstein, and W. Hong, "Tinydb: an acquisitional query processing system for sensor networks," *ACM Trans. Database Syst.*, vol. 30, no. 1, pp. 122–173, Mar. 2005.

[13] C. Avin and C. Brito, "Efficient and robust query processing in dynamic environments using random walk techniques," in *Proc. 3rd International Symposium on Information Processing in Sensor Networks (IPSN'04)*, Apr. 2004, pp. 277–286.

[14] B. J. Bonfils and P. Bonnet, "Adaptive and decentralized operator placement for in-network query processing," in *Proc. 2nd International Symposium on Information Processing in Sensor Networks (IPSN'03)*, Apr. 2003, pp. 47–62.

[15] C. Intanagonwiwat, R. Govindan, and D. Estrin, "Directed diffusion: a scalable and robust communication paradigm for sensor networks," in *Proc. 6th Annual International Conference on Mobile Computing and Networking (MobiCOM 2001)*, Aug. 2000, pp. 56–67.

[16] Y. Yao and J. Gehrke, "Query processing in sensor networks," in *Proc. 1st Biennial Conference on Innovative Data Systems Research*, Jan. 2003.

[17] Q. Ren and Q. Liang, "A quality-guaranteed and energy-efficient query processing algorithm for sensor networks," in *Proc. IEEE Wireless Communications and Networking Conference 2006 (WCNC2006)*, Apr. 2006.

[18] R. Gandhi, S. Khuller, and A. Srinivasan, "Approximation algorithm for partial covering problems," *J. of Algor.*, vol. 53, no. 1, pp. 55–84, Oct. 2004.

[19] J. D. Wilfrid and J. M. J. Frank, *Introduction to Statistical Analysis*. NY: McGraw-Hill, 1983.

[20] Q. Liang and Q. Ren, "Energy and mobility aware geographical multipath routing for wireless sensor networks," in *Proc. IEEE Wireless Communications and Networking Conference 2005 (WCNC 2005)*, Mar. 2005, pp. 1867–1871.

[21] J. M. Mendel, *Lessons in Estimation Theory for Signal Processing Communications, and Control.* NJ: Prentice Hall, 1995.

[22] A. Papoulis, *Probability, Random Variables, and Stochastic Processes.* NY: McGraw-Hill, 2002.

[23] "Products description," in *[On Line] WWW: http://xbow.com.*

[24] P. Olofsson, *Probability, Statistics, and Stochastic Processes.* NJ: Wiley, 2005.

Answer Quality and Network Lifetime Aware Query Processing Protocol in Tactical Sensor Networks

Qingchun Ren and Qilian Liang
Department of Electrical Engineering
University of Texas at Arlington
Arlington, TX 76019-0016 USA
E-mail: ren@wcn.uta.edu, liang@uta.edu

Abstract— **Starting from the characteristics of newly appeared wireless sensor networks, such as decentralized nature, limited computational power, imperfect information recorded, and energy scarcity of individual sensor nodes, we have done some works to solve energy constraint and quality required problems from active nodes election, information collection to query answer expression perspectives. In this paper, extending our previous works, we propose two methods to substitute cosine measure for vector similarity: Cosine-Length Measure (CLM) and Joint-Deference Measure (JDM). Through considering the impact of vector length on vector similarity, CLM alleviates the disadvantage of traditional VSM, in which the confidence of query answer may be degraded since truly similar nodes cannot be elected according to users' requirement. JDM upgrades the accuracy and degrades the complexity for the computation on similarity coefficient through simplifying the measure from vector domain to scalar domain. In addition, with the distributions of measurement error and environment noise known and/or unknown respectively, we formulate the criteria to determine the optimum sample size to meet users' pre-specified target precision. Through simulation, we check the validities and sensitivities of cosine measure, CLM and JMD methods on answer quality and network lifetime. Furthermore, our simulation results, in this paper, form a set of criteria for method selection based on specific applications.**

I. Introduction

Recent developments in integrated circuit technology have allowed the construction of low-cost sensor nodes, which are generally equipped with sensing capabilities, wireless communication and limited power supply, CPU and memory. These devices are expected to be embedded into environment to create very dense networks[1]. High level tasks, such as monitoring specific events, are accomplished by cooperation of multiple nodes to collect and process information. Wireless sensor networks (WSNs), which operate in unattended mode, represent an emerging new type of network. WSNs are intended for a broad range of environmental sensing applications from weather data collection to vehicle tracking and habitat monitoring[2][3].

The goal of monitoring through sensor nodes is to infer information about objects from measurements made from remote locations. Since inference processes are always less than perfect, there is an element of uncertainty regarding answers. When viewed from this perspective, the problem of uncertainty, which stands for the quality of query answers, is central to monitoring applications. Thus, to build useful information systems, it is necessary to learn how to represent and reason with imperfect information effectively and efficiently.

Uncertain information is typically handled by attaching a number, which represents a subjective measure of an uncertain element according to some observers, to the answer. The way in which the number is manipulated depends upon the theory that underlies the number. There are possibilistic databases[4] and probabilistic databases[5][6][7]. Moreover, probabilistic approach has started to be used by WSNs to process query with limited information[8].

Most of algorithms for determining query processing strategies in WSNs are static in nature. In [9], Bodorik proposed aborted join last (AJL) method to substitude static mechanism with adaptive one which owns low overhead delay to decide when to correct a strategy. Acquisitional query processing (ACQP)[10], Compared with typical methods, focuses on betaking the significant new query processing opportunity that arises in WSNs: smart sensor nodes have the capability to control over where, when, and how often data is physically acquired (i.e., sampled) and is delivered to query processing operators.

In energy constraint and quality required problems for query processing, we have done some works from active nodes election, information collection to query answer expression perspectives. QGEE[12] utilizes in-network query processing method to task wireless sensor database systems through declarative queries and uses confidence interval strategy to determine the closeness of a query answer to the true value. However, vector space model (VSM) is one of very efficient methods to quantify the correlation between a query and all candidate documents, but traditional cosine measure for similarity calculation is not a method that reflects the similarity among vectors accurately or completely (i.e., only from the angle aspect to express similarities). Moreover, sample size determination is another important issue for energy reservation and quality control. "How many measurements should be included in one sample (any subset of a population)?" is an essential question to be answered.

In this paper, we propose two methods to substitute cosine measure: Cosine-Length Measure (CLM) and Joint-Deference Measure (JDM). Through considering the impact of vector length on vector similarity, CLM alleviates the disadvantage of traditional VSM, in which the confidence of query answer may be degraded since truly similar nodes cannot be elected according to users' requirement. JDM upgrades the accuracy and degrades the complexity for the computation on similarity

coefficient through simplifying the measure from vector domain to scalar domain. In addition, knowing and/or without knowing the distributions of measurement error and environment noise respectively, we formulate the criteria to determine the optimum sample size to meet users' pre-specified target precision. Moreover, we check the validities and sensitivities of cosine measure, CLM and JMD methods for quality and network lifetime through simulation. The most important thing is that, the availability for those simulation results is not limited to the scenario for our specifical simulations. Since during the design of query vector, we remove the dependence on the absolute values related with network scenario and query, our results, in this paper, form a set of criteria for method selection based on specifical applications.

The remainder of this paper is organized as follows. Section II summarizes our previous work on QGEE algorithm. Our extending works are discussed in Section III. Simulation results are given in Section IV. Section V concludes this paper.

II. Quality-Guaranteed and Energy-Efficient (QGEE) Query Procession Protocol

QGEE employs an in-network query processing method to task networks through declarative queries, which is critical for reducing network traffic when accessing and manipulating sensor data. In QGEE algorithm, only a subset of nodes within a network will be chosen to acquire readings or samples corresponding to the fields or attributes referenced in queries. The goal of our approach is to reduce interference coming from measurements with extreme errors and to minimize energy consumption by providing service that is considerably necessary and sufficient for the needs of application.

From four aspects, QGEE implement quality control:

- *Query Vector Space Model (VSM) Design and Active Nodes Selection:* In QGEE, VSM is employed by us to combine all considering factors to select the most related nodes to participate query processing. A query correlation is designed to express the correlation between each node and a query. Moreover, query correlation is computed by nodes through a distributed way, and active nodes are chosen locally leveraging cooperations among nodes.
- *Optimal Location Determination:* We model the problem-determining optimal locations for a query, as a k-partial set cover problem. It is a NP problems which requires time that is exponential to the problem size. We exploit an approximation algorithm: SETCOVER[13], which can acquire the solution during polynomial time, to determine the value of k and the locations of these k disks on a plane. In QGEE, we choose centers of those k disks as our optimal locations.
- *Semi-Manufactured Query Answer Acquisition:* Since a statistic measurement on samples can rarely, if ever, be expected to be exactly equal to a parameter, it is important that an estimation is accompanied by a statement which describes the precision of this estimation. We utilize confidence intervals[14] to state both how close the value of a statistic being likely to be value of a parameter and the chance of being close.
- *Information Collection:* After active nodes are chosen, a data centric routing algorithm, EM-GMR[15] is employed by QGEE, which is a multipath, power-aware and mobility-aware routing scheme. It is used to establish route-tree from active nodes to front-end nodes for query answer return. EM-GMR uses reactive networking approach, in which it finds a route only when a message is to be delivered from source to destination. EM-GMR considers distance, remaining battery capacity, and mobility of each sensor node during route path setting up. This scheme could tremendously reduce frame loss rate and link failure rate since mobility is considered, so that incompleteness information caused by poor link quality can be reduced at certain degree.

In energy consumption control, first, in the query SVM design, node location is included besides measurement quality and remaining battery capacity, since it is directly related to the necessary number of active nodes to cover whole monitoring region. Through solving optimal location problem, we can employ as few as possible nodes to cover as large as possible monitoring region in order to carry out energy reservation task. Second, we tremendously reduce the frame loss rate and link failure rate through choosing more suitable nodes to set up route-tree for queries. With this improvement, we can reduce energy consumption for route-tree maintenance and information retransmission.

III. Extending Works for QGEE

A. Query Vector Space Model (VSM) Redesign

In information retrieval, VSM is one of very efficient methods to quantify the correlation between a query and all candidate documents. If we treat all sensor nodes as candidate documents for a query, the correlation between a query and nodes can be determined by utilizing the same principle in information retrieval. But we should redesign the VSM vector. Following factors are considered by us:

- Location
  Given a piece of space, number and location of nodes determine the monitoring coverage. In order to employ as few as possible nodes to cover as large as possible area, we should select those nodes located at some special locations, called optimal locations.
- Measurement Quality
  Since the cost and the measurement quality of sensor node are related to each other, sensor nodes owning various qualities are always deployed simultaneously in a WSN for economical reasons. Furthermore, through a query, database users supply not only what information they are interested in, but also the expectation on query answers' quality, i.e., the confidence of query answers. In this case, we should select suitable nodes to response queries.
- Battery
  Remaining battery capacity of sensor node is the third factor, but not the least important one. When the battery of a node is used up, the uncertainty of query answer, at some degree, will increase since data collected by this

node is missed. It inspires us to select those nodes with as high remaining battery capacity as possible, so that all expected information can be collected with best effort.

We employ VSM to incorporate above all factors into the selection of the most related nodes for query processing. We call those nodes active nodes. Vector Υ is designed as $\Upsilon \triangleq \{LC, QC, RBC\}$ to represent each candidate node.

- LC stands for the location correlation. It is the indicator of the distance between the location of a sensor node at (x,y) and the optimal location at (x_0,y_0). Smaller value of LC indicates a node is closer to a optimum location. It is defined as $LC = \frac{\sqrt{(x-x_0)^2+(y-y_0)^2}}{R}$. R is a constant to uniform LC. Usually, we choose nodes' sensor ranging as R.
- QC stands for the measurement quality correlation. It is defined as $QC = 1 - MEQ$. MEQ is the confidence of measurement bias. For example, for speed detecting sensor nodes, CXM539 [16], the bias is $\pm$1mGauss and owns 0.95 confidence. In this case, $MEQ = 0.95$.
- RBC stands for the remaining battery capacity correlation. It is defined as $RBC = \frac{BT_{max}-BT}{BT_{max}}$. BT is the remaining battery level. BT_{max} is the biggest value for BT can be.

As we know that, the typical composite vector similarity measure is the cosine measure, which represents the cosine of the angle between a query and a document as shown in (1).

$$sim_{vs}(q, x_i) = Q \cdot X_i = \frac{\sum_{j=1}^{m} v_j \cdot w_{ij}}{\sqrt{\sum_{j=1}^{m}(v_j^2) \cdot \sum_{j=1}^{m}(w_{ij}^2)}} \quad (1)$$

where m_i is the number of unique terms in a document collection. Document weight $w_{i,j}$ and query weight v_j are

$$w_{ij} = f_{ij} w_{ij} = f_{ij} log(N/d_j) \quad and$$
$$v_j = \begin{cases} log(N/d_j) & y_j \, is \, a \, term \, in \, q \\ 0 & otherwise. \end{cases} \quad (2)$$

However, we found that, besides the angle between two vectors, the length difference of vectors (the length of vector **h** is defined as $\mid \mathbf{h} \mid$) impacts the similarity of two vectors as well. We try to compare the similarity among several vectors in a 2-dimension space, noted by bold letters **A**, **B** and **C** (See Fig.1(a)). Observe that the angles between **A** and **B**, **C** and **B** are same, noted as angle θ. Based on the concept of cosine measure for vector similarity, hence, **A** and **C** have same similarity coefficient with **B**. Therefore, the cosine measure cannot identify vectors, which own same angle to the fiducial one. In this case, the function blind area of cosine measure will impact the performance of VSM. That is, the confidence of query answer may be degraded since truly similar nodes cannot be elected according to users' requirement.

Note that, cosine measure is not a method that reflects the similarity among vectors accurately or completely (i.e., only from the angle aspect to express similarities). In this paper, we propose two substitute methods to alleviate this disadvantage of traditional VSM. They are: Cosine-Length Measure (CLM) and Joint-Deference Measure (JDM). CLM is a modification

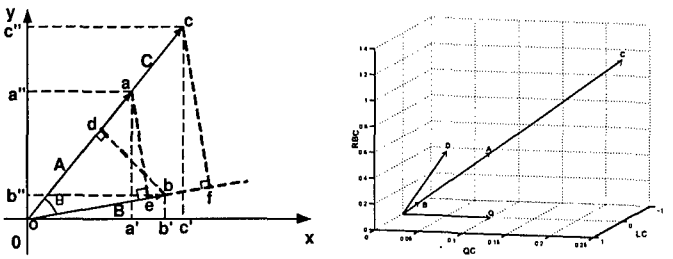

Fig. 1. (a) 2-dimension space for vector similarity and (b) 3-dimension space for vector similarity

of cosine measure, which takes the length difference between two vectors into account for similarity coefficient calculation. There are two ways to implement CLM. One is that we project the fiducial vector onto the measured vectors to calculate the length difference of vectors. As shown in Fig.1(a), fiducial vector **B** is projected onto the measured vector **A** and **C** individually, then ad stands for the length difference between **A** and **B**, as well as cd stands for the length difference between **C** and **B**. We call this method CLM I. The other is that we project the measured vector onto the fiducial vector. As shown in Fig.1(a), **A** and **C** are separately projected on **B**, then be stands for the length difference between **A** and **B** and fb stands for the length difference between **C** and **B**. We call this method CLM II.

Considering that a vector is a directed quantity that can be resolved into components/elements and the similarity of vector is the combination of all elements, JDM separately measure the similarity on each direction/element through measuring length difference, then linearly combine them together to achieve the joint similarity to act as the similarity coefficient. For instance, as shown in Fig.1(a), $a'b'$ stands for the length difference between **A** and **B** at x axis, and $a''b''$ stands for the length difference at y axis. Similarly for **C** and **B**, $c'b'$ and $c''b''$ stand for the length difference at x and y axis respectively.

1) ***Cosine-Length Measure I (CLM I)***:

$$SC_{clmI}(Q, \Upsilon) = \frac{1}{2}\{cos\theta + \vartheta_I(\Delta l)\}$$
$$= \begin{cases} \frac{1}{2}(1 + \frac{|Q|}{|\Upsilon|}) \frac{\Sigma_{j=1}^{t} r_j q_j}{\sqrt{\Sigma_{j=1}^{t} r_j^2 \Sigma_j^t q_j^2}} & H_o \, is \, held \\ \frac{1}{2}(1 + \frac{|\Upsilon|}{|Q|}) & otherwise \end{cases} \quad (3)$$

where H_0 is $\mid \Upsilon \mid \geq \mid Q \mid \frac{\Sigma_{j=1}^{t} r_j q_j}{\sqrt{\Sigma_{j=1}^{t} r_j^2 \Sigma_j^t q_j^2}}$. $\vartheta_I(\Delta l)$ is the part corresponding to the length difference Δl of vectors. In this paper, t equals to 3 based on the definition on query vector Υ. $\theta \in [0, \frac{\pi}{2}]$, since LC, QC and RBC are all positive numerics.

For the $\vartheta_I(\Delta l)$ term in (3), we exploit the uniformed length difference between the node vector Υ and the query vector Q at Υ's direction. In CLM I, opposite to cosine measure, even though the angle of measured vectors to a fiducial vector might be equal, the

difference introduced by length is not always identical too. Therefore, CLM I method can successfully remove the function blind area of cosine measure, For instance, shown in Fig.1(a), SC_{clm} of **A** does not equal to **C**'s any more based on CLM I, since obviously the length difference da for **A** and **B** is shorter than dc for **C** and **B**.

2) ***Cosine-Length Measure II (CLM II)***:
Similarly to CLM I, but we project the measured vectors onto the fiducial vector. Then the similarity coefficient calculation is modified as in (4).

$$\begin{aligned} SC_{clmII}(Q,\Upsilon) &= \frac{1}{2}\{cos\theta + \vartheta_{II}(\Delta l)\} \\ &= \begin{cases} \frac{1}{2}(1+\frac{|\Upsilon|}{|Q|})\frac{\Sigma_{j=1}^{t} r_j q_j}{\sqrt{\Sigma_{j=1}^{t} r_j^2 \Sigma_j^t q_j^2}} & H_o \; is \; held \\ \frac{1}{2}(1+\frac{|Q|}{|\Upsilon|}) & otherwise \end{cases} \end{aligned} \quad (4)$$

Here H_0 is $\mid Q \mid \geq \mid \Upsilon \mid \frac{\Sigma_{j=1}^{t} r_j q_j}{\sqrt{\Sigma_{j=1}^{t} r_j^2 \Sigma_j^t q_j^2}}$. CLM II can gain the same advantage as CLM I, since obviously the length difference eb for **A** and **B** is shorter than ef for **C** and **B**.

3) ***Joint-Deference Measure (JDM)***:

$$SC_{jdm}(Q,\Upsilon) = \frac{1}{t}(\sum_{i=1}^{t} SIM_i) \quad (5)$$

JDM simplifies the problem of measuring vector similarity into measuring scalar similarity, i.e., SC_{jdm} is decomposed into amount of parts - SIM_i along individual elements of vector. The factor $\frac{1}{t}$ in front of (5) comes from the equal gain combination combination for acquiring the joint similarity according to all vector elements. In this paper, based on the query vector design, (5) is specified as in (6).

$$\begin{aligned} SC_{jdm}(Q,\Upsilon) &= \frac{1}{3}(SIM_{lc} + SIM_{qc} + SIM_{rbc}) \\ &= 1 - \frac{1}{3}\{\frac{\mid LC - LC_q \mid}{LC_q} + \frac{\mid QC - QC_q \mid}{QC_q} \\ &+ \frac{\mid RBC - RBC_q \mid}{RBC_q}\} \end{aligned} \quad (6)$$

where SIM_{lc}, SIM_{qc} and SIM_{rbc} are the similarities between a node and a query at the location, measurement quality and battery aspects separately.
Note that, SC_{jdm} is a linear combination of similarities at all elements. Instead of treating each element equally, we can easily change the weights of elements to implement adaptive combination based on users' expectation. That can be a future work of us.

To evaluate the performance of our CLM and JDM methods, we set up a network scenario, in which there are 4 candidate nodes $a \sim d$ for a query q. Query vectors, noted by $A \sim D$ and Q, for all nodes and query are shown in Table I. We use cosine measure, our CLM and JDM to calculate their similarity coefficients individually. The results are shown in Table I.

Note that, cosine measure can only differentiate node d and nodes $a \sim d$'s similarities to query q, since SCs for nodes a, b and e are same (i.e., SC=0.7071). However, CLM and JDM methods can successfully identify the similarities to query q for noes $a \sim d$ individually. We let A, B and C has the same angle with Q, but, the distance from B to Q is the shortest one among A, B and C at node vectors' direction, and the distance from A to Q is the shortest one among A, B and C at q's direction. Note that, node b's SC is bigger than a and c's for CLM I (i.e., $0.6386 > 0.6036$ *and* 0.4538) and node a's SC is bigger than b and c's for CLM II (i.e., $0.8536 > 0.4516$ *and* 0.6415). Furthermore, we let the angle from D to Q is bigger than the one from A to Q, while the distance from D to Q is same as A to Q. Observe that, node a's SC is larger than node d's for CLM I and CLM II (i.e., $0.6036 > 0.4261$ and $0.8536 > 0.4745$). All above observations are consist with our analysis when we designing CLM and JDM methods.

TABLE I
VECTOR SIMILARITY MEASUREMENT USING COSINE MEASURE, COSINE-LENGTH MEASURE AND JOINT-DIFFERENCE MEASURE.

SC	Q	A	B	C	D
(x, y) (m)	(10,10)	(10,10)	(10,10)	(10,10)	(10,10)
Measure Quality(%)	90	90	98.04	75	95
Battery Level (J)	5.0	4.5	4.902	3.751	4.5025
LR (m)	0.0	0.0	0.0	0.0	0.0
MQ (%)	0.1	0.1	0.0196	0.25	0.05
RBL (J)	0.0	0.1	0.0196	0.2448	0.0995
COSINE	-	0.7071	0.7071	0.7071	0.449
CLM I	-	0.6036	0.6386	0.4538	0.4261
CLM II	-	0.8536	0.4516	0.6415	0.4745
JDM	-	0.9667	0.9637	0.8612	0.9483

B. Sample Size Determination

We have chosen a set of nodes, i.e., active nodes, to respond a query. Then, the situation on the region of interest can be inferred from the data obtained in a sample generated by active nodes. While, "How many measurements should be included in one sample (any subset of a population)?" and "How should the answer be presented with more information on confidence?" are two targets in this Section. Sample size determination refers to the process of determining exactly how many samples should be measured/observed in order that the sampling distribution of estimators meets users' pre-specified target precision [17]. Moreover, a statistic measurement on samples can rarely, if ever, be expected to be exactly equal to a parameter, thus it is important that an estimation is accompanied by a statement which describes the precision of this estimation.

As a matter of fact, nodes' readings are subject to many small and random errors which are caused by limitations of device's hardware and environmental noise. Consequently, uncertainty is inherent regarding to true values. In this paper, a node's reading x is formulated as:

$$x = v + e_m + \eta \quad (7)$$

where v is the true value, e_m is the measurement error introduced by limitations of device's hardware, and η is the

environmental noise. We assume e_m and η are independent random variables and the mean for both of them is zero.

Statistical inference is any procedure by which one generalizes to a population from the data obtained in a sample. In the precision description of the estimation, confidence interval (CI)[?] provides a method of stating both how close the value of a statistic being likely to be value of a parameter and the chance of being close. A CI of an attribute denoted by U_i is a interval $[l_i, h_i]$ such that l_i and h_i are real-valued, and that the condition $h_i \geq l_i$ holds. In the following, we discuss the determination of confidence interval and sample size under knowing or unknowing the distribution information separately.

1) Knowing the distribution of e_m and η: Based on the Central Limit Theorem, we assume $\eta \sim N(0, \frac{N_0}{2})$ and $e_m \sim N(0, \sigma_e^2)$. Generally, in product's technical datasheet, manufactories supply the information on measurement errors. For example, as we mentioned above, the bias for CXM539 is $\pm$1Gauss with 0.95 confidence. That means for sensor nodes CXM593, $\sigma_e^2 = 0.1302$. For general cases, if we know the maximum bias Δx and its confidence p, we can obtain the general expression of σ_e^2. That is

$$\sigma_e^2 = \frac{\Delta x^2}{[Q^{-1}(\frac{1-p}{2})]^2} \tag{8}$$

where $Q(x)$ stands for Q-Function, defined as $Q(x) \triangleq \int_x^\infty \frac{1}{2\pi} e^{-\frac{y^2}{2}} dy$.

Therefore, node reading also complies with a Gaussian distribution with μ_x-mean and σ_x-standard deviation given in (9). The PDF of node reading $f_X(x)$ is shown in (10).

$$\mu_x = v \quad and \quad \sigma_x = \sqrt{\sigma_e^2 + \frac{N_0}{2}} \tag{9}$$

$$f_X(x) = \frac{1}{\sqrt{2\pi(\sigma_e^2 + \frac{N_0}{2})^2}} e^{-\frac{(x-v)^2}{2(\sigma_e^2 + \frac{N_0}{2})^2}} \tag{10}$$

To infer the situation on the region of interest from the remote sensing, we do point estimates for the population mean v with sample mean $\hat{v}_n = \frac{1}{n}\sum_{j=1}^n x_j$, which is an unbiased estimation (i.e., the estimator aims at the true value or is correct average [18]) through random sampling. Here n is the sample size. Note that, the sampling distribution of $\hat{v}_n$ has mean μ_x and standard deviation $\frac{1}{n}\sigma_x^2$. Also, the quantity $\frac{\hat{v}_n - v}{\frac{\sigma_x}{n}}$ has a normal distribution. Consequently, in p percent of the samples the interval from $\hat{v}_n - \frac{z_{\frac{1-p}{2}}\sigma_x}{\sqrt{n}}$ to $\hat{v}_n + \frac{z_{\frac{1-p}{2}}\sigma_x}{\sqrt{n}}$ will include the value of v. Here, $z_{\frac{1-p}{2}}$ is the $100\frac{(1-p)}{2}$ percentile obtained from the normal distribution. That is,

$$P_r\{\hat{v}_n - \frac{z_{\frac{1-p}{2}}\sigma_x}{\sqrt{n}} < v < \hat{v}_n + \frac{z_{\frac{1-p}{2}}\sigma_x}{\sqrt{n}}\} \geq p \tag{11}$$

With (11), we obtain a bounded value, i.e., $[\hat{v}_n - \frac{z_{\frac{1-p}{2}}\sigma_x}{\sqrt{n}}, \hat{v}_n + \frac{z_{\frac{1-p}{2}}\sigma_x}{\sqrt{n}}]$, which owns p confidence (not probability). We call this kind of query answers from active nodes as "semi-manufactured" query answers.

The margin of error of a confidence interval is defined to be the value added or subtracted from the estimator which determines the length of the CI. The length of CI expresses the amount of uncertainty. Summary, there are four main factors affect the length of CI. There are: sample size, sample mean, confidence level and sample standard deviation. In practice, when one computes a confidence interval with specified confidence and width, one must decide the sample size to use. This decision involves a trade-off between energy consumption and estimation confidence. In QGEE, given the margin Δx of error between the estimator $\hat{v}_n$ and the true value v, to specify our capability for ensuring this error not to be smaller than p, the criterion for sample size determination is stated as:

$$P_r\{|\hat{v}_n - v| \leq \Delta x\} \geq p \tag{12}$$

Solving (12) and (11) for sample size n, we obtain (13). In other words, with the sample size determined by (13), we can state that the CI will be of length $2\Delta x$, or that the precision of the estimate is $\pm\Delta x$. Moreover, the sample size is in inverse proportion to the length of CI.

$$n = \lfloor \frac{z_{\frac{1-p}{2}}^2(\sigma_e^2 + \frac{N_0}{2})}{\Delta x^2} \rfloor \tag{13}$$

2) Without knowing the distribution of e_m and η:

In some cases, it is not feasible to acquire the information on the distribution of e_m and η. The method designed above may not be available any longer to determine the confidence interval and sample size in this circumstance. We extend our work into scenarios with large sample and small sample individually.

i ***Large Sample Scenario:***

Even though, we have no idea on the distribution of e_m and η. The Central Limit Theorem specifies that $\hat{v}_n \sim N(0, \frac{s^2}{n})$. Here s is the sample standard variance. Since s is almost certainly close to σ_x, the quantity $\frac{\hat{v}_n - v}{\frac{s}{n}}$ is approximately normal with mean 0 and variance 1. Therefore, we can safely substitute σ_x with s in (11) and (13), so that to determine the confidence interval and sample size with specified confidence and width. They are:

$$P_r\{\hat{v}_n - \frac{z_{\frac{1-p}{2}}s}{\sqrt{n}} < v < \hat{v}_n + \frac{z_{\frac{1-p}{2}}s}{\sqrt{n}}\} \geq p \tag{14}$$

$$n = \lfloor (\frac{z_{\frac{1-p}{2}}s}{\Delta x})^2 \rfloor \tag{15}$$

ii ***Small Sample Scenario:***

Since, for small sample size, s may not be close to σ_x, and $\hat{v}_n$ may not be approximately normal. But the quantity $\frac{\hat{v}_n - v}{\frac{s}{\sqrt{n}}}$, even though which will not have a normal distribution any more, has the Student's t distribution with $n-1$ degrees of freedom, which we denote t_{n-1}. Consequently, we have

$$P_r\{\hat{v}_n - t_{\frac{1-p}{2}}(n-1)\frac{s}{\sqrt{n}} < v < \hat{v}_n + t_{\frac{1-p}{2}}(n-1)\frac{s}{\sqrt{n}}\} \geq p \tag{16}$$

The adequate sample size, which ensures the length of CI, i.e., $[\hat{v}_n - t_{\frac{1-p}{2}}(n-1)\frac{s}{\sqrt{n}}, \hat{v}_n + t_{\frac{1-p}{2}}(n-1)\frac{s}{\sqrt{n}}]$,

is $2\Delta x$ with p confidence, should satisfy (17).

$$\frac{\sqrt{n}}{t_{\frac{1-p}{2}}(n-1)} \geq \frac{s}{\Delta x} \tag{17}$$

C. Confidence Computation on Query Answer

- *MAXIMUM Aggregation:* In MAXIMUM aggregation operation, we have design (18)[12] to acquire the final confidence interval.

$$l_{max} = arg\max_i\{l_i\}, \quad and \quad h_{max} = arg\max_i\{h_i\} \tag{18}$$

Since $Z_{max} \triangleq arg\max_i(\hat{v}_{n_i})$, the confidence of Z_{max} being covered by the confidence interval according to (18) is

$$\begin{aligned} p_{max} &= F_{Z_{max}}(h_{max}) - F_{Z_{max}}(l_{max}) \\ &= \prod_{i=1}^{\psi} Q(\frac{\sqrt{n_i}(h_{max}-\mu_{x_i})}{\sigma_{x_i}}) \\ &- \prod_{i=1}^{\psi} Q(\frac{\sqrt{n_i}(l_{max}-\mu_{x_i})}{\sigma_{x_i}}) \end{aligned} \tag{19}$$

- *MINIMUM Aggregation:* In MINIMUM aggregation operation, we have design (20) [12]to acquire the final confidence interval.

$$l_{min} = arg\min_i\{l_i\}, \quad and \quad h_{min} = arg\min_i\{h_i\} \tag{20}$$

Since $Z_{min} \triangleq arg\min_i(\hat{v}_{n_i})$, the confidence of Z_{min} being covered by the confidence interval according to (20) is

$$\begin{aligned} p_{min} &= F_{Z_{min}}(h_{min}) - F_{Z_{min}}(l_{min}) \\ &= \prod_{i=1}^{\psi}\{1 - Q(\frac{\sqrt{n_i}(l_{min}-\mu_{x_i})}{\sigma_{x_i}})\} \\ &- \prod_{i=1}^{\psi}\{1 - Q(\frac{\sqrt{n_i}(h_{min}-\mu_{x_i})}{\sigma_{x_i}})\} \end{aligned} \tag{21}$$

- *AVERAGE Aggregation:* In AVERAGE aggregation operation, we have design (22) [12]to acquire the final confidence interval.

$$l_{avg} = \frac{1}{\psi}\sum_{j=1}^{\psi} l_i, \quad and \quad h_{avg} = \frac{1}{\psi}\sum_{j=1}^{\psi} h_i \tag{22}$$

Since $Z_{avg} \triangleq \frac{1}{\psi}\sum_{i=1}^{\psi}\hat{v}_{n_i}$, the confidence of Z_{avg} being covered by the confidence interval according to (22)is

$$\begin{aligned} p_{avg} &= \int_{l_{avg}}^{h_{avg}} f_{Z_{avg}}(z_{avg})dz_{avg} \\ &= Q(\frac{\sqrt{n_i}(l_{avg}-\mu_{v_i})}{\sigma_{v_i}}) - Q(\frac{\sqrt{n_i}(h_{acg}-\mu_{v_i})}{\sigma_{v_i}}) \end{aligned} \tag{23}$$

IV. Simulations and Performance Evaluation

We run Monte Carlo simulations to remove the randomicity of simulation results and to compare the performance of cosine measure and our CLM and JDM methods. In our simulations, 100 temperature sensor nodes are randomly deployed in a area $\mathring{A}$ ($10 \times 10m^2$). Individual sensor nodes is connected to other nodes in its vicinity through wireless communication interface, and it uses a multihop routing protocol (i.e., EM-GMR[15]) to communicate with nodes that are spatially distant. All nodes are interconnected to a front-end node directly/indirectly. Queries are injected into this WSN through this query operator, and, on the opposite direction, collected data are returned to this query operator to obtain query answer for users. Within this WSN, each node owns equal computing and sensing capability (i.e., sensor ranging is $1m$), but measurement quality for sensor parts may be not identical.

Assume the query operator receives a total of M data samples originated from active nodes elected by different SVM methods in $\mathring{A}$. We utilize the data sample from each active node to represent the true value within the disk region monitored by this active node. We define the reconstruction distortion as in (24) to evaluate the performance for individual methods.

$$\varepsilon \triangleq \frac{1}{M}\sum_{i=1}^{M}\{S(x) - \hat{S}(x)\} \qquad x \in \mathring{A} \tag{24}$$

Here $S(x)$ is the source of interest in $\mathring{A}$. When $S(x)$ stands for the answer's quality, reconstruction distortion ε stands for the distortion between the expected quality and the actually achieved quality for query answers. The positive value of ε means even though higher quality answer is expected by users the confidence for answer actually achieved is some poorer/lower - negative distortion, and negative value means more confident answer is acquired than the expected one - positive distortion. Under various expected qualities from 0.55 to 1.0, we obtain a branch of curves for cosine measure, CLM and JDM separately (See Fig.2).

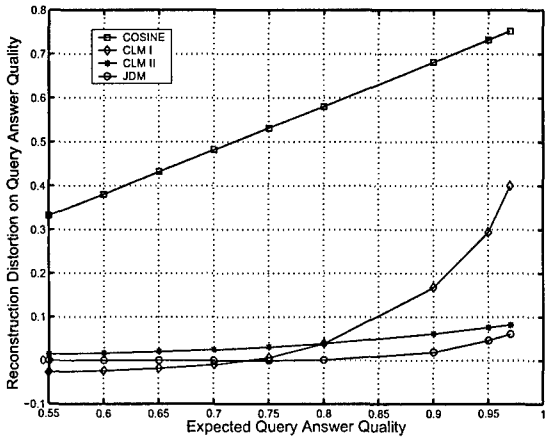

Fig. 2. Reconstruction Distortion for Query-Answer Quality Caused by Different SVM Methods Utilized

Note that, CLM and JDM surpass cosine measure in terms of quality distortion, since the ε for cosine measure is around

$\frac{0.5375-0.1375}{0.5375} \times 100 = 74.42\%$ larger than the ones for CLM and JDM. That is, it is more difficult for cosine measure to make the confidence of answer satisfy users' expectation than CLM and JDM. We also observe that CLM I can achieve more confident answer when expected quality is smaller than 0.75, while wore answers when expected quality is larger than 0.75 than by CLM II and JDM. In addition, the stabilities for CLM II and JDM are better than cosine measure and CLM I with the expected quality changed, i.e., the biggest changes are just 0.0625.

When $S(x)$ stands for the network lifetime that is defined as the period all nodes used up their batteries, reconstruction distortion ε stands for the distortion between the expected network lifetime and the actually achieved network lifetime. In our simulations, we set the expected network lifetime 50000 seconds. Under various expected qualities from 0.55 to 1.0, we obtain a branch of curves for cosine measure, CLM and JDM separately (See Fig.3).

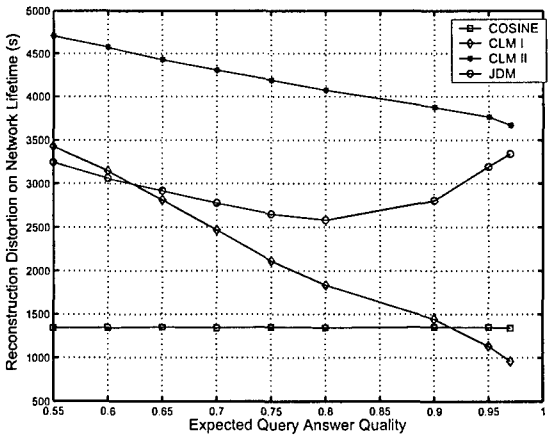

Fig. 3. Reconstruction Distortion for Network Lifetime Caused by Different SVM Methods Utilized

Note that, generally cosine measure surpasses CLM and JDM in terms of network lifetime distortion, except that CLM I achieves longer lifetime when expect quality is higher than 0.9. In addition, cosine measure owns higher stability with the change of expected qualities than CLM and JDM, i.e., the largest change is only 125 seconds. Among CLM I, CLM II and JDM, it is a watershed where expected quality equals 0.62. That is, JDM can elect higher remaining battery nodes to responde query than CLM I and CLM II at the left side of 0.62, while CLM I performances better than CLM II and JDM for the rest circumstances.

From above simulation results, we note that cosine measure, CLM and JDM methods show various sensitivity for answer quality and network lifetime, although we consider measurement quality, node location and battery equally. Hence, JDM method should be the first choose if answer quality is the best consideration for query processing, otherwise cosine measure should be the choose when hoping to achieve the longest network lifetime, especially when the expected quality is less than 0.9. Therefore, there is a tradeoff between answer quality and network lifetime. We should choose the SVM methods based on the specifical applications. For instance, when expected quality is not smaller than 0.8, CLM I can be used to reach the middle point, which achieves not only some higher confidence answer, but also some longer network lifetime.

In Table II, we compare the answer qualities for MAXIMUM, MINIMUM and AVERAGE data aggregations. In addition, we also check the impact of sample size (from 5 to 100) on answer quality. p_1 is the probability that the true answer locate within the confidence interval obtained through (18), (20) and (22). p_2 is computed through the PDF acquired through (19), 21) and (23).

TABLE II

	MAXIMUM		MINIMUM		AVERAGE	
	p_1	p_2	p_1	p_2	p_1	p_2
5	0.955	0.95825s	0.965	0.95839	0.747	0.73641
20	0.955	0.96017	0.96	0.96068	0.981	0.9746
50	0.96	0.96123	0.964	0.9611	1.0	0.99959
100	0.955	0.96118	0.97	0.96217	1.0	1.0

Note that, the very small difference between p_1 and p_2, even at various sample size and data aggregation, demonstrates the correctness of confidence interval and PDF of measurement we designed.

V. Conclusions

Starting from the characteristics of newly appeared wireless sensor networks, such as decentralized nature, limited computational power, imperfect information recorded, and energy scarcity of individual sensor nodes, we have done some works to solve energy constraint and quality required problems from active nodes election, information collection to query answer expression perspectives. In this paper, extending our previous works, we propose two methods to substitute cosine measure for vector similarity: Cosine-Length Measure (CLM) and Joint-Deference Measure (JDM). Through considering the impact of vector length on vector similarity, CLM alleviates the disadvantage of traditional VSM, in which the confidence of query answer may be degraded since truly similar nodes cannot be elected according to users' requirement. JDM upgrades the accuracy and degrades the complexity for the computation on similarity coefficient through simplifying the measure from vector domain to scalar domain. In addition, with the distributions of measurement error and environment noise known and/or unknown respectively, we formulate the criteria to determine the optimum sample size to meet users' pre-specified target precision. Through simulation, we check the validities and sensitivities of cosine measure, CLM and JMD methods on answer quality and network lifetime. Furthermore, our simulation results, in this paper, form a set of criteria for method selection based on specific applications.

Acknowledgement

This work was supported by the U.S. Office of Naval Research (ONR) Young Investigator Program Award under Grant N00014-03-1-0466.

REFERENCES

[1] G. J. Pottie and W. J. Kaiser, "Wireless integrated network sensors," *Commun. of the ACM.*, vol. 43, no. 5, pp. 551–558, May 2000.

[2] J. Warrior, "Smart sensor networks of the future," in *Sensor Magazine*, Mar. 1997.

[3] A. Cerpa, M. H. J. Elson, and J. Zhao, "Habitat monitoring: application driver for wireless communications technology," in *Proc. 2110 ACM SIGCOMM Workshop on Data Communications in Latin America and the Caribbean*, Apr. 2001.

[4] H. Prade and C. Testemal, "Generalizing database relational algebra for the treatment of incomplete or uncertain information and vague queries," *Information Sciences*, vol. 34, no. 2, pp. 115–143, 1984.

[5] R. Cavallo and M. Pittarelli, "The theory of probabilistic databases," in *Proc. 13th Very Large Database Conference*, Sept. 1987, pp. 71–81.

[6] M. Pittarelli, "An algebra for probabilistic databases," *IEEE Trans. Knowledge Data Eng.*, vol. 6, no. 2, pp. 293–303, 1994.

[7] ——, "Probabilistic databases for decision analysis," *International J. Intell. Sys.*, vol. 5, no. 4, pp. 209–236, 1990.

[8] R. Biswas, S. Thrun, and L. J. Guibas, "A probabilistic approach to inference with limited information in sensor networks," in *Proc. 3rd International Symposium on Information Processing in Sensor Networks (IPSN'04)*, Apr. 2004, pp. 269–276.

[9] P. Bodorik, J. S. Riordon, and J. S. Pyra, "Deciding to correct distributed query processing," *IEEE Trans. Knowledge Data Eng.*, vol. 5, no. 3, pp. 253–265, 1992.

[10] S. R. Madden, M. J. Franklin, J. M. Hellerstein, and W. Hong, "Tinydb: an acquisitional query processing system for sensor networks," *ACM Trans. Database Syst.*, vol. 30, no. 1, pp. 122–173, Mar. 2005.

[11] B. J. Bonfils and P. Bonnet, "Adaptive and decentralized operator placement for in-network query processing," in *Proc. 2nd International Symposium on Information Processing in Sensor Networks (IPSN'03)*, Apr. 2003, pp. 47–62.

[12] Q. Ren and Q. Liang, "A quality-guaranteed and energy-efficient query processing algorithm for sensor networks," in *Proc. IEEE Wireless Communications and Networking Conference 2006 (WCNC2006)*, Apr. 2006.

[13] R. Gandhi, S. Khuller, and A. Srinivasan, "Approximation algorithm for partial covering problems," *J. of Algor.*, vol. 53, no. 1, pp. 55–84, Oct. 2004.

[14] J. D. Wilfrid and J. M. J. Frank, *Introduction to Statistical Analysis*. NY: McGraw-Hill, 1983.

[15] Q. Liang and Q. Ren, "Energy and mobility aware geographical multipath routing for wireless sensor networks," in *Proc. IEEE Wireless Communications and Networking Conference 2005 (WCNC 2005)*, Mar. 2005, pp. 1867–1871.

[16] "Products description," in *[On Line] WWW: http://xbow.com.*

[17] J. M. Mendel, *Lessons in Estimation Theory for Signal Processing Communications, and Control.* NJ: Prentice Hall, 1995.

[18] P. Olofsson, *Probability, Statistics, and Stochastic Processes.* NJ: Wiley, 2005.

REPORT DOCUMENTATION PAGE

Form Approved
OMB No. 0704-0188

PLEASE DO NOT RETURN YOUR FORM TO THE ABOVE ADDRESS.

1. REPORT DATE *(DD-MM-YYYY)*	2. REPORT TYPE	3. DATES COVERED *(From - To)*
15-06-2006	Bi-annual Performance/Technical Report	12/01/2005 - 5/31/2006

4. TITLE AND SUBTITLE

Bi-annual (12/2005--05/2006) Performance/Technical Report
for ONR YIP Award under Grant N00014-03-1-0466
Studies on Radar and Non-radar Sensor Networks

5a. CONTRACT NUMBER

5b. GRANT NUMBER

N00014 – 03 –1 –0466

5c. PROGRAM ELEMENT NUMBER

6. AUTHOR(S)

Liang, Qilian

5d. PROJECT NUMBER

5e. TASK NUMBER

5f. WORK UNIT NUMBER

7. PERFORMING ORGANIZATION NAME(S) AND ADDRESS(ES)

University of Texas at Arlington
Office of Sponsored Projects
PO Box 19145
Arlington, TX 76019

8. PERFORMING ORGANIZATION REPORT NUMBER

9. SPONSORING/MONITORING AGENCY NAME(S) AND ADDRESS(ES)

Office of Naval Research
875 N. Randolph St.
One Liberty Center
Arlington, VA 22203-1995

10. SPONSOR/MONITOR'S ACRONYM(S)

ONR

11. SPONSOR/MONITOR'S REPORT NUMBER(S)

12. DISTRIBUTION/AVAILABILITY STATEMENT

Approved for Public Release; Distribution is Unlimited.

13. SUPPLEMENTARY NOTES

14. ABSTRACT

During the period of 12/1/2005 -- 5/30/2006, we expanded our research from generic wireless sensor networks to radar sensor networks. For radar sensor networks, we performed the following preliminary studies: 1) Waveform design and diversity in radar sensor networks with applications to automatic target recognition without or with delay-doppler uncertainty. 2) We proposed a Knowledge-based Ubiquitous and Persistent Sensor networks (KUPS) for threat assessment, of which ``sensor'' is a broad characterization concept. 3) Spatial-temporal-frequency diversity for RSN. For non-radar sensor networks, we conducted the following research: 1) Channel Capacity of Virtual MIMO-Based Wireless Sensor Networks with Imperfect CSI; 2) Cross-Layer Design for MIMO-Based Wireless Sensor Networks; 3) Statistical Analysis in Wireless Sensor Networks with Application to Resources Allocation; 4) MAC Protocol Design for UWB-Based Wireless Sensor Networks; 5) Query Processing Optimization in Wireless Sensor Networks. Fourteen papers were produced during the past six months, and are attached to this report.

15. SUBJECT TERMS

Radar Sensor Network, Automatic Target Recognition, Waveform Design and Diversity, Threat Assessment, Space-Time Adaptive Processing, Channel Capacity, Cross-Layer Design, MIMO, MAC Protocol, Query Processing.

16. SECURITY CLASSIFICATION OF:			17. LIMITATION OF ABSTRACT	18. NUMBER OF PAGES	19a. NAME OF RESPONSIBLE PERSON
a. REPORT	b. ABSTRACT	c. THIS PAGE			Qilian Liang
U	U	U	UU	140	19b. TELEPHONE NUMBER *(Include area code)* 817-272-1339